Theses and Dissertations--Chemistry   Chemistry

2018

CARBON QUANTUM DOTS: BRIDGING THE GAP BETWEEN CHEMICAL STRUCTURE AND MATERIAL PROPERTIES

Timothy J. Pillar-Little Jr.
University of Kentucky, tjli224@uky.edu
Author ORCID Identifier:
iD https://orcid.org/0000-0001-6365-9417
Digital Object Identifier: https://doi.org/10.13023/ETD.2018.108

Right click to open a feedback form in a new tab to let us know how this document benefits you.

CARBON QUANTUM DOTS: BRIDGING THE GAP BETWEEN CHEMICAL
STRUCTURE AND MATERIAL PROPERTIES

DISSERTATION

A dissertation submitted in partial fulfillment of the requirements for the degree of Doctor of
Philosophy in the College of Arts and Sciences at the University of Kentucky

By

Timothy James Pillar-Little Jr.

Lexington, Kentucky

Director: Dr. Doo Young Kim, Professor of Chemistry

Lexington, Kentucky

2017

ABSTRACT OF DISSERTATION

CARBON QUANTUM DOTS: BRIDGING THE GAP BETWEEN CHEMICAL
STRUCTURE AND MATERIAL PROPERTIES

Carbon quantum dots (CQDs) are the latest generation of carbon nanomaterials in applications where fullerenes, carbon nanotubes, and graphene are abundantly used. With several attractive properties such as tunable optical property, edge-functionalization, and defect-rich chemical structure, CQDs have the potential to revolutionize optoelectronics, electro- and photocatalysis, and biomedical applications. Chemical modifications through the addition of heteroatoms, chemical reduction, and surface passivation are found to alter the band gap, spectral position, and emission pathways of CQDs. Despite extensive studies, fundamental understanding of structure-property relationship remains unclear due to the inhomogeneity in chemical structure and a complex emission mechanism for CQDs.

This dissertation outlines a series of works that investigate the structure-property relationship of CQDs and its impact in a variety of applications. First, this relationship was explored by modifying specific chemical functionalities of CQDs and relating them to differences observed in optical, catalytic, and pharmacological performance. While a number of scientific articles reported that top-down or bottom-up synthesized CQDs yielded similar properties, the results herein present dissimilar chemical structures as well as photoluminescent and metal sensing properties. Second, the role of nitrogen heteroatoms in top-down synthesized CQD was studied. The effect of nitrogen atoms on spectral position and fluorescence quantum yield was considerably studied in past reports; however, thorough investigation to differentiate various nitrogen related chemical states was rarely reported. By finely tuning both the quantity of nitrogen doping and the distribution of nitrogen-related chemical states, we found that primary amine and pyridine induce a red-shift in emission while pyrrolic and graphitic nitrogen produced a blue-shift in emission. The investigation of nitrogen chemical states was extended to bottom-up synthesized CQDs with similar results. Finally, top-down, bottom-up, nitrogen-doped and chemically

reduced CQDs were separately tested for their ability to act as photodynamic anti-cancer agents. This series of experiments uncovered the distribution of reactive oxygen species produced during light exposure which elucidated the photodynamic mechanisms of cancer cytotoxicity. The results presented in this dissertation provide key insight into engineering finely-tailored CQDs as the ideal nanomaterial for a broad range of applications.

KEYWORDS: Materials Chemistry, Carbon Nanomaterials, Structure-Property Relationship, Optoelectronics, Electrocatalysis, Biophotonics

Timothy James Pillar-Little Jr.

3/9/2018

CARBON QUANTUM DOTS: BRIDGING THE GAP BETWEEN CHEMICAL
STRUCTURE AND MATERIAL PROPERTIES

By

Timothy James Pillar-Little Jr.

Dr. Doo Young Kim
_____
Director of Dissertation

Dr. Mark A. Lovell
_____
Director of Graduate Studies

3/9/2018
_____
Date

I dedicate this work to the people who supported me in this dream of mine: my parents, Timothy Little Sr. and Wendy Little; my wife, Elizabeth Pillar-Little; and my many friends. Thank you everyone for your words of encouragement, your advice, and your love.

ACKNOWLEDGEMENTS

my two greatest role models in my life. Dad, you always set out to meet or exceed your goals no matter the cost or uphill battle you face. I have learned so much from you over all these years and you have taught me the skills that have helped me be the person I am today. Mom, you are absolutely the strongest person I know with your determination and fighting spirit. Thank you for being the rock I cling to in the storm. Your words of encouragement, those long phone calls listening to my complaints, and those big hugs I get when we see each other have helped me to get to this point. I know that I will go very far in life if I am one-tenth the person you are daily. Thank you both for everything: your laughter, your love, and your example. I am proud to have you two as parents and I love you both very much.

I would also like to acknowledge my wife, Dr. Elizabeth Pillar-Little, for so much that I can't scratch the surface of what positive impact you have in my life. To put it simply (if there is such a thing), I am thankful that you are my best friend, my biggest supporter and ever-present lifeline when I get lost. You have been my foundation through this whole graduate school experience in both the high and low points. We have both been through great milestones together and I can't wait to see what the next big thing is. I've had a great time so far and the adventure is only better with my best friend and amazing wife at my side. I love you very much Liz and thank you from the bottom of my heart for all that you do.

To the friends I have made along the way, thank you for your support. It makes me happy to know I have such great people behind me cheering me on. Whether you were around for a short time or you are still trying to get me out of the house and do "people things", you all have a special place in my heart. I specifically want to call out Matt Bryant Cheney as one of these great friends in my life. I could not be more honored to have such a great Best Man at my wedding, you have been a great help in so many ways and you give the best toasts. I will always cherish our introspective talks and impromptu hangouts with or without Miss Scarlett. Stay super chill in your life even when you're not, I love you like a brother and thank you for everything.

Last but certainly not least, this work would not exist without the generous contribution from our funding sources: the National Science Foundation (NSF), the

TABLE OF CONTENTS

Chapter One: Carbon Nanomaterials, Carbon Quantum Dot Basics and Potential Applications

Chapter Two: Top-Down vs Bottom-Up Synthesis: Does Synthetic Approach Yield Different Carbon Quantum Dots?

Chapter Three: Temperature-Dependent Nitrogen Doping and its effect on the Optical Properties of Graphene Quantum Dots

Chapter Four: Photoluminescent and Electrochemical Properties of Nitrogen-doped Carbon Nanodots

Chapter Five: Structure-Function Relationship of Carbon Quantum Dots and Photo-induced Cytotoxicity Effects

Chapter Six: Conclusions and Future Directions

LIST OF TABLES

LIST OF FIGURES

Chapter Five

Chapter Six

LIST OF SCHEMES

Chapter One: Carbon Nanomaterials, Carbon Quantum Dot Basics and Potential Applications

Carbon nanomaterials have been found to have great potential in applications such as optoelectronics, bioimaging and catalysis due to their ease of functionalization and inexpensive synthesis. However, chemical modifications often induce undesirable effects such as poor aqueous solubility and hinder the same potential in various applications. A new kind of carbon nanomaterial, termed carbon quantum dots or CQDs, has shown even greater potential in these applications with inherently high aqueous solubility, photoluminescent quantum yield and size-dependent fluorescence. These properties are retained or even enhanced upon chemical modification which elevates CQDs above many carbon nanomaterials.

As nanoscale material properties are largely driven by quantum mechanical effects, this chapter will first briefly summarize the differences between bulk and nanoscale properties such as electronic structure and the resulting photophysical properties. A summary of the most notable carbon nanomaterials will follow with specific detail on graphene and graphene oxide as initial observations of CQD properties were often compared to these systems. Additionally, the specific properties of CQDs will be detailed along with their advantages over other carbon nanomaterials. In the last section of this chapter, a detailed explanation of how CQDs can be used as viable alternatives to current materials in optoelectronics, bioimaging, photodynamic therapy and catalysis will be discussed.

1.1   Summary of Carbon Nanomaterials

1.1.1   Differences Between Bulk Materials and Nanoscale Materials

Graphite and graphene are clear examples of how substantial differences between properties can arise as a material from the bulk phase approaches the nanoscale phase. Graphite is typically used in pencil lead and lubricants for its ability to easily slip along electrostatically bound planes. Graphene, on the other hand, has been shown to be an electrically superconducting solid that has sparked a meteoric rise in organic electronics. In the bulk phase, gold is a non-tarnishing, chemically inert, high melting

point metal. These properties allow for uses of gold that include currency, jewelry, electronics, and orthodontic bridges. Nanoparticles of gold (less than 10 nm) however, are very reactive, have a much lower melting point and become magnetic. This enhanced reactivity allows for gold nanoparticles to be used as catalysts.[1] Historically, colored glass has been made from gold nanoparticles as they appear red through the absorption of green light.

Overall, there are two main features that influence these changes from the bulk to the nanoscale. The first of these is related to surface chemistry changes in the nanoparticle. For rounded solids like spherical particles, atomic locations can lie on the surface or in the particle (interior to the surface). For polyhedral geometries, atoms can lie on the face, along the edge, on the corners of the structure, or interior to the surface. In either case, each of these locations is connected to neighboring atoms with a different degree of coordination, also known as the coordination number. A higher coordination number is directly related to the stability of the atom in that location. For the example above, coordination number are ranked from highest to lowest as follows: interior, surface/face, edge, and corners. By correlating stabilization energies of these differently-coordinated atoms, it can be said that those atoms with low coordination numbers will be the most reactive towards adsorbates, giving rise to catalytic activity. However these edge and corner sites may irreversibly bind to adsorbates due to a lack of inherent stability.[1-2] This irreversible binding inhibits catalytic activity and is commonly referred to catalytic poisoning. As the particle size decreases, more atoms take the role of edge and corner sites and thus are poisoned more quickly than larger particles.

As the surface chemistry is inherent to the chemical nature of the nanoparticle, the energy bandgap is inherent to the electronic nature of the nanoparticle. The electronic structure of a nanoparticle is a purely quantum mechanical property, therefore it is imperative to describe the electronic structure of bulk materials, nanomaterials and molecules. Returning to the previous discussion, the second feature that gives nanomaterials unique properties compared to their bulk phases is related to the band gap between the valence band and the conduction band. The overall concept is that as

materials shrink in size from the bulk phase to the nanoscale to atomic and molecular dimensions, their density of states changes from a band structure to discreet energy levels as seen in Figure 1.1 below.[3]
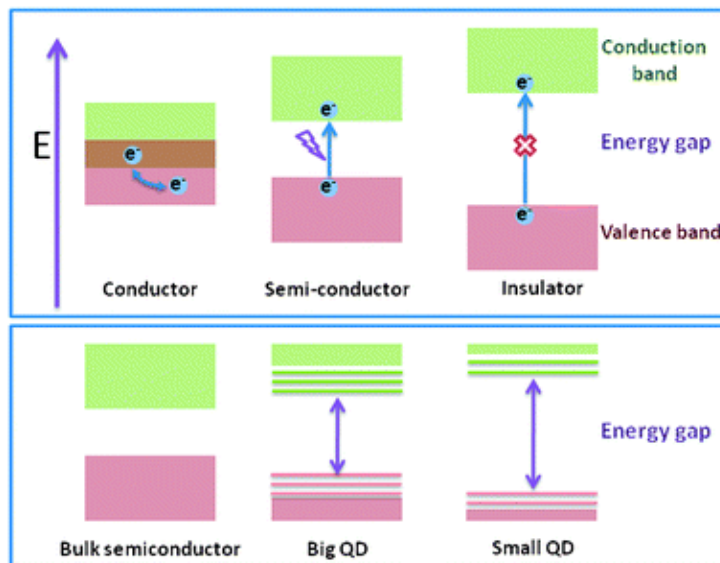
Figure 1.1: Electronic structure of bulk conductor, semiconductor, and insulator materials (top panel) and semiconductor nanoparticles (bottom panel). Reproduced from Ref. 21 with permission from The Royal Society of Chemistry.

When this energy difference exceeds that of thermal energy, the material has electronic structure similar to a molecule as opposed to the band structure seen in solids. This phenomenon is better known as the quantum confinement effect (QCE), or the quantum size effect, and is attributed to how nanoscale materials exhibit different properties than in the bulk phase. In bulk semiconducting materials, upon absorption of energy an electron in the valence band is promoted to the conduction band and a hole is left behind; this electron-hole pair is called an exciton. In bulk systems, both the electron and hole can freely move with little energy loss due to the periodicity of the material. Often the physical separation between the electron and hole is on the order of a few nanometers and is referred as the Bohr exciton radius, as it follows a hydrogen-like (one electron) wavefunction. If the absorbed energy is low, the electron and hole are electrostatically bound to one another and can recombine easily with nearly no energy emitted. QCE is observed when the size of a material approaches the Bohr exciton radius. Some reports have shown that this effect can occur in particles with

diameters as large as 50 nm but in the case of most inorganic quantum dots, this size is often between 2 and 10 nm.[4] As the size of the particle decreases to molecular or atomic sizes, the exciton is further confined and the energy band gap structure becomes identical to a molecular electronic structure. Figure 1.2 depicts the quantum confinement effect as a function of the size of a quantum dot.
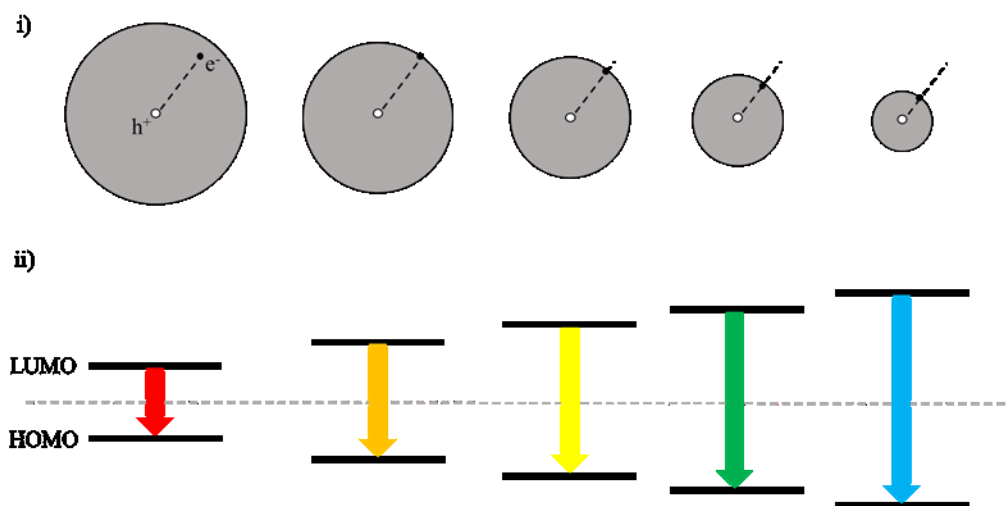
Figure 1.2: i) As the size of the nanoparticle decreases, the exciton (electron-hole pair) becomes spatially confined. ii) As a consequence of the quantum confinement effect, recombination energy becomes larger as the exciton is further confined.

The carbon quantum dots discussed in this thesis are unlike inorganic nanoparticles in that they are large enough to exhibit QCE but there are also separate fluorophores that act as molecular states. In essence, the electronic structure is a kind of blend of the energy band gap theory in bulk semiconductors and the fine electronic structure of molecules. Despite this blending, we can describe the electronic structure of carbon quantum dots using a modified Jablonski diagram as shown below in Figure 1.3.
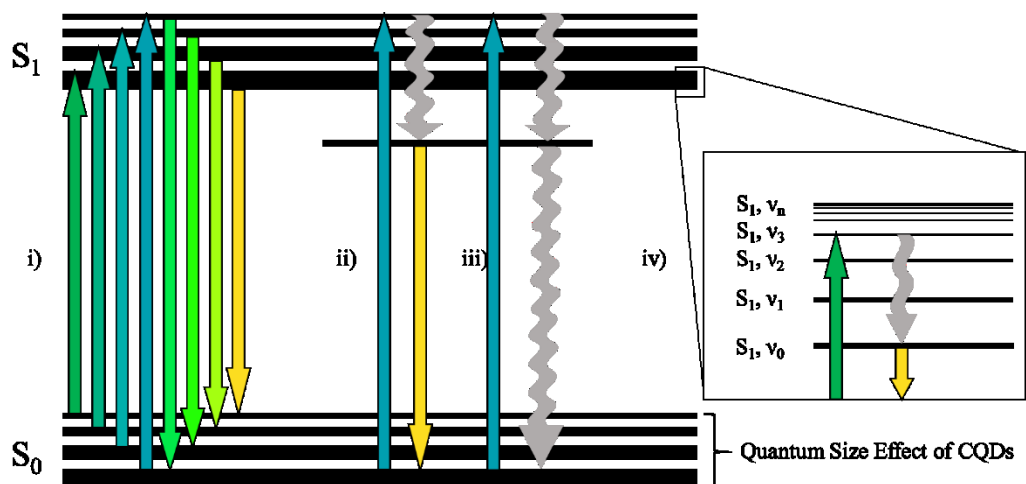
Figure 1.3: A modified Jablonski diagram to illustrate the electronic structure of carbon quantum dots (CQDs).

This figure is divided into four parts corresponding to the events upon the absorption of a photon. Part *i* is a depiction of the quantum confinement effect (QCE). Smaller CQDs have a larger bandgap between the ground state, S_0 and the excited state, S_1, than larger CQDs. Upon excitation, non-radiative processes remove energy from the excited state and the emitted photon has less energy than the initial excitation energy. This is referred to as the Stokes shift and results in red-shifted emission compared to the excitation. Part *ii* illustrates the role of the defect state fluorophore which may be functional groups or heteroatom dopants. Upon excitation, non-radiative processes occur which transfer energy to the defect state fluorophore with some amount of energy loss. Once there, the emitted photon from the defect state fluorophore is substantially red-shifted compared to the excitation energy. Part *iii* shows the effect of defects that are themselves non-radiative. These often take the form of "dark states" which trap the excited state energy and dissipate it non-radiatively through solvent effects or vibrational relaxation. Part *iv* depicts vibrational relaxation in the excited state, a very common non-radiative process. As energy is quantized, excitation may bypass the lowest excited state, S_1 and excite a higher vibrational state of the excited electronic state, such as S_1, v_1. In the figure, it is shown that the excess excited state energy is shed to the lowest excited state through vibrational relaxation. Kasha's rule states that efficient emission of photons must occur from the lowest excited state despite receiving excitation energy that exceeds that of the lowest excited state. In other

words, efficient photon emission from S_1 is largely excitation-independent with greater energy than the S_0-S_1 band gap.

By utilizing the chemical structure and electronic structure, there is great potential to use carbon quantum dots as optoelectronic, photovoltaic and photodynamic nanomaterials. The next sections of this chapter will discuss the development of carbon nanomaterials from the largest sizes to the smallest dimensions, finally with carbon quantum dots themselves. In these sections, it is discussed in detail the similarities and differences various carbon nanomaterials have with one another. In addition, information on structural and functional characteristics are described for each of these systems. After that, the relevant need for carbon nanomaterial research is discussed as well as how carbon quantum dots contribute to various applications and settings.

1.1.2 Bulk Carbons

Scientific interest in carbon nanomaterials has evolved from the desire to make alternatively sourced materials that compete with current technology made with rarer inorganic materials such as cadmium or platinum. These alternative sources can exist in many forms with a range of complexities but bulk carbons are often the starting material for producing carbon nanomaterials. Coal, for example, is carbonized plant matter that is found in underground deposits and widely used as fuel for energy production. As there is no repeating chemical structure, it is difficult to characterize coal as anything other than a bulk material. Nevertheless, there is a rich variety of elements which commonly include carbon, hydrogen, nitrogen, oxygen, and sulfur. Other rare elements can be found in coal but usually the quantity is low and depends on the geographic region. The main group elements form a myriad of functional groups such as thiols, azides, lactones, ethers, benzene rings, and other unique functionalities as identified by X-ray Photoelectron Spectroscopy (XPS) and Fourier Transform Infrared Spectroscopy (FTIR).[5-8] A less complex form of bulk carbon is acetylene black (or carbon black) made from processes such as the thermal decomposition of acetylene gas. This kind of bulk carbon has less atomic impurities than coal. This reduces the overall variety of functional groups to fused benzene rings, cycloalkanes/cycloalkenes, and alkyl chains.[9] It is important to note that there is no regular structure to acetylene

black and as such, it is also known as non-graphitic carbon. Heating non-graphitic carbon to very high temperatures (above 1500 °C) can convert some of this carbon to graphitic carbon, depending on local structure. However, some nongraphitic carbon cannot be converted even with temperatures above 3000 °C.[10]

The bulk carbon material with the least complexity is graphite which consists of stacked sheets of one-atom thick crystalline carbon (later known as graphene). A simple structure for graphite is shown below in Figure 1.3.[11] This figure illustrates the stacking effect between sheets which are weakly bound together by van der Waals forces and overlapping p_z orbitals that form π-bonding orbitals perpendicular to the plane containing carbon atoms, also referred as the basal plane. The structure of graphite provides unique properties compared to other allotropes of carbon. For example, graphite is an excellent conductor of heat and electricity compared to diamond along the basal plane. The stacking axis however is much less electrically conductive due to the large distance between planes (0.335 nm)[12] compared to the proximity of neighboring carbon atoms on each plane (0.142 nm).[13] The stacked arrangement of sheets also allows them to "slide" along each other under applied mechanical force. This reduced friction makes graphite useful for pencils and lubricants as the crystallographic sheets are easily moved by slip forces.
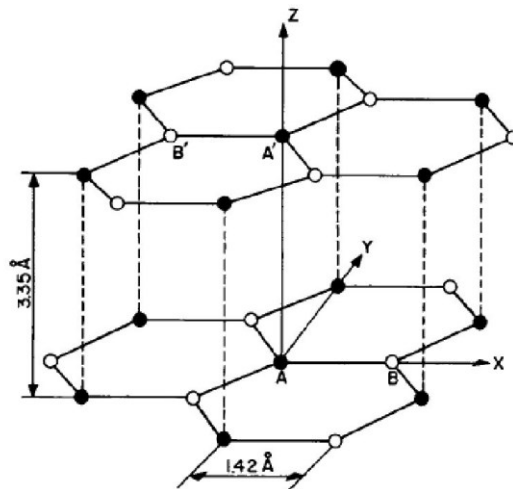
Figure 1.4: The crystal structure of graphite. The picture shows two planes of crystalline carbon in a stacked configuration. Reproduced with permission from ref. 13.

1.1.3　Graphene and Graphene Oxide

In 2004, Andre Geim and Konstantin Novoselov mechanically exfoliated pyrolytic graphite until all that remained was a single-atom thick film of carbon, termed graphene, with some films containing up to three stacked graphenes. In terms of material quality, it was found that these single-layer films could be isolated to crystals about 10 μm in size with few defects. Multi-layer graphene films with thickness $d \geq 3$ nm (more than 10 layers) could be as large as 100 μm in size. Both single- and multi-layer films were analyzed for their electronic properties which found some unprecedented results. First, graphene films were measured using field-effect and magnetoresistance measurements to extract the carrier mobility, μ. This defined as a measurement of how quickly an electron (μ_e) or hole (μ_h) can move through a metal or semiconductor. Typically, room temperature organic semiconductor crystals have $\mu_e = 0.1 - 20$ cm^2/V•s under the best conditions.[14] Inorganic semiconductors, on the other hand, have μ values many orders of magnitude higher such as Si with $\mu_e = 1350$ cm^2/V•s and $\mu_h = 480$ cm^2/V•s.[15] Surprisingly, it was found that graphene boasts a μ_e between 3000 and 10000 cm^2/V•s, depending on the quality of sample.[16] Since then, graphene μ_e measurements have improved and the highest electron mobility recorded is over 200000 cm^2/V•s.[17] Since the discovery of graphene, the field of organic electronics has experienced a renaissance of new research in both theoretical and experimental sciences.

As the focus of this thesis is about carbon quantum dots, it is important to understand the evolution of carbon-based nanomaterials both for their fundamental properties and useful applications. As graphene was making its mark in the scientific community, some researchers chose to explore systems of graphene that include oxygen heteroatoms in their structure. This oxidized form of graphene, termed graphene oxide, has provided new opportunities to use graphene-like materials in ways not previously allowable by the all-carbon chemical structure of graphene.

Graphene oxide (GO) is synthesized by either the Brodie, Staudenmaier, or Hummers method; all of which begin with harshly oxidizing graphite with strong acids and intercalating agents. Of course, there are more methods to synthesize graphene

oxide, but most of these are variations of the above. Regardless of the synthetic method, the produced graphene oxide is essentially graphene with additional oxygen-containing functional groups such as hydroxyls, carbonyls, and carboxylic acids. Additionally, there may be "defects" such as oxygen atoms that bridge across neighboring aromatic regions like ethers or along the same aromatic ring as in an epoxide. In essence, GO can be seen as a defect-ridden version of graphene compared to the nearly defect-free graphene sheets produced by mechanical exfoliation. Though graphene oxide can be produced in sheets as large as micrometers in diameter; the ether and epoxide defects can be targets for oxidative cleavage which fragment the GO into smaller pieces on the order of tens to hundreds of nanometers.

The added oxygen-containing functional groups also prevent the stacking behavior seen in multi-layer graphene and graphite. In aqueous media, the hydrogen bonding interaction is between the functional groups on GO and water, allowing for excellent aqueous dispersability and reduced aggregation. In non-polar solvents, a sort of clustering occurs as hydrogen bonding will be limited to the functional groups on other GO particles. Aqueous solubility allows for use in many more industrial applications than graphene as environmental and health hazards are eliminated by not using organic solvents for processing and purification. In addition, solubility in aqueous systems provides a means to use GO in biological and pharmacological applications.[18-20] It is important to note that these oxygen-containing functional groups can be changed to finely tune specific properties such as solubility, fluorescence, and metal sensing.[21] For example, when GO is reduced by either a chemical,[22] thermal,[23] or electrochemical method,[24] the oxygen-containing defects are converted to less oxidized functional groups. Using longer reduction times or more potent reducing agents can cause full reduction of the functional group to hydrogen. In concert with the removal of functional groups, the photoluminescent properties (e.g.: absorbed or emitted light) of GO are shifted to shorter wavelengths. This can be done by shrinking the π-conjugation in accordance with the quantum confinement effect, or by removing so-called "dark states" which are non-radiative defects. Both of these concepts will be discussed in further detail later in this chapter.

1.1.4 Carbon Nanotubes: One-Dimensional Nanomaterials

Another unique conformation of sp^2-hybridized carbon is the carbon nanotube, abbreviated CNT, which is essentially rolled-up graphene sheets. The main classifications of CNT are single-walled carbon nanotubes (SWNTs) and multi-walled carbon nanotubes (MWNTs) which are concentrically layered carbon nanotubes. Since first observed by Iijima in 1991,[25] CNTs have displayed several interesting properties that can be applied to a variety of potential uses. The cylindrical shape of carbon nanotubes whose atoms are covalently bound provides unusually high material strength — particularly against compression and tension. Interestingly, CNTs with very high ratios of the length of the CNT to its diameter, termed aspect ratio, are much softer and pliable along the main axis considering the rigidity of the tube towards compression and tension. As shown below in Figure 1.4,[26] carbon nanotubes can have a few different atomic arrangements within the cylindrical structure: armchair, zigzag, and chiral.[27-28] All of these conformations of CNTs have excellent thermal conductivity along the length of the tube (transverse axis). In addition, chiral CNTs show unique electronic properties much like graphene.[27] Overall, the thermal and electrical properties of CNTs have since been heavily researched for the purposes of electronics and microelectronics while the mechanical properties and functionalization of CNT edge have largely been exploited for use in membrane technology,[29-30] pharmacological research,[31-34] and for structural support of nanocomposites.[35] Though CNTs have the potential to be used in these applications, the challenge is producing uniform CNTs of high yield and low cost.
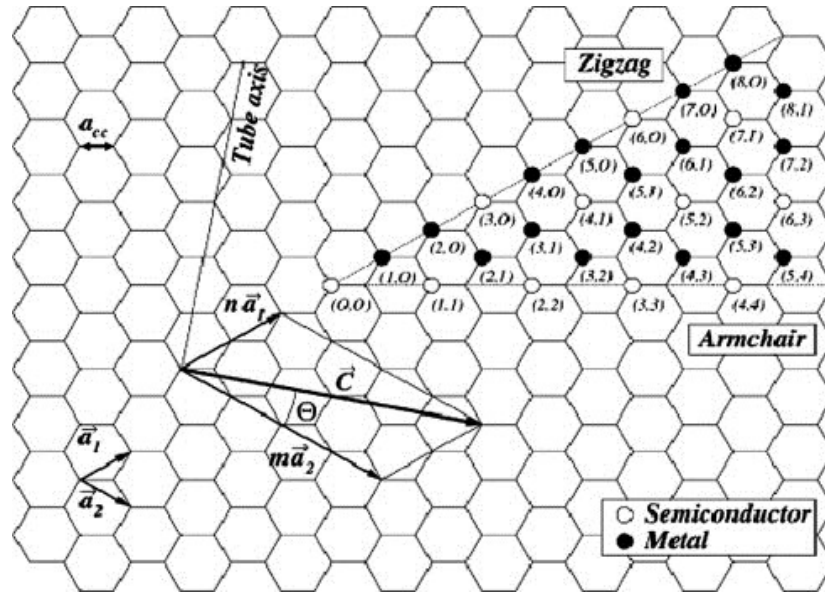
Figure 1.5: The 2D graphene sheet diagram showing a vector structure classification used to define CNT structure. Reproduced from ref. 36.

This challenge originates from the insufficient understanding of the growth mechanism of CNTs. In simple terms, CNT growth can be described by the vapor-solid-solid method (VSS) which is similar to the vapor-liquid-solid method that models the growth mechanism for many other nanomaterials.[36] Briefly, the VSS model illustrates that nanotube growth is initiated by a metal catalyst which absorbs carbon vapors, diffuses the carbon vapors into the surface of the metal catalyst (forming a solid solution) and finally deposits the carbon to the substrate as more vapors are absorbed. Interestingly, Hoffman *et al.*[37] and Puretzky *et al.*[38] observed with *in situ* high-resolution TEM that the metal catalyst can grow carbon nanotubes in two different ways based on a series of parameters. In Figure 1.5 below,[39] the CNTs are grown as deposited carbon pushes up the metal catalyst from the substrate or CNTs are grown on top of the metal catalyst as the metal-substrate interface is fixed.

11
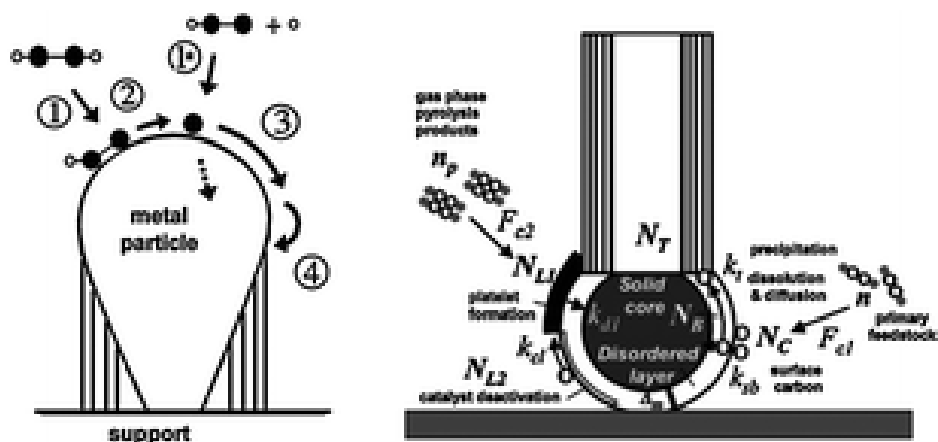
Figure 1.6: Popular models of carbon nanotube growth mechanism (sources: Hofmann *et al*. (left) and Puretzky *et al*. (right)). Reproduced with permission from ref. 49.

Overall, the growth mechanism has been difficult to elucidate due to the varied nature of each synthetic method. In short, there are three approaches in which CNTs are grown. The first of which takes large bulk carbons and atomizes them in a vacuum chamber. The atoms are then recombined upon cooling to form CNTs downstream of the atomization source. This breakdown of large carbons will be frequently addressed as the "top-down" approach. Common methods for this approach are an arc-discharge between graphite electrodes[40-41] and a laser ablation of graphite rods.[42-43] These techniques can produce large quantities of either SWNTs or MWCNTs (depending on specific parameters) but with a large distribution of sizes and a low purity. The second of these approaches takes small organic precursors and builds them up into the desired product, also known as the "bottom-up approach". This approach usually follows a scheme in which a mixture of hydrocarbon gas and an inert carrier gas is first pumped into a chamber. From here, popular methods for this kind of synthesis deviate greatly such as thermal chemical vapor deposition (CVD) in which a tube furnace is used to initiate CNT growth;[38] or microwave-assisted CVD in which microwave energy is used to generate a highly-reactive plasma.[44-45] Many variations on the bottom-up approach can be employed such as using larger liquid-phase hydrocarbons[46] through a bubbler system instead of gases, using a resistive material as the heat source to initiate reaction also known as the hot filament CVD method,[47] or ultra-high vacuum (P < 10⁻⁶ Pa) to encourage rapid cooling from the heat source to the substrate for defect-free material

growth.[48] Overall, the bottom-up approach gives low to average yields, medium to high purity, and a narrower distribution of sizes compared to the top-down approach.

In the next chapter of this thesis, we explore the top-down versus bottom-up approach to synthesizing carbon quantum dots (CQDs). Surprisingly, CQDs are unlike carbon nanotubes in that different synthetic approaches do not yield similar materials. In fact, both of these synthetic approaches instead yield similarly-sized carbon quantum dots with greatly varied chemical structures. As such, the synthetic approach was found to be critically important to finely tune optical and catalytic properties.

1.1.5   Carbon Quantum Dots and their Advantages

In 2004, a new kind of zero-dimensional carbon nanomaterial was inadvertently discovered by Xu *et al*. by the electrophoretic analysis of single-walled CNTs.[49] This fluorescent nano-sized carbon fragment, called the carbon quantum dot (CQD),[50] has since made a significant impact on research pertaining to catalysis, optoelectronics, photovoltaics, biomass conversion, bioimaging, and photodynamic therapy. Like the previously discussed carbon-based materials, CQDs can have greatly varied synthetic methods, chemical structures and functional group distributions – all of which affect performance in specific applications.[51-54] CQDs began their rise in optoelectronic research by applying oxidative cutting toward graphene oxide nanoflakes about 100 nm in size. The products of this reaction, termed "graphene quantum dots" or "GQDs", were found to be fluorescent with a low photoluminescent quantum yield (PLQY) of 1 to 3%.[55] In addition, these GQDs emitted blue or green light upon UV excitation. Currently, modifications to the synthesis such as changing the precursor or employing hydrothermal treatment yield GQDs with PLQY upwards of 25%.[53-54, 56-78]

PLQY can be simply defined as the ratio of emitted photons to absorbed photons. However as shown in the equation below, PLQY relates all photophysical processes with both radiative and non-radiative rate constants. In this equation, Φ_{PL} represents the photoluminescent (or fluorescent) quantum yield, k_r is the radiative rate constant, k_{isc} is the non-radiative rate constant for intersystem crossing, k_{ic} is the non-radiative rate constant for internal conversion, and k_{nr} is the sum of all non-radiative rate constants.

$$\Phi_{PL} = \frac{k_r}{k_r + k_{isc} + k_{ic} + \cdots} = \frac{k_r}{k_r + k_{nr}}$$

The PLQY of a sample can be measured directly with an integrating sphere. This sphere has a highly reflective coating on its interior that allows light to be well dispersed across the volume of the sphere. In essence, the sphere allows the emitted light to maintain a uniform "glow" as opposed to the potentially directional emission of some samples. The sample is compared to the solvent (a blank in this case) in which it is dispersed and the differences in the excitation light intensity received by the detector from sample to blank as well as the fluorescence intensity emitted by the sample give rise to the PLQY.

PLQY can also be measured indirectly by using the slope of fluorescence intensity vs absorbance of a standard fluorescent dye (such as Rhodamine 6G) with a known PLQY and comparing the slope of the same parameters of the sample as shown in the following equation. Despite this being a relative measurement, the instrumental error is minimized as all parameters are fixed during the experiment. The few errors that may arise are using standards that photobleach quickly, improper dilution technique, or using concentrations of fluorescent dyes whose absorbance falls out of the range of linearity $(0.01 - 0.1)$.

$$\Phi_{PL,sample} = (\frac{I_{sample}}{A_{sample}})(\frac{A_{standard}}{I_{standard}})(\frac{\eta_{sample}}{\eta_{standard}})$$

Further analysis of the chemical structure determined that these top-down synthesized quantum dots were mainly comprised of large domains of fused aromatic rings with edge-terminating functional groups like hydroxyls, carbonyls, and carboxylic acids. This gives CQDs very unique features not found in other carbon nanomaterials such as hydrophilicity without post-synthesis modification, a tunable sp^2 to sp^3 carbon ratio, and facile, inexpensive synthesis. CQDs are often divided in the literature by two synthetic approaches: known as the top-down or bottom-up method. Top-down methods, like the Hummers' method, take bulk carbon materials and subject them to harsh oxidation with compounds such as sulfuric acid, nitric acid, or potassium permanganate.[8, 79-81] Modifications to the top-down synthesis of CQDs make production cleaner by removing the harsh oxidants altogether as in electrochemical methods,[52, 66, 73, 82] hydrothermal treatment,[55, 83-86] or by chemically treating waste

products like lemon peels, urine, or even barbecued meat.[72, 87-90] Presently, the greatest challenge in the top-down method is the extensive amount of work-up required to purify CQDs such as ultracentrifugation, dialysis, neutralization, and vacuum filtration among many others.

Bottom-up methods, on the other hand, build up CQDs using a range of organic molecules as small as glucose or citric acid[60, 91-93] to large polymers like polyethylene glycol.[94-95] Bottom-up methods are more diverse compared to top-down methods due to their simplistic nature. The earliest example of producing CQDs by this method is the hotplate pyrolysis of citric acid by Dong *et al.*[60] Since then, many studies have utilized solvothermal[80, 96-97] and hydrothermal reactors[67, 98-99] or microwave ovens[63, 75, 84, 93, 100-101] in effort to restrict the inhomogeneous nature of CQDs. The advantage (and disadvantage) of using the bottom-up method is the sheer number of parameters one can use to influence the reaction. In hydrothermal synthesis, for example, parameters such as pressure, temperature, fill factor and mixing ratios can greatly change the chemical functionality of the produced CQD.[98, 102] Chapter 3 explores this further using a hydrothermal method to add nitrogen heteroatoms to CQDs as a function of treatment temperature. From this work, a large difference was observed not only in the quantity of nitrogen added, but also in the location (i.e.: edge-terminating or within the sp^2 nanodomain). Unique to CQDs, the approach of synthesis results in nearly identical products. Features such as graphene-like sp^2-carbon domains a few nm in size and edge-terminating functional groups are common to both the top-down and bottom-up synthetic approaches. The largest difference between these two kinds of CQDs is the presence of a surface passivation layer resulting from an incomplete bottom-up synthesis. Preventing the formation of the surface passivation layer can only be done with longer reaction times, which ultimately result in large carbonaceous aggregates whose properties approach those of bulk carbon materials. Thus, the surface passivation layer has been closely studied due to its effects on optical and catalytic properties.

Interestingly, research in this field has described CQDs as the combination of two very different nanomaterials. The chemical structure of CQDs closely matches that of graphene oxide (e.g. large sp^2 nano-domains, functional group defects) but on a much smaller scale of about 2-20 nm. Optical properties of CQDs are best explained by

inorganic quantum dots made from CdSe, CdTe and ZnS. These quantum dots are nanoparticles with a crystal structure similar to the bulk phase but with sizes on the order of a few nanometers. As with all materials in the nanoscale, the exciton (electron-hole pair) generated upon the absorption of light recombines and emits a photon upon relaxation from the excited state. The observed photoluminescence is defined by the size of the nanoparticle and is referred to as the quantum confinement effect (QCE). In QCE, the exciton can no longer move freely and is confined by the dimensions of the nano-sized particle. This forces recombination to occur at nearly the same energy as the excitation energy; thereby creating a size-dependent photoluminescence (E_{PL} α $1/r^2$) that is only observed with particles on the nanoscale. In other words, the smaller the particle, the more energy required to form the exciton, which induces a blue-shift in absorption and emission compared to larger particles. There are methods to tune exciton confinement other than size-dependence which covalently modify the outer edges of the quantum dot with other semiconductor molecules that physically separate the exciton from the outside environment. These "core/shell" structures were made famous with CdSe/ZnS quantum dots due to long excited state lifetimes (> 10 ns), high photoluminescence quantum yields with tunable emission based on size and composition, and a strong resistance to photobleaching effects.[103-104]

Despite the comparison to previously studied nanomaterials like graphene oxide and inorganic quantum dots, there is still a large gap in understanding the structure-function relationship in CQDs due to the myriad of parameters that can be changed. Since CQDs are carbon-based macromolecules there is a notable effect on photoluminescence from changes in pH, functional group modification, surface passivation, and solvent. Elucidating the structure-function relationship is crucial for using CQDs in real-world scenarios such as bioimaging or photodynamic therapy. For example, tuning the optical properties of CQDs toward infrared or near infrared wavelengths would make CQDs a highly effective anti-cancer drug that boasts low or no toxicity to healthy tissues and organs. Although applications that utilize carbon-based nanomaterials are still being developed, they are still nonetheless important to study and understand such that we can use them to bring technology to regions of the world that do not currently receive these benefits due to high resource demand or low

resource supply. The next section of this chapter describes how CQDs could be used in various industries and what work needs to be done to make these effective cooperative materials or even replacements in these applications.

1.2   Applications of Carbon Quantum Dots

1.2.1   Optoelectronics and Displays

The market on which carbon quantum dots have the most impact may be the electronics sector which includes optoelectronics like light emitting diodes and photovoltaics. The major hurdle semiconducting molecules face in this industry include a fairly low charge carrier mobility and poor uniformity compared to inorganic semiconductors. In recent years, much research has been devoted to developing organic semiconductors that are comparable to their inorganic equivalents. The benefits of organic semiconductors comes from the fact that they provide much more mechanical flexibility and are much easier to process into films with varying thicknesses. This allows for devices with unique shapes or curvatures to be developed such as flexible displays or electrodes that can be set onto human or animal tissues.

Organic light emitting diodes (OLEDs) are becoming more commonly used in displays such as televisions and smartphone devices as there are several advantages over conventional LEDs displays. First, conventional LED technology works as a backlight which illuminates the whole display with white light. Using a backlight with downstream color filters to make a picture causes very dark colors and blacks to show as a deep grey, preventing a truly black pixel and causing unnecessary power consumption. OLEDs on the other hand, emit specific wavelength light with applied voltage, making them both the illumination source and color filter for each pixel. This allows for better picture quality and contrast as each pixel is formed from a "building-up" of different wavelengths of light as opposed to color filtering. Blooming does not occur with OLED displays as dark pixels can be formed by simply removing the applied voltage.

Beyond reducing electronic noise and power consumption, achieving realistic blacks, and building flexible displays for consumer electronics, OLED technology can be used to make better displays for medical applications. This can feed forward into

better spatial and color resolution of images and thus, more accurate diagnoses in patients. For example, current medical-grade LED displays suffer from artifacts produced by a backlit display which can be misinterpreted in diagnoses. Usually this occurs when the contrast between neighboring shades of gray are difficult to differentiate. This problem is exacerbated with increasing viewing distance, such as in multiple-monitor workstations or consultation displays used by medical professionals. There is also a problem concerning LED display lifetime: the screen is brightest at the beginning of its lifetime but can degrade upwards of 25% within the first year of use. This is due to the photobleaching of the material: an irreversible light-activated process that alters the chemical structure and the optical properties.

Unfortunately, OLED displays are still more expensive than LED displays even after removing the cost of the LED backlight. This high cost originates from a difficult manufacturing process coupled with the high price of pure materials. Briefly, an OLED is constructed on a layer-by-layer process much like an LED and a schematic is shown below in Figure 1.7.[105-107]
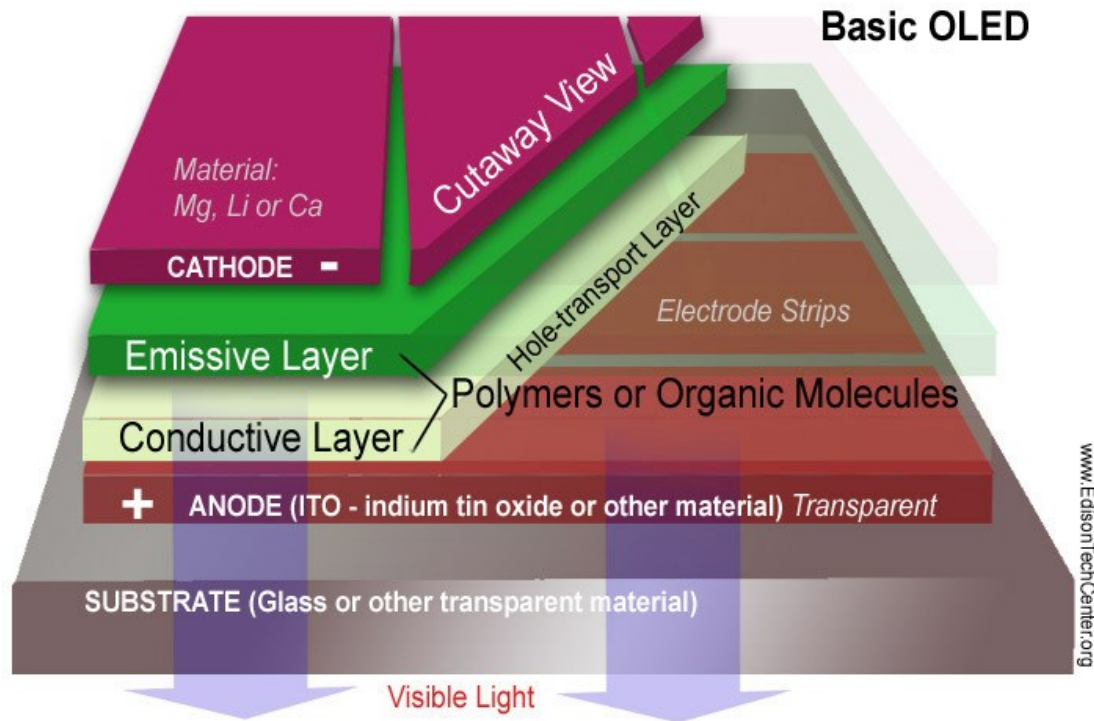
Figure 1.7: The diagram above is a simple modern OLED. There are a many new ways to construct the OLED using a variety of layer configurations. Displays will have additional layers such as an active matrix TFT (thin film transistor) which control pixel regions. Reproduced with permission from ref. 130.

First, a substrate is coated with an anode material which commonly is indium tin oxide (ITO) which is usually performed in a variety of methods such as sputtering or vacuum deposition. Both of these methods require very high purity ITO but have long been reliable manufacturing processes.[106] Carbon-based alternatives have been developed for ITO but they often do not deliver the same performance or are difficult to scale up. Next, a conductive polymer is deposited on the ITO anode which allows efficient electron transfer from the anode to the cathode. These polymers are usually a blend of polyaniline and poly(styrenesulfonate) (PANI:PSS) or poly(ethylenedioxythiophene) and poly(styrenesulfonate) (PEDOT:PSS).[106] After coating with conductive polymer, a layer of light-emitting molecules or polymers is added. These molecules are responsible for the light produced *via* radiative recombination of the electrons donated by the cathode with the holes transported from the anode. There are many light-emitting molecules that can serve as the emitting layer

19

as the electronic properties (i.e. wavelength of light emitted) are dependent on the chemical structure.

Polyfluorenes, shown below in Figure 1.8, contain chemical motifs commonly found in current OLED molecules such as fused aromatic ring structures, electrostatic π-stacking regions, and tunable edge chemistry.[108] The two key features - a π-conjugated backbone and functionalized bridging groups - together give rise to the high performance of polyfluorenes in OLEDs. In addition, both of these motifs can be chemically modified and engineered for a specific purpose such as enhancing solubility in liquid crystals, allowing efficient packing in larger crystals, or tuning the absorption/emission wavelengths.[109]
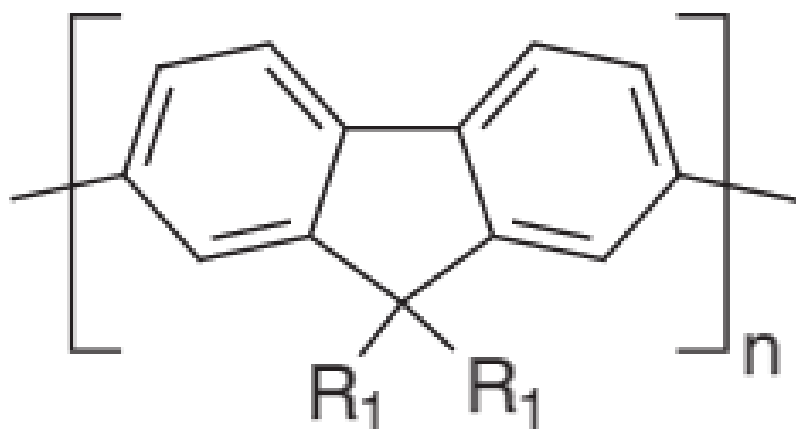
Figure 1.8: Chemical structure of a polyfluorene. Reproduced with permission from ref. 131.

With a macromolecular structure and a diameter on the order of a few to tens of nanometers, CQDs could be used as a non-polymeric alternative to OLED technology. In addition to tunable edge chemistry, CQDs have a characteristic quality that allows their sp^2-carbon nanodomains to be controllably grown into desired sizes by utilizing bottom-up synthesis. Manipulating the size of the nanodomain allows for tunable fluorescence according to the quantum confinement effect. Heteroatom dopants such as nitrogen and sulfur, which have been extensively researched in their effects on optical properties, can easily be inserted into either the edge or sp^2-core. Both of these sites, as shown in Chapters 2 and 3, affect optical properties in different ways. CQDs also carry the added benefit of high solubility in polar solvents, especially in water.

This allows for solution processing of OLED without the use of harsh organic solvents, reducing the health risks associated with manufacturing as well as the overhead costs of mitigating these same risks. Overall, knowledge in the structure-emission property relationship will allow for inexpensive, non-toxic materials that could be used in OLED displays. High-performance displays that are financially accessible and more environmentally-friendly would provide great support to the many applications discussed previously.

1.2.2 Solar Technology: Photovoltaics

Recently, many advances in solar cell and fuel cell research have elevated the technology to be competitive with the low-cost, high energy density of fossil fuels. However, the high cost of solar energy devices prevents large-scale production and the shift toward combustion-less electricity production. Solar cells, or photovoltaic (PV) cells, harness solar light which is then directly converted into usable electricity. Using solar energy as a means of generating electricity is an attractive option due to qualities such as high device stability with a small carbon footprint and high solar availability. The unique situation born out of the pursuit of alternative energy generation and combating climate change effects has initiated programs like the Sunshot Initiative put forward by the U.S Department of Energy (in collaboration with the National Renewable Energy Laboratory) which funds research toward low-cost photovoltaics.[110-118] At the start of this program in 2010, the cost per watt of electricity produced by utility-scale photovoltaics was $3.80. In five years, researchers have developed strategies and materials to drive down the cost per watt to $1.64, nearly 70% lower than in 2010 and well on track for the $1.00 per watt target of 2020.

In the simplest sense, photovoltaics operate upon the basis of energy level differences that generate electrons and holes much like a diode. When a photon interacts with a semiconducting material, if the photon has energy greater than or equal to the HOMO-LUMO gap, an electron in the ground state is promoted to the excited state. In the excited state, the electron can be moved in a variety of ways which build the foundation of modern electronics. In the schematic below, a PV is designed with two active layers: an N-type, or electron rich, layer or a P-type, or electron-deficient (or

21

hole-rich) layer. These two are joined together to make a P-N junction in which the electrons from the N-type layer migrate to the hole-rich P-type layer and vice versa. After this migration is complete, there is a buildup of positive charges on the N-type side of the junction and negative charges on the P-type side of the junction called the depletion layer. This new layer is resistant to charge carrier mobility and thus requires a forward bias (positive applied voltage to the N-type layer and negative applied voltage to the P-type layer) to generate current.

Current PV technology is divided into three groups: PV devices that only use organic molecules as the active photovoltaic material, those that only use inorganic materials, and hybrid organic-inorganic photovoltaic devices. Organic PV technology has been promising due to low-cost and more environmentally friendly materials but suffers from low power conversion efficiencies (PCE) of about 1-6%.[119] All-inorganic solar cells have experienced a meteoric rise as the top of the line devices in the photovoltaics industry with high PCE of 15 to 25%.[120] Unfortunately, these kinds of cells utilize expensive catalysts which neutralizes their commercial application. Hybrid organic-inorganic devices such as the organolead perovskite ($CH_3NH_3PbX_3$ where X = halogen) have boasted incredible PCE of over 20% using inexpensive materials.[121] However, using lead-based materials poses a potential environmental issue in which regulations may increase device cost and would cripple their utility-scale commercialization.

As before with optical electronics like LEDs, photovoltaics made using CQDs would be more beneficial compared to current materials. As the sp^2-nanodomain size can be tuned through synthetic means, the wavelengths of light absorbed are also tuned. This allows for large-scale synthesis of CQDs that could potentially span the entire range of the solar spectrum (250 – 2500 nm). Previous reports have found a use for CQDs in photovoltaics but only in the UV-blue region with marginal PCE compared to the organolead perovskites.[122]

1.2.3 Fuel Cell Catalysts

Fuel cells, on the other hand, aim to convert abundant resources like water or carbon dioxide into hydrogen or small hydrocarbons, respectively. These devices have many advantages over current combustion engine technology. First, the electricity produced is a less wasteful process than combustion engines that convert chemical to thermal to mechanical to electrical energy. In fuel cells, chemical energy is directly converted to electrical energy which can immediately be used. Applications where fuel cells can thrive lie are in portable and stationary systems such as personal or household power generators and transportation applications like light vehicles. Water and carbon dioxide can be effectively converted to fuel but have vastly different pathways each with their own challenges and advantages.

Fuel cells that convert water into hydrogen gas are heavily sought after due to the massive abundance of water on Earth coupled with the high gravimetric energy density of hydrogen (142 MJ kg^{-1}).[123] The inherent problems with hydrogen fuel cells are two-fold. First, though hydrogen contains a high gravimetric energy density with the only combustion product being water vapor. Considering the cost of compressing hydrogen gas into specially made containers that can be kept cool, the price of harvesting hydrogen as a fuel source is astronomical compared to current fossil fuel storage and extraction methods. In the meantime, research has shifted toward devices that do not produce fuel to be stored, but rather produce only enough for immediate use over longer periods of time. Aqueous solution electrochemical fuel cells have recently emerged as a strong force in alternative energy research due to high catalytic performance over many cycles. These kinds of fuel cells convert water into oxygen and hydrogen gas directly. Generally, there are a few chemical reactions in which this occurs as shown in Figure 1.10.[124]

Electrolyte	ORR reactions	Thermodynamic electrode potential at standard conditions, V
Acidic aqueous solution	$O_2 + 4H^+ + 4e^- \rightarrow H_2O$	1.229
	$O_2 + 2H^+ + 2e^- \rightarrow H_2O_2$	0.70
	$H_2O_2 + 2H^+ + 2e^- \rightarrow 2H_2O$	1.76
Alkaline aqueous solution	$O_2 + H_2O + 4e^- \rightarrow 4OH^-$	0.401
	$O_2 + H_2O + 2e^- \rightarrow HO_2^- + OH^-$	−0.065
	$HO_2^- + H_2O + 2e^- \rightarrow 3OH^-$	0.867
Non-aqueous aprotic solvents	$O_2 + e^- \rightarrow O_2^-$	a
	$O_2^- + e^- \rightarrow O_2^{2-}$	b

a, b: The thermodynamic potentials for the 1-electron reduction reaction to form a superoxide, and its further reduction to O_2^{2-}, are not listed in Table 2.1 because their values are strongly dependent on the solvent used.

Figure 1.9: Oxygen Reduction Reactions in various media. Adapted with permission from ref. 149.

The above reactions comprise the two- and four-electron Oxygen Reduction Reaction, or ORR, listed in acid, alkaline, and non-aqueous media, respectively. The current status of this technology is promising in that many researchers have made water splitting fuel cells that perform well and are long-lasting. However the catalysts that recombine hydrogen and oxygen gas into water are often made of platinum and make investing into these technologies too expensive for the average consumer. Pt catalysts for the ORR reaction require almost ten times that amount. In addition, these high-performance Pt catalysts can participate in side reactions during ORR that yield intermediates and byproducts that poison the catalyst and lead to premature fouling.[125] In an effort to overcome these problems, researchers have shifted their focus to developing inexpensive, non-noble metal (or even non-metal) catalysts that are resistant to poisoning effects.

1.2.4   Elemental Scarcity: Impact on Society

Fossil fuels, which include resources like coal, petroleum, and natural gas, have long been the primary source for electricity production due to attractive qualities such as: high energy density, stability over time, transportability, and the ease of conversion to other fuels and products. These qualities allow for inexpensive transport and storage in

domestic facilities as well as to global regions with little natural fossil fuel resources. As of 2015, the United States produced nearly 66% of all electricity that year from coal and natural gas sources and 30% of all CO_2 emission.[126]

As previously discussed, the state-of-the-art technology for photovoltaics and fuel cells requires precious rare metals such as platinum or indium for peak performance. If these technologies were more accessible to everyone by lowering costs, then the impact of the technology itself would be better experienced by all. For example, if photovoltaics were used as the primary source of electricity production then smog-ridden cities such as Beijing, Mumbai, Houston, and Los Angeles would begin to experience clearer air.[127] In some of these regions, air pollution levels are already above acceptable minimums for air quality guidelines set by the World Health Organization. By 2050, it has been predicted that air pollution and pollution-related complications will be a leading cause of death alongside heart disease and cancer.[128]

The scarcity of certain metals also brings about the topic of climate change as biomes that contain rich mineral deposits such are often deforested or mountaintops removed. Briefly, as more carbon-, nitrogen- and sulfur-containing gases and particulates are expelled from the ground to the atmosphere, they trap a small portion of the total sunlight that reaches earth. As a consequence of basic photophysics, molecules that absorb light are excited with this extra energy and must release it in order to relax back to the lowest energy state. More often than not, this release is emitted as heat and over time, this builds up and warms the local environment. From here, there are many fates in which heat can be transferred but if we consider the earth and its atmosphere as a nearly closed system with sunlight irradiating the earth at all times, there is ultimately a faster building up of heat than it can be quenched, giving rise to the greenhouse effect. If the greenhouse effect remains unchecked, weather-related problems can arise such as polar ice caps melting, sea levels rising, and more intense weather events such as flooding, drought, hurricanes and blizzards.

1.2.4.1 Non-noble and metal-free catalysts

Alternative fuel cell catalysts to noble metals fall into two divisions: those that simply replace the metals with other non-precious metals and those that are completely

metal-free. Catalysts that aim to replace expensive metals like Pt or Pd with much cheaper metals like Fe are referred as "non-noble" catalysts. In biological settings, the most recognizable catalyst of this kind is the heme group found in hemoglobin. The structure shown below in Figure 1.11 consists of a sp^2-conjugated framework of pyrroles linked to each other.
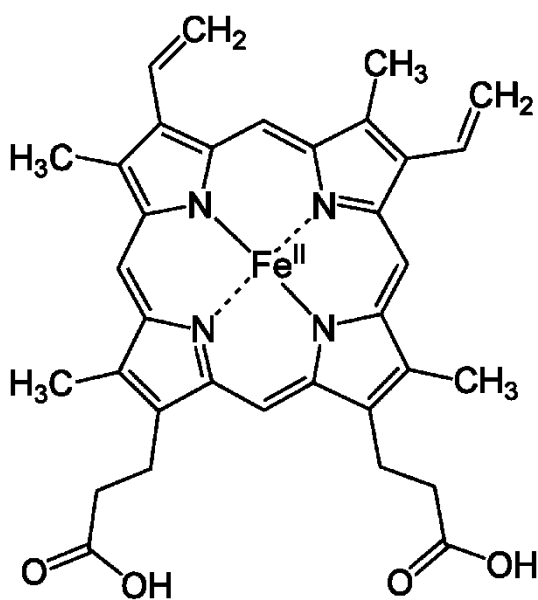
Figure 1.10: Chemical structure of heme, a tetrapyrrolic macrocycle which provides four binding sites to Fe^{2+}.

In hemoglobin, the heme group (four in total in hemoglobin) acts as a binding site designed to reversibly bind diatomic oxygen end-on toward the iron (II) atom. Interestingly, the heme can be poisoned much like platinum if cyanide ions (CN^-) or carbon monoxide molecules insert themselves in place of molecular oxygen. The binding with CN^- and CO is competitive with oxygen due to the stronger binding affinity of these molecules to the iron (II) ion. CN^- or CO at low concentrations can induce symptoms such as headaches and nausea. Higher concentrations may lead to unconsciousness and ultimately, permanent organ damage or death.[129]

Due to the large presence heme and hemoglobin have in our natural world, it is unsurprising that many non-noble catalysts for reducing oxygen *via* the ORR incorporate some degree of heme-like structure. In a broad sense, some of the best non-noble metal catalysts are made with a carbon- and nitrogen-containing precursor,

typically a nitrogenous polymer like poly(acrylonitrile), and an iron-[130] or zinc-containing precursor that may either be in an ionic salt like ferrous chloride tetrahydrate or in a chelated environment like tris-1,10-phenanthroline iron (II) perchlorate.[131] These precursors are then subjected to a pyrolytic method in which metal-, carbon-, and nitrogen-containing structures are formed. The unique performance of these catalysts arises from the abundance of active sites that molecular oxygen can access.

The idea of moving further away from noble metal catalysts has been realized in the metal-free catalysts. One notable example in the literature is the nitrogen-doped carbon nanotube (NCNT). NCNTs, like many of the other previously mentioned catalysts, have nitrogen-containing active sites that are anchored by a carbonaceous backbone. Much work has been done on the NCNT to elucidate the preferred active site, for which there are many candidates: amine N, pyridinic N, pyrrolic N, quaternary N, and holes made from the intersection of these such as the triple pyridinic N site.

CQDs could be used as an environmentally friendly, metal-free catalyst or co-catalyst in fuel cell applications as they can be synthesized using waste products or from simple organic molecules without expensive reagents or complex methods. This addresses the difficult problem of elemental scarcity but does not consider that a CQD catalyst should work as well as or better than the current top-of-the-line catalysts that heavily rely on platinum. One advantage CQDs have over other non-metal catalysts is the ease in which heteroatoms can be incorporated into its chemical structure with moderate control. Chapter 4 discusses the role of nitrogen dopants in CQDs and provides insight toward future work in CQD catalysis by taking advantage of facile synthesis and inhomogeneity.

1.2.5 Bioimaging and Photodynamic Therapy

Another promising use of carbon-based nanomaterials is in medicinal applications such as bioimaging[18, 95, 132-133] and photodynamic therapy.[66, 134-137] Bioimaging and photodynamic therapy are, in their simplest explanations, very similar photophysical concepts. Briefly, bioimaging is the use of light as a probe to determine features ranging from the sub-cellular to large working systems like organs. Typically there are three processes that a bioimaging agent must endure before bioimaging can be realized. The

first is the absorption event in which specific wavelengths of light are absorbed by the material. The second is the non-radiative relaxation processes that can occur within the material to lose excess energy such as vibrational relaxation, solvent reorganization, or internal conversion. The third process is the emission event. Referring back to the Jablonski diagram in Section 1.1.1, the energy of the photon emitted from the relaxation of the excited state back to the ground state is less than the initial energy absorbed due to the non-radiative relaxations. The key to bioimaging lies in optimizing all three of these steps to produce light of a narrow range of wavelengths such that they can be easily detected. The most important obstacle to overcome in bioimaging is that the imaging target (i.e. tissue, cells, etc.) absorbs almost all visible wavelengths of light. In addition, higher energy electromagnetic radiation such as near and far ultraviolet light can harm the imaging target in several ways. Considering all of these obstacles together, that leaves researchers with a narrow range of wavelengths that can be used to study biological systems. This range of wavelengths lies between 650 – 900 nm and is called the optical therapeutic window. The depth of tissue penetration varies on the wavelength used. Blue light (450 nm) will penetrate to a depth of about 0.1 mm. Yellow light (600 nm) penetrates a depth of about 2.0 mm and red light (680 nm) about 3.0 mm.[138]

Photodynamic therapy is the use of light that excites a photosensitizer (PS) in order to initiate a chemical reaction within the cellular matrix. Primarily, photodynamic therapy has been used as a treatment modality for skin cancers and melanoma due to the low penetration depth of early drugs. This low penetration depth correlates to the extensive scattering of blue light coupled with high absorptivity of the cell membrane. As with bioimaging, light that is efficiently absorbed by the PS must fall into the optical therapeutic window since it is optically masked by the cell membrane. The key difference between bioimaging and photodynamic therapy is that upon excitation the excess energy of the PS ideally is used to generate reactive oxygen species (ROS) through charge transfer or energy transfer. Figure 1.12 below details the products obtained through the charge transfer mechanism, also known as Type I products, and the energy transfer mechanism, or Type II products.[139]
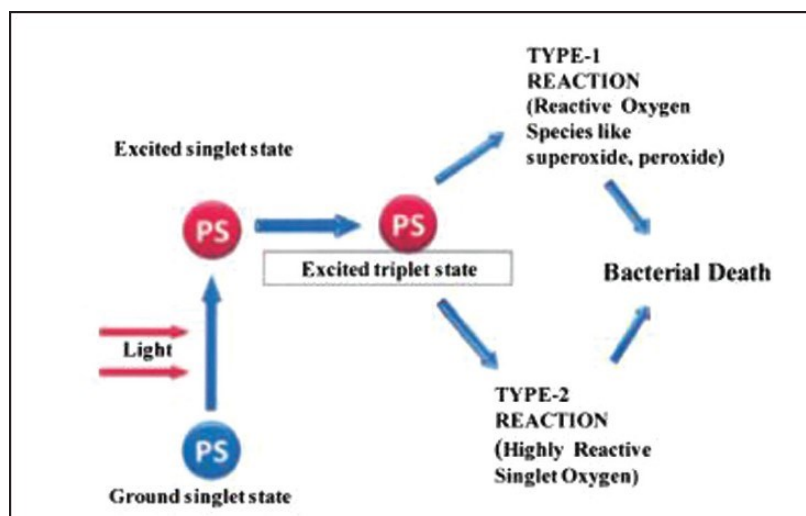
Figure 1.11: Mechanism of action in photodynamic therapy. Reproduced with permission from ref. 159.

As seen above, there are many ROS that can be produced in the cell but with varying behaviors. The lifetime and oxidizing power of each ROS varies greatly. Unfortunately, these two are often mutually exclusive. For example, strong ROS like $OH^\bullet$ are non-selective and thus have short lifetimes. Weaker, more selective ROS like H_2O_2, $O_2^{\bullet-}$ and $^1O_2$ have longer lifetimes. In other words, short lifetime species are the stronger oxidants and the longer lifetime species are generally weaker. This notion is well-tolerated in the scientific and medical communities as it allows much more control in therapeutic sessions. In other words, photosensitizers that generate singlet oxygen are preferred over those that generate the strongly oxidizing radical species. This prevents so-called "over-treatment" which may damage healthy cells that are not the target of photodynamic therapy.

In photodynamic therapy, inorganic quantum dots have been utilized for their broad absorption characteristics and narrow emission wavelengths by acting as the energy transfer system to a photosensitizer that generates singlet oxygen. Samia et al.[140] used 488 nm blue light to indirectly excite a silicon-based photosensitizer that produces $^1O_2$ ($^1O_2$ QY = 43% using CdSe quantum dots with PLQY = 65%) upon 580 nm excitation. This experiment was done to explore how FRET-based photosensitizer systems such as the [silicon PS]-[CdSe QD] pair would function *in vivo* and what chemical features are required for efficient $^1O_2$ generation. For practical use, this system would need to be

modified such that optical absorption and emission wavelengths of the CdSe QD, as well as the absorption of the photosensitizer, would be toward the infrared, where light scattering and absorption is low in tissues. In general, without complex coatings that cover the inorganic quantum dot, the risk of damaging healthy tissues is too high for clinical trials. This is not only for the possible leaching of toxic ions but also for the lack of understanding in how the quantum dots are cleared from a human or animal system. It was found by Liu *et al.*[141] in mouse studies that these kinds of quantum dots could remain in the liver, spleen, and bone marrow for months after the initial administration. Considering that photodynamic therapy may not eradicate a tumor over the course of one session, this accumulation may cause additional complications after photodynamic treatment.

Carbon quantum dots have been strongly considered as viable alternatives to the inorganic quantum dots in bioimaging and medical treatment.[50, 52, 57, 101, 137, 142-145] Advantages that CQDs have compared to other QD like CdTe, PbS, or ZnS stem from the ease of manipulation. Additionally, CQDs have been shown to exhibit good photostability compared to organic dyes.[50, 54, 146-147] Most important however, is the excellent compatibility that CQDs exhibit toward living systems. Bottom-up synthesized CQDs that are easily synthesized with naturally derived precursors such as waste biomass or simple molecules like citric acid or glucose provide an inexpensive, scalable route to manufacturing.

All of the previous advantages make CQDs attractive as potential replacements to current bioimaging and photodynamic therapy applications. Some properties of semiconducting QDs like CdTe or ZnS can be applied to CQDs such as the quantum confinement effect on optical properties. Unfortunately, the large distribution of functional group defects, which can be edge-terminating or within fused aromatic regions, often cloud the clarity of a structure-function relationship due to the inhomogeneity of the carbon quantum dot. Chapters 2 and 3 in this dissertation will address some of the work made toward elucidating a better structure-function relationship for optical properties toward bioimaging applications. Chapter 4 demonstrates the role that nitrogen heteroatoms in CQDs contribute toward catalyzing the oxygen reduction reaction which is critical for use in fuel cells. Chapter 5 is largely

devoted to the structure-function relationship between CQD and photodynamic therapy.

1.3   Chapter 1 References

1.   Roduner, E., Size matters: why nanomaterials are different. *Chemical Society Reviews* **2006,** *35* (7), 583-592.

2.   Khodashenas, B.; Ghorbani, H. R., Synthesis of silver nanoparticles with different shapes. *Arabian Journal of Chemistry* **2015**.

3.   Zrazhevskiy, P.; Sena, M.; Gao, X., Designing multifunctional quantum dots for bioimaging, detection, and drug delivery. *Chemical Society Reviews* **2010,** *39* (11), 4326-4354.

4.   Koole, R.; Groeneveld, E.; Vanmaekelbergh, D.; Meijerink, A.; de Mello Donegá, C., Size Effects on Semiconductor Nanoparticles. In *Nanoparticles: Workhorses of Nanoscience*, de Mello Donegá, C., Ed. Springer Berlin Heidelberg: Berlin, Heidelberg, 2014; pp 13-51.

5.   Hill, G. B.; Lyon, L. B., A NEW CHEMICAL STRUCTURE FOR COAL. *Industrial & Engineering Chemistry* **1962,** *54* (6), 36-41.

6.   Chen, Y.; Mastalerz, M.; Schimmelmann, A., Characterization of chemical functional groups in macerals across different coal ranks via micro-FTIR spectroscopy. *International Journal of Coal Geology* **2012,** *104*, 22-33.

7.   Schwager, I.; Yen, T. F., Determination of nitrogen and oxygen functional groups in coal-derived asphaltenes. *Analytical Chemistry* **1979,** *51* (4), 569-571.

8.   Hu, C.; Yu, C.; Li, M. Y.; Wang, X. N.; Yang, J. Y.; Zhao, Z. B.; Eychmuller, A.; Sun, Y. P.; Qiu, J. S., Chemically Tailoring Coal to Fluorescent Carbon Dots with Tuned Size and Their Capacity for Cu(II) Detection. *Small* **2014,** *10* (23), 4926-4933.

9.   Jawhari, T.; Roid, A.; Casado, J., Raman spectroscopic characterization of some commercially available carbon black materials. *Carbon* **1995,** *33* (11), 1561-1565.

10.   Schaeffer, W. D.; Smith, W. R., Effect of Heat Treatment on Reinforcing Properties of Carbon Black. *Industrial & Engineering Chemistry* **1955,** *47* (6), 1286-1290.

11.   Salar Bagherpour, D. H. E.-D. S. E., Fibre Reinforced Polyester Composites. *InTech* **2012**.

12.   Yoo, E.; Kim, J.; Hosono, E.; Zhou, H.-s.; Kudo, T.; Honma, I., Large Reversible Li Storage of Graphene Nanosheet Families for Use in Rechargeable Lithium Ion Batteries. *Nano Letters* **2008,** *8* (8), 2277-2282.

13.   Zhu, Y.; Murali, S.; Cai, W.; Li, X.; Suk, J. W.; Potts, J. R.; Ruoff, R. S., Graphene and Graphene Oxide: Synthesis, Properties, and Applications. *Advanced Materials* **2010,** *22* (35), 3906-3924.

14.   Coropceanu, V.; Cornil, J.; da Silva Filho, D. A.; Olivier, Y.; Silbey, R.; Brédas, J.-L., Charge Transport in Organic Semiconductors. *Chemical Reviews* **2007,** *107* (4), 926-952.

15.   Arora, N. D.; Hauser, J. R.; Roulston, D. J., Electron and hole mobilities in silicon as a function of concentration and temperature. *IEEE Transactions on Electron Devices* **1982,** *29* (2), 292-295.

16.   Geim, A. K.; Novoselov, K. S., The rise of graphene. *Nature Materials* **2007,** *6* (3), 183-191.

17.   Bolotin, K. I.; Sikes, K. J.; Jiang, Z.; Klima, M.; Fudenberg, G.; Hone, J.; Kim, P.; Stormer, H. L., Ultrahigh electron mobility in suspended graphene. *Solid State Communications* **2008,** *146* (9), 351-355.

18.   Kim, H.; Namgung, R.; Singha, K.; Oh, I.-K.; Kim, W. J., Graphene Oxide–Polyethylenimine Nanoconstruct as a Gene Delivery Vector and Bioimaging Tool. *Bioconjugate Chemistry* **2011,** *22* (12), 2558-2567.

19.   Wang, Y.; Li, Z.; Wang, J.; Li, J.; Lin, Y., Graphene and graphene oxide: biofunctionalization and applications in biotechnology. *Trends in Biotechnology* **2011,** *29* (5), 205-212.

20.   Chung, C.; Kim, Y.-K.; Shin, D.; Ryoo, S.-R.; Hong, B. H.; Min, D.-H., Biomedical Applications of Graphene and Graphene Oxide. *Accounts of Chemical Research* **2013,** *46* (10), 2211-2224.

21.   Dreyer, D. R.; Park, S.; Bielawski, C. W.; Ruoff, R. S., The chemistry of graphene oxide. *Chemical Society Reviews* **2010,** *39* (1), 228-240.

22.   Stankovich, S.; Dikin, D. A.; Piner, R. D.; Kohlhaas, K. A.; Kleinhammes, A.; Jia, Y.; Wu, Y.; Nguyen, S. T.; Ruoff, R. S., Synthesis of graphene-based nanosheets via chemical reduction of exfoliated graphite oxide. *Carbon* **2007,** *45* (7), 1558-1565.

23.   Gao, X.; Jang, J.; Nagase, S., Hydrazine and Thermal Reduction of Graphene Oxide: Reaction Mechanisms, Product Structures, and Reaction Design. *The Journal of Physical Chemistry C* **2010,** *114* (2), 832-842.

24.   Toh, S. Y.; Loh, K. S.; Kamarudin, S. K.; Daud, W. R. W., Graphene production via electrochemical reduction of graphene oxide: Synthesis and characterisation. *Chemical Engineering Journal* **2014,** *251*, 422-434.

25.   Iijima, S., Helical microtubules of graphitic carbon. *Nature* **1991,** *354* (6348), 56-58.

26.   Aqel, A.; El-Nour, K. M. M. A.; Ammar, R. A. A.; Al-Warthan, A., Carbon nanotubes, science and technology part (I) structure, synthesis and characterisation. *Arabian Journal of Chemistry* **2012,** *5* (1), 1-23.

27.   Eatemadi, A.; Daraee, H.; Karimkhanloo, H.; Kouhi, M.; Zarghami, N.; Akbarzadeh, A.; Abasi, M.; Hanifehpour, Y.; Joo, S. W., Carbon nanotubes: properties, synthesis, purification, and medical applications. *Nanoscale Research Letters* **2014,** *9* (1), 393.

28.   Rao, C. N. R.; Voggu, R.; Govindaraj, A., Selective generation of single-walled carbon nanotubes with metallic, semiconducting and other unique electronic properties. *Nanoscale* **2009,** *1* (1), 96-105.

29.   Das, R.; Ali, M. E.; Hamid, S. B. A.; Ramakrishna, S.; Chowdhury, Z. Z., Carbon nanotube membranes for water purification: A bright future in water desalination. *Desalination* **2014,** *336*, 97-109.

30.   Lee, B.; Baek, Y.; Lee, M.; Jeong, D. H.; Lee, H. H.; Yoon, J.; Kim, Y. H., A carbon nanotube wall membrane for water treatment. **2015,** *6*, 7109.

31.   Simon-Deckers, A.; Gouget, B.; Mayne-L'Hermite, M.; Herlin-Boime, N.; Reynaud, C.; Carrière, M., In vitro investigation of oxide nanoparticle and carbon nanotube toxicity and intracellular accumulation in A549 human pneumocytes. *Toxicology* **2008,** *253* (1), 137-146.

32.   Sayes, C. M.; Liang, F.; Hudson, J. L.; Mendez, J.; Guo, W.; Beach, J. M.; Moore, V. C.; Doyle, C. D.; West, J. L.; Billups, W. E.; Ausman, K. D.; Colvin, V. L., Functionalization density dependence of single-walled carbon nanotubes cytotoxicity in vitro. *Toxicology Letters* **2006,** *161* (2), 135-142.

33.   Bottini, M.; Bruckner, S.; Nika, K.; Bottini, N.; Bellucci, S.; Magrini, A.; Bergamaschi, A.; Mustelin, T., Multi-walled carbon nanotubes induce T lymphocyte apoptosis. *Toxicology Letters* **2006,** *160* (2), 121-126.

34.   Ji, S.-r.; Liu, C.; Zhang, B.; Yang, F.; Xu, J.; Long, J.; Jin, C.; Fu, D.-l.; Ni, Q.-x.; Yu, X.-j., Carbon nanotubes in cancer diagnosis and therapy. *Biochimica et Biophysica Acta (BBA) - Reviews on Cancer* **2010,** *1806* (1), 29-35.

35.   Arash, B.; Park, H. S.; Rabczuk, T., Mechanical properties of carbon nanotube reinforced polymer nanocomposites: A coarse-grained model. *Composites Part B: Engineering* **2015,** *80*, 92-100.

36.   Kolasinski, K. W., Catalytic growth of nanowires: Vapor–liquid–solid, vapor–solid–solid, solution–liquid–solid and solid–liquid–solid growth. *Current Opinion in Solid State and Materials Science* **2006,** *10* (3), 182-191.

37.   Hofmann, S.; Csányi, G.; Ferrari, A. C.; Payne, M. C.; Robertson, J., Surface Diffusion: The Low Activation Energy Path for Nanotube Growth. *Physical Review Letters* **2005,** *95* (3), 036101.

38.   Puretzky, A. A.; Geohegan, D. B.; Jesse, S.; Ivanov, I. N.; Eres, G., In situ measurements and modeling of carbon nanotube array growth kinetics during chemical vapor deposition. *Applied Physics A* **2005,** *81* (2), 223-240.

39.   Nessim, G. D., Properties, synthesis, and growth mechanisms of carbon nanotubes with special focus on thermal chemical vapor deposition. *Nanoscale* **2010,** *2* (8), 1306-1323.

40.   Shi, Z.; Lian, Y.; Liao, F. H.; Zhou, X.; Gu, Z.; Zhang, Y.; Iijima, S.; Li, H.; Yue, K. T.; Zhang, S.-L., Large scale synthesis of single-wall carbon nanotubes by arc-discharge method. *Journal of Physics and Chemistry of Solids* **2000,** *61* (7), 1031-1036.

41.   Journet, C.; Maser, W. K.; Bernier, P.; Loiseau, A.; de la Chapelle, M. L.; Lefrant, S.; Deniard, P.; Lee, R.; Fischer, J. E., Large-scale production of single-walled carbon nanotubes by the electric-arc technique. *Nature* **1997,** *388* (6644), 756-758.

42.   Zhang, Y.; Gu, H.; Iijima, S., Single-wall carbon nanotubes synthesized by laser ablation in a nitrogen atmosphere. *Applied Physics Letters* **1998,** *73* (26), 3827-3829.

43.   Scott, C. D.; Arepalli, S.; Nikolaev, P.; Smalley, R. E., Growth mechanisms for single-wall carbon nanotubes in a laser-ablation process. *Applied Physics A* **2001,** *72* (5), 573-580.

44.   Choi, Y. C.; Bae, D. J.; Lee, Y. H.; Lee, B. S.; Han, I. T.; Choi, W. B.; Lee, N. S.; Kim, J. M., Low temperature synthesis of carbon nanotubes by microwave plasma-enhanced chemical vapor deposition. *Synthetic Metals* **2000,** *108* (2), 159-163.

45.   Liu, R.-M.; Ting, J.-M., Growth of carbon nanotubes using microwave plasma-enhanced chemical vapor deposition process. *Materials Chemistry and Physics* **2003,** *82* (3), 571-574.

46.   Li, Q.; Yan, H.; Zhang, J.; Liu, Z., Effect of hydrocarbons precursors on the formation of carbon nanotubes in chemical vapor deposition. *Carbon* **2004,** *42* (4), 829-835.

47.   Jung, K. H.; Boo, J.-H.; Hong, B., Synthesis of carbon nanotubes grown by hot filament plasma-enhanced chemical vapor deposition method. *Diamond and Related Materials* **2004,** *13* (2), 299-304.

48.   Hövel, H.; Bödecker, M.; Grimm, B.; Rettig, C., Growth mechanisms of carbon nanotubes using controlled production in ultrahigh vacuum. *Journal of Applied Physics* **2002,** *92* (2), 771-777.

49.   Xu, X.; Ray, R.; Gu, Y.; Ploehn, H. J.; Gearheart, L.; Raker, K.; Scrivens, W. A., Electrophoretic Analysis and Purification of Fluorescent Single-Walled Carbon Nanotube Fragments. *Journal of the American Chemical Society* **2004,** *126* (40), 12736-12737.

50.   Zhu, S. J.; Zhang, J. H.; Tang, S. J.; Qiao, C. Y.; Wang, L.; Wang, H. Y.; Liu, X.; Li, B.; Li, Y. F.; Yu, W. L.; Wang, X. F.; Sun, H. C.; Yang, B., Surface Chemistry Routes to Modulate the Photoluminescence of Graphene Quantum Dots: From Fluorescence Mechanism to Up-Conversion Bioimaging Applications. *Advanced Functional Materials* **2012,** *22* (22), 4732-4740.

51.   Algarra, M.; Campos, B. B.; Radotic, K.; Mutavdzic, D.; Bandosz, T.; Jimenez-Jimenez, J.; Rodriguez-Castellon, E.; da Silva, J., Luminescent carbon nanoparticles: effects of chemical functionalization, and evaluation of Ag+ sensing properties. *Journal of Materials Chemistry A* **2014,** *2* (22), 8342-8351.

52.   Tan, X.; Li, Y.; Li, X.; Zhou, S.; Fan, L.; Yang, S., Electrochemical synthesis of small-sized red fluorescent graphene quantum dots as a bioimaging platform. *Chemical Communications* **2015,** *51* (13), 2544-2546.

53.   Hola, K.; Zhang, Y.; Wang, Y.; Giannelis, E. P.; Zboril, R.; Rogach, A. L., Carbon dots-Emerging light emitters for bioimaging, cancer therapy and optoelectronics. *Nano Today* **2014,** *9* (5), 590-603.

54.   Zhu, S. J.; Song, Y. B.; Zhao, X. H.; Shao, J. R.; Zhang, J. H.; Yang, B., The photoluminescence mechanism in carbon dots (graphene quantum dots, carbon nanodots, and polymer dots): current state and future perspective. *Nano Research* **2015,** *8* (2), 355-381.

55.   Sun, Y.; Wang, S.; Li, C.; Luo, P.; Tao, L.; Wei, Y.; Shi, G., Large scale preparation of graphene quantum dots from graphite with tunable fluorescence properties. *Physical Chemistry Chemical Physics* **2013,** *15* (24), 9907-9913.

56.   Chandra, S.; Pathan, S. H.; Mitra, S.; Modha, B. H.; Goswami, A.; Pramanik, P., Tuning of photoluminescence on different surface functionalized carbon quantum dots. *Rsc Advances* **2012,** *2* (9), 3602-3606.

57.   Chen, Z.; Wang, X. C.; Li, H.; Li, C.; Lu, Q. H.; Yang, G.; Long, J. G.; Meng, L. J., Controllable and mass fabrication of highly luminescent N-doped carbon dots for bioimaging applications. *Rsc Advances* **2015,** *5* (29), 22343-22349.

58.   Diac, A.; Focsan, M.; Socaci, C.; Gabudean, A. M.; Farcau, C.; Maniu, D.; Vasile, E.; Terec, A.; Veca, L. M.; Astilean, S., Covalent conjugation of carbon dots with Rhodamine B and assessment of their photophysical properties. *Rsc Advances* **2015,** *5* (95), 77662-77669.

59.   Dong, Y.; Chen, C.; Zheng, X.; Gao, L.; Cui, Z.; Yang, H.; Guo, C.; Chi, Y.; Li, C. M., One-step and high yield simultaneous preparation of single- and multi-layer graphene quantum dots from CX-72 carbon black. *Journal of Materials Chemistry* **2012,** *22* (18), 8764-8766.

60.   Dong, Y.; Shao, J.; Chen, C.; Li, H.; Wang, R.; Chi, Y.; Lin, X.; Chen, G., Blue luminescent graphene quantum dots and graphene oxide prepared by tuning the carbonization degree of citric acid. *Carbon* **2012,** *50* (12), 4738-4743.

61.   Fu, M.; Ehrat, F.; Wang, Y.; Milowska, K. Z.; Reckmeier, C.; Rogach, A. L.; Stolarczyk, J. K.; Urban, A. S.; Feldmann, J., Carbon Dots: A Unique Fluorescent Cocktail of Polycyclic Aromatic Hydrocarbons. *Nano Letters* **2015,** *15* (9), 6030-6035.

62.   Hu, X.; An, X.; Li, L., Easy synthesis of highly fluorescent carbon dots from albumin and their photoluminescent mechanism and biological imaging applications. *Materials Science & Engineering C-Materials for Biological Applications* **2016,** *58*, 730-736.

63.   Hu, X.; Cheng, L.; Wang, N.; Sun, L.; Wang, W.; Liu, W., Surface passivated carbon nanodots prepared by microwave assisted pyrolysis: effect of carboxyl group in precursors on fluorescence properties. *Rsc Advances* **2014,** *4* (36), 18818-18826.

64.   Hu, Y. P.; Yang, J.; Tian, J. W.; Yu, J. S., How do nitrogen-doped carbon dots generate from molecular precursors? An investigation of the formation mechanism and a solution-based large-scale synthesis. *Journal of Materials Chemistry B* **2015,** *3* (27), 5608-5614.

65.   Jiang, Z.; Nolan, A.; Walton, J. G. A.; Lilienkampf, A.; Zhang, R.; Bradley, M., Photoluminescent Carbon Dots from 1,4-Addition Polymers. *Chemistry-a European Journal* **2014,** *20* (35), 10926-10931.

66.   Asada, R.; Liao, F.; Saitoh, Y.; Miwa, N., Photodynamic anti-cancer effects of fullerene [C60]–PEG complex on fibrosarcomas preferentially over normal fibroblasts in terms of fullerene uptake and cytotoxicity. *Molecular and Cellular Biochemistry* **2014,** *390* (1), 175-184.

67.   Liu, L.; Li, Y.; Zhan, L.; Liu, Y.; Huang, C., One-step synthesis of fluorescent hydroxyls-coated carbon dots with hydrothermal reaction and its application to optical sensing of metal ions. *Science China Chemistry* **2011,** *54* (8), 1342.

68.   Liu, Y.; Liao, M.; He, X. L.; Liu, X.; Kou, X. M.; Xiao, D., One-step Synthesis of Highly Luminescent Nitrogen-doped Carbon Dots for Selective and Sensitive Detection of Mercury(II) Ions and Cellular Imaging. *Analytical Sciences* **2015,** *31* (10), 971-977.

69.   Ma, Z.; Ming, H.; Huang, H.; Liu, Y.; Kang, Z., One-step ultrasonic synthesis of fluorescent N-doped carbon dots from glucose and their visible-light sensitive photocatalytic ability. *New Journal of Chemistry* **2012,** *36* (4), 861-864.

70.   Niu, W. J.; Li, Y.; Zhu, R. H.; Shan, D.; Fan, Y. R.; Zhang, X. J., Ethylenediamine-assisted hydrothermal synthesis of nitrogen-doped carbon quantum dots as fluorescent probes for sensitive biosensing and bioimaging. *Sensors and Actuators B-Chemical* **2015,** *218*, 229-236.

71.   Peng, J.; Gao, W.; Gupta, B. K.; Liu, Z.; Romero-Aburto, R.; Ge, L.; Song, L.; Alemany, L. B.; Zhan, X.; Gao, G.; Vithayathil, S. A.; Kaipparettu, B. A.; Marti, A. A.; Hayashi, T.; Zhu, J.-J.; Ajayan, P. M., Graphene Quantum Dots Derived from Carbon Fibers. *Nano Letters* **2012,** *12* (2), 844-849.

72.   Sarswat, P. K.; Free, M. L., Light emitting diodes based on carbon dots derived from food, beverage, and combustion wastes. *Physical Chemistry Chemical Physics* **2015,** *17* (41), 27642-27652.

73.   Shinde, D. B.; Pillai, V. K., Electrochemical Preparation of Luminescent Graphene Quantum Dots from Multiwalled Carbon Nanotubes. *Chemistry-a European Journal* **2012,** *18* (39), 12522-12528.

74.   Sun, Y. X.; He, Z. W.; Sun, X. B.; Zhao, Z. D., Synthesis of Water-soluble Fluorescent Carbon Dots from a One-step Hydrothermal Method with Potato. In *Eighth China National Conference on Functional Materials and Applications*, Zhao, G. M.; Chen, L.; Tang, Y.; Long, B.; Nie, Z.; He, L.; Chen, H., Eds. 2014; Vol. 873, pp 770-776.

75.   Xu, M. H.; Xu, S. S.; Yang, Z.; Shu, M. J.; He, G. L.; Huang, D.; Zhang, L. L.; Li, L.; Cui, D. X.; Zhang, Y. F., Hydrophilic and blue fluorescent N-doped carbon dots from tartaric acid and various alkylol amines under microwave irradiation. *Nanoscale* **2015,** *7* (38), 15915-15923.

76.   Zhang, R.; Liu, Y. B.; Sun, S. Q., Preparation of highly luminescent and biocompatible carbon dots using a new extraction method. *Journal of Nanoparticle Research* **2013,** *15* (10).

77.   Zhang, Y.; He, J. H., Facile synthesis of S, N co-doped carbon dots and investigation of their photoluminescence properties. *Physical Chemistry Chemical Physics* **2015,** *17* (31), 20154-20159.

78.   Zhao, L. X.; Di, F.; Wang, D. B.; Guo, L. H.; Yang, Y.; Wan, B.; Zhang, H., Chemiluminescence of carbon dots under strong alkaline solutions: a novel insight into carbon dot optical properties. *Nanoscale* **2013,** *5* (7), 2655-2658.

79.   Li, L. L.; Wu, G. H.; Yang, G. H.; Peng, J.; Zhao, J. W.; Zhu, J. J., Focusing on luminescent graphene quantum dots: current status and future perspectives. *Nanoscale* **2013,** *5* (10), 4015-4039.

80.   Wang, L.; Zhu, S. J.; Wang, H. Y.; Qu, S. N.; Zhang, Y. L.; Zhang, J. H.; Chen, Q. D.; Xu, H. L.; Han, W.; Yang, B.; Sun, H. B., Common Origin of Green Luminescence in Carbon Nanodots and Graphene Quantum Dots. *Acs Nano* **2014,** *8* (3), 2541-2547.

81.   Zhu, S. J.; Zhou, N.; Hao, Z. Y.; Maharjan, S.; Zhao, X. H.; Song, Y. B.; Sun, B.; Zhang, K.; Zhang, J. H.; Sun, H. C.; Lu, L. J.; Yang, B., Photoluminescent graphene quantum dots for in vitro and in vivo bioimaging using long wavelength emission. *Rsc Advances* **2015,** *5* (49), 39399-39403.

82.   Ge, J.; Li, Y.; Zhang, B. P.; Ma, N.; Wang, J.; Pu, C.; Xiang, Y. C., Electrochemical tuning of optical properties of graphitic quantum dots. *Journal of Luminescence* **2015,** *166*, 322-327.

83.   Funke, A.; Ziegler, F., Hydrothermal carbonization of biomass: A summary and discussion of chemical mechanisms for process engineering. *Biofuels Bioproducts & Biorefining-Biofpr* **2010,** *4* (2), 160-177.

84.   Huang, H.; Li, C. G.; Zhu, S. J.; Wang, H. L.; Chen, C. L.; Wang, Z. R.; Bai, T. Y.; Shi, Z.; Feng, S. H., Histidine-Derived Nontoxic Nitrogen-Doped Carbon Dots for Sensing and Bioinnaging Applications. *Langmuir* **2014,** *30* (45), 13542-13548.

85.   Liu, M. Y.; Zhang, X. Q.; Yang, B.; Li, Z.; Deng, F. J.; Yang, Y.; Zhang, X. Y.; Wei, Y., Fluorescent nanoparticles from starch: Facile preparation, tunable luminescence and bioimaging. *Carbohydrate Polymers* **2015,** *121*, 49-55.

86.   Pan, D. Y.; Zhang, J. C.; Li, Z.; Wu, M. H., Hydrothermal Route for Cutting Graphene Sheets into Blue-Luminescent Graphene Quantum Dots. *Advanced Materials* **2010,** *22* (6), 734-+.

87.   Essner, J. B.; Laber, C. H.; Ravula, S.; Polo-Parada, L.; Baker, G. A., Pee-dots: biocompatible fluorescent carbon dots derived from the upcycling of urine. *Green Chemistry* **2016,** *18* (1), 243-250.

88.   Hu, Y. P.; Yang, J.; Tian, J. W.; Jia, L.; Yu, J. S., Green and size-controllable synthesis of photoluminescent carbon nanoparticles from waste plastic bags. *Rsc Advances* **2014,** *4* (88), 47169-47176.

89.   Zhang, R.; Liu, Y. B.; Yu, L. B.; Li, Z.; Sun, S. Q., Preparation of high-quality biocompatible carbon dots by extraction, with new thoughts on the luminescence mechanisms. *Nanotechnology* **2013,** *24* (22).

90.   Wang, J.; Sahu, S.; Sonkar, S. K.; Tackett Ii, K. N.; Sun, K. W.; Liu, Y.; Maimaiti, H.; Anilkumar, P.; Sun, Y.-P., Versatility with carbon dots - from overcooked BBQ to brightly fluorescent agents and photocatalysts. *RSC Advances* **2013,** *3* (36), 15604-15607.

91.   Deng, L.; Wang, X. L.; Kuang, Y.; Wang, C.; Luo, L.; Wang, F.; Sun, X. M., Development of hydrophilicity gradient ultracentrifugation method for photoluminescence investigation of separated non-sedimental carbon dots. *Nano Research* **2015,** *8* (9), 2810-2821.

92.   Song, Y. B.; Zhu, S. J.; Zhang, S. T.; Fu, Y.; Wang, L.; Zhao, X. H.; Yang, B., Investigation from chemical structure to photoluminescent mechanism: a type of carbon dots from the pyrolysis of citric acid and an amine. *Journal of Materials Chemistry C* **2015,** *3* (23), 5976-5984.

93.   Zhai, X.; Zhang, P.; Liu, C.; Bai, T.; Li, W.; Dai, L.; Liu, W., Highly luminescent carbon nanodots by microwave-assisted pyrolysis. *Chemical Communications* **2012,** *48* (64), 7955-7957.

94.   Chen, M. Y.; Wang, W. Z.; Wu, X. P., One-pot green synthesis of water-soluble carbon nanodots with multicolor photoluminescence from polyethylene glycol. *Journal of Materials Chemistry B* **2014,** *2* (25), 3937-3945.

95.   Zhu, S. J.; Zhang, J. H.; Song, Y. B.; Zhang, G. Y.; Zhang, H.; Yang, B., Fluorescent Nanocomposite Based on PVA Polymer Dots. *Acta Chimica Sinica* **2012,** *70* (22), 2311-2315.

96.   Lei, Z.; Xu, S.; Wan, J.; Wu, P., Facile synthesis of N-rich carbon quantum dots by spontaneous polymerization and incision of solvents as efficient bioimaging probes and advanced electrocatalysts for oxygen reduction reaction. *Nanoscale* **2016,** *8* (4), 2219-2226.

97.   Zhu, S. J.; Shao, J. R.; Song, Y. B.; Zhao, X. H.; Du, J. L.; Wang, L.; Wang, H. Y.; Zhang, K.; Zhang, J. H.; Yang, B., Investigating the surface state of graphene quantum dots. *Nanoscale* **2015,** *7* (17), 7927-7933.

98.   Ding, H.; Xiong, H. M., Exploring the blue luminescence origin of nitrogen-doped carbon dots by controlling the water amount in synthesis. *Rsc Advances* **2015,** *5* (82), 66528-66533.

99.   Du, F. Y.; Li, J. A.; Hua, Y.; Zhang, M. M.; Zhou, Z.; Yuan, J.; Wang, J.; Peng, W. X.; Zhang, L.; Xia, S.; Wang, D. Q.; Yang, S. M.; Xu, W. R.; Gong, A. H.; Shao, Q. X., Multicolor Nitrogen-Doped Carbon Dots for Live Cell Imaging. *Journal of Biomedical Nanotechnology* **2015,** *11* (5), 780-788.

100.   Lu, W. J.; Gong, X. J.; Yang, Z. H.; Zhang, Y. X.; Hu, Q.; Shuang, S. M.; Dong, C.; Choi, M. M. F., High-quality water-soluble luminescent carbon dots for multicolor patterning, sensors, and bioimaging. *Rsc Advances* **2015,** *5* (22), 16972-16979.

101.   Zheng, B. Z.; Liu, T.; Paau, M. C.; Wang, M. N.; Liu, Y.; Liu, L.; Wu, C. F.; Du, J.; Xiao, D.; Choi, M. M. F., One pot selective synthesis of water and organic soluble carbon dots with green fluorescence emission. *Rsc Advances* **2015,** *5* (15), 11667-11675.

102.   Luo, P. H.; Qiu, Y.; Guan, X. F.; Jiang, L. Q., Regulation of photoluminescence properties of graphene quantum dots via hydrothermal treatment. *Physical Chemistry Chemical Physics* **2014,** *16* (35), 19011-19016.

103.   Ghosh Chaudhuri, R.; Paria, S., Core/Shell Nanoparticles: Classes, Properties, Synthesis Mechanisms, Characterization, and Applications. *Chemical Reviews* **2012,** *112* (4), 2373-2433.

104.   Reiss, P.; Protiere, M.; Li, L., Core/Shell Semiconductor Nanocrystals. *Small* **2009,** *5* (2), 154-168.

105.   Aparna, M.; Pankaj, K.; Kamalasanan, M. N.; Subhas, C., White organic LEDs and their recent advancements. *Semiconductor Science and Technology* **2006,** *21* (7), R35.

106.   Islam, A.; Rabbani, M.; Bappy, M. H.; Miah, M. A. R.; Sakib, N. In *A review on fabrication process of organic light emitting diodes*, 2013 International Conference on Informatics, Electronics and Vision (ICIEV), 17-18 May 2013; 2013; pp 1-5.

107.   Center, E.   T.   LED   Lights   -   How   It   Works   -   History. http://www.edisontechcenter.org/LED.html (accessed July 5, 2017).

108.   Scherf, U.; List, E. J. W., Semiconducting Polyfluorenes—Towards Reliable Structure–Property Relationships. *Advanced Materials* **2002,** *14* (7), 477-487.

109.   Liu, J.; Tu, G.; Zhou, Q.; Cheng, Y.; Geng, Y.; Wang, L.; Ma, D.; Jing, X.; Wang, F., Highly efficient green light emitting polyfluorene incorporated with 4-diphenylamino-1,8-naphthalimide as green dopant. *Journal of Materials Chemistry* **2006,** *16* (15), 1431-1438.

110.   Mehos, M., C. Turchi, J. Jorgensen, P. Denholm, C. Ho, and K. Armijo, On the Path to SunShot: Advancing Concentrating Solar Power Technology, Performance, and Dispatchability. Laboratory, N. R. E., Ed. Golden, CO, 2016.

111.   Denholm, P., K. Clark, and M. O'Connell, On the Path to SunShot: Emerging Issues and Challenges in Integrating High Levels of Solar into the Electrical Generation and Transmission System. Laboratory., N. R. E., Ed. Golden, CO, 2016.

112.   Palmintier, B., R. Broderick, B. Mather, M. Coddington, K. Baker, F. Ding, M. Reno, M. Lave, and A. Bharatkumar, On the Path to SunShot: Emerging Issues and Challenges in Integrating Solar with the Distribution System. Laboratory, N. R. E., Ed. 2016.

113.   Feldman, D., and M. Bolinger, On the Path to SunShot: Emerging Opportunities and Challenges in Financing Solar. Laboratory, N. R. E., Ed. Golden, CO, 2016.

114.   Chung, D., K. Horowitz, and P. Kurup., On the Path to SunShot: Emerging Opportunities and Challenges in U.S. Solar Manufacturing. Laboratory., N. R. E., Ed. Golden, CO, 2016.

115.   Wiser, R., T. Mai, D. Millstein, J. Macknick, A. Carpenter, S. Cohen, W. Cole, B. Frew, and G. A. Heath, On the Path to SunShot: The Environmental and Public Health Benefits of Achieving High Penetrations of Solar Energy in the United States. Laboratory, N. R. E., Ed. Golden, CO, 2016.

116.   Woodhouse, M., R. Jones-Albertus, D. Feldman, R. Fu, K. Horowitz, D. Chung, D. Jordan, and S. Kurtz, On the Path to SunShot: The Role of Advancements in Solar Photovoltaic Efficiency, Reliability, and Costs. Laboratory, N. R. E., Ed. 2016.

117.   Barbose, G., J. Miller, B. Sigrin, E. Reiter, K. Cory, J. McLaren, J. Seel, A. Mills, N. Darghouth, and A. Satchwell. , On the Path to SunShot: Utility Regulatory and Business Model Reforms for Addressing the Financial Impacts of Distributed Solar on Utilities. Laboratory., N. R. E., Ed. Golden, CO, 2016.

118.   Energy), D. U. S. D. o., SunShot Vision Study. Energy), D. U. S. D. o., Ed. Washington, DC, 2012.

119.   Yu, J.; Zheng, Y.; Huang, J., Towards High Performance Organic Photovoltaic Cells: A Review of Recent Development in Organic Photovoltaics. *Polymers* **2014,** *6* (9).

120.   Miles, R. W.; Zoppi, G.; Forbes, I., Inorganic photovoltaic cells. *Materials Today* **2007,** *10* (11), 20-27.

121.   Fan, Z.; Sun, K.; Wang, J., Perovskites for photovoltaics: a combined review of organic-inorganic halide perovskites and ferroelectric oxide perovskites. *Journal of Materials Chemistry A* **2015,** *3* (37), 18809-18828.

122.   Paulo, S.; Palomares, E.; Martinez-Ferrero, E., Graphene and Carbon Quantum Dot-Based Materials in Photovoltaic Devices: From Synthesis to Applications. *Nanomaterials* **2016,** *6* (9).

123.   Züttel, A.; Remhof, A.; Borgschulte, A.; Friedrichs, O., Hydrogen: the future energy carrier. *Philosophical Transactions of the Royal Society A: Mathematical, Physical and Engineering Sciences* **2010,** *368* (1923), 3329.

124.   Song, C.; Zhang, J., Electrocatalytic Oxygen Reduction Reaction. In *PEM Fuel Cell Electrocatalysts and Catalyst Layers: Fundamentals and Applications*, Zhang, J., Ed. Springer London: London, 2008; pp 89-134.

125.   Shinozaki, K.; Zack, J. W.; Richards, R. M.; Pivovar, B. S.; Kocha, S. S., Oxygen Reduction Reaction Measurements on Platinum Electrocatalysts Utilizing Rotating Disk Electrode Technique: I. Impact of Impurities, Measurement Protocols and Applied Corrections. *Journal of The Electrochemical Society* **2015,** *162* (10), F1144-F1158.

126.   Administration, U. S. E. I., ELECTRIC POWER MONTHLY: with data for January 2016. Energy, U. S. D. o., Ed. 2016.

127.   Cady-Pereira, K. E.; Payne, V. H.; Neu, J. L.; Bowman, K. W.; Miyazaki, K.; Marais, E. A.; Kulawik, S.; Tzompa-Sosa, Z. A.; Hegarty, J. D., Seasonal and Spatial Changes in Trace Gases over Megacities from AURA TES Observations. *Atmos. Chem. Phys. Discuss.* **2017,** *2017*, 1-31.

128.   von Schneidemesser, E.; Monks, P. S.; Allan, J. D.; Bruhwiler, L.; Forster, P.; Fowler, D.; Lauer, A.; Morgan, W. T.; Paasonen, P.; Righi, M.; Sindelarova, K.; Sutton, M. A., Chemistry and the Linkages between Air Quality and Climate Change. *Chemical Reviews* **2015,** *115* (10), 3856-3897.

129.   Hall, A. H.; Rumack, B. H., Clinical toxicology of cyanide. *Annals of emergency medicine* **1986,** *15* (9), 1067-1074.

130.   Maruyama, J.; Okamura, J.; Miyazaki, K.; Uchimoto, Y.; Abe, I., Hemoglobin Pyropolymer Used as a Precursor of a Noble-Metal-Free Fuel Cell Cathode Catalyst. *The Journal of Physical Chemistry C* **2008,** *112* (7), 2784-2790.

131.   Shui, J.; Chen, C.; Grabstanowicz, L.; Zhao, D.; Liu, D.-J., Highly efficient nonprecious metal catalyst prepared with metal–organic framework in a continuous carbon nanofibrous network. *Proceedings of the National Academy of Sciences* **2015,** *112* (34), 10629-10634.

132.   Bhunia, S. K.; Saha, A.; Maity, A. R.; Ray, S. C.; Jana, N. R., Carbon Nanoparticle-based Fluorescent Bioimaging Probes. *Scientific Reports* **2013,** *3*.

133.   Wang, K.; Zhang, X. Y.; Zhang, X. Q.; Yang, B.; Li, Z.; Zhang, Q. S.; Huang, Z. F.; Wei, Y., Fluorescent Glycopolymer Nanoparticles Based on Aggregation-Induced Emission Dyes: Preparation and Bioimaging Applications. *Macromolecular Chemistry and Physics* **2015,** *216* (6), 678-684.

134.   Choi, Y.; Kim, S.; Choi, M. H.; Ryoo, S. R.; Park, J.; Min, D. H.; Kim, B. S., Highly Biocompatible Carbon Nanodots for Simultaneous Bioimaging and Targeted Photodynamic Therapy In Vitro and In Vivo. *Advanced Functional Materials* **2014,** *24* (37), 5781-5789.

135.   Fowley, C.; Nomikou, N.; McHale, A. P.; McCaughan, B.; Callan, J. F., Extending the tissue penetration capability of conventional photosensitisers: a carbon quantum dot-protoporphyrin IX conjugate for use in two-photon excited photodynamic therapy. *Chemical Communications* **2013,** *49* (79), 8934-8936.

136.   Ge, J.; Jia, Q.; Liu, W.; Lan, M.; Zhou, B.; Guo, L.; Zhou, H.; Zhang, H.; Wang, Y.; Gu, Y.; Meng, X.; Wang, P., Carbon Dots with Intrinsic Theranostic Properties for Bioimaging, Red-Light-Triggered Photodynamic/Photothermal Simultaneous Therapy In Vitro and In Vivo. *Advanced Healthcare Materials* **2016,** *5* (6), 665-675.

137.   Ge, J.; Lan, M.; Zhou, B.; Liu, W.; Guo, L.; Wang, H.; Jia, Q.; Niu, G.; Huang, X.; Zhou, H.; Meng, X.; Wang, P.; Lee, C. S.; Zhang, W.; Han, X., A graphene quantum dot photodynamic therapy agent with high singlet oxygen generation. *Nat Commun* **2014,** *5*, 4596.

138.   Cheong, W. F.; Prahl, S. A.; Welch, A. J., A review of the optical properties of biological tissues. *IEEE Journal of Quantum Electronics* **1990,** *26* (12), 2166-2185.

139.   Singh, H.; Khurana, H.; Singh, H.; Singh, M., Photodynamic therapy: Truly a marriage between a drug and a light. *Muller Journal of Medical Sciences and Research* **2014,** *5* (1), 48-55.

140.   Samia, A. C. S.; Chen, X.; Burda, C., Semiconductor Quantum Dots for Photodynamic Therapy. *Journal of the American Chemical Society* **2003,** *125* (51), 15736-15737.

141.   Liu, J.; Erogbogbo, F.; Yong, K.-T.; Ye, L.; Liu, J.; Hu, R.; Chen, H.; Hu, Y.; Yang, Y.; Yang, J.; Roy, I.; Karker, N. A.; Swihart, M. T.; Prasad, P. N., Assessing Clinical Prospects of Silicon Quantum Dots: Studies in Mice and Monkeys. *ACS Nano* **2013,** *7* (8), 7303-7310.

142.   Sarkar, S.; Das, K.; Ghosh, M.; Das, P. K., Amino acid functionalized blue and phosphorous-doped green fluorescent carbon dots as bioimaging probe. *Rsc Advances* **2015,** *5* (81), 65913-65921.

143.   Song, Y. B.; Zhu, S. J.; Yang, B., Bioimaging based on fluorescent carbon dots. *Rsc Advances* **2014,** *4* (52), 27184-27200.

144.   Markovic, Z. M.; Ristic, B. Z.; Arsikin, K. M.; Klisic, D. G.; Harhaji-Trajkovic, L. M.; Todorovic-Markovic, B. M.; Kepic, D. P.; Kravic-Stevovic, T. K.; Jovanovic, S. P.; Milenkovic, M. M.; Milivojevic, D. D.; Bumbasirevic, V. Z.; Dramicanin, M. D.; Trajkovic, V. S., Graphene quantum dots as autophagy-inducing photodynamic agents. *Biomaterials* **2012,** *33* (29), 7084-7092.

145.   Wen, X. M.; Yu, P.; Toh, Y. R.; Ma, X. Q.; Tang, J., On the upconversion fluorescence in carbon nanodots and graphene quantum dots. *Chemical Communications* **2014,** *50* (36), 4703-4706.

146.   Sk, M. A.; Ananthanarayanan, A.; Huang, L.; Lim, K. H.; Chen, P., Revealing the tunable photoluminescence properties of graphene quantum dots. *Journal of Materials Chemistry C* **2014,** *2* (34), 6954-6960.

147.   Chen, X. X.; Jin, Q. Q.; Wu, L. Z.; Tung, C. H.; Tang, X. J., Synthesis and Unique Photoluminescence Properties of Nitrogen-Rich Quantum Dots and Their Applications. *Angewandte Chemie-International Edition* **2014,** *53* (46), 12542-12547.

Chapter 2: Top-Down vs Bottom-Up Synthesis: Does Synthetic Approach Yield Different Carbon Quantum Dots?

This chapter details the work done to differentiate the chemical structures and observable properties of both top-down and bottom-up synthesized carbon quantum dots (CQDs). Often these two approaches of synthesis are grouped together in literature despite vastly different formation mechanisms. The careful and thorough analysis of the chemical structure was carried out using a variety of techniques including FTIR and XPS. A titration as well as a reverse titration elucidated the presence of ether and ester functional groups which are challenging distinguish from other types of functional groups like hydroxyl and other carbonyl-containing moieties by spectroscopic methods. It was ultimately found that top-down synthesized graphene quantum dots were relatively more ordered sp^2-bonded graphitic domains with a distinct two-dimensional shape. The "discus-like" graphene quantum dots (GQDs) were found to contain a central sp^2-hybridized carbon network which is terminated with functional groups such as hydroxyl, carbonyl and carboxyl groups. Bottom-up grown carbon nanodots (CNDs) are relatively more disordered with a three-dimensional structure. CNDs contain significant amounts of sp^3-hybridized carbon intertwined with sp^2-carbon. Much of the sp^3-carbon housed functional groups such as hydroxyl, carbonyl, carboxyl, ethers and esters.

After determining the fine chemical structure, optical measurements such as UV-Vis absorption, fluorescence, and metal-activated quenching were conducted. In agreement with our hypothesis, the GQDs and CNDs exhibited markedly different optical absorption and emission. In collaboration with Dr. Gary Blanchard of Michigan State University, time correlated single-photon counting (TCSPC) was used to determine fluorescence lifetimes. The GQD and CND samples show remarkable differences that are detailed later in this chapter. Additionally, chemical and hydrothermal reduction of GQDs show substantially different results, establishing a direct relationship between the chemical structure and fluorescence.

2.1   Introduction and Motivation

Carbon quantum dots (CQDs) are fluorescent nanoparticles that have been shown to exhibit excellent performance in various roles such as photo-[1-4] and electrocatalysts,[5-7] light emitting diodes,[8-13] molecular sensors,[14-16] metal ion sensors,[17-20] and anti-cancer agents.[10, 21-22] These nanomaterials are generally inexpensive to produce and show comparable performance to current inorganic quantum dots like CdSe, but with the additional advantage of low cytotoxicity.[23-25] Key features of CQDs include a nanocrystalline sp^2-carbon domain of variable size which is passivated by sp^3-carbon or other surface functional groups. CQDs are synthesized in two approaches: the top-down cutting of bulk carbons into graphene quantum dots (GQDs) and the bottom-up growth of small organic molecules such as sugars and carboxylic acids into carbon nanodots (CNDs). Despite the similar size of the two types of CQDs, relative atomic percent of C to O, and the presence of sp^2-C nano-domains and the optical properties observed are quite different. Although there are fluctuations in detailed results, the overall trend in the literature is that GQDs generally exhibit red-shifted emission than CNDs. On the other hand, CNDs show considerably higher photoluminescent quantum yield (PLQY) than GQDs.

Previous works which relate optical properties of CQDs to their chemical structure have advanced the fundamental understanding of how CQDs fluoresce. As of now, two major emission pathways have been extensively studied. The intrinsic emission arises from the σ-π* or π-π* transitions inherent to the carbonaceous "core" of CQDs which are made up of aromatic nano-domains of varying size. Extrinsic emission, also known as the molecule-like state, originates from n-π* transitions on the defects of carbon dots such as surface functional groups or vacancies in the graphitic plane. As such, the surface modification of carbon dots would affect extrinsic emission rather than intrinsic emission. For example, it was reported that incorporation of heteroatoms such as nitrogen into CNDs or GQDs increased fluorescence QY and shift the emission. As GQDs carry a more defect-free sp^2 nano-domain, N-doping modifies extrinsic emission by creating surface N groups such as amine and pyridine which can shift peak emission to the red and increase PLQY by eliminating non-radiative functional groups such as -

45

COOH.[26-27] The bottom-up approach to synthesize CNDs with a nitrogen source such as ethylenediamine ($NH_2CH_2CH_2NH_2$) tends to shift peak emission to the blue while greatly enhancing fluorescent quantum yield.

Due to increased control of the extrinsic emission, the effect of functional groups present at the edge of graphene quantum dots on photoluminescence has been extensively studied with post-synthetic methods such as surface passivation, functional group exchange and chemical or thermal reduction. For example, Li *et al.*[28] used computational methods to determine the effect of oxygen- and nitrogen-containing functional groups on the HOMO-LUMO gap of GQDs. A major significance of that work shows that carbon-oxygen double bonds found in aldehyde, carboxyl and amide functional groups are critical for tuning the HOMO-LUMO gap to lower energies. However, amines (R–NH_2) have been extensively used as the functional group of choice to reduce the HOMO-LUMO gap[14, 29-32] because of its simultaneous increase of PLQY. It has been shown both computationally[27] and experimentally[26] that the band gap decreases with increasing number of primary amines. Additionally, a study about the common origin of photoluminescence in carbon dots made through bottom-up and top-down methods was published by Wang *et al*. which primarily focused on the green luminescence found in both CNDs and GQDs.[33] By utilizing femtosecond transient absorption spectroscopy, it was found that edge states consisting of a carbon backbone and carbonyl/carboxyl groups are responsible for the similar n-π* optical behavior in CND and GQD samples.

In contrast to aforementioned contribution on qualitative understanding, significant progress has been made to understand the structure-function relationship. Huang *et al.* demonstrated this with a back potentiometric titration of GQDs made from carbon black to quantify carboxylic, lactonic and phenolic moieties.[34] As before, carbonyl groups were found to be critical for photoluminescence in GQDs by utilizing phenylenediamine to target ortho- and para-quinones. Alves *et al.* later utilized potentiometric titrations with non-linear regression analysis to quantify carboxylic, lactonic and phenolic groups on GQDs made from cellulose fibers.[35] Both of these

studies demonstrated that carboxylic acid groups were approximately twice as abundant as lactone or phenolic substituents.

The similarity in structure, the difference in function, and the relationship between CNDs and GQDs needs to be better understood so that we can fundamentally understand how to optimize CQDs for specific applications. To our knowledge there has not yet been a comprehensive analysis of the structure-function relationship of both CNDs and GQDs in this manner. The motivation of this work is two-fold: first, we aim to identify and differentiate the structure-function properties of CQDs produced by top-down and bottom-up approach. Second, we intend to use the structure-function relationship to develop a strategy for tailoring carbon quantum dots for specific applications. Those applications include bioimaging (Chapter 3 and 4), electrocatalysis (Chapter 4) and photodynamic therapy (Chapter 5).

2.2 Experimental Details and Methods

GQDs were synthesized by a top-down method by first mixing 100 mg of acetylene carbon black (Strem Chemicals) with 75 mL of concentrated HNO_3 (15.8 N, Fisher Scientific) and 25 mL of concentrated H_2SO_4 (95-98%, Sigma-Aldrich). This mixture was placed into a 250 mL three-neck round bottom flask with a condensing column attached. The flask was heated to 105 °C in an oil bath and kept under reflux for 4 hours. The acid-acetylene black mixture changed from a powdery black solution to a dark brown with small amounts of particulates over the four hour period. After cooling to room temperature, the solution was placed in an ice bath and slowly neutralized with KOH (solid pellet, BDH VWR Analytical) until a large precipitation of salt was formed. The GQD-unreacted acetylene black and salt mixture was vacuum filtered through 2.5 μm filter paper (Whatman) to remove most of the salt and large carbon particles. The neutralization and filtration processes were repeated until the stock GQD solution was pH = 6. Then, 25 mL of stock GQD solution was filtered through a 200 nm pore syringe filter (Supelco) to remove any remaining carbon microparticles. After the final filtration, a MWCO = 100-500 Da dialysis bag (Spectrum Laboratories, Inc.) was filled with the syringe-filtered solution and dialyzed against ultrapure water for one week to

remove dissolved salts. The resulting solution was used in this work as the GQD sample.

CNDs were synthesized by a bottom-up method in which 1 g of solid citric acid (Sigma-Aldrich) was introduced into a 10 mL beaker and heated on a hotplate for 10 minutes at 160 °C in a similar procedure to a previous work by Dong *et al.*[36] After melting, the citric acid liquid begins to effervesce vigorously which is the evolution of carbon dioxide and water vapor. This is a direct sign of the condensation and dehydration reactions that ultimately form C-C bonds in CNDs. At 10 minutes, the liquid is red-orange in color and is quenched using 100 mL of approximately 0.01 M KOH. To remove salt impurities, the same 200 nm filtration and MWCO = 100-500 Da dialysis procedures were performed to produce the CND sample for this work.

2.3   Results and Discussion

In order to understand the structure-function relationship between CNDs and GQDs, we must first measure the physical and chemical structure using both qualitative and qualitative methods. A comprehensive study of these structural aspects can provide useful information to correlate fluorescence, metal sensing, and surfactant behaviors. Figure 2.1 shows the low-magnification (left column) and high-magnification (right column) TEM images of CNDs (top row) and GQDs (bottom row). The low-magnification images were used to generate a histogram of particle diameter as seen in the insets of Figure 2.1.   CNDs are about 5 nm in diameter with a narrow size distribution ($\pm$ 8%) whereas GQDs are about an order of magnitude larger with a much wider size distribution ($\pm$ 31%). The lattice fringes (Fig 2.1, right column) which are about 0.24 nm apart in both carbon dots correspond to the (002) plane of graphene and signifies the presence of sp^2-carbon. It can be seen from the high-magnification images that the graphene-like structures do not cover the entirety of the carbon dot but are rather localized into smaller aromatic regions.
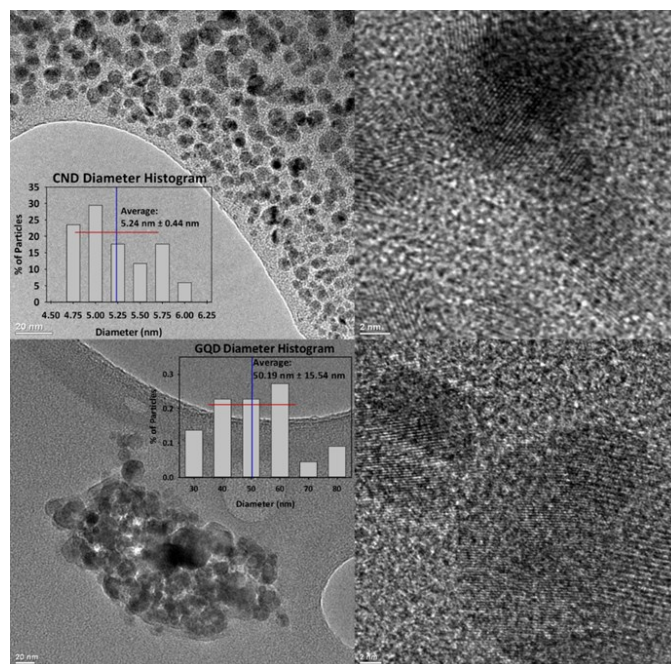
Figure 2.1: Low-magnification (left column) and high-magnification (right column) TEM images of CNDs (top row) and GQDs (bottom row). Histograms of carbon dot diameters for CNDs (top left inset) and GQDs (bottom left inset) with mean diameter (blue line) and standard deviation (red line).

X-ray photoelectron spectroscopy was utilized for the chemical analyses of carbon and oxygen in both CQD samples. CQDs generally have some amount of sp^2/sp^3 carbon structure, with a varied distribution of functional groups. As seen in Figure 2.2, the C1s spectrum shows CNDs have the largest peak as sp^2 C-C with a smaller amount of sp^3 C-C. In an ideal scenario, the bottom-up method would utilize both dehydration and carbonization reactions to form all sp^2 C-C bonds with some edge-terminating functional groups. However, since citric acid consists of three carboxylic acid groups each connected to a sp^3-hybridized carbon atom it is not unreasonable for partially reacted citric acid to be the source of sp^3-carbon. It is also possible that ether and ester functional groups may still be present in CNDs by incomplete carbonization reactions. The C1s binding energies for ether and ester functional groups are the same as hydroxyl (~286.5 eV) and carboxyl (~289.5 eV) and are included in the XPS assignments. The O1s spectrum is included in the right column of Figure 2 to show oxygen-containing functional groups. We observed the functional group distribution is quite similar to the C1s spectrum.

GQDs carry a similar chemical structure to CNDs but with varying quantities. As with CNDs, the dominant peak in the C1s spectra is sp^2-C. A small amount of sp^3-carbon is present in the GQD sample is indicative of an incomplete breakdown and oxidation of acetylene black. GQDs also show less overall oxygen-containing functional groups with the most of these being in the form of carbonyl groups. Ideally, the top-down method would cut GQDs out of the bulk carbon material and harshly oxidize the edges of the produced quantum dots. We hypothesize that the content of sp^3-carbon can be further reduced and oxygen functional group content can be increased with a longer duration of acid treatment. We do not expect ether or ester groups to be present in GQDs due to the harsh acidic treatment easily hydrolyzing the C-O bonds but the binding energies are similar to hydroxyl and carboxyl groups nonetheless.
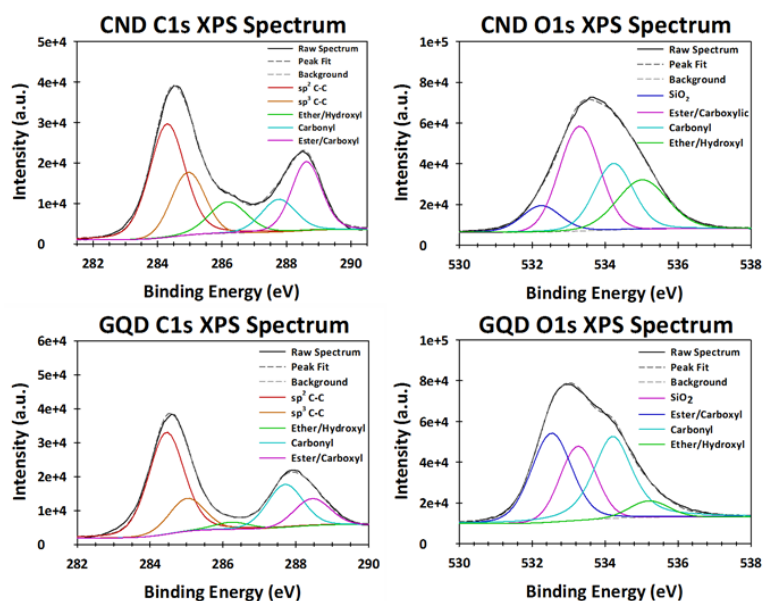
Figure 2.2: C1s (left column) and O1s (right column) XPS spectra of CNDs (top row) and GQDs (bottom row). Peaks were assigned using the NIST X-ray Photoelectron Spectroscopy Database.

FTIR can provide additional information about specific functional groups present in CQDs that XPS may not be able to obtain. For example, the differences in vibrational energy can separate a hydroxyl group from an ether group in FTIR spectra. Figure 2.3 shows the ATR-FTIR spectra of CQDs for qualitative functional group comparison. Both CQD samples have one peak in common with aromatic C-C peaks at 1400 cm^{-1} and 1560 cm^{-1}. As expected, the large differences seen in FTIR lie in the oxygen-containing functional groups. For GQDs there is a peak at 1240 cm^{-1} for the phenolic –OH stretch, a carboxylic acid C-O stretch at 1330 cm^{-1}, a carbonyl peak at 1710 cm^{-1} relating to both ketones and carboxyl C=O groups, a broad carboxylic acid shoulder starting at 2400 cm^{-1}, and a very broad peak starting at 2700 cm^{-1} and reaching a maximum at 3370 cm^{-1}. We speculate the large peak around 3200 cm^{-1} is attributed to hydrogen-bonding with adjacent oxygen-containing functional groups or even water as GQDs are very hygroscopic.

CNDs were found to have a wider distribution of functional groups. The broad peak around 1200 cm^{-1} was treated as two peaks. The left side of this broad peak at 1170 cm^{-1} is assigned as an aliphatic ether (R-O-R). The second assignment is an aromatic ether (Ar-O-R) which is a combination of the small peak at 1040 cm^{-1} and the right shoulder of the large peak at 1250 cm^{-1} which is due to the symmetric stretch and asymmetric C-O-C stretch, respectively. The dominant peak at 1710 cm^{-1} is again assigned to ketone and carboxylic C=O and the right shoulder of that peak (1740-1750 cm^{-1}) is assigned to ester and lactone (cyclic ester) functional groups as a result of incomplete carbonization. At 2570 cm^{-1} the broad carboxylic acid peak can be clearly seen. The broad peak at 2900 cm^{-1} and extending to 3000 cm^{-1} is assigned to the sp^3-carbon and sp^2-carbon C-H stretches. Lastly, the H-bonded -OH stretch at 3400 cm^{-1} could again be from adjacent oxygen-containing functional groups. We do not speculate as much water is absorbed by the CND due to the interference provided by surface passivation due to a larger amount of sp^3-carbon.
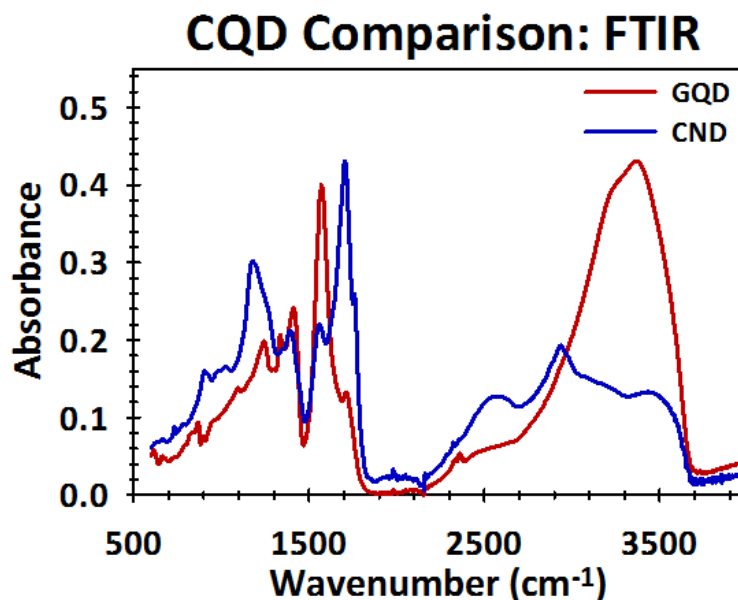
Figure 2.3: ATR-FTIR spectra of prepared CQD samples. These qualitative spectra were normalized to each other by the maximum peak absorbance.

Based on different sp^2- and sp^3-carbon ratios observed in the prepared carbon dots, we chose to perform an experiment where CNDs or GQDs would act as a surfactant toward MWCNTs. We hypothesized that both CQD samples would perform well as a surfactant and Figure 2.4 shows the time lapse over several months of three samples. In the center column of Figure 2.4, the control sample is 1 mg of MWCNTs dispersed in 10 mL of water. The samples in the left and right columns consist of the same proportions of reagents as the control sample but with 1 mg of dried GQD or CND sample added respectively. All three samples were placed in an ultrasonic bath for 30 minutes and then placed in an undisturbed location to prevent agitation. The MWCNT solution began to precipitate in about two hours. A day later, the MWCNT control was mostly precipitated and the GQD-MWCNT solution had started to settle with full precipitation after 15 days. After 150 days, the CND-MWCNT solution continued to be well-dispersed with no sign of MWCNT precipitation.

We speculate the chemical structure differences could be the reason behind the large discrepancy in surfactant performance. Surfactant activity for GQDs can be explained by the large sp^2 nano-domain of GQDs acting as a surfactant to the π-conjugated surface of the MWCNT. Edge-terminating functional groups allow GQDs to act as the

intermediate between MWCNTs and water. GQDs, however, have a tendency to self-stack (seen by the TEM images) causing large GQD aggregates to form that reduce surfactant activity. In the case of CNDs, the sp^3-carbon is hypothesized to act as a surface passivation layer which would adhere to the MWCNT surface. This layer would also provide a physical barrier between oxygen-containing functional groups of neighboring CNDs which prevents them from aggregating due to hydrogen bonding. This hypothesis is also supported by the TEM images as CNDs show very little aggregation. Additionally, hydroxyl and carboxyl groups of the CNDs will also stabilize the CND-MWCNT complex in water. Considering the relative size of a water molecule to a CND, it is reasonable to expect the hydroxyl and carboxyl groups are adequately hydrated in water.
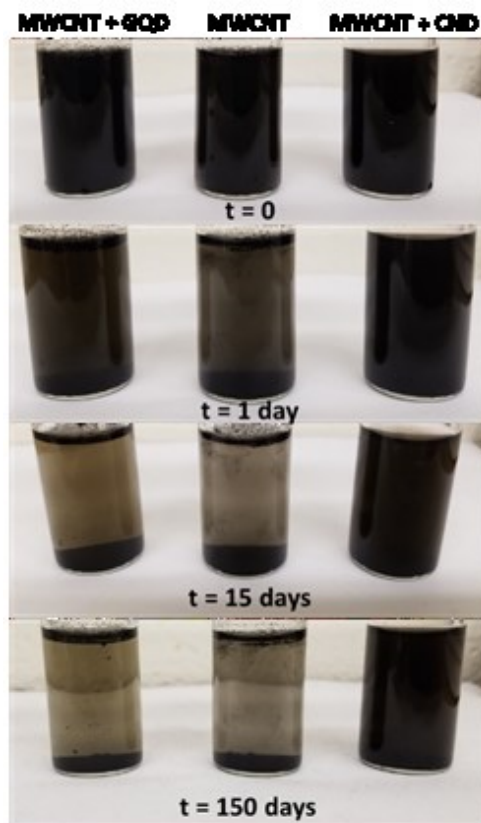
Figure 2.4: Time-lapse photographs of surfactant experiment. 1 mg of MWCNT was ultrasonically dispersed in 10 mL of water as a control sample (center). 1 mg of dried GQD and CND powder was added to identical solutions of the control sample to make the GQD-MWCNT solution (left) and CND-MWCNT solution (right).

The optical properties of carbon dots can also be traced back to the chemical structure. The top row of Figure 2.5 shows the UV-Visible absorbance spectra of CQD samples. As seen in the 0.04 mg mL^{-1} samples, the GQD absorbance peak around 280 nm is assigned to the π-π* transition of the sp^2-C aromatic region. This broad absorbance band is attributed to the large size distribution of GQDs (50 ± 15 nm). Consequently, this allows the exciton to delocalize amongst the carbon nano-domain more freely, lowering the energy required for exciton recombination. CNDs have a much smaller size distribution than GQDs (5 ± 0.4 nm) and subsequently, have narrower absorption peaks that lie toward higher energy. The peaks for both samples at wavelengths longer than 340 nm are assigned to the n-π* transitions related to excitations of nonbonding orbital electrons belonging to edge-terminating functional groups. Absorption peaks for GQDs extend far into the red end of the visible spectrum where CNDs sharply lose absorbance intensity around 360 nm.
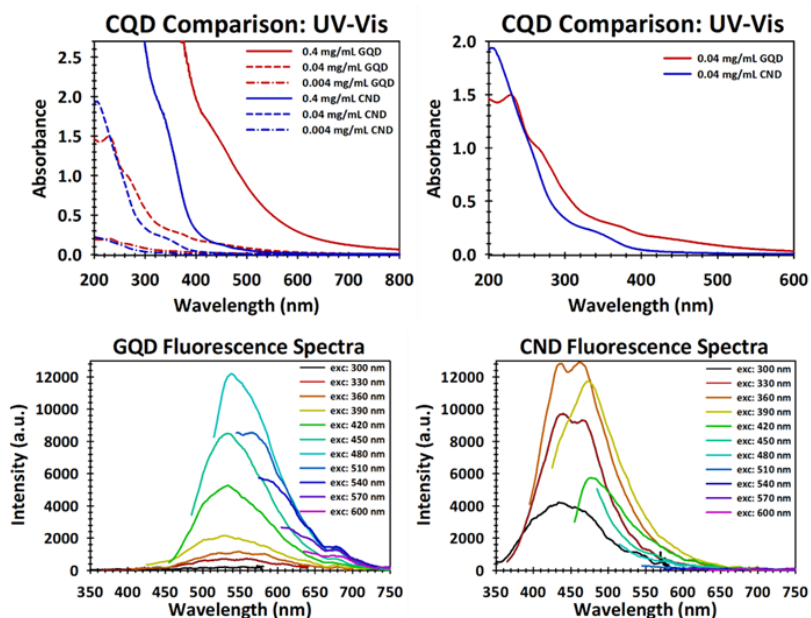
Figure 2.5: (top) UV-Visible Absorbance Spectra of GQDs (red) and CNDs (blue). GQDs have a prominent red shift in absorbance wavelength whereas CNDs have strongly absorb in the UV region (200-260 nm). Functional group distribution and overall size were found to be the sources of red-shifted absorbance in GQDs and surface passivation was attributed as the source of blue-shifted absorbance. (bottom) Excitation-dependent emission spectra of GQDs (left) and CNDs (right).

Excitation-dependent emission spectra for GQDs (Figure 2.5: bottom left) is comprised of 2 major bands with the first having peak emission wavelength at 530 nm and the second at 670 nm. Figure 2.6 in the shows the excitation spectra of each of the above emission wavelengths. For 530 nm emission, three excitation peaks were observed at 350 nm, 420 nm, and 465 nm. Comparing this information with absorbance data, it can be speculated that the peak emission of GQDs originates from the n-π* transition of functional groups. We hypothesize that though short wavelength light is strongly absorbed by the GQD, it undergoes non-radiative energy transfer by vibrational relaxation, exciton recombination to the sp^2-carbon nano-domain or energy transfer to defective functional groups which result in a lower-energy emission. The second major emission peak at 670 nm was found to be weakly excitation-dependent. According to the excitation spectra (Figure 2.6), this emission has a wide range of excitation wavelengths from 380 nm to 640 nm. Considering both the broadband excitation and the lack of excitation wavelength dependent emission, we hypothesize this peak as the direct emission of the sp^2-carbon nanodomain as per the quantum confinement effect. Unfortunately, without harsh chemical reduction of the edge-terminating groups (and thereby reducing the GQD solubility in water) we cannot verify this assignment. This emission peak at 670 nm with a maximum excitation wavelength of 530 nm is promising for developing GQDs for bioimaging and photodynamic therapy applications as the emission would be useful to treat skin tumors and melanomas. GQDs tailored with near-infrared (650 to 1350 nm) excitation and emission would be ideal as near-infrared light penetrates more effectively into deep tissues (i.e.: organs) than visible light.
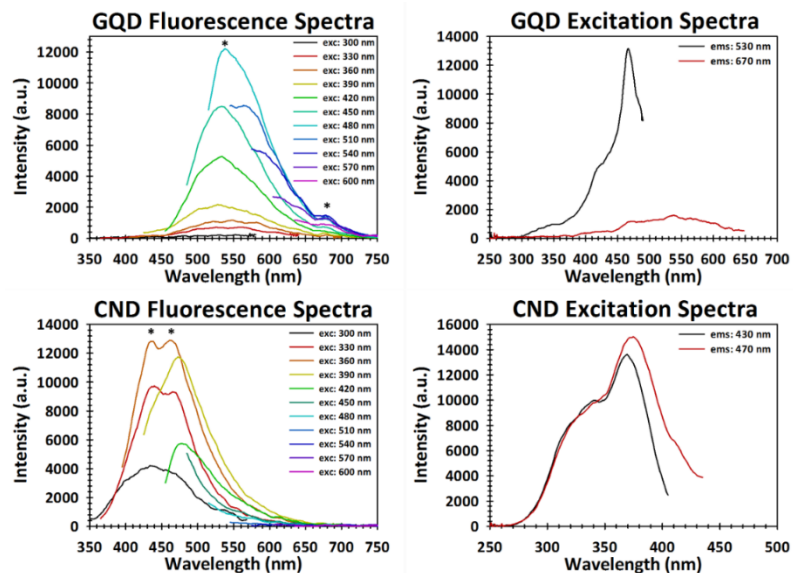
Figure 2.6: Fluorescence spectra of GQD and CND (left column) and corresponding excitation spectra (right column) taken at each respective mark. For example, GQD excitation spectra were taken at an emission wavelength of 530 nm and 670 nm.

CNDs have a very different emission profile (Figure 2.5: bottom right) than GQDs with a majority of the emission confined to wavelengths between 400 nm and 550 nm. As with absorbance, this 150 nm blue shift can be attributed to the size distribution of CNDs. The overall diameter of the CNDs is smaller than GQDs by an order of magnitude which would further confine the exciton to a smaller area. This would increase the energy of the HOMO-LUMO gap by reducing the number of discreet energy states. The quantum confinement effect is analogous to the particle-in-a-box system and is also seen in inorganic quantum dots like CdSe.[37] The role of surface passivation with sp³-carbon with surfactant behavior was discussed earlier in this section. However for optical properties this creates a "barrier" which directs non-radiative energy transfer toward intramolecular functional groups and not trap states, other CNDs, or solvent molecules thereby increasing PLQY. Surface passivation has also been used to increase the QY of carbon dots that are functionalized with agents much like branched polyethylenimine (BPEI).[38] We did not observe any emission lower than 300 nm excitation and the Stokes shift between the emission and excitation wavelengths were similar to GQDs implying that the optical behavior in this region is - like GQDs - tied to the n-π* transition of the functional groups.

56

In order to identify and quantify the functional groups for each carbon dot sample, we chose to perform metal sensing and titration experiments. Many researchers have explored the use of carbon dots as highly sensitive agents for determining metal ion concentrations in aqueous samples.[39-46] Overall, the metal ion that has been found to strongly quench carbon dots is Fe^{3+} which is electrostatically bound to the CQD via hydroxyl functional groups.[45, 46] The carboxylic acid group has not been studied as extensively as hydroxyl groups however Zeng *et al.*[47] demonstrated a carboxyl-modified polymer as a highly selective Cu^{2+} sensor. Therefore, we intended to probe the qualitative abundance of these two functional groups by performing a fluorescence quenching experiment with Cu^{2+} and Fe^{3+} salts. Figure 2.7 shows the concentration of metal ion plotted against the fluorescence intensity ratio. An $I/I_0 = 1$ corresponds to no fluorescence quenching and a value of zero represents complete quenching. The emission intensity was measured using an excitation wavelength of 360 nm for CNDs and 480 nm for GQDs which gives the maximum peak emission intensity as seen in Figure 2.6. GQDs quenched with both metal ions follow a similar pattern with Fe^{3+} quenching fluorescence more completely at lower concentrations. This qualitatively suggests there are less hydroxyl than carboxyl groups in GQDs which is consistent with XPS peak areas of hydroxyl and carboxyl groups for both C1s and O1s spectra. CNDs, on the other hand, show a significant difference in metal sensing as the highest concentration of Cu^{2+} does not completely quench fluorescence. This would suggest that there is a larger amount of carboxyl groups in CNDs compared to hydroxyl groups and is also supported by XPS peak areas in Figure 2.2.
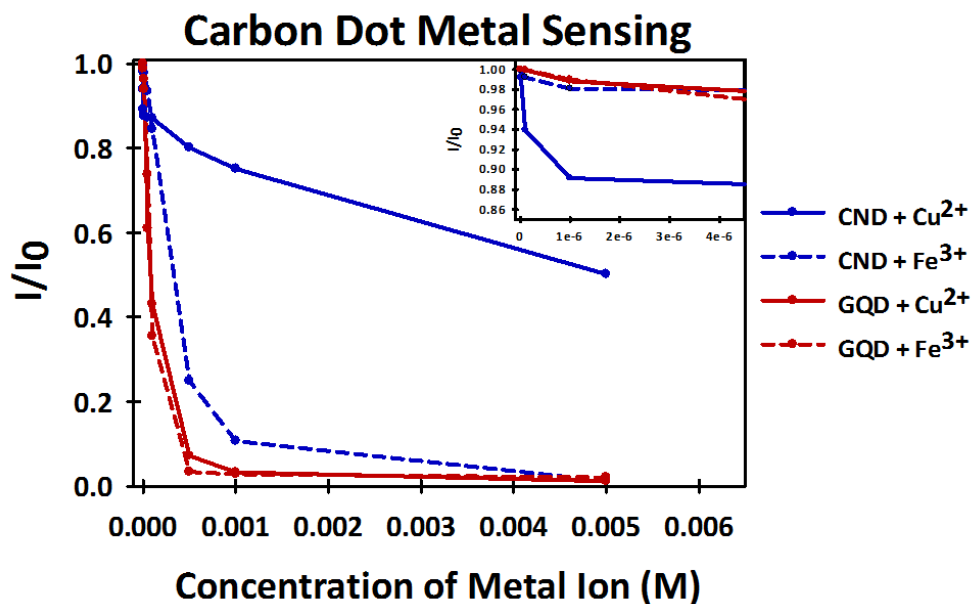
Figure 2.7: Metal sensing data for CNDs (blue) and GQDs (red) toward Cu^{2+} (solid line) and Fe^{3+} (dashed line). Plot represents concentration vs fluorescence intensity ratio. $I/I_0 = 1$ represents no fluorescence quenching and $I/I_0 = 0$ represents total fluorescence quenching. GQDs showed similar metal sensing behavior toward both copper (II) and iron (III) metal ions. CNDs responded to iron (III) ions in the same way as GQDs, but with a significant difference toward copper (II) ions. This was attributed to the increased amount of carboxyl groups on CNDs.

Titration experiments provided us with detailed quantitative information on the chemical structure of GQDs and CNDs. It was hypothesized that by using the pKa values of hydroxyl and carboxyl functional groups we could quantify the number of a specific functional group in CQD samples. Recently, Konkena et al.[48] published a work detailing the chemistry behind the dispersibility of graphene oxide in water which included titration data to identify and quantify specific functional groups. We chose to model our titration experiment with a similar approach. First, the control experiment (Figure 2.8 left – green symbol) was performed by titrating 15 mL of 0.01 M KOH with 0.01 M HCl. Then, we titrated the same volume of 0.01 M KOH with 1 mg of GQDs (Fig. 2.8 – red symbol) and CNDs (Fig. 2.8 – blue symbol). We hypothesized that the excess concentration of KOH would deprotonate all of the –OH and $-CO_2H$ groups without significantly reducing the concentration of KOH. The volume difference between the equivalence point of the control sample and the first equivalence point for the CND/GQD sample is correlated with the total number of hydroxyl groups. The

volume difference between the first and second equivalence points relates to the total number of carboxyl groups. The derivatives of these titration curves in Figure 2.9 were used to find the exact equivalence volumes for functional group calculations.

We found for the CND sample that the carboxylic acid equivalence point was very broad. We attribute this broadening to acid-catalyzed hydrolysis of ether and ester groups at pH < 7 which would cleave the ether and ester groups into either two hydroxyl groups or one hydroxyl and one carboxyl groups, respectively. As a means to quantify the amount of ether and ester groups in the CND sample, we had taken the previous CND sample that had been titrated with HCl and back titrated it with 0.01 M KOH. It was hypothesized that the difference between the number of carboxyl groups found in the forward and reverse titration would be equal to the number of ester functional groups. Likewise, the difference of hydroxyl functional groups would represent the number of ester groups plus twice the number of ether groups. Table 2.1 shows the quantities of each functional group determined by the titration experiments. In the forward titration, we found that the OH:CO_2H ratio of GQDs is 1.31:1 and 1.54:1 for CNDs. The back titration results of CNDs show a wider distribution of functional groups as acid hydrolysis of ethers and esters can produce more hydroxyl and carboxyl groups. Interestingly, we found a significant portion of ester groups and very little ether content. In total, of all the pH-sensitive functional groups on CNDs: 50% are hydroxyl, 37% are carboxyl, 12% are esters, and 1% are ethers.
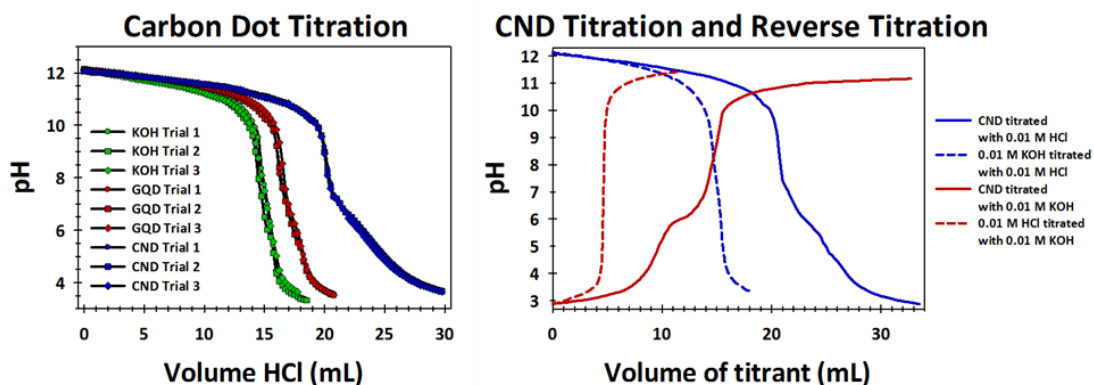
Figure 2.8: Titration data (left panel) for control (green), GQD (red), and CND (blue). Titration and reverse titration data (right panel) to investigate the presence of ether and ester groups after acid hydrolysis.
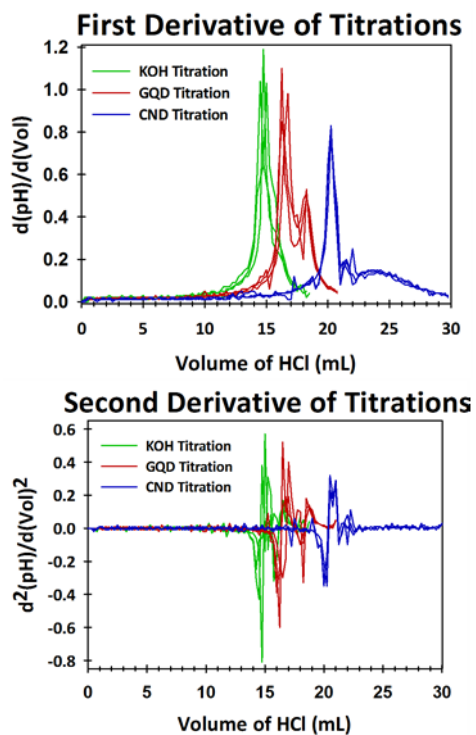
Figure 2.9: First and second derivative curve of titration experiments. The volume of HCl where the first derivative reaches a maximum or the second derivative crosses zero as a result of a sharp increase or decrease corresponds to the exact equivalence point.

Table 2.1: (top) Forward titration of GQD and CND to determine the quantity of hydroxyl and carboxyl groups. Titrations were performed in triplicate and show excellent convergence despite the lack of uniformity found in CQD. (bottom) Forward and reverse titrations were used in conjunction to determine the amount of ether and ester groups in CNDs. At the end of the forward titration, the pH is basic enough to cleave ester and ethers into one carboxyl and one hydroxyl or two hydroxyl groups, respectively.

First Equivalence Point				Second Equivalence Point		
	Vol of titrant (mL)	ΔVol (mL)	Mol -OH		Vol of titrant (mL)	ΔVol (mL)	Mol -CO_2H
Control	15.00±0.25	---	1.5e-4±2.5e-6	Control	---	---	---
GQD	16.46±0.26	1.46	1.46e-5±2.6e-6	GQD	17.58±0.14	1.12	1.12e-5±7e-7
CND	20.21±0.14	5.21	5.21e-5±1.4e-6	CND	23.83±0.29	3.61	3.61e-5±2.9e-6

First Equivalence Point				Second Equivalence Point		
	Vol of titrant (mL)	ΔVol (mL)	Mol -OH	Vol of titrant (mL)	Δvol (mL)	Mol -CO_2H
Forward: Control	15.19	---	1.52e-4	---		---
Forward: CND	20.18	4.99	4.99e-5	23.81	3.63	3.63e-5
Reverse: Control	4.52	---	4.52e-5	---		
Reverse: CND	15.73	6.41	6.41e-5	9.32	4.80	4.80e-5
Δ(Mol –OH) from forward and reverse titrations			1.42e-5	Δ(Mol –CO_2H) from forward and reverse titrations		1.17e-5
Mol additional –OH[1]			0.25e-5	Mol Ester		1.17e-5
Mol Ether			0.12e-5	1: after subtracting the –OH from ester groups		

We first hypothesized that these titration results would roughly resemble the previously mentioned XPS peak areas; however, those results show very different relative abundances of carboxyl to hydroxyl groups in both GQDs and CNDs. As before, XPS spectra show GQDs primarily contain carbonyl and carboxyl functional groups and little hydroxyl content. CNDs show nearly equal hydroxyl and carbonyl groups and a much higher amount of carboxyl content. We speculate that the difference in analytical methods could be the reason for this discrepancy. For example, the XPS measurement is conducted under vacuum with a solid sample and titrations were conducted in an excess of KOH solution. As a dried solid in vacuum, there is no source of proton addition or abstraction such as water to catalyze the conversion of carbonyls to hydroxyl groups. In basic aqueous media however, the carbonyl group can be hydrated to form a geminal diol via nucleophilic addition of hydroxyl ion (OH^-). Since our titration experiments were conducted in excess KOH, we can say this difference in hydroxyl groups is attributed to the aldehydes that were converted to geminal diols. We believe that the majority of carbonyl groups in CNDs would exist as aldehydes based on the large peak in Figure 2.3 around 2900 cm^{-1} that is assigned the sp^2 C-H stretch.

Since our titration experiments were conducted in excess KOH, we can say this difference in hydroxyl groups is attributed to the aldehydes that were converted to geminal diols. This conversion of the carbonyl group also occurs in acidic media by protonation of the carbonyl oxygen (and subsequent electrophilic attack by water) but we expect most, if not all, carbonyls have already been converted before the reverse titration. In either case, one carbonyl is converted to two pH-sensitive hydroxyl groups. This skews the hydroxyl group titration result to be roughly three times larger than observed for CNDs since the hydroxyl and carbonyl XPS peak areas are nearly the same. With that consideration in mind, this changes the $OH:CO_2H$ ratio from 1.54:1 to 0.51:1 which matches better with the XPS peak areas.

For GQDs, if we assume that all carbonyls were converted to two hydroxyls as we did for CNDs, the $C=O:CO_2H$ ratio would then be 0.65:1 which is still largely different than the XPS peak area ratios. We hypothesize that the carbonyl groups on GQDs are embedded into the carbon nano-domain system and are more like quinones than benzaldehydes. With GQD having a large π-conjugated system on the order of a few tens of nanometers, forming a diol with these carbonyl groups would disrupt the aromaticity of this system. Instead, we speculate that these carbonyls are more quinine-like and are converted into one phenol group in order to maintain aromaticity. A previous work by Isaacs et al. explored the mechanism behind the reduction of quinones to hydroquinones using ascorbic acid as a catalyst.[49] Based on the structure of GQDs, it is reasonable to expect some catalytic amount of vicinal –OH on a C-C double bond, which is the initiating functional group in that work. As such, we can treat the GQD's carbonyl groups as being catalytically converted to a single phenol. Therefore, the $-C=O:-CO_2H$ ratio would be 1.31:1 as observed in the titration data which is similar to the XPS peak areas.

By coupling these results with the sizes of CQDs found in TEM and the relative ratio of C1s peaks assigned in XPS, we can take the titration data further to fully quantify the average number of functional groups on a single carbon dot and ultimately build an accurate model of the carbon dots produced by top-down and bottom-up approaches. The representative images from the data collected in this work are shown

in Fig. 2.8 and 2.9. This work details the variety of methods to building model carbon dots for any synthesis. We feel this information is crucial to understanding the role that carbon quantum dots can serve for various applications including wastewater treatment or photodynamic therapy. In addition, these model compounds can provide computational chemists the structure needed to fully understand the mechanisms of fluorescence. Only with a great understanding of the structure-function relationship can researchers use CQD as inexpensive and high-performance materials in systems that require expensive catalysts.
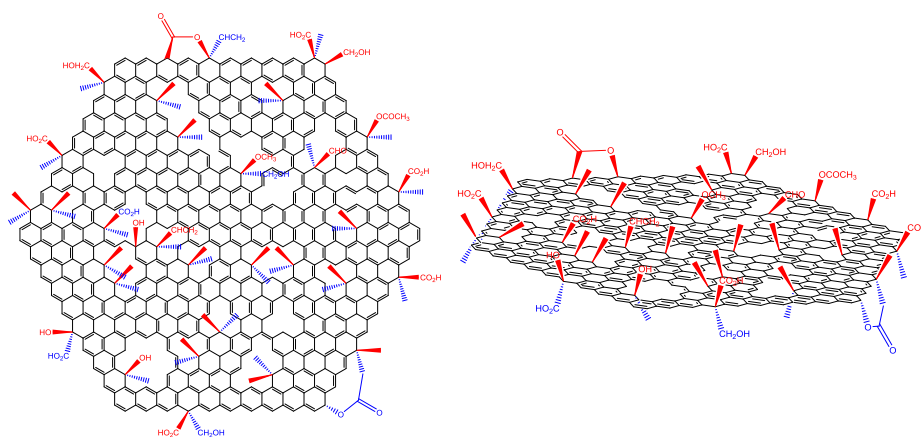
Figure 2.10: Representation of a bottom-up synthesized carbon nanodot using data from this work. For image clarity, methyl groups were added as a means to show the surface passivation instead of larger alkyl chains.
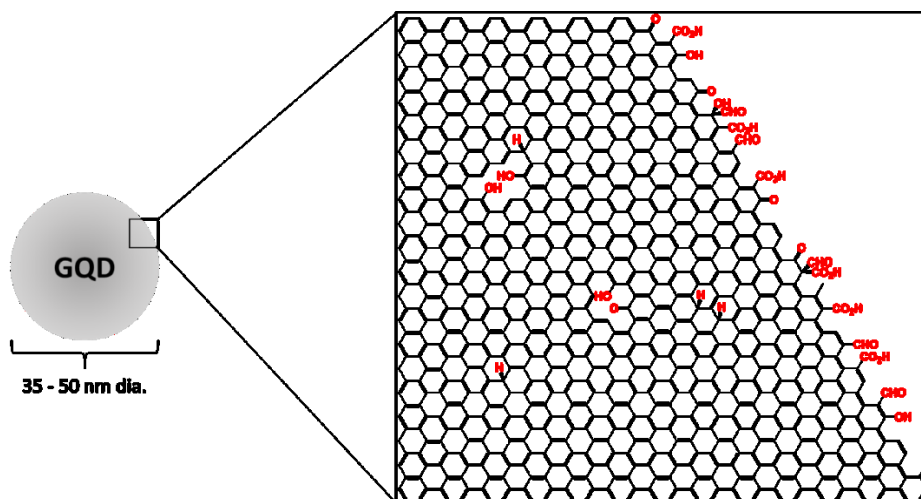
Figure 2.11: Representation of a top-down synthesized graphene quantum dot using data in this work. A 5 nm x 5 nm window is used to show the distribution of functional groups.

2.4 Lifetime Measurements of Carbon Quantum Dots in Collaboration with Michigan State University

A recent collaboration with Dr. Gary Blanchard from Michigan State University yielded interesting results concerning the lifetimes of CQDs made from either a top-down or bottom-up approach. Overall, five samples were submitted with two distinct sample sets. In the first sample set, CQDs were made using a top-down approach by chemically oxidizing carbon nano-onions (CNOs) with nitric and sulfuric acid. In this case, sulfuric acid acts as an intercalating agent which assists in "peeling off" layers of the carbon nano-onion. At the same time, nitric acid can strongly oxidize either the inherent defects of the CNO or the exposed edges of the carbon nano-onion layer. These two processes result in the formation of graphene quantum dots (GQDs). Generally, GQDs produced in this way are large, aromatic sp^2-carbon planes about 5 to 10 nm in diameter with edges terminated with hydroxyl, carbonyl, and carboxyl functional groups. The number and proportion of these functional groups vary from particle to particle but can be quantitatively averaged using X-ray Photoelectron Spectroscopy. Previous results with Atomic Force Microscopy suggest that the ox-GQD are not monodisperse but instead tend to aggregate into stacks of three to five.

In this study, we considered a recent report by Wang *et al.* in which ultrafast spectroscopy was used to identify emissive states in GQDs.[50] Historically, only two states have been discussed and are known commonly as the intrinsic and extrinsic states. The intrinsic state is hypothesized to originate solely from the aromatic sp^2-carbon nano-domain in which delocalized π-electrons are promoted to π^* orbitals. As the GQD relaxes from the excited state, non-radiative processes such as vibrational relaxation down to the lowest vibronic (vibrational-electronic) state compete with fluorescence. As the size of the aromatic nano-domain increases, more of this competition can occur which red-shifts the emission as per the quantum confinement effect. The extrinsic state (or surface state), on the other hand, arises from the edge-terminating functional groups. It is still under debate whether the extrinsic state is the combination of all emissive functional groups or individual fluorophores. The Wang *et al.* report details three distinct emissive states from the results of time-correlated single-

photon counting (TCSPC) as well as femtosecond transient absorption (TA) spectroscopy.[50] The first state suggests green fluorescence from a bright-state functional group that is affected by a nearby second bright-state functional group. The second emissive state originates from a standalone bright-state functional group, such as a hydroxyl either on the edge or as a defect in the aromatic nano-domain. This functional group has no other functional group neighbors with high electron density, therefore there is no channel to remove energy from this bright fluorophore. The third emissive state is assigned to the intrinsic state whose bandgap is sensitive to the size of the aromatic nano-domain. Interestingly, this report suggests the intrinsic state is an optically dark state and is not a primary component of GQD fluorescence. The source of GQD fluorescence is assigned to the standalone functional group (typically with blue-shifted emission) and synergistically coupled functional groups (typically with red-shifted emission).

As the theme of this dissertation is to uncover the structure-function relationship in carbon quantum dots we wanted to see if we could find a similar effect in fluorescent lifetime measurements. We prepared five samples belonging to two sample sets. The first sample set was synthesized by a top-down approach and some of these samples were reduced versions of GQD using either hydrothermal reduction or chemical reduction with $NaBH_4$. The second sample set contains a sample of bottom-up synthesized CQD for comparison.

The data we received from Dr. Blanchard originated from a parallel-polarized fluorescence detector and a perpendicularly-polarized fluorescence detector. This detector arrangement can provide fluorescence polarization and anisotropy data, which is discussed later in this section. The overall lifetime data is found by adding one parallel-polarized data set with two perpendicularly-polarized data sets. This accounts for all three dimensions in which the sample may emit a photon. The raw data was fit with OriginLab software using the following equation:

$$y = y_0 + Ae^{-Bt_1} + Ce^{-Dt_2}$$

This equation was used for fitting for two reasons: (i) it provides the best numerical fit for the data and (ii) we wanted to first assume a simple model relating to "core"

(aromatic nano-domain) and "defect" (functional groups) state emission. The variables in the equation are as follows. y_0 relates to the y-intercept of the fitted data, but we usually found this to be nearly zero as the exponential fits were more prominent. Terms A and C are the pre-exponential factors which relate to the contribution of each exponential to the fit. Terms B and D are relate to the observable lifetime in each fitted exponential. If we assume $y_0 = 0$ and integrate the equation, we can find the relative contribution of each time component as:

$$\frac{A*B}{A*B+C*D} + \frac{C*D}{A*B+C*D} = 1$$

This allows us to observe which time component is more prevalent in any given excitation and emission wavelength in which we have fitted data. A simple way to interpret this data is to consider that the lifetime relates to an event and the relative contribution of that component relates to the frequency of those events. Understanding this provides us with information on if core state emission or defect state emission is dominant at a specific excitation wavelength and emission wavelength pair.

First, we will compare two identically-synthesized GQD, termed ox-GQD. All of the data for the top-down synthesized GQD experiments are shown in Table 2.2. Ox-GQD have two major lifetime components when excited by 330 nm light: a short component at 700 ps and a longer lifetime component at 2600 ps. Generally, these lifetimes are unchanged (within < 5 % deviation) regardless of the emission wavelength which was 430 nm and 530 nm. However, looking at the relative contributions of each lifetime component, we see a substantial shift. At 430 nm emission, the short lifetime component is dominant with about 75 % of the total fit. At 530 nm emission, the long lifetime component becomes dominant at around 63 % of the total fit. As such, we hypothesize that the short lifetime component relates to the core state - experiencing less non-radiative decay and giving rise 430 nm emission. The fluorescence at 530 nm emission shows that non-radiative energy transfer from the core to the defect state has occurred and that the defect state is most responsible for the longer wavelength emission.

Chemical reduction is an effective means to alter the distribution of functional groups on ox-GQD. Using a mild reducing agent like NaBH$_4$ allows for the change of carbonyls to hydroxyls without significantly disrupting the remainder of the GQD. Shown below in Figure 2.10 is a comparison of XPS C1s spectra that shows ox-GQD and chemically reduced GQD (CR-GQD). It is clearly shown that chemical reduction using NaBH$_4$ converted carbonyls to hydroxyls. We suspect the increase of sp^3-carbon originates from the chemical reduction of quinone-like carbonyls to a hydroxyl group attached to a sp^3-carbon. Using an excitation wavelength of 330 nm and emission wavelength of about 450 nm, the ox-GQD show two components: one with a pre-exponential factor of nearly 70% and a lifetime of about 700 ps, the other with a pre-exponential factor of nearly 30% and a much longer lifetime of 2600 ps. Upon chemical reduction, the first time component shows 30% contribution with about 700 ps. The second time component makes up about 70% of the total spectrum with a lifetime again around 2600 ps. The lifetimes themselves are unaffected however the contributions of these lifetimes toward the total spectrum are greatly changed. With this data, we can affirm that the longer time component belongs to the functional groups. We hypothesize that the carbonyl groups extend the π-conjugation of the sp^2-carbon nano-domain whereas the hydroxyl groups remove electron density from the nano-domain, isolating itself as an independent fluorophore. With an increased density of hydroxyl groups, we find the dominant component of observed fluorescence originates from these isolated fluorophores.

Table 2.2: Results from fitted data obtained through TCSPC lifetime measurements. The top-down synthesized graphene quantum dots show similar lifetimes and relative contributions of lifetimes despite differing synthesis conditions. Upon chemical or hydrothermal reduction, there are significant changes in lifetimes and relative contributions of lifetimes compared to the original sample. As these reduction methods are generally mild, there is a clear structure-function relationship between the functional groups of GQD and observed fluorescence lifetimes.

	A	B (ps)	C	D (ps)	A*B	C*D	% A*B	% C*D
OX-GQD1:								
Ex 330, em 430	3253	694	235	2605	2257373	612175	78.6 %	21.4 %
Ex 330, em 530	3427	724	1595	2575	2480930	4108525	37.7 %	62.3 %
HT-GQD:								
Ex 330, em 430	3676	935	3152	6074	3436593	19142818	15.2 %	84.8 %
Ex 330, em 530	2407	1110	1460	5359	2672214	7825748	25.5 %	74.5 %
OX-GQD2:								
Ex 330, em 440	0.889	710	0.091	2568	631.2	233.7	73.0 %	27.0 %
Ex 330, em 510	0.639	686	0.296	2504	438.4	741.2	37.2 %	62.8 %
CR-GQD:								
Ex 330, em 430	0.570	730	0.362	2592	416.1	938.3	30.7 %	69.3 %
Ex 330, em 500	0.594	982.6	0.383	4466	583.7	1710.5	25.4 %	74.6 %
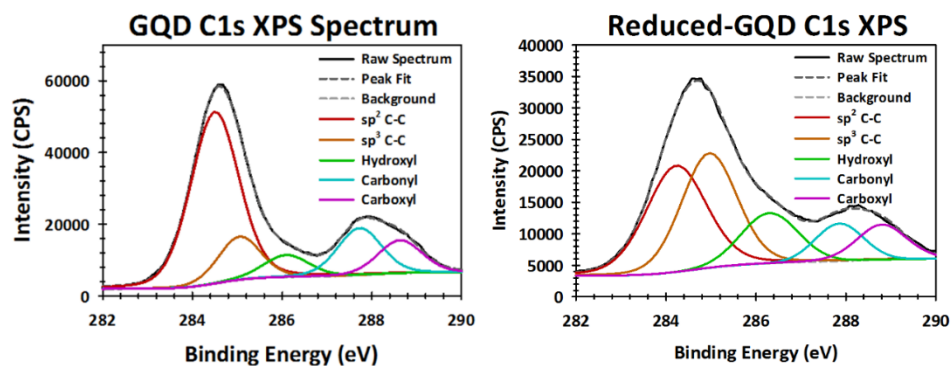
Figure 2.12: A comparison of C1s XPS Spectra for OX-GQD and CR-GQD. This shows the mild reduction of aromatic carbonyls to non-aromatic hydroxyls. Carboxylic acid groups were largely unaffected by chemical reduction with $NaBH_4$.

Interestingly, at longer emission wavelengths CR-GQD shows much longer lifetimes for both components (nearly 1000 ps and 4500 ps). Typically, chemical reduction increases the photoluminescent quantum yield (PLQY) by eliminating non-radiative decay channels attributed to the functional groups. In this case, since carbonyls are being converted to hydroxyls, it can be said that carbonyls are a non-radiative decay channel as an independent fluorophore. Usually for CR-GQD, the emission spectra (and the position where PLQY is measured) is shifted toward higher energy or is blue-shifted. As such, seeing the shift only in time component contribution and not in the lifetimes seems consistent with the altered chemical state of CR-GQD. At longer emission wavelengths however, interpretation is more difficult. We hypothesize that since the emission is enhanced toward the blue end of the visible spectrum, longer wavelength emission suffers as a result and PLQY is likewise suppressed. This reduction in PLQY would decrease the radiative rate constant and lengthen the lifetimes of all time components. A unique observation we found in these results is that both lifetime components are extended by about 150% which supports a global reduction in the radiative rate constant. Another interesting observation is that the pre-exponential factors of CR-GQD are relatively unchanged compared to the short wavelength results. We hypothesize that this means that during chemical reduction, the core is not significantly changed and the frequency of energy transfers from core to defect state is also relatively unchanged.

Hydrothermally reduced GQDs (HT-GQDs) show very different results than CR-GQD. First, we see both an increase of the lifetimes as well as a shift in pre-exponential factor. This is also shown in the longer wavelength emission but to a greater extent. As with CR-GQD, hydrothermal reduction can increase the PLQY and is contradictory to the results. However at high temperatures, hydrothermal treatment can also cut typically stable bonds that would not be cleaved by chemical reduction. As there is a greater effect of reduction by means of high-temperature hydrothermal treatment, the cleavage of emissive defect states could be the origin of the global increase of lifetimes. The most significant change in HT-GQD occurs with 330 nm excitation and 430 nm emission. We observe in this wavelength set that the high-temperature hydrothermal treatment has enhanced the defect state relative contribution to nearly 85%. This high percentage of the defect state can be explained in the following ways: (i) upon hydrothermal cutting, more functional groups are generated due to supercritical water acting as a reactant, and (ii) in comparison to CR-GQD, the peak fluorescence may be further blue-shifted and thus non-radiative decay channels dominate in this low PLQY wavelength. Unfortunately, we do not have any characterization data or steady-state fluorescence data of this sample to support either of these claims.

CND have a very different chemical structure than ox-GQD as seen in Fig. 2.11. First, there is a greater amount of sp^3-carbon which can encapsulate and shield sp^2-carbon nano-domains from the environment. This kind of passivation can hinder exciton mobility and reduce non-radiative decay channels. This is seen clearly in the much greater PLQY (at short wavelengths) of CND compared to ox-GQD. In the lifetime data (Table 2.3), there are three lifetime components for CNDs as opposed to the two components in GQD. Accordingly, the equation below was used for a three-component fit.

$$y = y_0 + Ae^{-Bt_1} + Ce^{-Dt_2} + Ge^{-Ht_3}$$

We speculate the very short lifetime of less than 100 ps relates to core state emission of fully or near-fully passivated sp^2-carbon nano-domains. We hypothesize that these small, fully-passivated aromatic regions have no means to transport energy other functional groups. With a lack of non-radiative decay channels, this allows the exciton

70

to quickly relax back to the ground state and emit a photon with a small Stokes shift. As before, the t_2 component relates to partially passivated sp^2-carbon nano-domains as seen in GQDs. Interestingly, the t_3 lifetime component for CND is about 3000 ps compared to 2600 ps for ox-GQD. According to our XPS spectra, there is a higher concentration of carbonyl and hydroxyl groups in CND than ox-GQD. As a result, the non-radiative decay channel related to carboxyl groups is suppressed, lengthening the lifetime of the defect state. These components and their relative contributions are also seen at longer emission wavelengths with little change overall. We suspect any changes, however small, may be in part to the inhomogeneity of the size of the sp^2-carbon nano-domain. Though CND are generally blue-shifted compared to ox-GQD, the excitation-dependence encompasses a wider range of wavelengths than ox-GQD. This is likely due to the broad range of wavelengths that can excite a myriad of nano-domain sizes. Additionally, the contributions of each time component (particularly t_2 and t_3) in CND mimic those of HT-GQD and CR-GQD. This is likely due to the similar amounts of functional groups (primarily hydroxyl) in CND and reduced GQD.
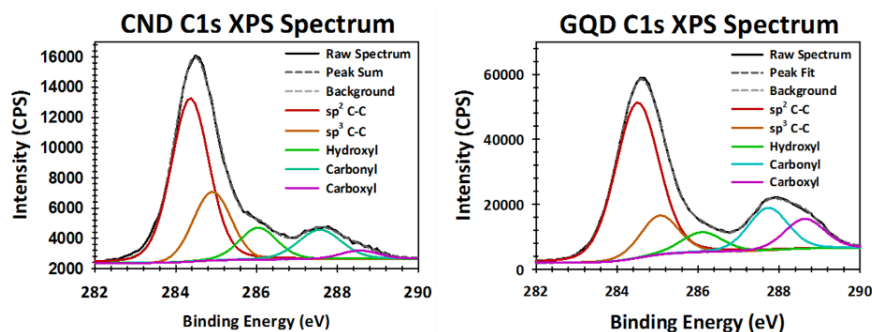
Figure 2.13: A comparison of C1s XPS Spectra between bottom-up synthesized carbon nanodots and top-down synthesized graphene quantum dots. The most significant difference lies in the elevated amount of sp^3-carbon in CNDs compared to GQDs. These two carbon nanoparticle do however have a slight difference in functional group distribution. CNDs have more hydroxyl groups whereas GQDs have more carbonyl groups.

Table 2.3: Results from fitted data obtained through TCSPC lifetime measurements. The bottom-up synthesized carbon nanodots show a large difference compared to the top-down synthesized graphene quantum dots. We attribute the first, very short lifetime component to relate to fully passivated aromatic regions. Without a means to transfer energy through non-radiative processes, the exciton fluoresces quickly. The other two lifetime components relate to similar emissive features found in GQDs: the core and the defect states.

	A	B (ps)	C	D (ps)	G	H (ps)	% A*B	%C*D	%G*H
CND:									
Ex 330, em 430	0.347	63.5	0.418	513.8	0.266	2678.5	0.023212	0.226243	0.750546
Ex 330, em 460	0.287	56.9	0.415	541.2	0.300	3087.9	0.01399	0.192408	0.793602
Ex 360, em 430	0.260	60.1	0.392	579.8	0.350	2790.8	0.012811	0.186344	0.800844
Ex 360, em 450	0.161	41.2	0.391	526.5	0.387	2806.8	0.005107	0.15851	0.836382
Ex 385, em 430	0.205	77.3	0.382	641.8	0.417	2983.3	0.010529	0.162897	0.826574
Ex 385, em 470	0.188	83.1	0.402	585.9	0.402	2823.2	0.011271	0.169926	0.818802
Ex 385, em 560	0.171	37.0	0.499	575.3	0.336	2808.8	0.005114	0.232044	0.762842

Overall, we found this collaboration promising in that we were able to determine another structure-function correlation with CQDs by observing the clear difference between the core and defect emissive states in GQDs and CNDs. There was also a distinct change in both the relative contributions and lifetimes of GQDs when chemically or hydrothermally reduced. This supports the importance of the "molecule-like state" as first discussed by Wang *et al.* in the overall fluorescence of GQDs and CNDs.[50] Finally, a third, very short-lived time component emerges upon studying the bottom-up synthesized CNDs. In this way, we were able to determine the effect that complete surface passivation has on observed fluorescence lifetimes. In the future, this author hopes to continue this collaboration and determine further the structure-function relationship in heteroatom-doped and other post-synthesis modified CQDs.

2.5   Chapter 2 References

1. Zhang, Z.; Zheng, T.; Li, X.; Xu, J.; Zeng, H., Progress of Carbon Quantum Dots in Photocatalysis Applications. *Particle & Particle Systems Characterization* **2016,** *33* (8), 457-472.

2. Li, F.; Tian, F.; Liu, C.; Wang, Z.; Du, Z.; Li, R.; Zhang, L., One-step synthesis of nanohybrid carbon dots and TiO2composites with enhanced ultraviolet light active photocatalysis. *RSC Adv.* **2015,** *5* (11), 8389-8396.

3. Martins, N. C. T.; Ângelo, J.; Girão, A. V.; Trindade, T.; Andrade, L.; Mendes, A., N-doped carbon quantum dots/TiO2 composite with improved photocatalytic activity. *Applied Catalysis B: Environmental* **2016,** *193*, 67-74.

4. Yu, H.; Zhao, Y.; Zhou, C.; Shang, L.; Peng, Y.; Cao, Y.; Wu, L.-Z.; Tung, C.-H.; Zhang, T., Carbon quantum dots/TiO2 composites for efficient photocatalytic hydrogen evolution. *Journal of Materials Chemistry A* **2014,** *2* (10), 3344-3351.

5. Hu, C.; Yu, C.; Li, M.; Wang, X.; Dong, Q.; Wang, G.; Qiu, J., Nitrogen-doped carbon dots decorated on graphene: a novel all-carbon hybrid electrocatalyst for enhanced oxygen reduction reaction. *Chemical Communications* **2015,** *51* (16), 3419-3422.

6. Lei, Z.; Xu, S.; Wan, J.; Wu, P., Facile synthesis of N-rich carbon quantum dots by spontaneous polymerization and incision of solvents as efficient bioimaging probes and advanced electrocatalysts for oxygen reduction reaction. *Nanoscale* **2016,** *8* (4), 2219-2226.

7. Shen, J.; Li, Y.; Su, Y.; Zhu, Y.; Jiang, H.; Yang, X.; Li, C., Photoluminescent carbon-nitrogen quantum dots as efficient electrocatalysts for oxygen reduction. *Nanoscale* **2015,** *7* (5), 2003-2008.

8. Chandra, S.; Pathan, S. H.; Mitra, S.; Modha, B. H.; Goswami, A.; Pramanik, P., Tuning of photoluminescence on different surface functionalized carbon quantum dots. *Rsc Advances* **2012,** *2* (9), 3602-3606.

9. Do, S.; Kwon, W.; Rhee, S.-W., Soft-template synthesis of nitrogen-doped carbon nanodots: tunable visible-light photoluminescence and phosphor-based light-emitting diodes. *Journal of Materials Chemistry C* **2014,** *2* (21), 4221-4226.

10. Hola, K.; Zhang, Y.; Wang, Y.; Giannelis, E. P.; Zboril, R.; Rogach, A. L., Carbon dots-Emerging light emitters for bioimaging, cancer therapy and optoelectronics. *Nano Today* **2014,** *9* (5), 590-603.

11. Sk, M. A.; Ananthanarayanan, A.; Huang, L.; Lim, K. H.; Chen, P., Revealing the tunable photoluminescence properties of graphene quantum dots. *Journal of Materials Chemistry C* **2014,** *2* (34), 6954-6960.

12. Zhu, S. J.; Song, Y. B.; Zhao, X. H.; Shao, J. R.; Zhang, J. H.; Yang, B., The photoluminescence mechanism in carbon dots (graphene quantum dots, carbon nanodots, and polymer dots): current state and future perspective. *Nano Research* **2015,** *8* (2), 355-381.

13. Zhu, S. J.; Zhang, J. H.; Liu, X.; Li, B.; Wang, X. F.; Tang, S. J.; Meng, Q. N.; Li, Y. F.; Shi, C.; Hu, R.; Yang, B., Graphene quantum dots with controllable surface oxidation, tunable fluorescence and up-conversion emission. *Rsc Advances* **2012,** *2* (7), 2717-2720.

14. Kim, T. H.; Ho, H. W.; Brown, C. L.; Cresswell, S. L.; Li, Q., Amine-rich carbon nanodots as a fluorescence probe for methamphetamine precursors. *Analytical Methods* **2015,** *7* (16), 6869-6876.

15. Kundu, A.; Nandi, S.; Das, P.; Nandi, A. K., Facile and green approach to prepare fluorescent carbon dots: Emergent nanomaterial for cell imaging and detection of vitamin B2. *J Colloid Interface Sci* **2016,** *468*, 276-83.

16. Liu, S. Y.; Zhao, N.; Cheng, Z.; Liu, H. G., Amino-functionalized green fluorescent carbon dots as surface energy transfer biosensors for hyaluronidase. *Nanoscale* **2015,** *7* (15), 6836-6842.

17. Hu, C.; Yu, C.; Li, M. Y.; Wang, X. N.; Yang, J. Y.; Zhao, Z. B.; Eychmuller, A.; Sun, Y. P.; Qiu, J. S., Chemically Tailoring Coal to Fluorescent Carbon Dots with Tuned Size and Their Capacity for Cu(II) Detection. *Small* **2014,** *10* (23), 4926-4933.

18. Ju, J.; Chen, W., Synthesis of highly fluorescent nitrogen-doped graphene quantum dots for sensitive, label-free detection of Fe (III) in aqueous media. *Biosensors & Bioelectronics* **2014,** *58*, 219-225.

19. Liu, Y.; Liao, M.; He, X. L.; Liu, X.; Kou, X. M.; Xiao, D., One-step Synthesis of Highly Luminescent Nitrogen-doped Carbon Dots for Selective and Sensitive Detection of Mercury(II) Ions and Cellular Imaging. *Analytical Sciences* **2015,** *31* (10), 971-977.

20. Zhang, R.; Chen, W., Nitrogen-doped carbon quantum dots: Facile synthesis and application as a "turn-off" fluorescent probe for detection of Hg2+ ions. *Biosensors & Bioelectronics* **2014,** *55*, 83-90.

21. Choi, Y.; Kim, S.; Choi, M. H.; Ryoo, S. R.; Park, J.; Min, D. H.; Kim, B. S., Highly Biocompatible Carbon Nanodots for Simultaneous Bioimaging and Targeted Photodynamic Therapy In Vitro and In Vivo. *Advanced Functional Materials* **2014,** *24* (37), 5781-5789.

22. Ge, J.; Lan, M.; Zhou, B.; Liu, W.; Guo, L.; Wang, H.; Jia, Q.; Niu, G.; Huang, X.; Zhou, H.; Meng, X.; Wang, P.; Lee, C.-S.; Zhang, W.; Han, X., A graphene quantum dot photodynamic therapy agent with high singlet oxygen generation. *Nature Communications* **2014,** *5*, 4596.

23. Zhu, S.; Meng, Q.; Wang, L.; Zhang, J.; Song, Y.; Jin, H.; Zhang, K.; Sun, H.; Wang, H.; Yang, B., Highly Photoluminescent Carbon Dots for Multicolor Patterning, Sensors, and Bioimaging. *Angewandte Chemie-International Edition* **2013,** *52* (14), 3953-3957.

24. Zhao, A. D.; Chen, Z. W.; Zhao, C. Q.; Gao, N.; Ren, J. S.; Qu, X. G., Recent advances in bioapplications of C-dots. *Carbon* **2015,** *85*, 309-327.

25. Fan, Z. T.; Li, S. H.; Yuan, F. L.; Fan, L. Z., Fluorescent graphene quantum dots for biosensing and bioimaging. *Rsc Advances* **2015,** *5* (25), 19773-19789.

26. Tetsuka, H.; Asahi, R.; Nagoya, A.; Okamoto, K.; Tajima, I.; Ohta, R.; Okamoto, A., Optically Tunable Amino-Functionalized Graphene Quantum Dots. *Advanced Materials* **2012,** *24* (39), 5333-5338.

27. Jin, S. H.; Kim, D. H.; Jun, G. H.; Hong, S. H.; Jeon, S., Tuning the Photoluminescence of Graphene Quantum Dots through the Charge Transfer Effect of Functional Groups. *ACS Nano* **2013,** *7* (2), 1239-1245.

28. Li, Y.; Shu, H.; Niu, X.; Wang, J., Electronic and Optical Properties of Edge-Functionalized Graphene Quantum Dots and the Underlying Mechanism. *The Journal of Physical Chemistry C* **2015,** *119* (44), 24950-24957.

29. Wang, H.; Sun, P.; Cong, S.; Wu, J.; Gao, L.; Wang, Y.; Dai, X.; Yi, Q.; Zou, G., Nitrogen-Doped Carbon Dots for "green" Quantum Dot Solar Cells. *Nanoscale Res Lett* **2016,** *11* (1), 27.

30. Zheng, B. Z.; Liu, T.; Paau, M. C.; Wang, M. N.; Liu, Y.; Liu, L.; Wu, C. F.; Du, J.; Xiao, D.; Choi, M. M. F., One pot selective synthesis of water and organic soluble carbon dots with green fluorescence emission. *Rsc Advances* **2015,** *5* (15), 11667-11675.

31. Chen, X. X.; Jin, Q. Q.; Wu, L. Z.; Tung, C. H.; Tang, X. J., Synthesis and Unique Photoluminescence Properties of Nitrogen-Rich Quantum Dots and Their Applications. *Angewandte Chemie-International Edition* **2014,** *53* (46), 12542-12547.

32. Zhu, S.; Zhang, J.; Tang, S.; Qiao, C.; Wang, L.; Wang, H.; Liu, X.; Li, B.; Li, Y.; Yu, W.; Wang, X.; Sun, H.; Yang, B., Surface Chemistry Routes to Modulate the Photoluminescence of Graphene Quantum Dots: From Fluorescence Mechanism to Up-Conversion Bioimaging Applications. *Advanced Functional Materials* **2012,** *22* (22), 4732-4740.

33. Wang, L.; Zhu, S. J.; Wang, H. Y.; Qu, S. N.; Zhang, Y. L.; Zhang, J. H.; Chen, Q. D.; Xu, H. L.; Han, W.; Yang, B.; Sun, H. B., Common Origin of Green Luminescence in Carbon Nanodots and Graphene Quantum Dots. *Acs Nano* **2014,** *8* (3), 2541-2547.

34. Huang, J.; Deming, C. P.; Song, Y.; Kang, X.; Zhou, Z.-Y.; Chen, S., Chemical analysis of surface oxygenated moieties of fluorescent carbon nanoparticles. *Nanoscale* **2012,** *4* (3), 1010-1015.

35. Alves, L. A.; de Castro, A. H.; de Mendonça, F. G.; de Mesquita, J. P., Characterization of acid functional groups of carbon dots by nonlinear regression data fitting of potentiometric titration curves. *Applied Surface Science* **2016,** *370*, 486-495.

36. Dong, Y.; Shao, J.; Chen, C.; Li, H.; Wang, R.; Chi, Y.; Lin, X.; Chen, G., Blue luminescent graphene quantum dots and graphene oxide prepared by tuning the carbonization degree of citric acid. *Carbon* **2012,** *50* (12), 4738-4743.

37. Wang, Y.; Herron, N., Nanometer-sized semiconductor clusters: materials synthesis, quantum size effects, and photophysical properties. *The Journal of Physical Chemistry* **1991,** *95* (2), 525-532.

38. Dong, Y.; Wang, R.; Li, H.; Shao, J.; Chi, Y.; Lin, X.; Chen, G., Polyamine-functionalized carbon quantum dots for chemical sensing. *Carbon* **2012,** *50* (8), 2810-2815.

39. Zhang, Y. L.; Wang, L.; Zhang, H. C.; Liu, Y.; Wang, H. Y.; Kang, Z. H.; Lee, S. T., Graphitic carbon quantum dots as a fluorescent sensing platform for highly efficient detection of Fe3+ ions. *Rsc Advances* **2013,** *3* (11), 3733-3738.

40. Huang, H.; Li, C. G.; Zhu, S. J.; Wang, H. L.; Chen, C. L.; Wang, Z. R.; Bai, T. Y.; Shi, Z.; Feng, S. H., Histidine-Derived Nontoxic Nitrogen-Doped Carbon Dots for Sensing and Bioinnaging Applications. *Langmuir* **2014,** *30* (45), 13542-13548.

41. Gaddam, R. R.; Vasudevan, D.; Narayan, R.; Raju, K., Controllable synthesis of biosourced blue-green fluorescent carbon dots from camphor for the detection of heavy metal ions in water. *Rsc Advances* **2014,** *4* (100), 57137-57143.

42. Algarra, M.; Campos, B. B.; Radotic, K.; Mutavdzic, D.; Bandosz, T.; Jimenez-Jimenez, J.; Rodriguez-Castellon, E.; da Silva, J., Luminescent carbon nanoparticles: effects of chemical functionalization, and evaluation of Ag+ sensing properties. *Journal of Materials Chemistry A* **2014,** *2* (22), 8342-8351.

43. Wang, L.; Li, B.; Xu, F.; Shi, X.; Feng, D.; Wei, D.; Li, Y.; Feng, Y.; Wang, Y.; Jia, D.; Zhou, Y., High-yield synthesis of strong photoluminescent N-doped carbon nanodots derived from hydrosoluble chitosan for mercury ion sensing via smartphone APP. *Biosens Bioelectron* **2016,** *79*, 1-8.

44. Sun, H.; Gao, N.; Wu, L.; Ren, J.; Wei, W.; Qu, X., Highly Photoluminescent Amino-Functionalized Graphene Quantum Dots Used for Sensing Copper Ions. *Chemistry-a European Journal* **2013,** *19* (40), 13362-13368.

45. Liu, L.; Li, Y.; Zhan, L.; Liu, Y.; Huang, C., One-step synthesis of fluorescent hydroxyls-coated carbon dots with hydrothermal reaction and its application to optical sensing of metal ions. *Science China Chemistry* **2011,** *54* (8), 1342.

46. Huang, H.; Liao, L.; Xu, X.; Zou, M.; Liu, F.; Li, N., The electron-transfer based interaction between transition metal ions and photoluminescent graphene quantum dots (GQDs): A platform for metal ion sensing. *Talanta* **2013,** *117*, 152-157.

47. Zeng, D.; Cheng, J.; Ren, S.; Sun, J.; Zhong, H.; Xu, E.; Du, J.; Fang, Q., A new sensor for copper(II) ion based on carboxyl acid groups substituted polyfluoreneethynylene. *Reactive and Functional Polymers* **2008,** *68* (12), 1715-1721.

48. Konkena, B.; Vasudevan, S., Understanding Aqueous Dispersibility of Graphene Oxide and Reduced Graphene Oxide through pKa Measurements. *The Journal of Physical Chemistry Letters* **2012,** *3* (7), 867-872.

49. S. Isaacs, N.; van Eldik, R., A mechanistic study of the reduction of quinones by ascorbic acid. *Journal of the Chemical Society, Perkin Transactions 2* **1997,** (8), 1465-1468.

50. Wang, L.; Zhu, S. J.; Wang, H. Y.; Wang, Y. F.; Hao, Y. W.; Zhang, J. H.; Chen, Q. D.; Zhang, Y. L.; Han, W.; Yang, B.; Sun, H. B., Unraveling Bright Molecule-Like State and Dark Intrinsic State in Green-Fluorescence Graphene Quantum Dots via Ultrafast Spectroscopy. *Advanced Optical Materials* **2013,** *1* (3), 264-271.

Chapter 3: Temperature-Dependent Nitrogen Doping and its effect on the Optical Properties of Graphene Quantum Dots

Parts of this chapter including text and images are taken from the published work "Differentiating the Impact of Nitrogen Chemical States on Optical Properties of Nitrogen-Doped Graphene Quantum Dots" *RSC Advances, 2017, 7, 48263 - 48267* with permission from the Royal Society of Chemistry. The aim of this work is to fundamentally understand the optical properties of top-down synthesized oxidized graphene quantum dots (ox-GQDs) and nitrogen-incorporated graphene quantum dots (N-GQDs). Nitrogen dopants were introduced by controlling hydrothermal temperature during post-synthetic addition of aqueous ammonia. This was found to be an effective method to incorporate different chemical states of nitrogen atoms into GQDs: amine, pyridinic, pyrrolic, and quaternary N. Each of these chemical states were identified using various characterization techniques and related to optical properties. The results herein show that hydrothermal treatment temperatures below 150 °C produce primarily surface-terminated amines and amides. Above 150 °C, nitrogen chemical states were dominated by pyridinic, pyrrolic and quaternary N. Additionally, pH-sensitive chemical states (amines and pyridines) were studied to investigate the pH-tunable chemical states and observed fluorescence.

3.1   Introduction and Motivation for Study

Graphene quantum dots (GQDs) are an emerging carbon-based nanomaterial with unique chemical structure and optical properties. Various methods have been utilized for the top-down synthesis of GQDs, including: chemical oxidation,[1-3] electrochemical preparation,[4] hydrothermal cutting,[5] and electric arc method.[6] The chemical structure of GQDs constitutes two components: a sp^2-hybridized graphitic domain and abundant chemical functional groups surrounding it. The band gap of GQDs can be tuned by modifying these components. First, the physical dimension of GQDs such as size and thickness influences band gap. Second, the band gap can be tuned by introducing heteroatoms either by modifying surface functional groups of GQDs or substituting carbon atoms in nanographene sheets.[7-10] These modifications enable the tuning of not only electronic property of GQDs but also their interfacial properties, thereby making

GQDs attractive for many applications such as bioimaging,[11] photodynamic therapy, [12] wound disinfection,[13] heavy metal sensing,[14] electrocatalysis,[15] and photovoltaic devices.[16] GQDs are more biocompatible than other types of carbon nanomaterials, for example, carbon nanotubes, graphene, and graphene oxide.[17-18] GQDs have a potential to replace expensive and toxic inorganic quantum dots such as CdSe.

Nitrogen is one of the most studied heteroatoms in the research of carbon materials. With five valence electrons, nitrogen has the role of electron donor in a carbonaceous system. Recent literature demonstrated the red-shifted photoluminescence (PL) of nitrogen-containing GQDs with enhanced quantum yield.[7-8] The red-shifted PL was attributed to the reduction of band gap. The incorporation of nitrogen atoms into a sp^2 carbon framework in the bottom-up synthesis of CQDs has likewise shown increased QY but with blue shifting of PL due to the strong electron affinity of nitrogen atoms which invokes a partial positive charge on adjacent carbon atoms.[19-20] In addition to optical properties, nitrogen doping on carbon nanomaterials have been shown to enhance the electrocatalytic activity toward oxygen reduction reaction (ORR).[19]

Recently, Tetsuka *et al.* reported that absorption/emission properties of amino-functionalized GQDs were finely tuned by controlling hydrothermal temperature from 70 °C to 150 °C.[7] In this report, the shift of spectral position and the enhancement of fluorescence intensity were mostly attributed to N-related surface functionalities such as primary amines and amides. However, the role of edge-terminating nitrogen sites, i.e.: pyridines and pyrroles, and core N sites such as quaternary N were largely neglected. The maximum content of nitrogen atoms was observed at the lowest hydrothermal temperature and the content of nitrogen became reduced as the temperature was raised.[7] In support of these experimental observations, a recent computational work likewise shows the quantity of amine N is connected to the red-shifted behavior of GQDs.[8] In contrast to the Tetsuka study, a recent article brought about the importance of pyridinic, pyrrolic and quaternary N sites. This study employed much higher hydrothermal temperatures (>150 °C) and observed blue-shifted emission with higher quantum yield (Φ = 34.5%).[9] Until now, there were very few studies differentiating the effect of different N chemical states (i.e., amines, pyridines,

pyrroles) on the optical properties of top-down-synthesized GQDs. However, a recent work by Qu *et al*. has shown a pronounced differentiation of pyrrolic and graphitic N states in the bottom-up synthesized carbon nanodots.[21] This report utilizes the hydrothermal dehydration of urea and citric acid to show a direct correlation between the quantity of graphitic N and increase of PLQY. In addition, varying the nitrogen source from urea to ethylenediamine greatly enhanced the PLQY to 94%. Carbon nanodots made in this way have also been employed as fluorescent probes for *in vitro* and *in vivo* studies with excellent cellular uptake and biocompatibility in mice.[22]

In this study, hydrothermal temperature was controlled as an effective method to incorporate different chemical states of nitrogen atoms into GQDs. Four different chemical states of nitrogen atoms (amine, pyridinic, pyrrolic, and quaternary) were identified and related to absorption/emission properties. Moreover, pH-dependent emission spectra was studied to probe chemical states of nitrogen atoms and to investigate the relation between nitrogen location and emission.

3.2   Materials, Methods and Characterization

Carbon nano-onions were prepared by the thermal annealing of commercially available nanodiamond powders (Nanostructured and Amorphous Materials, Inc., Houston, TX) at 1650 °C for 1h under the flow of helium in a graphitization furnace. H_2SO_4, HNO_3, K_2CO_3 and NH_4OH were purchased from Sigma-Aldrich. The 200 mL stainless steel hydrothermal reactor houses a PTFE sample chamber in which the ox-GQDs were reacted with aqueous ammonia. All samples were dialyzed against deionized water in 1 kDa MWCO dialysis bags purchased from Spectrum Labs.

The size of GQDs and N-GQDs were characterized by a JEOL JEM-2200FS, 200 kV electron acceleration voltage TEM and the thickness was measured with a Park Systems XE-70 AFM operating in non-contact mode. TEM samples were prepared by dipping a TEM copper grid (Ted Pella, lacey carbon support film) into a dilute solution of GQD sample. AFM samples were prepared by dropping 5 μL GQD sample onto a mica substrate disc and spin casting to dry. FTIR spectra were taken with a Thermo Scientific Model Nicolet 6700 FTIR Spectrometer operating with a diamond ATR crystal. FTIR samples were prepared by dropping 5 μL GQD samples onto the ATR

crystal and drying in an oven until a thick film was observed. The XPS characterization was conducted with a Thermo Scientific Model K-Alpha XPS instrument. The XPS samples were prepared by dropping 5 µL of GQD sample onto a silicon wafer and drying between depositions until a thick film could be observed. Absorption spectra were collected with a Thermo Scientific Evolution 201 Spectrophotometer and emission spectra were recorded with a Jobin-Yvon Spectromax 4 Spectrofluorometer. Optical properties were measured using a quartz cuvette with 10 mm path length. Photoluminescent quantum yield measurements (PLQY) were taken using the Integrating Sphere Attachment on the Horiba Fluoromax-C-Plus. The excitation slit width is 0.2 nm and the emission slit width is 2 nm for all samples.

The synthesis of oxidized GQDs (ox-GQDs) and the subsequent nitrogen incorporation (N-GQDs) are described as follows. ox-GQDs were prepared by reacting 100 mg of carbon nanoonions with a 1 : 3 ratio of concentrated H_2SO_4 : HNO_3 under 95 °C reflux and vigorous stirring for 4 hours. The reaction was terminated when the reflux solution became clear and brownish in color. Afterwards, this solution was first centrifuged at 4000 rpm for 90 minutes to allow the precipitation of unreacted carbon nano-onions. Then, the supernatant was neutralized with K_2CO_3 and dialyzed for 6 days with a dialysis bag (1 kDa MWCO) to remove excess ions from the neutralization. After dialysis, the resulting solution contains the purified ox-GQD in water. N-GQDs were prepared by reacting ox-GQDs with NH_4OH in a hydrothermal reactor, as similar to the report by Tetsuka *et al.*[7] First, ox-GQDs were mixed with 5.0 M NH_4OH (1:2 v/v). The mixture was then placed into a 200 mL stainless steel autoclave reactor for 5 hours. The hydrothermal temperature of the reaction was varied from 90–190 °C. N-GQD-X prepared at a specific temperature such as 150 °C will now be referred as NGQD-150. A simplified scheme of this procedure is shown below in Scheme 3.1.
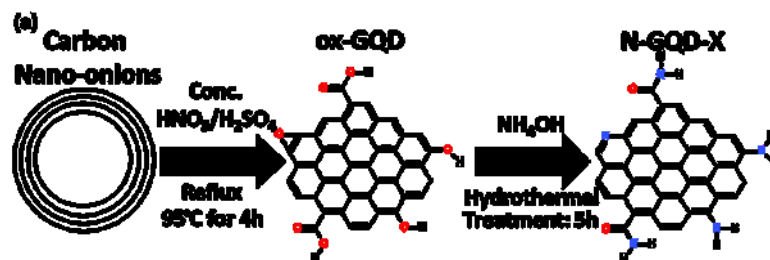
Scheme 3.1: Synthetic scheme of ox-GQD and N-GQD-X. Structures are representative and do not reflect the exact chemical structure of carbon nano-onions, ox-GQDs, and N-GQDs.

Morphology and chemical structure are important factors to determine the optical behaviour of ox-GQDs and N-GQDs. The size and the thickness of ox-GQDs and N-GQDs were characterized by TEM (JEOL JEM-2200FS, 200 kV) and atomic force microscopic (AFM) characterizations (Park Systems XE-70). The results of TEM and AFM characterizations are shown in Fig. 3.1b-g. The size of ox-GQDs varies from 20-30 nm. As the functional groups are modified, electrostatic interactions and hydrogen bonding may induce some amount of aggregation which can be seen for N-GQDs. AFM characterization of ox-GQDs and N-GQDs revealed isolated particles. As shown in the histogram (Fig. 3.1f and 3.1g), both ox-GQD and N-GQD show an average thickness of 2.5 nm, indicating that both particles are made of multiple stacks of graphene nanosheets.[5]
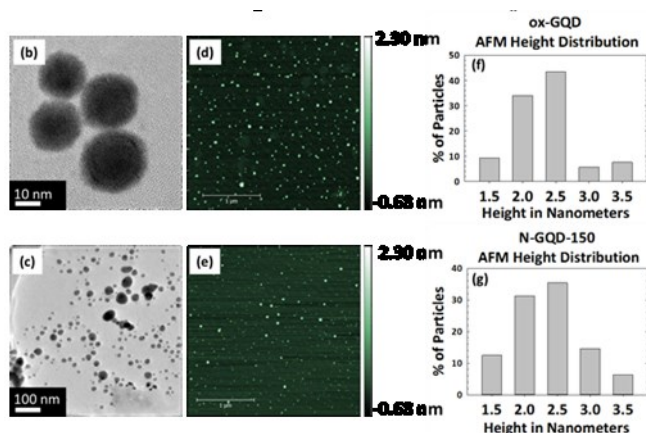
Figure 3.1: TEM images of ox-GQD (b) and N-GQD (c), AFM images of ox-GQD (d) and N-GQD (e), and the histogram of the thickness of ox-GQDs (f) and N-GQDs (g).

Hydrothermal temperature (90 – 190 °C) greatly influenced the chemical functionalities and the incorporated nitrogen atoms in N-GQDs prepared. The chemical structure of N-GQDs and chemical states of nitrogen incorporated were probed by FT-IR and XPS analyses. FT-IR spectra were recorded with a Thermo Scientific Model Nicolet 6700 FT-IR Spectrometer and are displayed in Fig. 3.2. As shown in Fig. 3.2, FT-IR spectra of ox-GQD exhibited the presence of hydroxyl, carbonyl and carboxyl groups located at 1000 cm^{-1} (C-O), 1700 cm^{-1} (C=O), 2500 cm^{-1} (CO$_2$H) and 3300 cm^{-1} (-OH), respectively. Compared to ox-GQDs, a new peak appeared at 1070 cm^{-1} in N-GQD-150, which is assigned to C-N bond. In addition, the peak at 1700 cm^{-1} became broadened due to the overlay of amide and carbonyl C=O. The carboxylic acid peak at 2500 cm^{-1} was suppressed in N-GQD-150, supporting the conversion of carboxylic group into amine or amide. Most notably, the broad peak at 3300 cm^{-1} in ox-GQD due to hydrogen bonded O-H stretching became much narrower in N-GQD, indicating the substitution of hydroxyls to primary and secondary amines.

XPS characterization was conducted with a Thermo Scientific Model K-Alpha XPS instrument. The high resolution spectra were deconvoluted using Avantage software by Thermo Scientific. Peak position for each chemical state is detailed in the main text as well as in Table 3.1. XPS analyses were conducted after drying of GQD solution mounted on a silicon wafer. Fig. 3.3a shows hypothetical structure of N-GQDs where nitrogen atoms are incorporated into various sites. The nitrogen-incorporated sites include pyridinic N (398.5 eV, N1), amine N (399.7 eV, N2), pyrrolic N (400.2 eV, N3), and quaternary N (401.3 eV, N4). N1s peaks were assigned according to the NIST Standard Reference Database.[23] The assignments of XPS peaks to different chemical states by previous studies and this report are summarized in Table 3.1.
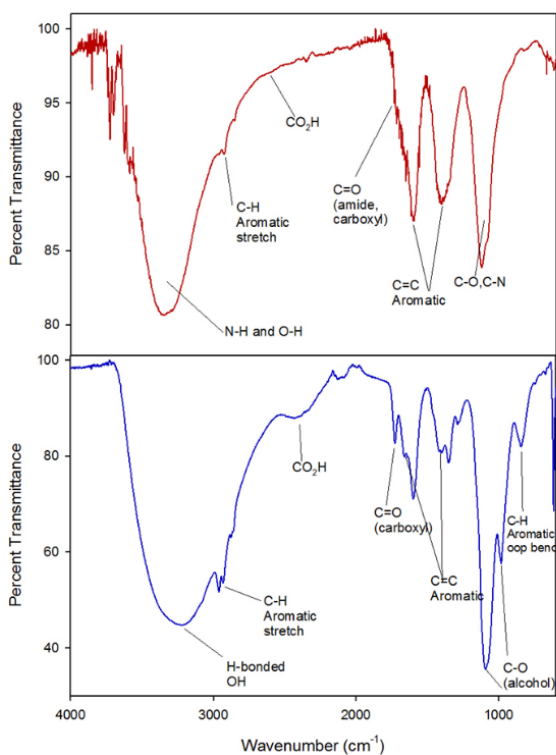
Figure 3.2: FTIR Spectra of N-GQD-150 (top) and ox-GQD (bottom).

Table 3.1: XPS N1s peak assignments in recent literature and this work.

Experimental Work	Year Published	~398.5 eV	~399.5 eV	~400 eV	>401 eV
Tetsuka et al.[7]	2012	---	Amine N (399.7 eV)	---	---
Dai et al.[9]	2014	---	Pyrrolic N (399.7 eV)	---	Graphitic N (401.6 eV)
Li et al.[10]	2012	Pyridinic N (398.5 eV)	---	---	Pyrrolic N (401 eV)
NIST Database[23]	2012	Pyridinic N (398.6 eV)	Amine N (399.4 eV)	Pyrrolic N (399.9 eV)	Graphitic N (401.3 eV)
This work	2015	Pyridinic N (398.5 eV)	Amine N (399.3 eV)	Pyrrolic N (400.2 eV)	Graphitic N (401.3 eV)

Fig. 3.3 shows the high resolution XPS N1s peaks of N-GQDs synthesized at N-GQD-90, N-GQD-150, and N-GQD-190. The high resolution XPS N1s peaks of N-GQDs were deconvoluted to resolve the relative fraction of N1, N2, N3 and N4. While N-GQD-90 and N-GQD-150 are mainly deconvoluted with N1, N2, and N3, the N-GQD-190 showed the significant fraction of N4 (quaternary N). Fig. 3.3b shows the evolution of the relative fraction of N1 - N4 sites present in N-GQDs synthesized at different hydrothermal temperature. Clearly, the total N content of N-GQDs increased from 5% to 8% when hydrothermal temperature was raised up to 150 °C. Then the content of N went down at 170 °C and 190 °C. The reduction of nitrogen content for N-GQD-170 and N-GQD-190 is likely due to the hydrothermal cutting of ox-GQD, as consistent with the results reported by Luo *et al.*[24] Overall, the content of amine groups (N2) tends to go down as temperature becomes higher. On the other hand, the content of other types of N edge sites such as pyridinic (N1) and pyrrolic (N3) rises until the temperature reaches 150 °C. At the temperature above 150 °C, the relative fraction of pyridinic N and pyrrolic N decrease. These N sites are converted to quaternary N in N-GQD-190.
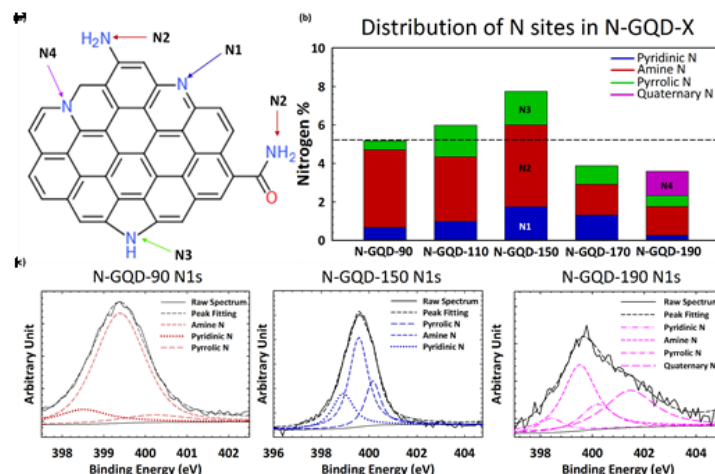
Figure 3.3: (a) A simplified representation of nitrogen-incorporated GQDs. The four chemical states of nitrogen are listed as N1 (pyridinic), N2, (amine/amide), N3 (pyrrolic) and N4 (quaternary or graphitic). (b) The percentage of N chemical states in N-GQDs determined by N1s high resolution XPS spectra. The average nitrogen content (5.3 ± 1.7 %) is denoted by the dashed line. (c) High resolution XPS N1s spectra of N-GQD-90, N-GQD-150 and N-GQD-190.

3.3   Results, Discussion and Conclusions

Absorption and emission spectra of GQDs and N-GQDs were investigated. Absorption spectra were recorded with a Thermo Scientific Evolution 201 Spectrophotometer and Emission spectra were recorded with a Jobin-Yvon Spectromax 4 Spectrofluorometer. The excitation-dependent PL spectra for ox-GQD, N-GQD-90, N-GQD-150, and N-GQD-190 are shown in Figure 3.5. Fig. 3.4a shows the photograph of GQDs and N-GQDs dispersed in water under UV lamp (λ = 365 nm). While N-GQD-90 and N-GQD-150 show green to yellow emission, N-GQD-170 and N-GQD-190 exhibited much stronger blue emission.

Fig. 3.4b presents UV-VIS absorption spectra of ox-GQDs and N-GQDs. The UV-Vis absorption spectra display three bands (300nm, 370nm, and 470nm). The 300 nm peak of ox-GQDs is assigned to the π-π* transition and it is shifted to 280 nm in N-GQDs. This blue-shift is attributed to the strong electron affinity of nitrogen atoms, which were reported to enhance the delocalization of electrons in the graphene nanodomain.[9-10] The peak at 370 nm is prominent for all N-GQDs and it is assigned to the n-π* transition. This 370 nm band is shifted to shorter wavelength (350 nm) upon the increase of hydrothermal treatment temperature. This particular band is attributed to the effect of non-bonding orbitals from pyridinic N and pyrrolic N as previously described by Li *et al.*[10] Lastly, the absorbance band at 470 nm that relates to another surface state n-π* transition tends to become weaker as the hydrothermal temperature gets higher. The 470 nm band is likely due to the amine N and shows the maximum absorbance in N-GQD-90 as shown in a previous report.[7] From these results, the different surface states associated with pyridinic N, pyrrolic N, and amine N show their individual impact on the absorption profile of the N-GQD. It should also be noted that hydrothermal temperature-dependent evolutions of UV-VIS spectra are consistent with nitrogen-related chemical states revealed in the XPS analysis discussed above.
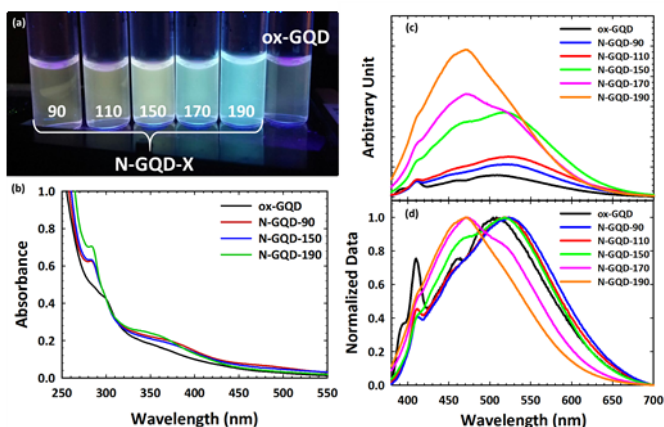
Figure 3.4: (a) The photograph of ox-GQDs and N-GQDs under a UV lamp (364 nm). (from left: N-GQD-90, N-GQD-110, N-GQD-150, N-GQD-170, N-GQD-190, and ox-GQD) (b) UV-visible absorbance, (c) emission spectra, and (d) normalized emission spectra of ox-GQDs and N-GQD-90, N-GQD-110, N-GQD-150, N-GQD-170, and N-GQD-190. Emission spectra of GQDs were taken at λ_{ex} = 360 nm.

Fig. 3.4c shows the emission spectra of ox-GQD and N-GQDs. Emission spectra were taken at excitation wavelength of 360 nm. As can be seen, emission intensity gradually increases as the hydrothermal temperature was raised. There are two major bands observed in the emission spectra of N-GQDs: 470 nm and 525 nm. Compared to ox-GQD, N-GQD-90 and N-GQD-110 show the red-shift of emission from 500 nm to 525 nm. The 525 nm emission is attributed to the surface state associated with amine N sites. N-GQD-150 shows the emergence of a prominent new band at 470 nm. This band is related to the maximal content of pyrrolic N.[10] For N-GQD-170, the emission at 525 nm is suppressed; however, the emission at 470 nm is greatly enhanced. Based upon the results of XPS analysis, the 470 nm emission comes primarily from pyrrolic N, while the 525 nm emission is related to the amine N sites. N-GQD-190 shows the emission enhancement at 470 nm is even greater and is assigned to the addition of quaternary N. The measured PLQY for the samples is as follows: ox-GQD = 0.48 %, N-GQD-90 = 2.51 %, N-GQD-150 = 10.07 %, N-GQD-190 = 5.89 %. Similarly with Qu *et al.*,[21] our results likewise show that the presence of pyrrolic N and quaternary N strongly contributes to the enhanced PLQY. Overall, the samples which were hydrothermally treated at low temperatures contain large concentrations of amine and pyridinic N and displayed red-shifted emission profiles. Conversely, high hydrothermal treatment temperatures drive nitrogen addition toward pyrrolic and quaternary N sites.

These absorption and emission results clearly demonstrate the resolved energetics of four different N-related chemical states in N-GQD.

In order to further probe surface functionalities of GQDs and N-GQDs, the emission of ox-GQD and N-GQDs was explored as a function of pH. The effects of tuning the quantity of carboxylic acids and phenols have been studied by Mei *et al.*[25] and Luo *et al.*[24] Both functional groups were found to promote non-radiative processes with red-shifted emission. Although pH-dependence of GQDs and polyethylene glycol (PEG)-modified GQDs were reported by Zhu *et al.*[26] and Jin *et al.,*[8] N-GQDs with primary amines/amides, pyridinic, etc. toward the change of pH has been rarely reported. In ox-GQDs, the pH-sensitive functional groups are carboxylic acids (pKa ~ 5) and phenols (pKa ~ 10). Fig. 3.6a shows the pH dependence of ox-GQDs shows a similar trend as previous reports.[8, 26] Major pH-induced changes observed for ox-GQDs are the enhancement of emission intensity from pH = 5 to pH = 7 and the suppression of emission intensity from pH = 7 to pH = 9. While pH influences the emission intensity of ox-GQD, a slight shift of emission position was also observed. The spectral position change is clearly coupled with the protonation/de-protonation of carboxylic acids and phenols around their respective pKa values. The origin may be due to either the variation of absorption cross-section in the formed charged species or non-radiative interaction with environment. The normalized emission spectra in Fig. 3.6b show slightly red-shifted emission maxima with increasing pH which can also be linked to additional non-radiative processes such as collisional quenching.
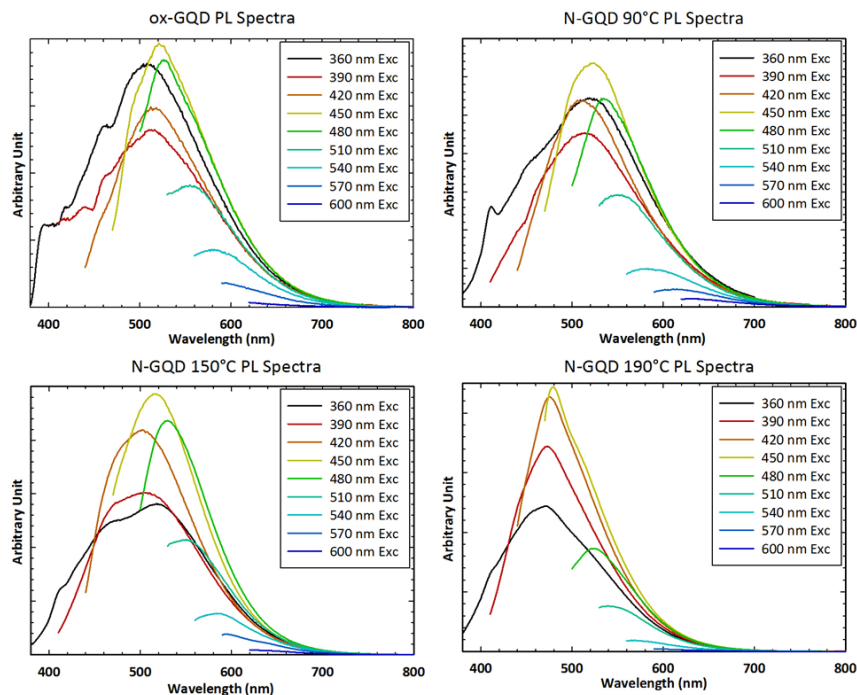
Figure 3.5: Emission spectra of ox-GQD (top left), N-GQD-90 (top right), N-GQD-150 (bottom left), and N-GQD-190 (bottom right).
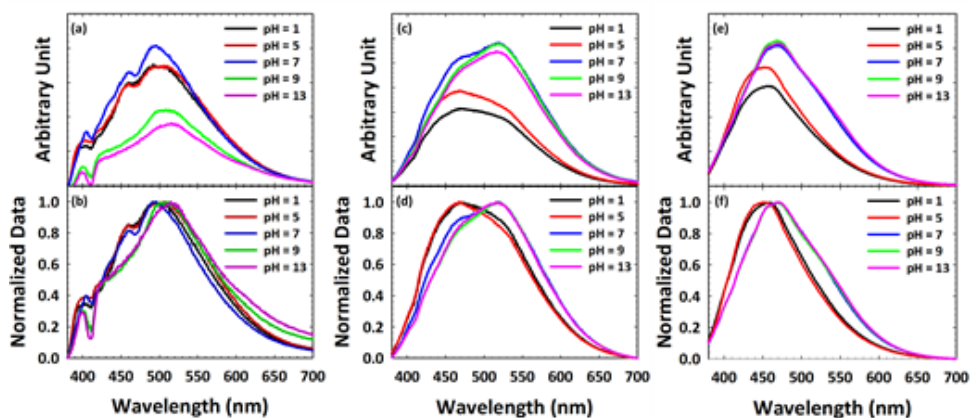
Figure 3.6: Emission spectra of (a,b) ox-GQD, (c,d) N-GQD-150 and (e,f) N-GQD-190 excited with 360 nm light plotted as a function of pH.

Figure 3.6c and 3.6d show the pH dependent emission of N-GQD-150. The most pronounced change in PL intensity is the significant emission enhancement at 520 nm from pH 5 to pH 7. Little change is observed above pH 7. This change of emission intensity is attributed to protonation/deprotonation of either pyridine N or amine N sites which both have a pKa ~ 5. The contrast between ox-GQDs and N-GQD-150 clearly indicates the difference in surface chemistry of the two GQDs. As reported in the work

by Luo[24], hydrothermal treatment removes hydroxyl groups, so little change in PL intensity above pH 7 is expected. The different behaviour of the emission peaks at 460 nm and 520 nm indicates that the two peaks have different origins. The normalized PL spectra of N-GQD-150 (Fig. 3.6d) show the red-shift of emission as the pH changes from 5 to 7.

The PL spectra of N-GQD-190 (Fig. 3.6e and f) shows the pH dependence similar to that of N-GQD-150, but to a lesser extent. This is likely due to the reduced total content of nitrogen in N-GQD-190, along with the smallest quantity of pH-sensitive functional groups (amine and pyridine) among all N-GQD samples. The origin of the emission around 470 nm in N-GQD-150 and N-GQD-190 is hypothesized as pyrrolic and quaternary nitrogen. These two functional groups have a negligible pH dependence in aqueous media, so the 470 nm emission would be unaffected by pH change. The enhanced emission intensity at pH > 7 is due to the contribution of 520 nm emission coming from amine and pyridinic N sites. As can be seen in Fig. 3.6e and 3.6f, N-GQD-190 also shows the red-shifted emission maxima but to a lesser degree due to its smaller quantity of amine and pyridinic N sites.

The results herein clearly demonstrate the relation between nitrogen-related surface states and emission property. Overall, with the increase of the hydrothermal temperature, the amount of pyridinic and pyrrolic nitrogens relative to amine nitrogen is enhanced. The total content of nitrogen atoms was found to be maximal at 150 °C. At lower temperatures, amine groups were predominant as a result of a kinetically-favored addition of aqueous ammonia. At higher temperature, surface amines are converted to edge-sites (pyridinic or pyrrolic), core N sites (quaternary), or partially removed signifying a thermodynamically favourable process. These results clearly differentiate the impact of N chemical states on optical behaviour of GQDs. This understanding is critical for developing finely tuned, high-performance nanoparticles that are also more environmentally-friendly. Fundamentally understanding the effects that specific nitrogen chemical states have on carbon nanomaterials will bolster their potential use in optoelectronics, bioimaging, photo- and electrocatalytic applications.

3.4   Chapter 3 References

1. Peng, J.; Gao, W.; Gupta, B. K.; Liu, Z.; Romero-Aburto, R.; Ge, L.; Song, L.; Alemany, L. B.; Zhan, X.; Gao, G.; Vithayathil, S. A.; Kaipparettu, B. A.; Marti, A. A.; Hayashi, T.; Zhu, J.-J.; Ajayan, P. M., Graphene Quantum Dots Derived from Carbon Fibers. *Nano Letters* **2012,** *12* (2), 844-849.

2. Dong, Y.; Chen, C.; Zheng, X.; Gao, L.; Cui, Z.; Yang, H.; Guo, C.; Chi, Y.; Li, C. M., One-step and high yield simultaneous preparation of single- and multi-layer graphene quantum dots from CX-72 carbon black. *Journal of Materials Chemistry* **2012,** *22* (18), 8764-8766.

3. Tao, H.; Yang, K.; Ma, Z.; Wan, J.; Zhang, Y.; Kang, Z.; Liu, Z., In Vivo NIR Fluorescence Imaging, Biodistribution, and Toxicology of Photoluminescent Carbon Dots Produced from Carbon Nanotubes and Graphite. *Small* **2012,** *8* (2), 281-290.

4. Shinde, D. B.; Pillai, V. K., Electrochemical Preparation of Luminescent Graphene Quantum Dots from Multiwalled Carbon Nanotubes. *Chemistry-a European Journal* **2012,** *18* (39), 12522-12528.

5. Pan, D. Y.; Zhang, J. C.; Li, Z.; Wu, M. H., Hydrothermal Route for Cutting Graphene Sheets into Blue-Luminescent Graphene Quantum Dots. *Advanced Materials* **2010,** *22* (6), 734-+.

6. Bottini, M.; Balasubramanian, C.; Dawson, M. I.; Bergamaschi, A.; Bellucci, S.; Mustelin, T., Isolation and Characterization of Fluorescent Nanoparticles from Pristine and Oxidized Electric Arc-Produced Single-Walled Carbon Nanotubes. *The Journal of Physical Chemistry B* **2006,** *110* (2), 831-836.

7. Tetsuka, H.; Asahi, R.; Nagoya, A.; Okamoto, K.; Tajima, I.; Ohta, R.; Okamoto, A., Optically Tunable Amino-Functionalized Graphene Quantum Dots. *Advanced Materials* **2012,** *24* (39), 5333-5338.

8. Jin, S. H.; Kim, D. H.; Jun, G. H.; Hong, S. H.; Jeon, S., Tuning the Photoluminescence of Graphene Quantum Dots through the Charge Transfer Effect of Functional Groups. *ACS Nano* **2013,** *7* (2), 1239-1245.

9. Dai, Y.; Long, H.; Wang, X.; Wang, Y.; Gu, Q.; Jiang, W.; Wang, Y.; Li, C.; Zeng, T. H.; Sun, Y.; Zeng, J., Doping: Versatile Graphene Quantum Dots with Tunable Nitrogen Doping. *Particle & Particle Systems Characterization* **2014,** *31* (5), 509-509.

10. Li, Y.; Zhao, Y.; Cheng, H.; Hu, Y.; Shi, G.; Dai, L.; Qu, L., Nitrogen-Doped Graphene Quantum Dots with Oxygen-Rich Functional Groups. *Journal of the American Chemical Society* **2012,** *134* (1), 15-18.

11. Zhu, S.; Zhang, J.; Qiao, C.; Tang, S.; Li, Y.; Yuan, W.; Li, B.; Tian, L.; Liu, F.; Hu, R.; Gao, H.; Wei, H.; Zhang, H.; Sun, H.; Yang, B., Strongly green-photoluminescent graphene quantum dots for bioimaging applications. *Chemical Communications* **2011,** *47* (24), 6858-6860.

12. Markovic, Z. M.; Ristic, B. Z.; Arsikin, K. M.; Klisic, D. G.; Harhaji-Trajkovic, L. M.; Todorovic-Markovic, B. M.; Kepic, D. P.; Kravic-Stevovic, T. K.; Jovanovic, S. P.; Milenkovic, M. M.; Milivojevic, D. D.; Bumbasirevic, V. Z.; Dramicanin, M. D.; Trajkovic, V. S., Graphene quantum dots as autophagy-inducing photodynamic agents. *Biomaterials* **2012,** *33* (29), 7084-7092.

13. Sun, H.; Gao, N.; Dong, K.; Ren, J.; Qu, X., Graphene Quantum Dots-Band-Aids Used for Wound Disinfection. *ACS Nano* **2014,** *8* (6), 6202-6210.

14. Sun, H.; Gao, N.; Wu, L.; Ren, J.; Wei, W.; Qu, X., Highly Photoluminescent Amino-Functionalized Graphene Quantum Dots Used for Sensing Copper Ions. *Chemistry-a European Journal* **2013,** *19* (40), 13362-13368.

15. Li, Q.; Zhang, S.; Dai, L.; Li, L.-s., Nitrogen-Doped Colloidal Graphene Quantum Dots and Their Size-Dependent Electrocatalytic Activity for the Oxygen Reduction Reaction. *Journal of the American Chemical Society* **2012,** *134* (46), 18932-18935.

16. Li, Y.; Hu, Y.; Zhao, Y.; Shi, G.; Deng, L.; Hou, Y.; Qu, L., An Electrochemical Avenue to Green-Luminescent Graphene Quantum Dots as Potential Electron-Acceptors for Photovoltaics. *Advanced Materials* **2011,** *23* (6), 776-780.

17. Zhang, R.; Liu, Y. B.; Sun, S. Q., Preparation of highly luminescent and biocompatible carbon dots using a new extraction method. *Journal of Nanoparticle Research* **2013,** *15* (10).

18. Wu, C.; Wang, C.; Han, T.; Zhou, X.; Guo, S.; Zhang, J., Insight into the Cellular Internalization and Cytotoxicity of Graphene Quantum Dots. *Advanced Healthcare Materials* **2013,** *2* (12), 1613-1619.

19. Gong, K.; Du, F.; Xia, Z.; Durstock, M.; Dai, L., Nitrogen-Doped Carbon Nanotube Arrays with High Electrocatalytic Activity for Oxygen Reduction. *Science* **2009,** *323* (5915), 760.

20. Wang, S.; Yu, D.; Dai, L., Polyelectrolyte Functionalized Carbon Nanotubes as Efficient Metal-free Electrocatalysts for Oxygen Reduction. *Journal of the American Chemical Society* **2011,** *133* (14), 5182-5185.

21. Qu, D.; Zheng, M.; Zhang, L.; Zhao, H.; Xie, Z.; Jing, X.; Haddad, R. E.; Fan, H.; Sun, Z., Formation mechanism and optimization of highly luminescent N-doped graphene quantum dots. *Scientific Reports* **2014,** *4*, 5294.

22. Zheng, M.; Liu, S.; Li, J.; Xie, Z.; Qu, D.; Miao, X.; Jing, X.; Sun, Z.; Fan, H., Preparation of highly luminescent and color tunable carbon nanodots under visible light excitation for in vitro and in vivo bio-imaging. *Journal of Materials Research* **2015,** *30* (22), 3386-3393.

23. A. V. Naumkin, A. K.-V., S. W. Gaarenstroom, C. J. Powell NIST XPS Standard Reference Database. Version 4.1.

24. Luo, P. H.; Qiu, Y.; Guan, X. F.; Jiang, L. Q., Regulation of photoluminescence properties of graphene quantum dots via hydrothermal treatment. *Physical Chemistry Chemical Physics* **2014,** *16* (35), 19011-19016.

25. Mei, Q.; Zhang, K.; Guan, G.; Liu, B.; Wang, S.; Zhang, Z., Highly efficient photoluminescent graphene oxide with tunable surface properties. *Chemical Communications* **2010,** *46* (39), 7319-7321.

26. Zhu, S. J.; Zhang, J. H.; Liu, X.; Li, B.; Wang, X. F.; Tang, S. J.; Meng, Q. N.; Li, Y. F.; Shi, C.; Hu, R.; Yang, B., Graphene quantum dots with controllable surface oxidation, tunable fluorescence and up-conversion emission. *RSC Advances* **2012,** *2* (7), 2717-2720.

Chapter 4: Photoluminescent and Electrochemical Properties of Nitrogen-doped Carbon Nanodots

It was hypothesized that bottom-up synthesized carbon quantum dots, commonly named as carbon nanodots (CNDs), were capable of achieving a higher quantum yield and exhibit greater catalytic activity due to the ease of incorporating nitrogen heteroatoms into the nanocarbon host. Motivated by this, we report the bottom-up synthesis of CNDs and the impact of added nitrogen on photoluminescence and electrochemical activity. A time-dependent pyrolytic synthesis followed by nitrogen addition via hydrothermal treatment is employed to elucidate the effect of nitrogen chemical states (amine, pyrrolic, pyridinic and graphitic N) on CND fluorescence. CNDs formed with short pyrolysis times were observed to uptake much more nitrogen than those formed with longer pyrolysis times. As a result, the quantum yield of CNDs made with short pyrolysis time followed by hydrothermal nitrogen treatment is much greater. We sought to extend this work by determining if there was a structure-function relationship between the degree of pyrolysis and the uptake of nitrogen heteroatoms on the electrocatalytic oxygen reduction reaction (ORR). As with optical properties, short pyrolysis time greatly enhanced the desirable four-electron ORR which is critical for implementing metal-free catalysts in fuel cells. This work illustrates the advantages of the bottom-up method toward optimizing heteroatom incorporation and their effects on optical and catalytic properties.

4.1   Introduction and Motivation

CNDs are one category of CQDs, in particular, prepared be the bottom-up synthesis of small organic precursors such as citric acid,[1] glucose,[2] ascorbic acid,[3] and folic acid.[4] CNDs are the counterpart of "top-down" synthesized graphene quantum dots (GQDs). Similar to GQDs, CNDs also have a myriad of synthetic methods such as thermopyrolysis,[1-2] hydrothermal preparation,[5-8] microwave-assisted pyrolysis,[9-12] and silane coupling.[13-14] The morphologies of CNDs are often spherical with[2, 13-16] or without[17-19] a clearly defined graphene nanodomain depending on their preparation.[1-2] One potentially important advantage of CNDs over GQDs is their capability to incorporate larger amounts of heteroatoms (B, N, and S) into their internal structure

with dopant concentrations as high as 20 wt %.[20] This can be done by adding heteroatom-containing molecules during the bottom-up synthesis. For example, adding a nitrogen source such as ethylenediamine to bottom-up synthetic methods has been extensively shown to greatly enhance their photoluminescent quantum yields (PLQY) several-fold compared to undoped counterparts.[15, 21-25]

Previously, Hu *et al.*[26] demonstrated the synthesis of nitrogen-doped CNDs with citric acid as the carbon source. CNDs were effectively synthesized via dehydration and condensation reactions to form new sp^2 C-C bonds. Furthermore, the CNDs produced with citric acid (22% nitrogen with ethylenediamine) give high PLQY with $\Phi = 0.55$ which are comparable to inorganic quantum dots.[27] Though this is an efficient method of synthesizing highly fluorescent CNDs with a high yield; the results often vary due to the inhomogeneity of nitrogen chemical states.[18, 28-29] While nitrogen incorporation into bottom-up synthesized CNDs shows a clear promise to promote PQY, the role of nitrogen content and its chemical states are unclear. If the location of heteroatom dopants in CND synthesis were finely controlled, the potential of CNDs in real world applications such as bioimaging,[2, 20, 30-32] sensing[15, 19, 24] and photocatalysis[33] could be truly realized.

Previous computational works reported controversial effects of specific chemical states of nitrogen in GQDs and CNDs. have been studied in theoretical simulations with varying interpretations. Sk *et al.*[34] reported that graphitic N lowers the band gap for GQDs by 0.97 eV when the nitrogen is edge-substituted and by 0.76 eV when nitrogen is center-substituted.[18] On the other hand, pyridinic and pyrrolic N was found to widen the band gap and shift emission toward shorter wavelengths. Increasing the atom percent of nitrogen in these simulations resulted in a larger blue shift. A computational work by Margraf *et al.*[35] for CNDs containing sp^2 nanodomains suggested geometric considerations more so than hybridization and heteroatom content could manipulate the electronic structure. In this simulation, nitrogen atoms were incorporated as amine, imine and cyano groups. It was found that heteroatoms modify the electronic structure by being incorporated in the sp^2-network, which is consistent with the aforementioned computational work on GQDs.[34]

In addition, Strauss *et al.*[10] reports that pyridinic N shifts the emission wavelength toward higher energy and increases the rates of radiative decay in CNDs. These simulations considered molecules with large sp^2-hybridized graphene planes much like GQDs. In the same report, CND luminescence was divided into two major mechanisms. First, emission at short wavelengths originates from the excitation of the intrinsic sp^2 nanodomain which is in agreement with previous reports.[36-37] Second, longer wavelength emission does not originate from the graphene-like nanodomain but rather through a separate excited state deactivation pathway; similar to the so-called defect state in previous experimental work.[36, 38] Xu *et al.*[39] proposed that the defect state is central to processes such as photoreduction of metal ions into metal nanoparticles by localizing the exciton to the surface of a CND. By this feature of exciton localization, Strauss *et al.*[10] found the ability for the CND to act as both an electron donor and an electron acceptor depending on the local environment. This result is promising as it expands the potential role of CNDs in optoelectronics[40] as well as photochemical water splitting.[41]

CNDs are particularly unique with characteristics such as: green chemistry synthesis with inexpensive reagents and a high yield, a uniform size distribution, and excellent photoluminescence performance. As previously mentioned, these attributes work in concert to create useful carbogenic nanoparticles for many applications. This work focuses on the incorporation of nitrogen into CNDs of varying degrees of carbonization. The two-step synthetic procedure is depicted in Figure 4.1. CNDs are formed from the pyrolysis of citric acid and followed by nitrogen addition via hydrothermal treatment. When the nitrogen addition is conducted in the early stages of pyrolysis, the hypothesis is that nitrogen atoms are both incorporated (graphitic N) and surface-terminated (pyridinic, pyrrolic and amine N). On the other hand, when the nitrogen addition was conducted after extended pyrolysis, nitrogen is hypothesized to be located preferentially in edge-defects. After synthesizing these two differently nitrogen-incorporated CNDs; their structure and optical properties were investigated. The presence of incorporated nitrogen is hypothesized to greatly enhance the fluorescent quantum yield over surface-terminated nitrogen functional groups. The hypothesis is supported by a recent work by Sun *et al.*[42] which shows that dopant

concentrations of graphitic N greatly enhance fluorescent quantum yield in GQDs. This works aims to further elucidate the structure-function relationship between added nitrogen heteroatoms in CNDs and optical properties as the aforementioned reports do not come to a consensus on the role of specific nitrogen chemical states. Additionally, we chose to pursue this work to make a strong comparison with the N-doped GQDs from Chapter 3.

As an extension of the chemical structure and optical properties relationship in CNDs, we hypothesized that the ease of nitrogenation found with the bottom-up approach would enable us to study the potential that carbon nanodots may have as electrocatalysts. N-doped carbon nanomaterials have been previously found to greatly enhance ORR activity.[39, 43-44] Recent literature demonstrates the use of NCNDs in electrochemical reactions such as the oxygen reduction reaction (ORR). This report shows the promise of using inexpensive reagents to produce effective fuel cell catalysts.[45] However, key details of the ORR catalytic process such as active sites, electron transfer number and product formation were generally unexplained and referred to previous works with analogous systems such as N-doped carbon nanotubes or graphene-based nanomaterials.

Though comparing NCNDs and their catalytically active sites to other nanomaterials is a natural course of scientific logic, it is this author's opinion that this explanation is not adequate for fundamental understanding. It is important to recall in Chapter 2 that bottom-up synthesized CQDs could have significant deviation from the carbon backbone of carbon nanotubes and graphene-like nanomaterials like graphene oxide or GQDs. Therefore, we began to explore the catalytic performance of NCNDs by utilizing them for ORR and critically analyzing the impact of specific nitrogen-containing functional groups on catalytic performance and electron transfer number.

4.2   Experimental Details and Methods

CNDs were prepared by adapting the previous work by Dong *et al.*[1] Two grams of citric acid (CA) powder were weighed into a 50 mL beaker and placed on a hotplate set to 160^0C. At first, CA is melted and the point at which all the CA is melted is referred to as t_0. At t_0, the pyrolysis of CA seems to occur by the formation of bubbles.

The bubbles are generated by the vaporization of water as well as gaseous carbon dioxide formed during the pyrolysis and carbonization of CA. About 1 minute after t_0, a uniformly pale yellow liquid is observed. The pyrolytic reaction was quenched by adding 100 mL of 0.1 M KOH solution. The obtained CNDs were labeled as "1 min CNDs". These CNDs seem to be a loose polymer of carbonized citric acid with a mixture of sp^2- and sp^3-hybridized carbon. The proposed structure of 1 min CNDs can be seen in Scheme 1. When the reaction continues to pyrolyze without KOH quenching, the color of the liquid changes from pale yellow to bright yellow, to orange, and finally to orange-red. The observed color change is consistent with the previous work by Dong *et al.* and is indicative of newly formed C-C sp^2-hybridized carbon.[1] At 10 minutes after t_0, the liquid becomes a deep red indicating more complete carbonization of CNDs. Any longer carbonization than 15 minutes using hotplate pyrolysis dries the product out and can burn the product. This can still create quantum dots, but their solubility in water is reduced and their photoluminescence was found to be negligible. The carbonization of CNDs is quenched by 100 mL of 0.1 M KOH solution and the resultant CNDs are labeled as "10 min CNDs". In order to remove the excess ions K^+ and OH^-, dialysis was performed on 1 min and 10 min CNDs using 1 kDa MWCO dialysis membranes for about 3 days. Both 1 min CNDs and 10 min CNDs were treated with aqueous ammonia in a Teflon-lined stainless steel autoclave reactor. The nitrogen-doped CNDs are referred to as "1 min NCNDs" and "10 min NCNDs". The hydrothermal treatment was conducted for 5 hours at 180 °C. The NCNDs were subjected to the same dialysis procedure to remove excess ammonia. All of the hydrothermally treated CNDs have a control solution of 1 min CNDs and 10 min CNDs that were subjected to the same hydrothermal conditions but in the absence of aqueous ammonia. These are referred to as "1 min HT-CNDs" and "10 min HT-CNDs", respectively.
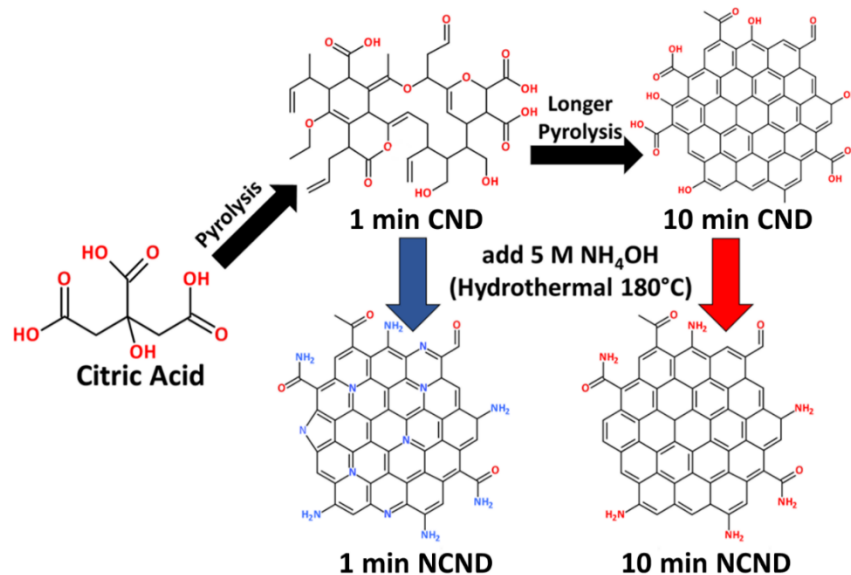
Scheme 4.1: Synthesis of the as-prepared CNDs which were prepared by the thermal pyrolysis of solid citric acid at 155 °C.

4.3   Results and Discussion

AFM and TEM experiments were conducted to probe the morphology of CND samples. 1 min and 10 min CNDs for AFM analysis were prepared by spin-casting the sample on an atomically flat mica substrate. The AFM characterization was conducted by a Park Systems XE-70 Advanced Scanning Probe Microscope operating in a non-contact mode and the AFM images were post-processed with the software package Gwyddion.[46] The AFM topography images of 1 min CNDs and 10 min CNDs are displayed in Figure 4.1A and 4.1B showing all nanoparticles are well isolated. Line profiles (Fig. 4.1C, 1D) of 25 different particles in the AFM topographic images were used to measure the thickness of CNDs. The average CND thickness was found to be about 1.3 nm for 1 min CNDs and 1.0 nm for 10 min CNDs. This reduction in height for 10 min CNDs is likely due to the extended carbonization of carboxylic and ether functional groups to sp^2-hybridized C-C bonds with longer pyrolysis time. TEM imaging was carried out on 1 min CNDs as shown in Figure 4.1E. The average diameter was found to be about 5 nm. 1 min NCNDs show a well formed sp^2 nanodomain by the presence of graphene lattice fringes with a spacing of about 0.24 nm as shown in Fig. 4.1E.[47]
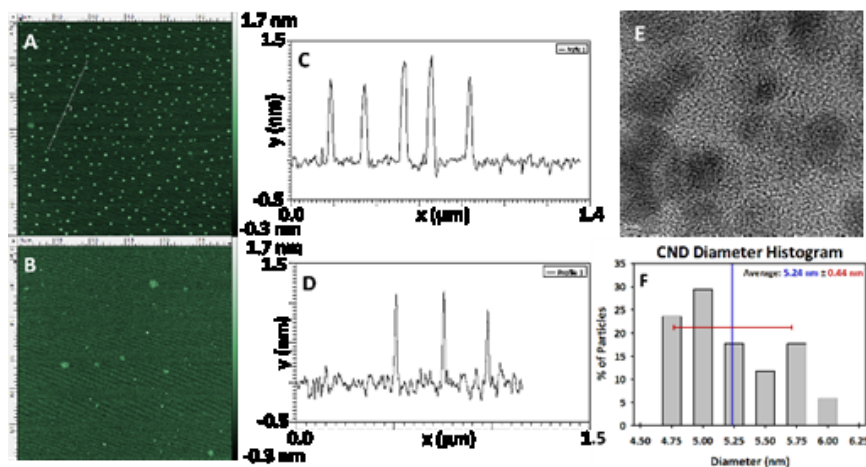
Figure 4.1: AFM Images of A) 1 min CNDs and B) 10 min CNDs. Line profile of C) 1 min CNDs and D) 10 min CNDs. E) HRTEM of 1 min NCNDs and F) Diameter Histogram of 1 min NCNDs.

The chemical structure of each CND sample was determined by XPS analysis. The survey spectra for all samples are shown in Figure 4.2A. Figure 4.2B illustrates the relative percentage of C, N, and O atoms present in citric acid and 4 CNDs. It is clear that 1 min NCNDs has the highest nitrogen content among all CNDs. 10 min NCNDs show noticeably lower nitrogen content which is attributed from the reduction in defect sites as the sp^2 nanodomain is more completely formed with longer pyrolysis time. For citric acid, the C1s high resolution spectrum shows peaks corresponding to sp^3 C-C (284.9 eV), C-O (286.5 eV), and CO_2H (290.0 eV) which is consistent with the molecular structure of citric acid. Upon the short pyrolysis of citric acid, the top panel of Figure 4 shows the 1 min CNDs XPS peaks related to sp^2 C-C (284.4 eV), sp^3 C-C (284.9 eV) C-O (286.5 eV), C=O (288.0 eV) and CO_2H (290.5 eV). With even further pyrolysis time, the sp^3 C-C peak (formed via carbonization of CA) in the C1s spectrum of 1 min CNDs evolves to sp^2 C-C due to the further degree of carbonization as seen in the XPS spectra of 10 min CNDs (Figure 4.2D). The peaks relating to potassium, in which KOH is used to quench the CND pyrolysis, can be observed at about 293 eV for $K2p_{3/2}$ and 295 eV for $K2p_{1/2}$.[48] These two peaks are separated by ~2.7 eV, which was used to assign these peaks as potassium in the C1s spectra.

100
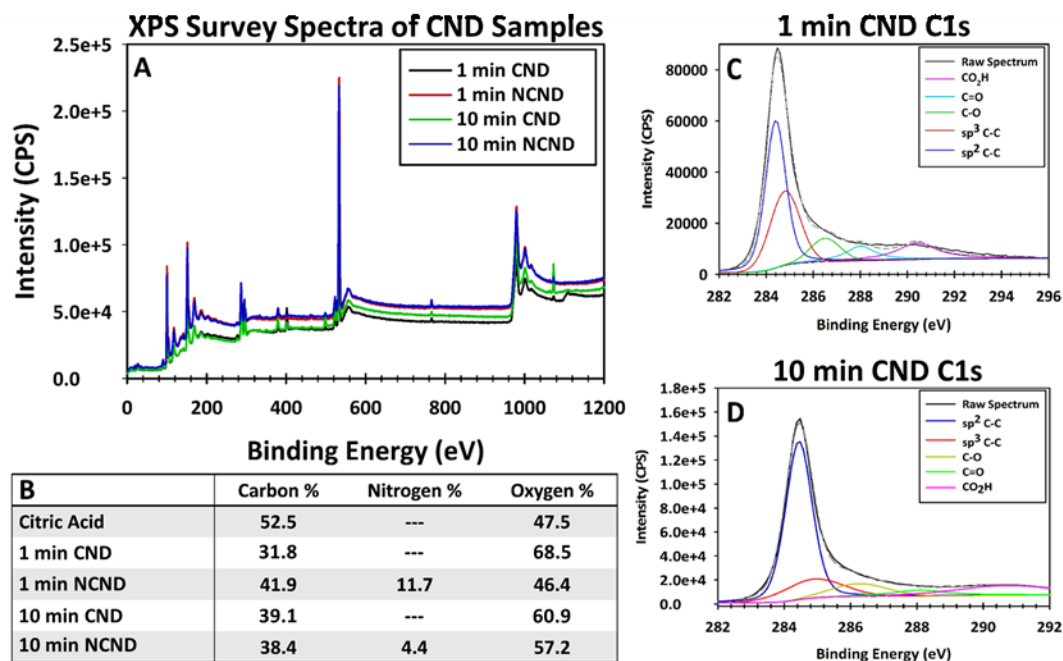
Figure 4.2: A) XPS Survey Spectra of CNDs, B) XPS relative atom percent of C, N, O and high resolution C1s spectra of C) 1 min CNDs and D) 10 min CNDs.

When aqueous ammonia was added to produce 1 min NCNDs as seen in the top row of Figure 4.3, the sp^3 C-C peak at 284.9 eV disappeared and the sp^2 C-C peak increased in intensity suggesting the formation of aromatic C=C bonds. The C-O peak shifts to lower binding energy (285.8 eV), verifying that C-N bonds are formed. This is in concert with the broad N1s spectra that contains peaks relating to pyridinic (398.5 eV), amine (399.3 eV) pyrrolic (400.5 eV), and graphitic (401.3 eV) nitrogen chemical states. Abundant and various nitrogen sites indicate the conversion of carboxyl and hydroxyl groups to amino and amido moieties as well as the uptake of nitrogen into the carbon network.

In 10 min NCNDs (Figure 4.3: bottom row), the C1s spectra remains similar to 10 min CNDs though the carboxylic functionality (290 eV) is partially converted to C-N (285.8 eV) and C=O (~288 eV). The attachment of nitrogen is similar to 1 min NCNDs though with less nitrogen content and without graphitic N. These results support the hypothesis that the location of added nitrogen atoms can be controlled using pyrolysis time as a parameter during the synthesis of carbon nanodots. During the early stages of pyrolysis, nitrogen can be incorporated into the graphene nanodomain in the form of

graphic N; however with longer pyrolysis time the graphene nanodomain is more completely formed thus removing the ability to add graphitic nitrogen. By treating highly disordered CNDs, more nitrogen can be incorporated into the graphene framework which would potentially enhance the fluorescent quantum yield.
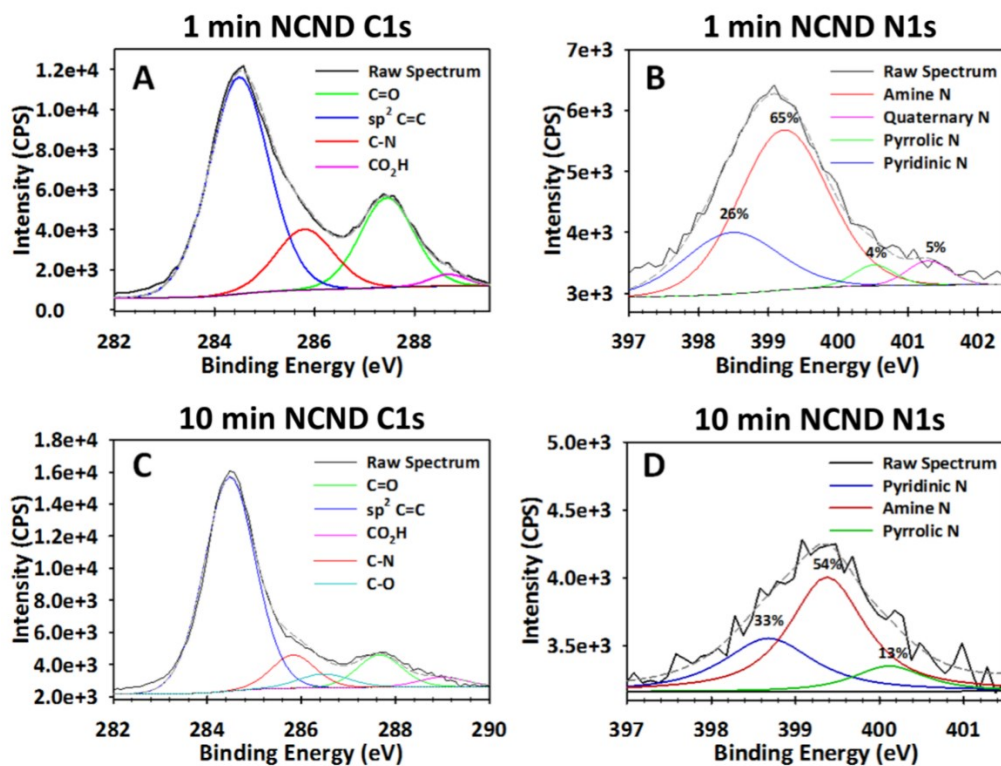
Figure 4.3: High resolution XPS spectra of A, B) 1 min NCNDs and C, D) 10 min NCNDs. In addition to higher N content, 1 min NCNDs also contain more diverse nitrogen chemical states than 10 min NCNDs.

Table 4.1: Functional Group Distribution of 10 min CNDs before and after hydrothermal treatment with water. These XPS results show the conversion of carboxylic to carbonyl functional groups and with additional loss to hydroxyl groups.

	10 min CND	**10 min HT-CND**
sp^2 C-C	71.0 %	67.0 %
Hydroxyl	8.9 %	5.3 %
Carbonyl	4.6 %	25.7 %
Carboxyl	15.5 %	2.0 %

In a control experiment, 10 min CNDs were subjected to the same hydrothermal treatment (5 hours, 180 °C) without aqueous ammonia to analyze the chemical effect of hydrothermal treatment. The distribution of functional groups was analyzed using the C1s high resolution XPS experiments. Table 4.1 illustrates that hydrothermal treatment reduces the fraction of hydroxyl (~286 eV) and carboxylic acid (~289 eV) functional groups.

As shown in Figure 4.4, four different CNDs (1 min CNDs, 1 min NCNDs, 10 min CNDs, and 10 min NCNDs) were also studied by FTIR spectroscopy. The left panel of Fig. 4 shows the comparison between 1 min CNDs and 1 min NCNDs. The peak at 1600 cm^{-1} reflects the formation of C=C bonds and the peak at 1250 cm^{-1} suggests the formation of C-O-C bonds. These two bonds are formed during the carbonization process with the formation of aromatic C=C bonds. After hydrothermal reaction with aqueous ammonia, 1 min NCNDs reveal the shift of the –OH band at 3400 cm^{-1} to lower energy at 3200 cm^{-1} which is indicative of the formation of N-H bond. In addition, the intensity of the peak at 2600 cm^{-1} is greatly suppressed, suggesting that carboxyl groups were replaced with amide groups. This is also supported by the shift of the peak at 1730 cm^{-1} (CO$_2$H) to 1670 cm^{-1} (CONH$_2$). In addition, a new peak arises at 1320 cm^{-1}, which can be assigned to the C-N stretching mode of amines and amides. These results clearly indicate the addition of amine and amide nitrogen to CNDs after hydrothermal treatment with aqueous ammonia. A significant increase of the peak at 1600 cm^{-1} in NCNDs indicates the completion of aromatic rings by the carbonization of dangling bonds.

The right panel of Figure 4.4 shows the FTIR spectra of 10 min CNDs and 10 min NCNDs. The enhanced carbonization of 10 min CNDs is indicated by the presence of distinctive peaks at 1400 and 1600 cm^{-1} which are assigned to aromatic C=C stretching modes. In addition, the intensity of the peak at 2600 cm^{-1} relating to carboxyl groups is greatly suppressed in 10 min CNDs, compared to 1 min CNDs, which indicate more complete pyrolysis of 10 min CNDs. After hydrothermal reaction with aqueous ammonia, carboxylic groups are converted to amides and hydroxyl groups are converted to amines. This can be seen with the reduction of the peaks at 2600 cm^{-1} and at 3400 cm^{-1}. In addition, 10 min NCNDs shows the pronounced peak at 1260 cm^{-1} which is attributed to the C-N stretching mode. This band shows an elevated addition of nitrogen in 10 min NCNDs supporting the hypothesis that a complete CND is formed at later pyrolysis time and that primarily surface-terminated nitrogen is added to 10 min NCNDs. This is in stark contrast to 1 min NCNDs whose nitrogen attachment not only includes surface-termination nitrogen chemical states but also includes graphitic N.
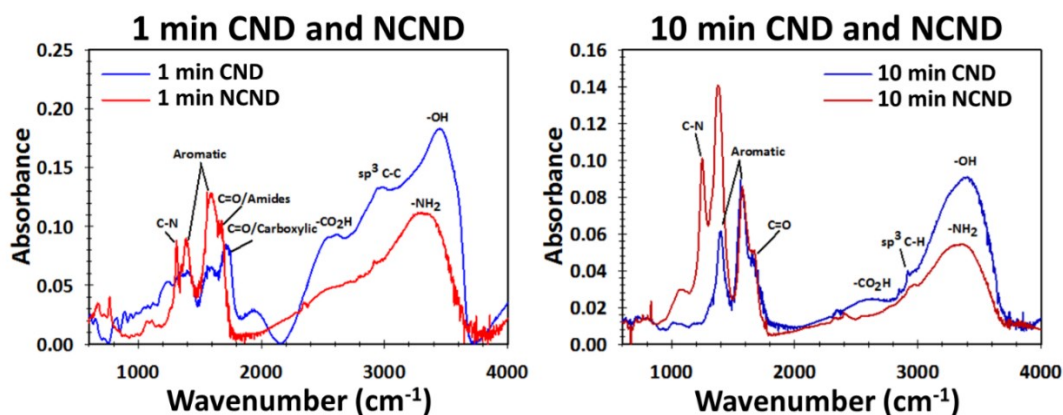
Figure 4.4: FTIR spectra of as-prepared CNDs. Noticeable changes in the spectra are seen with the addition of nitrogen such as the peak evolutions around 1700 cm^{-1} and 3200-3400 cm^{-1}.

The UV-Vis absorption spectra of different CNDs (i.e., 1 min CNDs, 1 min NCNDs, 10 min CNDs, and 10 min NCNDs) are presented in Figure 4.5. The UV-Vis absorption spectra clearly show the effect of pyrolysis and incorporated nitrogen atoms. After pyrolyzing citric acid for 1 min and 10 min, the absorption is enhanced in the visible region. This is due to the formation of sp^2-bonded carbon conjugation in the aromatic rings as the nanodomains in CNDs are formed. While 1 min CNDs show

slightly extended absorption extended to 300 nm, the 10 min CNDs show drastic enhancement of visible absorption at 340 nm. This band at 340 nm was assigned to the π-π* transition. This enhancement of this feature in 10 min CNDs at 350 nm show a more complete formation of sp^2 nanodomains after 10 minutes of pyrolysis.

After the hydrothermal treatment with aqueous ammonia, 1 min NCNDs show a drastic increase of absorption toward longer wavelength with significant absorbance between 300 nm and 450 nm. This band is assigned the n-π* transition relating to the defect states in the forms of pyridinic, amine, pyrrolic and graphitic N. Overall, the red shifted and absorption intensity effects are much greater for 1 min NCNDs than 10 min NCNDs, indicating that the nitrogen incorporation occurred more efficiently in 1 min CNDs. This is consistent with the results from XPS analysis. More efficient nitrogen addition can be explained by different structural features between 1 min CNDs and 10 min CNDs. While nitrogen atoms can be freely added into a loose polymer dot (1 min CNDs) via both edge functionalization and doping, completely carbonized CNDs (10 min CNDs) are restricted to the internal incorporation of nitrogen and thus only contain surface-terminating nitrogen groups.

Overall, the red shifted band in the absorption spectra is much more pronounced for 1 min NCNDs than 10 min NCNDs, indicating that the nitrogen incorporation occurred more efficiently in 1 min CNDs. This is consistent with the results from XPS analysis. More efficient nitrogen addition can be explained by different structural features between 1 min CNDs and 10 min CNDs. While nitrogen atoms can be freely added into a loose polymer dot (1 min CNDs) via both edge functionalization and doping, completely carbonized CNDs (10 min CNDs) are restricted to the internal incorporation of nitrogen and thus only contain surface-terminating nitrogen groups. The fluorescence quantum yields of four CNDs were also measured and are shown the inset of Figure 4.5. The QY of 1 min CNDs were unable to be determined because of weak absorbance and fluorescence. Upon amination, the QY of 1 min NCNDs was found to be about 35%. 10 min CNDs show a QY of 3% whereas 10 min NCNDs was found to be 11%.
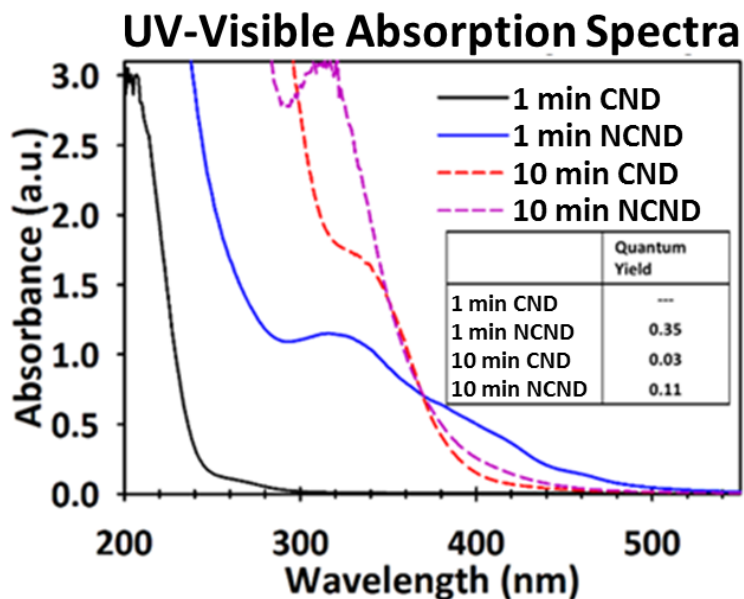
Figure 4.5: UV-Visible Absorption Spectra of CNDs. The addition of nitrogen to 1 min CNDs shows great absorption enhancement in the visible region. 10 min CNDs do not show as much enhancement in the visible region however increase the absorption of UV light at 340 nm.

The emission spectra of the four CNDs were also compared, as shown in Figure 4.6. While 1 min CNDs shows weak fluorescence centered at 420 nm, the 10 min CNDs show much stronger fluorescence centered at 450 nm. The stronger and red-shifted emission of 10 min CNDs, compared to 1 min CNDs, reflects that 10 min CNDs have more complete sp2-conjugated aromatic rings due to the extended pyrolysis. The comparison of emission spectra between 1 min NCNDs and 10 min NCNDs presents the effect of added nitrogen. After the treatment of 1 min CNDs, the excitation maxima shifts from 360 nm to 420 nm and the emission peak position shifts from 420 nm to 450 nm. The shift of excitation wavelength from 360 nm to 420 nm is attributed to the new band formed by the added nitrogen. 10 min NCNDs show excitation peaks in the range of 330 nm to 390 nm. 1 min NCNDs show stronger and red-shifted fluorescence, compared to 10 min NCNDs, which is consistent with the larger amount of added nitrogen.

Hydrothermally treated CNDs without added ammonia were also studied for their optical properties. Their excitation-dependent emission spectra can be found in Figure 4.7. Hydrothermal treatment affected the fluorescence of 1 min CNDs significantly. A

notable increase in absorption at 340 nm was observed as well as a 40 times enhancement in PL intensity with 50 nm blue shift in peak emission wavelength. 10 min CNDs had a very different result under hydrothermal treatment. An absorbance increase was observed with a blue shift from 350 to 330 nm and a two-fold increase in emission intensity. It is hypothesized that the removal of the oxygen-containing functional groups correlates with the increase of absorbance and emission intensity. Additionally, the peak emission wavelength undergoes a blue shift from 450 nm to 430 nm. Luo *et al*. performed a similar hydrothermal treatment of GQDs to find that epoxide and hydroxyl functional groups were removed upon treatment.[49] The results of that treatment likewise show an increase of emission intensity with a corresponding blue shift in peak emission. In that report, this is assigned to the removal of oxygen-containing functional groups which are known to cause a red shift in emission. Such a removal would also promote emission from the higher energy C π* LUMO+2 to the C π HOMO instead of the lower energy defect state (O π* LUMO).[37] This results in the removal of a non-radiative decay channel thereby increasing the fluorescent quantum yield as well as blue shifting the peak emission wavelength.
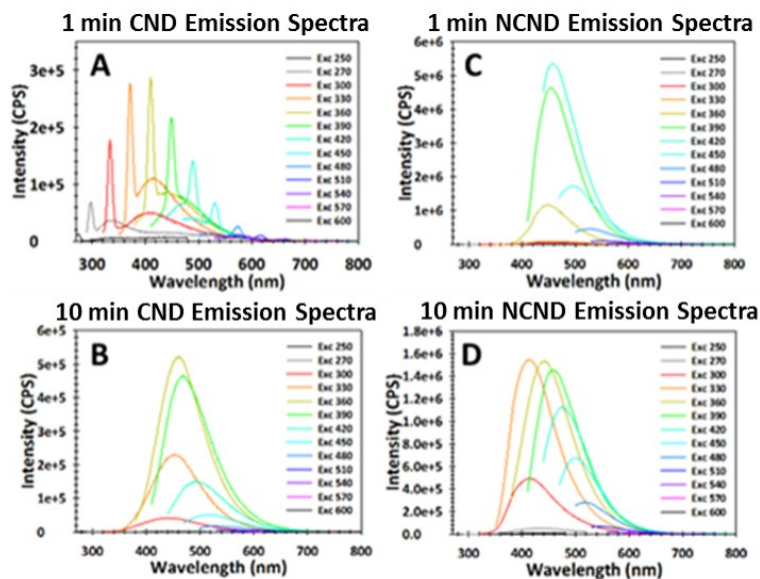
Figure 4.6: Excitation-dependent emission spectra of A) 1 min CNDs, B) 10 min CNDs, C) 1 min NCNDs and D) 10 min NCNDs. An increase in emission intensity is observed with both longer pyrolysis time and nitrogenation. However, the largest increase is found in 1 min NCNDs due to the higher N content.
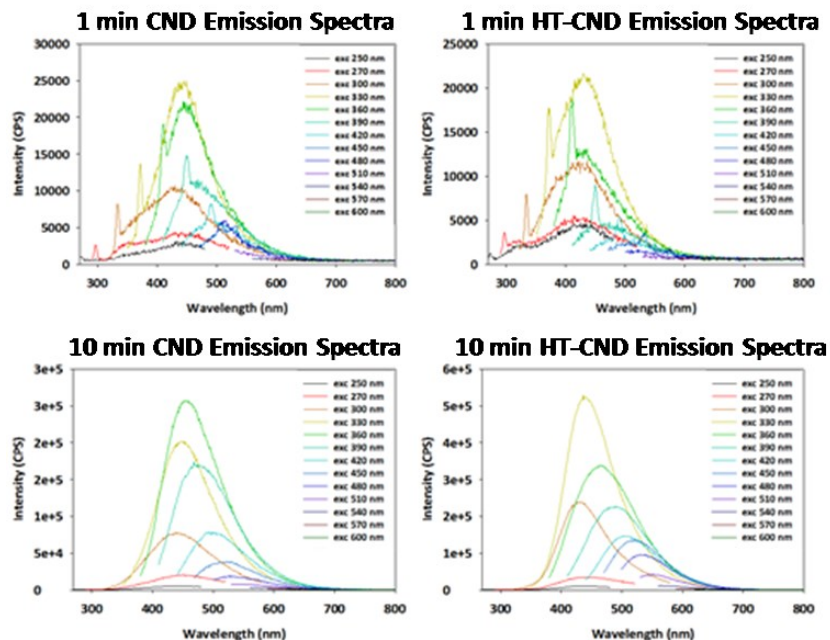
Figure 4.7: Comparison of PL Spectra of 1 and 10 min CNDs with hydrothermally treated 1 and 10 min CNDs. Upon hydrothermal reduction, the peak emission wavelengths of both 1 and 10 min HT-CNDs are blue-shifted by about 30 nm. Characterization suggests this originates from the collapse of the surface passivation layer to form small aromatic fluorophores.

As found previously, 1 min NCNDs contain a larger nitrogen content as well as graphitic N compared to 10 min NCNDs. We hypothesized that 1 min NCNDs would outperform 10 min NCNDs in catalyzing ORR. The results of the linear sweep voltammetric (LSV) experiments can be seen in Figure 4.8 (bottom left). Both 1 min and 10 min NCNDs show an increase in disk current density and onset potential compared to bare MWCNTs. Interestingly, it seems from the disk current density that 10 min NCNDs have a substantial increase of hydrogen peroxide formation compared to 1 min NCNDs. Coupling this data set with Koutecky-Levich (K-L) (Figure 4.8 bottom right) analysis clearly shows the highest electron transfer number is obtained by 1 min NCNDs, indicating that more oxygen is reduced to water by a four electron process than the energetically unfavourable two electron process.

A complication in any ORR analysis is determining at what potential a particular reaction occurs as there are many simultaneous reactions. Ideally, a direct four electron process would be favoured over the two electron reduction to the peroxide ion followed by another two electron reduction to water. In order to determine the preferred reaction

pathway in NCNDs, hydrogen peroxide was used as the analyte for ORR instead of O_2. By performing cyclic voltammetry, it was found (Figure 4.9) that both 1 min and 10 min NCNDs perform similarly in reducing H_2O_2 to H_2O. When increasing the concentration of H_2O_2 ten-fold, the peak currents also increased by similar amounts. This suggests that both 1 min and 10 min NCNDs are equally effective at reducing H_2O_2 to H_2O by a two electron process.

Interestingly, when the ring electrode was set to a potential that oxidizes H_2O_2 to O_2 in excess H_2O_2 as shown in Figure 4.10, there was a significant response at potentials below -0.2 V with 10 min NCNDs that shows strong reduction of both O_2 and H_2O_2 to H_2O. These results, coupled with those in Figures 4.8 and 4.9 suggest that 10 min NCNDs catalyze the energetically less favourable two electron pathway effectively with a higher onset potential. When performing the same experiment with 1 min NCNDs there was some change in current density with a slight enhancement of current density at -0.2 V and a decrease in current at potentials below -0.8 V. This signifies the four electron reduction is preferred over the two electron reduction process and that the conversion of O_2 to H_2O_2 is not catalyzed by 1 min NCNDs.
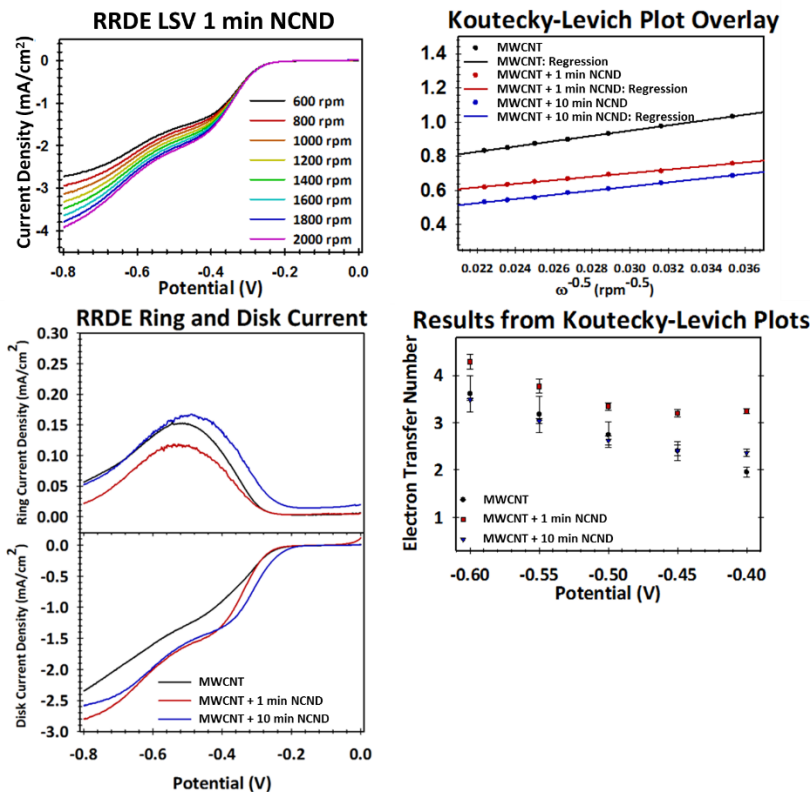
Figure 4.8: Determination of Electron Transfer Number of 1 min and 10 min NCNDs. A rotation ring-disk electrode (RRDE) is used in LSV measurements (top left) to build the Koutecky-Levich Plot (top right) by varying electrode rotation speed in the presence of O_2. Current densities of the ring and disk electrode in RRDE LSV illustrate the electrochemical preference between a four electron and two electron process for each sample. (bottom left) Koutecky-Levich Plot shows the electron transfer number as a function of potential. (bottom right)
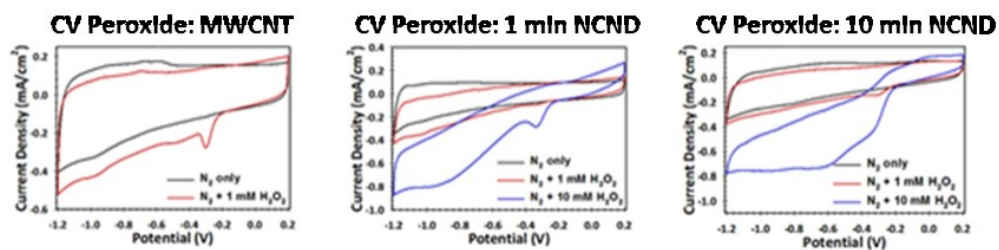
Figure 4.9: Cyclic voltammetry experiments in which nitrogen is bubbled into a solution containing a known concentration of hydrogen peroxide. With H_2O_2 as the only source of oxygen, it is clear that both 1 min and 10 min NCNDs perform equally well in reducing hydrogen peroxide to water. However, the potential windows at which this reduction occurs varies due to the chemical structure of each type of NCNDs.
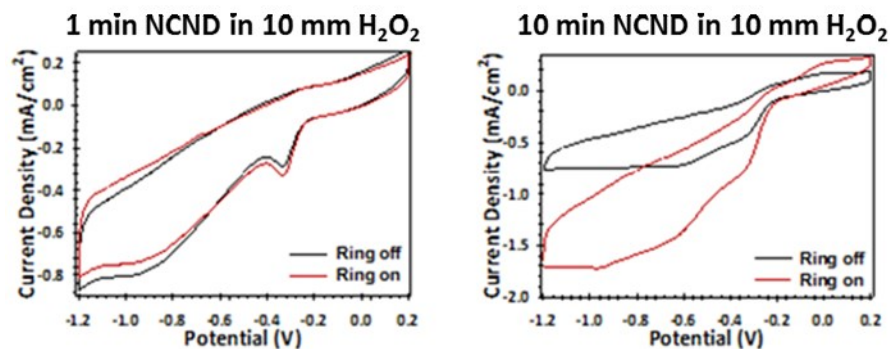
Figure 4.10: CV experiments which utilize turning the ring electrode on to oxidize excess H_2O_2 to O_2. Since 1 min NCNDs favour reducing O_2 to H_2O by a four electron process, there will be no significant increase in current density. 10 min NCNDs favour the two electron reduction of O_2 to H_2O_2 which will be re-oxidized by the ring electrode, showing a substantial increase in current density.

There are two main conclusions to found with these results. First, pyrolysis time plays a significant role in preparing fluorescent CNDs. If the CNDs synthesized are left in a loose polymer-like state, there will be little to no absorbance or fluorescence to be observed. As a result, the QY will be negligibly small due to the lack of π-π* transitions from the sp^2 nanodomains or n-π* transitions from optically active defect sites. Once a suitable pyrolysis time is reached, the CNDs are well formed which boost the quantum yield to measureable amounts. The control sample of hydrothermally treated 1 min CNDs and 10 min CNDs were found to show the same order of quantum yields (~10%) suggesting that hydrothermal treatment without heteroatom dopants simply complete the carbonization process.

Second, the amount and the location of added nitrogen play a significant role in synthesizing highly fluorescent CNDs as well as tune the specific reaction pathway for the electrochemical oxygen reduction reaction. Nitrogen addition to 10 min CNDs results in the formation of pyridinic, amine, and pyrrolic N chemical states. The total nitrogen content was found to be 4.4% and the QY was enhanced fourfold from 3% to 11%. However, when nitrogen is added to the weakly fluorescing loose polymer 1 min CNDs, fluorescent quantum yields of at least thirty percent are easily obtainable due to the increased availability of nitrogen attachment sites in 1 min CNDs. This is seen by the total nitrogen content of 1 min NCNDs being much higher (11.7%) than 10 min NCNDs and the nitrogen chemical states, which in addition to the surface-terminating

111

groups, contain graphitic N. This graphitic N contributes delocalized electrons to the interior of the π-conjugated carbon nanodomain. From this, it can be concluded that nitrogen chemical states that are directly bonded to the sp^2-hybridized carbons are responsible for the enhancement of quantum yield in carbon dots.

We hypothesize that not only does graphitic N contribute to the delocalization of electrons throughout the carbon nanodomain but the charge distribution may also improve ORR catalysis from the electron-poor (positively charged) carbons that neighbor the graphitic N heteroatom (negatively charged). In this electrostatic situation, dissolved oxygen (being electron-rich) will migrate toward the electron-poor carbon active site and begin the oxygen reduction reaction. Without further experimentation, it is difficult to say if this particular electrostatic environment from graphitic N is responsible for the substantial enhancement of electron transfer number to the more favorable four electron process. We speculate this is the case as when performing cyclic voltammetry experiments in 10 mM H_2O_2, we find that 1 min NCNDs are greatly outperformed by 10 min NCNDs. In H_2O_2, the electron density is spread out across two additional O-H bonds and the O-O bond is lengthened. This would negatively influence electrostatic attraction toward the partially positively charged carbon, thus hindering the two electron ORR pathway.

These results further confirm the potential of carbon nanodots as highly fluorescent organic nanoparticles for use in bioimaging, optoelectronics and electrocatalysis by optimizing the bottom-up approach to synthesis. However, this potential is met with great challenge as the chemical states of nitrogen addition are often mixed and with varying content. The previous chapters of this dissertation have shown the importance of understanding the chemical structure-function relationship. Future work would involve finely controlling the total nitrogen content and the specific chemical state as well. Proposed experiments are detailed in Chapter 6 that aim to accomplish this goal. Chapter 5 will show a new CQD function that can be implemented in light-activated functions in biological systems, also known as biophotonics. The CQD structure-function relationship will be explored for one of these functions, photodynamic therapy, in which light is used to initiate cytotoxicity.

4.4   Chapter 4 References

1. Dong, Y.; Shao, J.; Chen, C.; Li, H.; Wang, R.; Chi, Y.; Lin, X.; Chen, G., Blue luminescent graphene quantum dots and graphene oxide prepared by tuning the carbonization degree of citric acid. *Carbon* **2012,** *50* (12), 4738-4743.

2. Yang, Z.-C.; Wang, M.; Yong, A. M.; Wong, S. Y.; Zhang, X.-H.; Tan, H.; Chang, A. Y.; Li, X.; Wang, J., Intrinsically fluorescent carbon dots with tunable emission derived from hydrothermal treatment of glucose in the presence of monopotassium phosphate. *Chemical Communications* **2011,** *47* (42), 11615-11617.

3. Jia, X.; Li, J.; Wang, E., One-pot green synthesis of optically pH-sensitive carbon dots with upconversion luminescence. *Nanoscale* **2012,** *4* (18), 5572-5575.

4. Zhang, R.; Chen, W., Nitrogen-doped carbon quantum dots: Facile synthesis and application as a "turn-off" fluorescent probe for detection of Hg2+ ions. *Biosensors & Bioelectronics* **2014,** *55*, 83-90.

5. Kim, H.; Kwon, W.; Choi, M.; Rhee, S. W.; Yong, K., Photoelectrochemical Hydrogen Generation Using C-dot/ZnO Hierarchical Nanostructure as an Efficient Photoanode. *Journal of the Electrochemical Society* **2015,** *162* (6), H366-H370.

6. Liu, S. Y.; Zhao, N.; Cheng, Z.; Liu, H. G., Amino-functionalized green fluorescent carbon dots as surface energy transfer biosensors for hyaluronidase. *Nanoscale* **2015,** *7* (15), 6836-6842.

7. Lopez, T. D. F.; Gonzalez, A. F.; Diaz-Garcia, M. E.; Badia-Laino, R., Highly efficient Forster resonance energy transfer between carbon nanoparticles and europium-tetracycline complex. *Carbon* **2015,** *94*, 142-151.

8. Shi, W. J.; Fan, H.; Ai, S. Y.; Zhu, L. S., Preparation of fluorescent graphene quantum dots from humic acid for bioimaging application. *New Journal of Chemistry* **2015,** *39* (9), 7054-7059.

9. Lu, W. J.; Gong, X. J.; Yang, Z. H.; Zhang, Y. X.; Hu, Q.; Shuang, S. M.; Dong, C.; Choi, M. M. F., High-quality water-soluble luminescent carbon dots for multicolor patterning, sensors, and bioimaging. *RSC Advances* **2015,** *5* (22), 16972-16979.

10. Strauss, V.; Margraf, J. T.; Dolle, C.; Butz, B.; Nacken, T. J.; Walter, J.; Bauer, W.; Peukert, W.; Spiecker, E.; Clark, T.; Guldi, D. M., Carbon Nanodots: Toward a Comprehensive Understanding of Their Photoluminescence. *Journal of the American Chemical Society* **2014,** *136* (49), 17308-17316.

11. Xu, M. H.; Xu, S. S.; Yang, Z.; Shu, M. J.; He, G. L.; Huang, D.; Zhang, L. L.; Li, L.; Cui, D. X.; Zhang, Y. F., Hydrophilic and blue fluorescent N-doped carbon dots from tartaric acid and various alkylol amines under microwave irradiation. *Nanoscale* **2015,** *7* (38), 15915-15923.

12. Zheng, B. Z.; Liu, T.; Paau, M. C.; Wang, M. N.; Liu, Y.; Liu, L.; Wu, C. F.; Du, J.; Xiao, D.; Choi, M. M. F., One pot selective synthesis of water and organic soluble carbon dots with green fluorescence emission. *RSC Advances* **2015,** *5* (15), 11667-11675.

13. Zhang, W.; Yu, S. F.; Fei, L.; Jin, L.; Pan, S.; Lin, P., Large-area color controllable remote carbon white-light light-emitting diodes. *Carbon* **2015,** *85*, 344-350.

14. Zhang, W. F.; Jin, L. M.; Yu, S. F.; Zhu, H.; Pan, S. S.; Zhao, Y. H.; Yang, H. Y., Wide-bandwidth lasing from C-dot/epoxy nanocomposite Fabry-Perot cavities with ultralow threshold. *Journal of Materials Chemistry C* **2014,** *2* (8), 1525-1531.

15. Zhai, Y.; Zhu, Z.; Zhu, C.; Ren, J.; Wang, E.; Dong, S., Multifunctional water-soluble luminescent carbon dots for imaging and Hg2+ sensing. *Journal of Materials Chemistry B* **2014,** *2* (40), 6995-6999.

16. Zhu, S. J.; Zhou, N.; Hao, Z. Y.; Maharjan, S.; Zhao, X. H.; Song, Y. B.; Sun, B.; Zhang, K.; Zhang, J. H.; Sun, H. C.; Lu, L. J.; Yang, B., Photoluminescent graphene quantum dots for in vitro and in vivo bioimaging using long wavelength emission. *RSC Advances* **2015,** *5* (49), 39399-39403.

17. Bourlinos, A. B.; Stassinopoulos, A.; Anglos, D.; Zboril, R.; Karakassides, M.; Giannelis, E. P., Surface functionalized carbogenic quantum dots. *Small* **2008,** *4* (4), 455-458.

18. Yang, Z.; Xu, M.; Liu, Y.; He, F.; Gao, F.; Su, Y.; Wei, H.; Zhang, Y., Nitrogen-doped, carbon-rich, highly photoluminescent carbon dots from ammonium citrate. *Nanoscale* **2014,** *6* (3), 1890-1895.

19. Zhu, S.; Meng, Q.; Wang, L.; Zhang, J.; Song, Y.; Jin, H.; Zhang, K.; Sun, H.; Wang, H.; Yang, B., Highly Photoluminescent Carbon Dots for Multicolor Patterning, Sensors, and Bioimaging. *Angewandte Chemie-International Edition* **2013,** *52* (14), 3953-3957.

20. Jiang, Z.; Nolan, A.; Walton, J. G. A.; Lilienkampf, A.; Zhang, R.; Bradley, M., Photoluminescent Carbon Dots from 1,4-Addition Polymers. *Chemistry-a European Journal* **2014,** *20* (35), 10926-10931.

21. Do, S.; Kwon, W.; Rhee, S.-W., Soft-template synthesis of nitrogen-doped carbon nanodots: tunable visible-light photoluminescence and phosphor-based light-emitting diodes. *Journal of Materials Chemistry C* **2014,** *2* (21), 4221-4226.

22. Gong, X.; Lu, W.; Paau, M. C.; Hu, Q.; Wu, X.; Shuang, S.; Dong, C.; Choi, M. M. F., Facile synthesis of nitrogen-doped carbon dots for Fe3+ sensing and cellular imaging. *Analytica Chimica Acta* **2015,** *861*, 74-84.

23. Li, Z.; Yu, H.; Bian, T.; Zhao, Y.; Zhou, C.; Shang, L.; Liu, Y.; Wu, L.-Z.; Tung, C.-H.; Zhang, T., Highly luminescent nitrogen-doped carbon quantum dots as effective fluorescent probes for mercuric and iodide ions. *Journal of Materials Chemistry C* **2015,** *3* (9), 1922-1928.

24. Wang, W.; Lu, Y.-C.; Huang, H.; Wang, A.-J.; Chen, J.-R.; Feng, J.-J., Facile synthesis of N, S-codoped fluorescent carbon nanodots for fluorescent resonance energy transfer recognition of methotrexate with high sensitivity and selectivity. *Biosensors & Bioelectronics* **2015,** *64*, 517-522.

25. Xu, Q.; Zhao, J.; Liu, Y.; Pu, P.; Wang, X.; Chen, Y.; Gao, C.; Chen, J.; Zhou, H., Enhancing the luminescence of carbon dots by doping nitrogen element and its application in the detection of Fe(III). *Journal of Materials Science* **2015,** *50* (6), 2571-2576.

26. Hu, X.; Cheng, L.; Wang, N.; Sun, L.; Wang, W.; Liu, W., Surface passivated carbon nanodots prepared by microwave assisted pyrolysis: effect of carboxyl group in precursors on fluorescence properties. *RSC Advances* **2014,** *4* (36), 18818-18826.

27. Reiss, P.; Protiere, M.; Li, L., Core/Shell Semiconductor Nanocrystals. *Small* **2009,** *5* (2), 154-168.

28. Qian, Z.; Ma, J.; Shan, X.; Feng, H.; Shao, L.; Chen, J., Highly Luminescent N-Doped Carbon Quantum Dots as an Effective Multifunctional Fluorescence Sensing Platform. *Chemistry-a European Journal* **2014,** *20* (11), 2983-2983.

29. Han, X. G.; Zhong, S. H.; Pan, W.; Shen, W. Z., A simple strategy for synthesizing highly luminescent carbon nanodots and application as effective down-shifting layers. *Nanotechnology* **2015,** *26* (6).

30. Choi, Y.; Kim, S.; Choi, M. H.; Ryoo, S. R.; Park, J.; Min, D. H.; Kim, B. S., Highly Biocompatible Carbon Nanodots for Simultaneous Bioimaging and Targeted Photodynamic Therapy In Vitro and In Vivo. *Advanced Functional Materials* **2014,** *24* (37), 5781-5789.

31. Hola, K.; Zhang, Y.; Wang, Y.; Giannelis, E. P.; Zboril, R.; Rogach, A. L., Carbon dots-Emerging light emitters for bioimaging, cancer therapy and optoelectronics. *Nano Today* **2014,** *9* (5), 590-603.

32. Song, Y. B.; Zhu, S. J.; Yang, B., Bioimaging based on fluorescent carbon dots. *RSC Advances* **2014,** *4* (52), 27184-27200.

33. Ma, Z.; Ming, H.; Huang, H.; Liu, Y.; Kang, Z., One-step ultrasonic synthesis of fluorescent N-doped carbon dots from glucose and their visible-light sensitive photocatalytic ability. *New Journal of Chemistry* **2012,** *36* (4), 861-864.

34. Sk, M. A.; Ananthanarayanan, A.; Huang, L.; Lim, K. H.; Chen, P., Revealing the tunable photoluminescence properties of graphene quantum dots. *Journal of Materials Chemistry C* **2014,** *2* (34), 6954-6960.

35. Margraf, J. T.; Strauss, V.; Guldi, D. M.; Clark, T., The Electronic Structure of Amorphous Carbon Nanodots. *Journal of Physical Chemistry B* **2015,** *119* (24), 7258-7265.

36. Hu, X.; An, X.; Li, L., Easy synthesis of highly fluorescent carbon dots from albumin and their photoluminescent mechanism and biological imaging applications. *Materials Science & Engineering C-Materials for Biological Applications* **2016,** *58*, 730-736.

37. Tang, L.; Ji, R.; Li, X.; Teng, K. S.; Lau, S. P., Energy-level structure of nitrogen-doped graphene quantum dots. *Journal of Materials Chemistry C* **2013,** *1* (32), 4908-4915.

38. Zhu, S.; Zhang, J.; Tang, S.; Qiao, C.; Wang, L.; Wang, H.; Liu, X.; Li, B.; Li, Y.; Yu, W.; Wang, X.; Sun, H.; Yang, B., Surface Chemistry Routes to Modulate the Photoluminescence of Graphene Quantum Dots: From Fluorescence Mechanism to Up-Conversion Bioimaging Applications. *Advanced Functional Materials* **2012,** *22* (22), 4732-4740.

39. Xu, J.; Sahu, S.; Cao, L.; Bunker, C. E.; Peng, G.; Liu, Y.; Fernando, K. A. S.; Wang, P.; Guliants, E. A.; Meziani, M. J.; Qian, H.; Sun, Y.-P., Efficient Fluorescence Quenching in Carbon Dots by Surface-Doped Metals - Disruption of Excited State Redox Processes and Mechanistic Implications. *Langmuir* **2012,** *28* (46), 16141-16147.

40. Zhang, X.; Zhang, Y.; Wang, Y.; Kalytchuk, S.; Kershaw, S. V.; Wang, Y.; Wang, P.; Zhang, T.; Zhao, Y.; Zhang, H.; Cui, T.; Wang, Y.; Zhao, J.; Yu, W. W.; Rogach, A. L., Color-Switchable Electroluminescence of Carbon Dot Light-Emitting Diodes. *ACS Nano* **2013,** *7* (12), 11234-11241.

41. Martindale, B. C. M.; Hutton, G. A. M.; Caputo, C. A.; Reisner, E., Solar Hydrogen Production Using Carbon Quantum Dots and a Molecular Nickel Catalyst. *Journal of the American Chemical Society* **2015,** *137* (18), 6018-6025.

42. Sun, J.; Yang, S.; Wang, Z.; Shen, H.; Xu, T.; Sun, L.; Li, H.; Chen, W.; Jiang, X.; Ding, G.; Kang, Z.; Xie, X.; Jiang, M., Ultra-High Quantum Yield of Graphene Quantum Dots: Aromatic-Nitrogen Doping and Photoluminescence Mechanism. *Particle & Particle Systems Characterization* **2015,** *32* (4), 434-440.

43. Tuci, G.; Zafferoni, C.; Rossin, A.; Luconi, L.; Milella, A.; Ceppatelli, M.; Innocenti, M.; Liu, Y.; Pham-Huu, C.; Giambastiani, G., Chemical functionalization of N-doped carbon nanotubes: a powerful approach to cast light on the electrochemical role of specific N-functionalities in the oxygen reduction reaction. *Catalysis Science & Technology* **2016,** *6* (16), 6226-6236.

44. Sharma, P. P.; Wu, J.; Yadav, R. M.; Liu, M.; Wright, C. J.; Tiwary, C. S.; Yakobson, B. I.; Lou, J.; Ajayan, P. M.; Zhou, X.-D., Nitrogen-Doped Carbon Nanotube Arrays for High-Efficiency Electrochemical Reduction of CO2: On the Understanding of Defects, Defect Density, and Selectivity. *Angewandte Chemie International Edition* **2015,** *54* (46), 13701-13705.

45. Lei, Z.; Xu, S.; Wan, J.; Wu, P., Facile synthesis of N-rich carbon quantum dots by spontaneous polymerization and incision of solvents as efficient bioimaging probes and advanced electrocatalysts for oxygen reduction reaction. *Nanoscale* **2016,** *8* (4), 2219-2226.

46. Necas, D.; Klapetek, P., Gwyddion: an open-source software for SPM data analysis. *Central European Journal of Physics* **2012,** *10* (1), 181-188.

47. Peng, J.; Gao, W.; Gupta, B. K.; Liu, Z.; Romero-Aburto, R.; Ge, L.; Song, L.; Alemany, L. B.; Zhan, X.; Gao, G.; Vithayathil, S. A.; Kaipparettu, B. A.; Marti, A. A.; Hayashi, T.; Zhu, J.-J.; Ajayan, P. M., Graphene Quantum Dots Derived from Carbon Fibers. *Nano Letters* **2012,** *12* (2), 844-849.

48. A. V. Naumkin, A. K.-V., S. W. Gaarenstroom, C. J. Powell NIST XPS Standard Reference Database. Version 4.1.

49. Luo, P. H.; Qiu, Y.; Guan, X. F.; Jiang, L. Q., Regulation of photoluminescence properties of graphene quantum dots via hydrothermal treatment. *Physical Chemistry Chemical Physics* **2014,** *16* (35), 19011-19016.

Chapter 5: Structure-Function Relationship of Carbon Quantum Dots and Photo-induced Cytotoxicity Effects

Carbon quantum dots (CQDs) have been pursued for use in biophotonics due to their low cost, facile synthesis, and controllable optical properties. In this study, two types of CQDs were synthesized by different methods designated as top-down and bottom-up and their chemical structure and properties were compared. CQDs have been shown to display a unique balance of low dark cytotoxicity and strong photodynamic effect, but the mechanism for this photodynamic activity has not been determined. To the best of our knowledge, this is the first extensive study to investigate relations between chemical structure of CQDs and their photodynamic effect, and to track the mechanism of action in photodynamic therapy (PDT). Spectroscopic and chemical methods were employed to differentiate the chemical structure while cell viability, singlet oxygen ($^1O_2$), and DNA damage studies elucidated the photodynamic mechanism of action for each CQD sample. Graphene quantum dots (GQDs) synthesized by a top-down method exhibited superior light-activated cell cytotoxicity compared to carbon nanodots (CNDs) synthesized by a bottom-up method. The photodynamic index of GQDs was found to be 40 - 150 times larger than commerically available drugs. Singlet oxygen was quantitatively measured and found to be a primary cause for the observed photodynamic effect. Measurements with selective quenchers of $^1O_2$ and radical species such as (2,2,6,6-tetramethylpiperidin-1-yl)oxidanyl (TEMPO), sodium iodide and sodium azide indicated that the photodynamic mechanism of CQDs is through strong Type I and Type II photodynamic effects.

5.1   Introduction and Motivation

Photodynamic therapy (PDT) is a non-invasive therapeutic approach that benefits from effective cellular penetration, low inherent cytotoxicity, and strong light-activated cytotoxicity. Originally used as a treatment only for skin conditions such as vitiligo[1] it has recently been explored for actinic keratosis and basal cell carcinoma treatment.[2] The major challenge of PDT as a viable treatment is imposed by the tissue penetration depth of light. For example, UV and visible light is energetic enough to generate reactive oxygen species (ROS), however UV light ($\lambda < 400$ nm) risks damaging healthy

118

tissue as well. Visible light (400 – 760 nm) is safe for healthy tissues but has a short penetration depth ranging from sub-millimeter with blue light to a few millimeters with red light.[3] In the case of visible light, photodynamic medical treatments are limited to cutaneous and subcutaneous applications. Wavelengths between 650 nm and 1350 nm, commonly referred to as the optical therapeutic window due to low light absorption by tissues coupled with forward-directed scattering,[4] are ideal for optimal tissue penetration though many complications have emerged in efforts to develop near-IR absorbing compounds.

The development of PDT agents has primarily focused on small molecule photosensitizers, but their absorption and emission ranges often lie outside of the optical therapeutic window. Carbon nanomaterials have been extensively studied due to their tunable optical properties. This tuning can be performed by manipulating the size of the nanomaterial, known as the quantum confinement effect. Similar to inorganic semiconducting systems,[5] extending the size of the carbon nanomaterial narrows the optical bandgap due to the spatial confinement of excitons.[6] However, previous studies have shown that carbon nanomaterials exhibiting near-IR absorption and emission suffer from poor solubility in aqueous media.[7] Without the aid of surfactants, materials such as carbon nanotubes (CNTs) can aggregate into bundles which rupture the cell membrane and become inherently cytotoxic.[8-9] Several articles have reported on the cytotoxicity of CNTs cytotoxicity in the dark where in some cases the CNTs are even more cytotoxic than metal oxide nanoparticles.[10-14] However, there are also reports suggesting that inherent cytotoxicity can be controlled using sidewall functionalization.[10, 12-13, 15] All of these previous reports cast some doubt on the use of CNTs, as effective and non-toxic PDT agents.

Recently carbon quantum dots (CQDs), have emerged as a promising deep-tissue PDT agent with manipulated optical properties via chemical functionalization.[16-19] This new type of carbon-based nanoparticle has gained significant interest due to their widely tunable optical properties,[20-21] ease of synthesis[22-24] and modification,[25-27] resistance to photobleaching[28] as well as excellent biocompatibility.[18, 29] Briefly, a CQD can be described as a flat sheet of sp^2-hybridized carbon a few nanometers in size

with abundant functional groups (e.g. hydroxyl, carbonyl, carboxyl) terminating the sheet in all directions. These nanoparticles can also be spherical or elliptical in shape due to the presence of sp^3-hybridized carbon. In addition, CQDs can be synthesized with inexpensive starting materials such as citric acid in a bottom-up fashion[30-31] or carbon black by a top-down method.[32-33]

CQDs have shown efficacy as PDT agents in the areas of anti-bacterial and wound treatment.[19, 34-36] The detailed study by Ge *et al.* reported that CQDs are able to populate their triplet states and the photodynamic activity was purely through the Type II pathway.[19] This article also reported no detection of radical ROS in their EPR measurement. Other than the presence of heteroatom dopants (N, O, and S) as the result of the hydrothermal synthesis, there is little to no explanation of what chemical features in these CQDs provide such promising results. The same article also proposed a route to produce $^1O_2$ from a ground state $^3O_2$ by its energy transfer from excited singlet state of CQD despite its lifetime (on the order of nanoseconds) being simply too short to convert $^3O_2$ to the highly reactive $^1O_2$. However, it was expertly demonstrated using tetracene and pentacene that the effective photodynamic performance of CQDs requires efficient generation of triplet states for Type II photodynamic processes. Typically, these excited triplet states have lifetimes on the order of a few microseconds in CQDs as observed by Mueller *et al.*[37]

Unfortunately compared with near-IR responsive CNTs, CQDs generally suffer from low optical absorption and emission in the IR and near-IR range. However, this can be circumvented by controlling the morphology of a CQD with bottom-up synthesis as shown by Kumawat *et al.* or by removing internal defects in CQDs resulting in the extension of conjugation length as reported by Fan *et al.*[38-39] In light of the extensive studies on CQDs exhibiting photodynamic effects towards inducing cytotoxicity in cancer cells and tumors, a fundamental understanding of what structural parameters allow CQDs to be useful PDT agents remains unclear.

In this work, we have taken advantage of the predictable and easily controlled modification of CQDs in order to correlate specific structural and chemical features with efficacy in PDT. This project was a collaborative effort between our group and

Dr. Edith Glazer and Dr. David Heidary at the University of Kentucky. We explored the roles of sp^2-carbon content, edge-terminating functional groups (i.e. hydroxyl or carbonyl) and heteroatoms dopants on the impact toward PDT efficacy. It was found that the aromatic core from a top-down synthesis along with a variety of oxygen-containing functional groups yielded the highest performing PDT agents. By incorporating nitrogen into top-down synthesized CQDs or chemically reducing these carbon nanomaterials, we observed inhibited PDT performance. The bottom-up synthesis approach yielded a poorly performing PDT agent, which was enhanced by nitrogen-doping. Overall, it was observed that both synthetic methods and post-synthesis modifications can enhance the light/dark performance ratio, also known as the photodynamic index, over forty-fold larger than that of aminolevulinic acid (ALA) reported in the literature.[40] DNA damage experiments demonstrated that reactive oxygen radical species are photodynamically produced by CQDs in addition to $^1O_2$, signifying the Type I photodynamic mechanism. By employing ROS-selective quenching agents, we identified the correlation between specific chemical features of CQDs and the mechanism of action which, to our knowledge, had not been proven experimentally. Our results suggest that CQDs exhibit strong PDT activity in both the Type I (radical species production) and Type II (direct $^1O_2$ production) processes. This activity was also found to be tunable by chemical modification of functional groups. Additionally, it was determined with a comparison of bottom-up synthesized CQDs that surface passivation layers may inhibit PDT activity. Understanding the interplay between chemical structure and mechanism of action for the PDT effect will be essential to develop CQDs as non-toxic, low-cost, and highly effective PDT agents.

5.2   Experimental Details and Methods

Synthesis of GQD. Carbon nano-onions (5 nm in diameter) in a concentrated HNO_3/H_2SO_4 solution were refluxed at 105 °C for 5 h. The resulting solution was neutralized with KOH and filtered using a Buchner funnel (20 μm pore size) to remove salts and large particulates. 50 mL of filtered solution was placed into a dialysis bag (MWCO: 1 kDa) for 1 week to remove any remaining salts and then concentrated to 0.5 mg mL^{-1}.

Synthesis of NGQD (nitrogen-doped GQD). 5 mL of 0.5 mg mL^{-1} GQDs were mixed with 5 mL of concentrated NH_4OH (28 wt %) and placed in a hydrothermal (HT) reactor with no additional gas pressure applied. The HT reactor was placed in an oven at 180 ºC for 5 h and left to cool overnight. The resulting solution was gently heated to remove excess NH_3 and then dialyzed for 1 week to remove excess ions. The final concentration was 0.5 mg mL^{-1}.

Synthesis of rGQD. 10 mg of GQD were mixed with 10 mL of DI water and placed in a 20 mL vial. Then, 200 mg of $NaBH_4$ was added to the same vial and kept it stirring at room temperature for 1 hour. After that, the resulting solution was neutralized with dilute H_2SO_4. Next, above solution was dialyzed for 1 week using 1 kDa MWCO dialysis bag to remove any remaining salts and rGQD were obtained. Finally, the concentration of rGQD solution was adjusted to 0.5 mg mL^{-1}.

Synthesis of CND. 1 gram of solid citric acid in a 50 mL beaker was placed on a hotplate at 160 ºC for pyrolysis for 10 mins. At the end of this time, the liquid CNDs were quenched with 100mL of 0.1 M KOH solution to prevent aggregation and further reaction. The resulting solution was dialyzed for 1 week and concentrated to 0.5 mg mL^{-1}.

Synthesis of NCND (nitrogen doped CND). NCNDs were prepared in the same manner as NGQDs. 5 mL of 0.5 mg mL^{-1} CNDs were mixed with 5 mL of concentrated NH_4OH (28 wt%) and placed in a hydrothermal (HT) reactor with no additional gas pressure applied. The HT reactor was placed in an oven at 180 ºC for 5 h and left to cool overnight. The resulting solution was gently heated to remove excess NH_3 and then dialyzed for 1 week to remove excess ions. The final concentration was 0.5 mg mL^{-1}.

TEM Analysis. Samples were dropcast (20 µL) onto copper TEM grid with lacey carbon (400 mesh, Ted Pella) and left to dry in air overnight. High resolution TEM images of the samples were collected by a JEOL 2010F TEM. The acceleration voltage of 200 kV was used.

XPS Analysis. XPS analysis was conducted to probe elemental composition and the chemical states of elements. Samples were dropcast (5 µL drops) onto Si wafers several times and vacuum dried overnight at 40 °C to remove water and adventitious carbon. XPS experiments were conducted with a K-alpha X-ray Photoelectron Spectrometer (ThermoScientific).

FTIR Analysis. To probe chemical functional groups and chemical structure of the samples, ATR-FTIR analysis was conducted. Samples were dried in a powder and then placed onto ATR-FTIR crystal (diamond, Thermo Nicolet iS50 FTIR). Background spectrum was obtained with the bare crystal in air. FTIR spectra were corrected for adsorbed water and CO_2.

UV-VIS absorption and fluorescence (FL) characterization. Samples were diluted 10x for UV-Vis absorption and FL studies. FL studies used a series of excitation wavelengths with the slits set to 5 nm spectral band-widths. UV-Vis spectra were collected with an absorption spectrometer (Thermo Scientific, Evolution 201) and FL spectra were collected with a fluorescence spectrometer (Horiba, Fluoromax-3).

Cell viability in the presence and absence of light. The effect of the compounds on cell viability was determined in the HL60 cell lines. HL60 cells were plated in 96-well plates at a density of 30,000 cells per well in extracellular solution followed by the addition of compounds and incubated for 1 hr at 37 ºC with 5% CO_2. The plates were then irradiated for 1 min with a 450 nm LED array or kept in the dark, followed by the addition of opti-MEM supplemented with 2% FBS such that the final solution contained 1% FBS. The plates were incubated in the dark for 72 hrs at 37 ºC with 5% CO_2. Viability was determined upon the addition of 440 µM resazurin in PBS with the final concentration being 73 µM per well. The plates were incubated for three hours followed by measurement of fluorescence using a Tecan SPECTRAFluor Plus plate reader. The plates were read with the gain set to 60 and an excitation wavelength filter of 535 nm and emission of 595 nm. All data were collected in triplicate and normalized to wells incubated without compound and without cells. EC50 values were determined by plotting the concentration of compound vs the %viability and fit to the equation for a sigmoidal dose response using the software Prism.

Cell viability of nanodots attached to PDMS. Samples were covalently attached to poly(dimethylsiloxane) (PDMS) by first attaching 3-aminopropyl(triethoxysilane) (APTES) using standard methods and following up with EDC/NHS coupling using standard protocol at a diameter of 7.0 mm and placed at the bottom of the well in a 96-well plate. HL60 cells were added at 30,000 cells per well in ECS and incubated with the PDMS nanodot- coated disks for 1 hr. The plate was then irradiated for 1 min with an indigo LED, followed by the addition of opti-MEM containing 2% FBS. Viability was measured after 72 hrs as described above.

Measurement of reactive oxygen species via DNA damage: Samples were prepared in 10 mM sodium phosphate buffer with 40 μg/mL of pUC 19 plasmid. CQD samples were added at a final concentration of 0.25 mg mL^{-1} and all quenchers were diluted in water and added at a final concentration of 50 mM. Samples were irradiated for 5 min with an indigo LED array (145 J/cm^2) or kept in the dark. The 100 μM Rose Bengal positive control sample was only irradiated for 1 min with the indigo LED array (29.1 J/cm^2) to avoid complete damage to DNA. Samples were stained with 6x gel loading dye (NEB) and loaded onto a 1.0% agarose gel (Invitrogen). Gel electrophoresis was run in 1x Tris Acetate Buffer at 100 V with a current of 3.00 A for 1 hour. Gels were stained with ethidium bromide in 1x TA buffer for an hour and de-stained in 1x TA buffer for 45 min. Gels were imaged and quantified on a VersaDoc (Bio-Rad).

Measurement of singlet oxygen with SOSG. Singlet oxygen sensor green (Invitrogen) was prepared as a 5 mM solution in methanol. The SOSG was diluted to 5 μM in ECS and transferred to a 96-well plate. Compounds were added to a separate 96-well plate, serially diluted in ECS, and then transferred to the 96-well plate containing SOSG. Fluorescence was measured on a SPECTRAFluor Plus (Tecan) plate reader with an excitation of 485 nm and emission of 530 nm. The plate was then irradiated for 1 min with the indigo LED (29.1 J/cm^2) followed by fluorescence measurement. The change in emission signal before and after exposure to the indigo LED was plotted against the concentration of the compound.

124

5.3   Results, Discussion and Conclusions

To determine if photodynamic efficacy could be altered by varying the distribution of sp^2- and sp^3-carbon moieties in CQDs, carbon dots were synthesized with both top-down and bottom-up methods. For clarity, top-down produced carbon dots will be referred to as "graphene quantum dots" (GQDs) similar to reports that use synthetic techniques such as chemical oxidation[32, 39, 41] and electrochemical exfoliation.[42-44] The bottom-up approach produced carbon dots termed "carbon nanodots (CNDs)" as described in previous studies with microwave pyrolysis[31, 45-46] and hydrothermal treatment.[47-48] The overall synthetic schemes for GQD and CND are shown below in Scheme 1a and 1b, respectively.
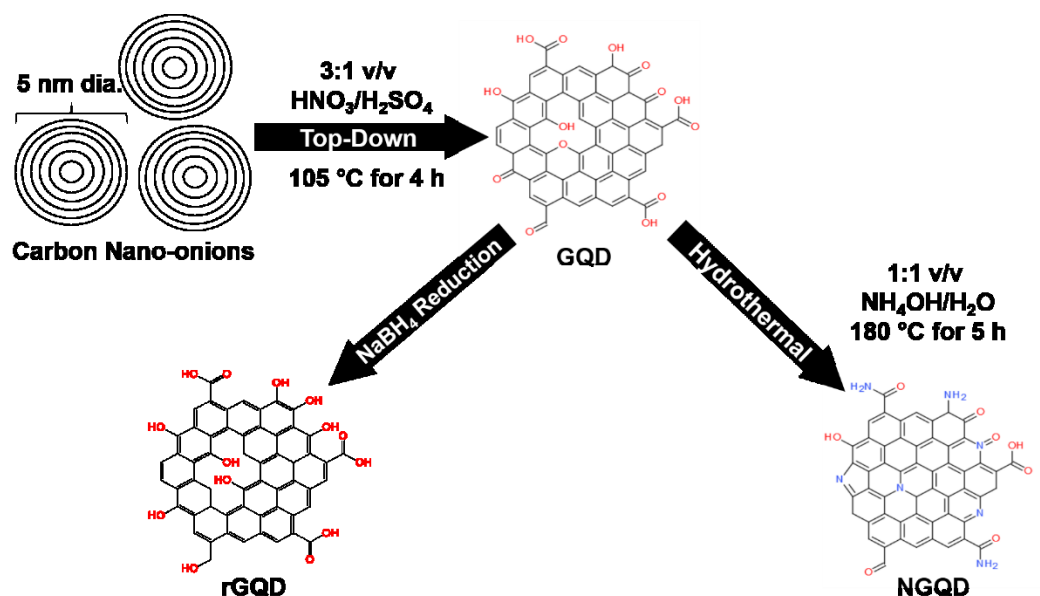
Scheme 5.1: Top-down synthesis of GQDs from carbon nano-onions. Post-synthesis modifications yield NGQDs by hydrothermally treating GQDs with aqueous ammonia or rGQDs by chemical reduction with $NaBH_4$.
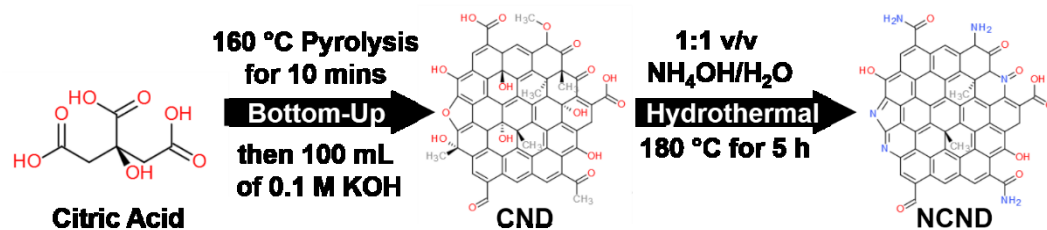
Scheme 5.2: Bottom-up synthesis of CNDs from citric acid. Post-synthesis modification yields NCND by hydrothermally treating CNDs with aqueous ammonia.

TEM experiments (Figure 5.1) determined that the undoped CQDs have an average diameter of 4.8 nm for GQDs and 8.8 nm for CNDs, which were not affected by post-synthesis modifications. In high-resolution TEM, lattice fringes of ~0.2 nm in size were observed for GQDs and CNDs, which corresponds to (1120) plane of a graphene sheet, which indicates that the carbon dots include sp^2-hybridized carbon domains. This hybridization was confirmed by both Fourier Transform Infrared spectroscopy (FTIR) and X-ray photoelectron spectroscopy (XPS).
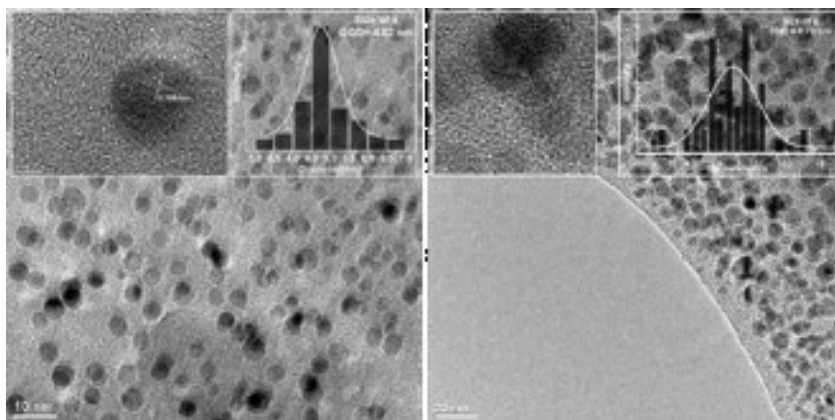
Figure 5.1: TEM images of carbon quantum dots. (Left) graphene quantum dots (GQDs) produced by a top-down method were about 5 nm in diameter. (Right) a bottom-up synthetic method produced carbon nanodots (CNDs) which had a larger diameter of about 9 nm. High-resolution TEM (inset) images show lattice fringes (about 0.22 nm spacing) relating to graphene-like structures in both sets of quantum dots.

The chemical states of carbon and nitrogen present in each CQD sample were determined by XPS (Figure 5.2 and 5.3, 5.10). The C1s spectra show that GQDs have a slightly larger sp^2-carbon to sp^3-carbon ratio compared to CNDs. This enhanced sp^2-carbon content originates from the high sp^2 content of the precursor, carbon nano-onions. Upon intercalation with sulfuric acid and oxidation by nitric acid, the fullerene-like layers become separated to form graphene-like sheets that are edge-terminated with oxygen-containing chemical groups.
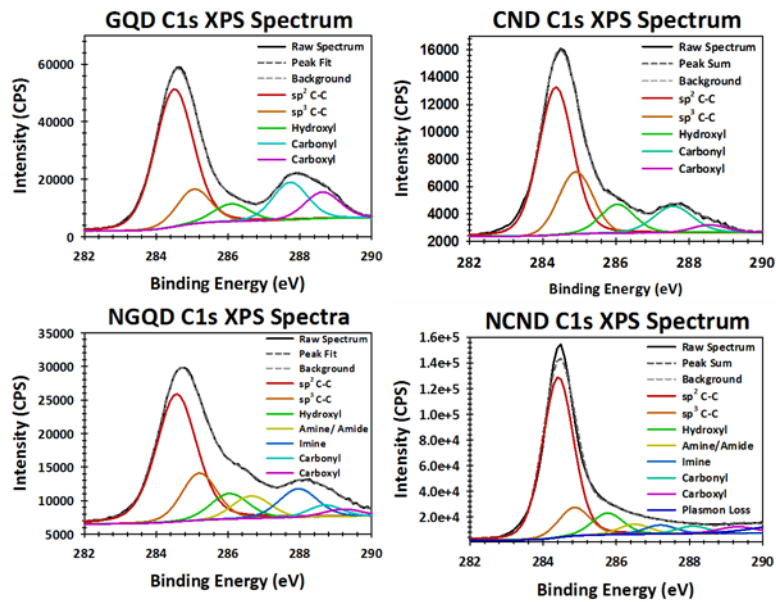
Figure 5.2: XPS C1s spectra of GQD (top left), NGQD (bottom left), CND (top right) and NCND (bottom right). All samples show significant sp^2-carbon content with varying amounts of sp^3-carbon. After nitrogen doping, this sp^3-carbon is enhanced in the GQD series due to hydrothermal cutting effects. In the CND series, the sp^3-carbon content is enhanced as the surface passivation layer collapses and condenses into more sp^2-carbon content.

Upon pyrolysis of citric acid above its melting temperature, two processes occurred, condensation and carbonization, which both form the CND framework. During condensation, two –OH form an ether or one –CO_2H and one –OH group form an ester, with dehydration occurring in both processes. Under these pyrolysis temperatures (> 160°C), water is evaporated to atmosphere making this process irreversible. Carbonization is also an irreversible reaction in which CO_2 is evolved in favor of forming the much stronger C=C bond and ultimately, the sp^2 nano-domain. Additional sp^3-carbon in CNDs is attributed to the incomplete carbonization of citric acid during the pyrolysis. This sp^3-carbon disrupts and passivates the sp^2 nano-domains and may contribute to the spherical structure of CNDs.

Determining the structure-function relationship requires a detailed analysis of the chemical structure. We chose to characterize our samples with the combination of XPS and FTIR to probe the specific distribution of chemical states in each CQD. XPS experiments show that both CND and GQD have similar overall oxygen contents but with varying distributions of functional groups (i.e.: hydroxyl, carbonyl and carboxyl).

127

GQDs tend to possess more carbonyl and carboxylic acid moieties as the result of the harsh oxidation condition with nitric acid during synthesis. CNDs, in comparison, have more hydroxyl groups and less carboxylic acid groups. Carboxyl groups are often gasified as CO_2 during pyrolysis. The peaks have been assigned with 286 eV for C-O, 288 eV for carbonyl groups associated with aldehydes, ketones, and esters, and 289 eV is assigned to carboxylic acids due to the strong electron withdrawing effect of the oxygen which shift the binding energy of the C1s electron higher.

Nitrogen-incorporated samples (NGQDs and NCNDs) have C1s spectra similar to their undoped counterparts but with notable changes in sp^3-carbon content. These quantitative results can be found in Table 5.1. An additional set of peaks relating to amine, amide and imine N appears around 287 eV. The N1s spectra of NGQD and NCNDs (Fig. 5.3) show similar relative peak intensities where amine/amide N (~ 399.5 eV) is the dominant species, followed closely by pyridinic (398.5 eV), pyrrolic (400.2 eV), and N-oxide (403 eV). Interestingly, there is a substantial amount of quaternary N (401.6 eV) present in NGQD despite having more sp^2-C before nitrogenation. We attribute this to the high temperature used for hydrothermal treatment (180 °C) which can replace defects in the sp^2 nano-domain with nitrogen.
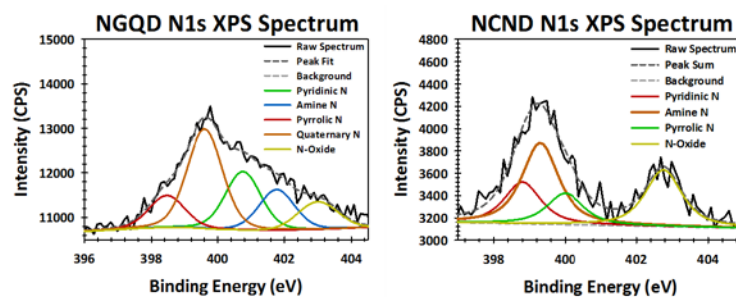
Figure 5.3: XPS N1s spectra of NGQD (left) and NCND (right) produced by similar hydrothermal treatment conditions. Though the process to add nitrogen was the same for both samples, it was found that NGQDs carry more functional group diversity than the bottom-up synthesized NCNDs. Unique to each sample, NGQDs has a substantial amount of graphitic N whereas NCNDs contains more N-oxide functionality.

FTIR spectra of GQDs confirmed the previous XPS interpretations, by revealing peaks assigned to hydroxyl (1200 and 3400 cm^{-1}), carbonyl (1700 cm^{-1}), carboxyl (1750 and 2500 cm^{-1}), and aromatic carbon (1400 and 1550 cm^{-1}) (Figure 5.4). After

hydrothermal reaction of GQDs with aqueous ammonia, NGQDs show new peaks characteristic of a successful reaction. The simultaneous shift from the 1200 and 3400 cm^{-1} peaks to 1050 cm^{-1} and 3300 cm^{-1} is attributed to the replacement of hydroxyl groups (C-O and O-H stretches) with N-containing functional groups (C-N and N-H stretches), respectively. Carboxylic acid groups are converted to amide groups, signified by the shift of the peak from 1750 cm^{-1} to 1650 cm^{-1} and the loss of the well-defined peak at 2500 cm^{-1}. rGQD, shown in Figure 5.11, shows a suppression of peaks relating to carbonyl groups at 1750 cm^{-1} and 3300 cm^{-1}. This is coupled with the increase of peak intensity at 1100 cm^{-1} corresponding to hydroxyl groups. There is also a minor suppression related to the loss of carboxylic acid groups, which is consistent with the XPS spectra in Figure 5.10. This result shows the conversion of carbonyl groups to hydroxyl groups by NaBH$_4$ reduction.
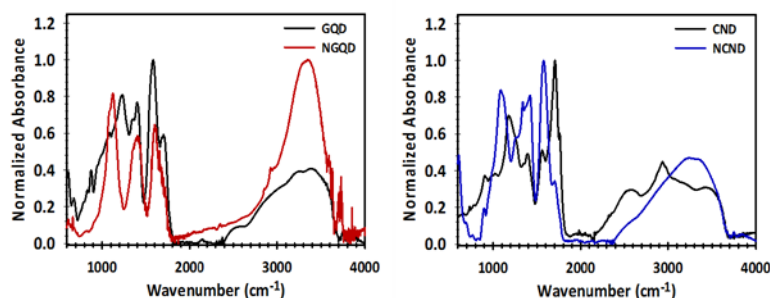
Figure 5.4: FTIR Spectra of GQD/NGQD (left) and CND/NCND (right) samples.

The FTIR spectra of CNDs show similar oxygen-containing functional groups like GQDs but with intensities that correspond to the varied functional group distribution. Unique to CNDs, there is a significant sp^3-carbon peak (C-H stretch) at 2950 cm^{-1} that is removed upon hydrothermal treatment. Like GQDs, the same shift of –OH to –NH$_2$ occurs when ammonia is added to CNDs. Additionally, the peaks at 1700 and 1750 cm^{-1} are greatly suppressed upon nitrogenation, signifying the conversion of carboxyl groups to amides and reducing carbonyls to hydroxyls which then are converted to primary amines.

Optical measurements (i.e.: absorption and photoluminescence) were used to identify the optimal wavelength for the cell viability and DNA damage studies

discussed later. In general, compared with GQDs, CNDs tend to absorb/emit at shorter wavelengths due to smaller sp^2 nanodomains that are well passivated which block non-radiative relaxation. This is also the case in Fig. 5.5 where CQD samples of the same concentration (0.05 mg mL^{-1}) were analyzed by UV-Visible absorption spectroscopy. Upon nitrogenation, both CND and GQD samples globally increase their absorbance at all wavelengths. However, it is important to note that NGQDs absorb a wider range of visible light than all the other CQD samples.
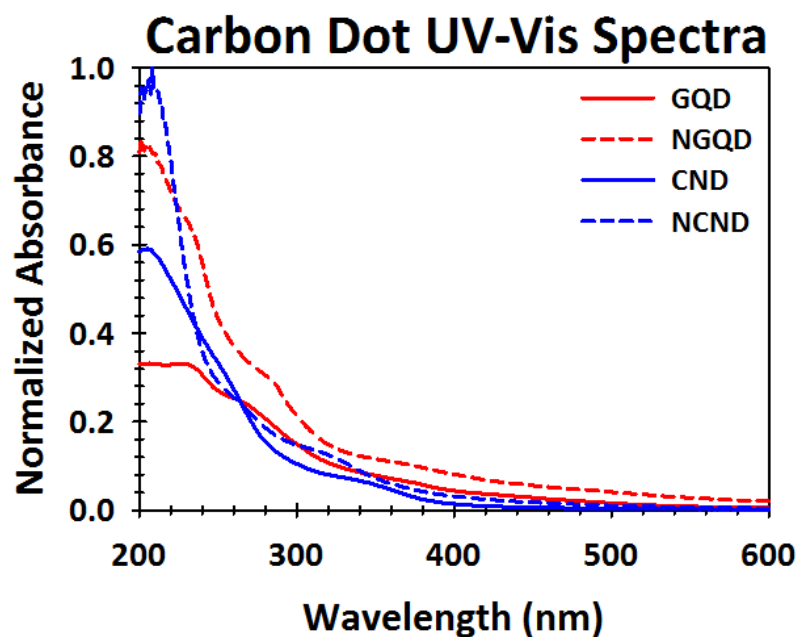
Figure 5.5: UV-Vis Absorbance spectra of each CQD sample. GQDs (red solid line) absorbs visible light more than CNDs (blue solid line) which absorbs primarily UV light. Upon nitrogenation (dashed lines), absorbance is enhanced for all samples universally across the measured wavelengths.

Overall, the photoluminescence (PL) of CQDs in this report exhibit optical properties similar to the report by Wang et al. that detail intrinsic emission from the aromatic carbon core and extrinsic emission originating from molecule-like fluorophores.[49] GQDs and NGQDs both have similar excitation-dependent emission profiles with 520 nm peak emission at 450 nm excitation which relates to extrinsic emission. However NGQDs show peak emission with 420 nm excitation (Figure 5.6). Chemical reduction of GQD resulted in peak emission wavelengths that were shifted to shorter wavelengths (Figure 5.12). In comparison with GQDs, CNDs display blue-

shifted photoluminescence with 450 nm peak emission upon to excitation at 330 nm. We attribute the blue-shift of emission to surface-passivated aromatic domains formed during synthesis. Compared to CNDs, nitrogen-doped CNDs (NCNDs) were blue shifted by 30 nm with the same excitation wavelength. Based on previous XPS and FTIR characterization, the most common feature between these five CQD samples is the sp^2-hybridized nano-domain.
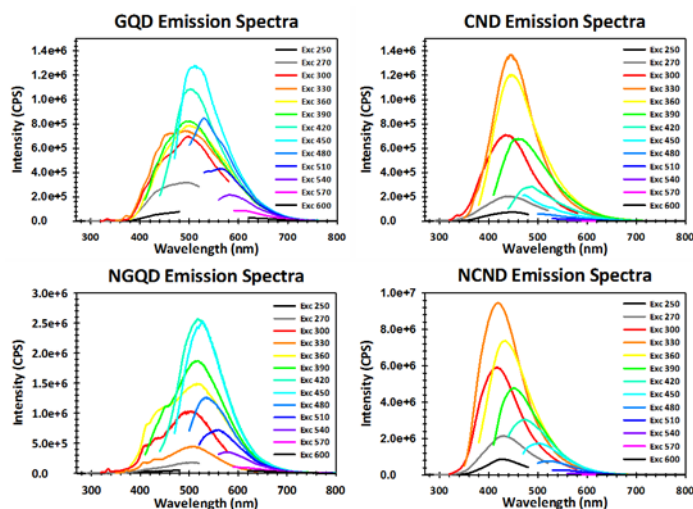
Figure 5.6: Photoluminescence spectra of GQD (top left), NGQD (bottom left), CND (top right), and NCND (bottom right). GQDs and their nitrogen-doped counterparts have similar emission profiles however CNDs and NCNDs vary greatly in both peak emission wavelength and intensity.

As with optical absorption and emission profiles, the photoluminescent quantum yield (PLQY) is used to identify which CQDs show stronger radiative or non-radiative decay channels. This information allows for greater understanding of Type I processes which require charge transfer versus Type II processes which require energy transfer. If there is significant competition of the PDT agent with its own fluorescence, neither charge transfer nor energy transfer will be a dominant process, reducing PDT efficacy. Table 5.2 shows the absolute photoluminescent quantum yield (PLQY) of each CQD sample which was determined using an integrating sphere. Overall, nitrogenation and chemical reduction increase the PLQY of both CNDs and GQDs. Enhancement by the addition of nitrogen has been extensively studied for its effect on optical properties.[17,] [20] Reduction of existing carbonyl functional groups to hydroxyls which has also been shown to increase photoluminescent QY. NaBH$_4$-reduced GQDs (rGQDs)

demonstrated similar PL increases (Figure 5.12) as those shown in other reports.[50-51] The PLQY enhancement is attributed to the reduction of dark state carbonyl to the bright state hydroxyl.[52]

CNDs inherently have a higher PLQY than GQDs due to the effect of surface passivation. By restricting the mobility of the exciton, direct emission takes precedence over non-radiative decay channels such as vibrational relaxation and energy transfer. NCNDs show a significant increase of PLQY compared to CNDs which is again consistent with reports that dope nitrogen into carbon quantum dots. Based on XPS analysis from Figures 5.2 and 5.3, we assign the PLQY enhancement in NCNDs to the collapse of sp^3-C passivation layer and the increase of dipole moments associated with nitrogen-related chemical states which are pyridinic, amine/amide, pyrrolic and N-oxides. As with NGQDs, the hydrothermal treatment of CND at this temperature could cause cutting effects. However we hypothesize the sp^3 surface passivation layer of CNDs may act as protection from hydrothermal cutting effects. GQDs, without a significant passivation layer, would not experience this same protection and be vulnerable to hydrothermal cutting or disruption of the contiguous sp^2-carbon nanodomain with the electron-rich graphitic N. These modifications have been shown to have a significant effect on photoluminescent properties.[53-54]

Efficacy of CQDs as PDT agents was evaluated in a leukemic cell line (HL60). The cells were dosed with CQDs and irradiated for 1 minute with 450 nm light or kept in the dark. Viability was measured after 72 hrs. As hypothesized, the efficacy of CNDs and GQDs as a PDT agent was dependent on chemical and structural changes.

GQDs were the most effective PDT agent among all the CQD samples tested (Figure 5.7). In HL60 cells, GQD and NGQD concentrations up to 0.5 mg mL^{-1} were not cytotoxic (Figure 5.7c and d). When GQDs were exposed to 450 nm light, cytotoxicity occurred with an EC_{50} value of 10^{-3} mg mL^{-1}. These results give a GQD photodynamic index of nearly 725, which is 40 times more potent than commercial PDT drugs such as aminolevulinic acid (ALA).[40] Additionally, GQDs that were chemically reduced or hydrothermally N-doped show a decreased photodynamic index compared to unmodified GQDs.
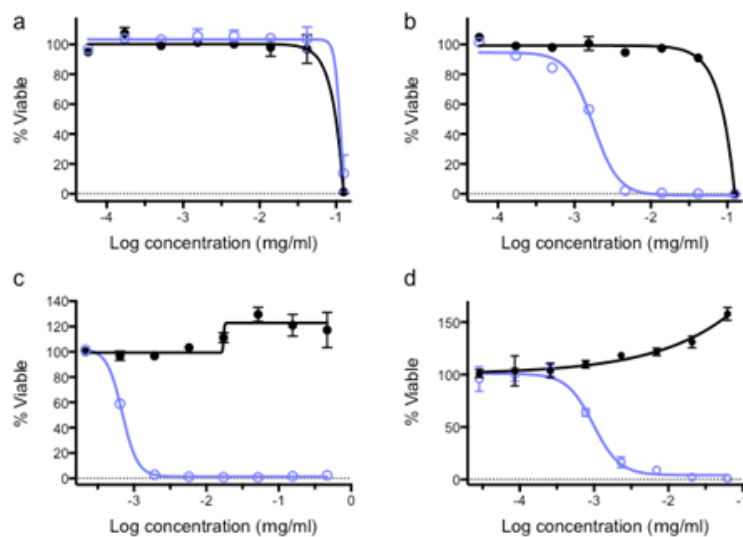
Figure 5.7: Efficacy of compounds as PDT agents determined in HL60 cells. Cell viability determined for a) CND, b) NCND, c) GQD, and d) NGQD. Compounds were dosed with the cells and either exposed to indigo light (blue line) or kept in the dark (black line).

Unmodified CNDs had no PDT activity in HL60 cells. Cytotoxicity occurred at concentrations of over 0.1 mg mL^{-1} in the absence or presence of irradiation. Interestingly, N-doped CNDs "switch on" a much stronger photodynamic effect toward cancer cells. We speculate that the collapse of the sp^3 surface passivation layer coupled with the new nitrogen-containing functional groups allow for facile electron transfer allowing the generation of ROS (OH· or OOH·). The lack of a surface passivation layer could allow for intimate contact between ROS precursors such that the newly formed nitrogenated functional groups can participate in redox processes. Likewise, the presence of a surface passivation layer may prevent this contact resulting in little or no PDT activity as seen in CNDs.

After the cell viability experiments, we considered that a physical mechanism such as cell lysis (or contact-kill mechanism) could be partially responsible for those results. Figure 5.16 illustrates that covalently anchored CQDs show no cytotoxicity, implying that cytotoxicity most likely occurred due to uptake of the CQD into the cytosol, possible through endocytosis.

In order to explore the structure-function relationship of CQDs, the amount of (^{1}O$_2$) singlet oxygen generated by different types of CQDs were tracked (Figure 5.8). CNDs

133

produced very little singlet oxygen and only with very high concentrations did the NCNDs show measurable production of singlet oxygen. These results correlate with cell cytotoxicity. Compared to CNDs, GQDs had nearly six times the $^1O_2$ generation. Interestingly, any modification to the GQD suppressed the PDT efficacy which correlates with the cellular cytotoxicity. In contrast to CNDs, NGQDs show about a five-fold increase of generated $^1O_2$ and rGQD show a nearly four-fold increase of generated $^1O_2$. At very high concentrations of 0.1 mg mL^{-1}, the 5 µM singlet oxygen sensor green dye (SOSG) becomes saturated with singlet oxygen. This results in a decrease of emission by SOSG dye. The 0.1 mg mL^{-1} data points fall into the range where dark cytotoxicity becomes a problem with CNDs and NCNDs and were not used for comparison with any of the CQD samples. These results could infer: (i) when the pristine aromatic core of GQD is disrupted by graphitic N, photodynamic activity is lost; and (ii) carbonyl functional groups may relate to photodynamic activity as upon chemical reduction with NaBH$_4$, there is a severe decrease in singlet oxygen production. Overall, top-down synthesized GQDs, NGQDs, rGQDs outperform bottom-up synthesized CNDs and NCNDs, implying that structural defects in sp^2-carbon domains and oxygenated edge-terminating chemical groups are crucial for efficient production of singlet oxygen.

Singlet oxygen production
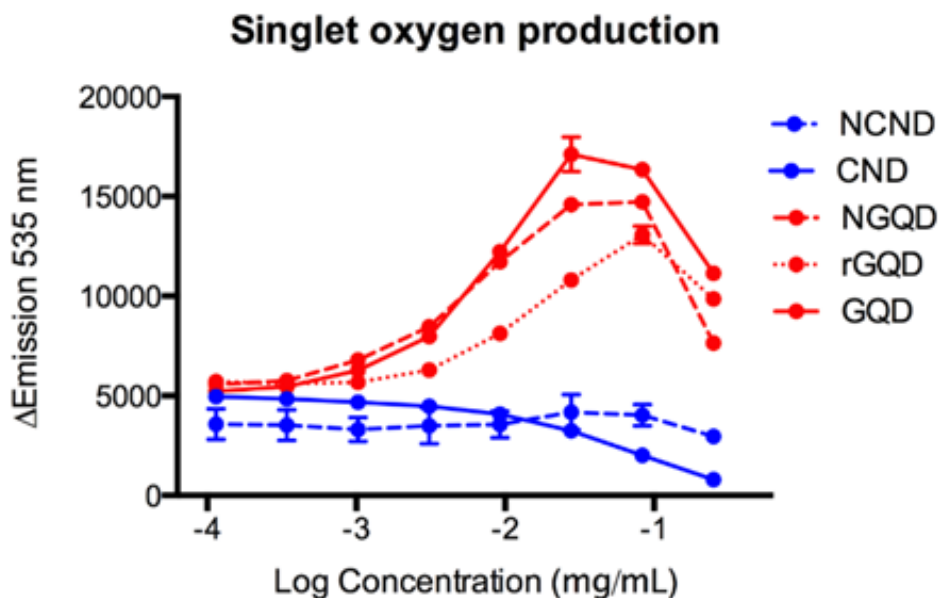
Figure 5.8: Relative measurement of singlet oxygen as a function of CQD concentration. The GQD series show significant production of singlet oxygen compared to the CND series. Upon any chemical modification of GQDs such as reduction or nitrogen-doping, the amount of produced singlet oxygen drops. In all studies the fluorescent SOSG dye was used as the measure of singlet oxygen.

The PDT mechanism could be due to a Type I (radical species production) or a Type II (direct $^1O_2$ production) mechanism. To further elucidate the mechanism of action, damage of DNA plasmid was used as a reporter. Compounds were incubated with plasmid and illuminated in the presence or absence of ROS selective quenchers. As ROS is generated, the supercoiled plasmid sustains either single or double strand breaks, resulting in relaxed circle or linear plasmid. The amount of these plasmid species was quantified for GQDs and NGQDs (Figure 5.9). The results for the other CQDs can be found in the Supporting Information (Figure 5.14 and 5.15).
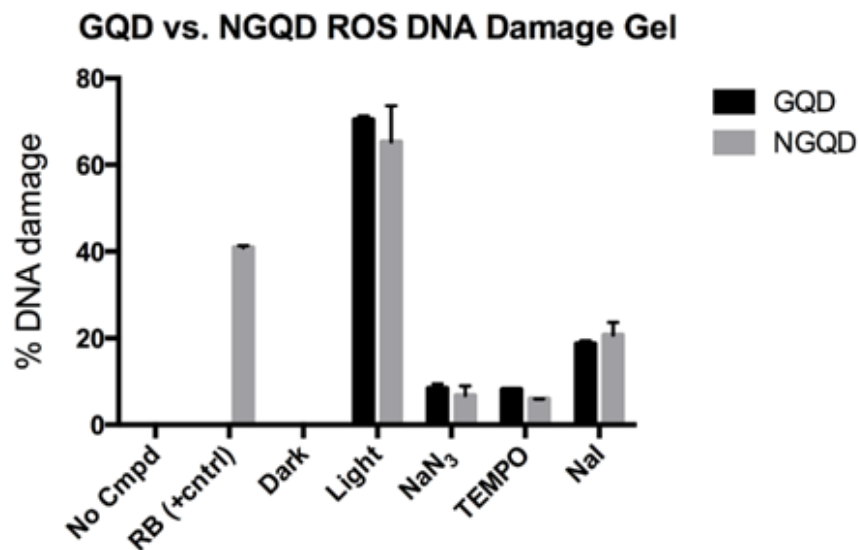
Figure 5.9: Gel electrophoresis results of DNA damage experiment. It can be seen that there is a moderate amount of plasmid fragmentation when exposed to GQDs and light. Without either GQDs or light, there is no measurable fragmentation. Additionally, quenching agents such as TEMPO or ascorbic acid help determine the photodynamic mechanism of action by selectively blocking specific reactive oxygen species. NGQDs show similar behavior to GQDs but with less effect.

As expected, GQD-plasmid solution without light irradiation clearly shows very little damage to the plasmid DNA. The irradiated GQD-plasmid and NGQD-plasmid sample shows significant damage – even more so than 100 μM Rose Bengal (RB). DNA damage was measured in the presence of several selective quenching molecules. Sodium azide (NaN$_3$) was used to selectively quench singlet oxygen ($^1O_2$). TEMPO, a common radical scavenger, was used to trap radical ROS and sodium iodide (NaI) as a hydroxyl radical quenching agent. DNA damage was significantly reduced for both GQDs, NGQDs and rGQDs when the solutions were irradiated in the presence of NaN3, TEMPO, or NaI (Figure 5.9 and Figure 5.15). These results indicate that singlet oxygen is not the only ROS species produced by GQDs and their modified counterparts. In fact, there is little preference for one specific ROS and that the mixture of superoxide, hydrogen peroxide, hydroxyl radical, and other radical species produced play a substantial part in the photodynamic death of cancer cells. In the case of NCNDs (Figure S5), which showed strong light-activated cytotoxicity, the photodynamic mechanism of action is largely driven by radical ROS. We hypothesize that the

combination of added nitrogen heteroatoms and collapse of the surface passivation layer generate an active site in which electron transfer can more freely occur.

The overall mechanism of action for CQDs involves both Type I and Type II processes. For GQDs and their derivatives, oxygenated functional groups and defects (vacancies) are crucial to generate singlet oxygen species and reactive radicals. We suspect that carbonyl functional groups of unmodified GQDs are responsible for $^1O_2$ production as chemical reduction with $NaBH_4$ reduces singlet oxygen production significantly. From the DNA damage experiments, unmodified GQDs also show the greatest quenching with NaI, further suggesting that the carbonyl group is also responsible for hydroxyl radical production. Conversely, quenching with NaI shows that rGQD produce the smallest amount of hydroxyl radicals, enabling other ROS species to carry Type I PDT activity. NGQDs are particularly interesting as they produce intermediate results between GQDs and rGQDs in cell viability, $^1O_2$ production, and DNA damage experiments. We have observed through FT-IR and XPS characterization that the conversion of carbonyl functional groups diverges into both imines and hydroxyl groups. As such, we hypothesize that the imine functional group either is inactive or weakly active for the Type I process and the smaller amount of hydroxyl groups produced gives rise to the intermediate results. For nitrogen-doped CNDs, the mechanism of action is more towards a Type I process due to a very low singlet oxygen production and total suppression of DNA damage when TEMPO is the quenching agent. We cannot determine whether the PDT activity of these functional groups (molecule-like states) comes from direct energy transfer to molecular oxygen from their own excited triplet state, or via indirect energy transfer between the intrinsic state and the molecule-like state. Nonetheless, the trends found across GQDs, NGQDs, and rGQDs in this study suggest that specific functional groups (i.e.: carbonyls, hydroxyls and imines) may play an important role toward the Type I and Type II mechanisms of action. To the best of our knowledge, this is the first report in which the detailed structure-function relationships of CQDs are investigated in the context of photodynamic therapy.

GQDs and other chemically modified CQDs used for photodynamic anti-cancer therapy demonstrated excellent PDT activity toward HL60 cancer cell lines using 450 nm light as the excitation source. Through a battery of experiments including singlet oxygen measurements and DNA damage experiments performed with gel electrophoresis, it was found that GQDs outperformed CNDs. Uniquely, nitrogenation of the bottom-up synthesized CNDs switched on the PDT activity whereas chemical modification of GQDs show an inhibitive effect. Ideally, IR-absorbing CQD would be a better PDT agent due to the potential for deep tissue penetration. However, this work provides a strong foundation about the structure-photodynamic effect relation and the mechanism of action. For the first time, both Type I and Type II photodynamic processes were observed based on the ROS produced by the photoactivation of GQDs, NGQDs, and rGQDs. Furthermore, we propose that carbonyl, hydroxyl and imine groups of CQDs play a critical role in determining the detailed mechanism of PDT activity through Type I and Type II pathways. With this information, there is now great promise to engineer IR-absorbing CQDs for non-toxic and cost-effective photodynamic agents with a diverse mechanism of action.

5.4 Supporting Tables and Figures
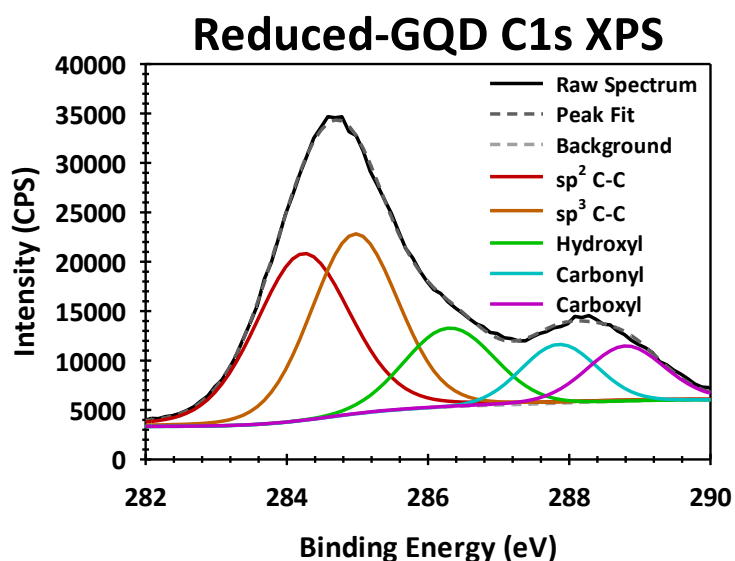
Figure 5.10: rGQD XPS high resolution spectrum. Compared to the unmodified GQD, there is a substantial decrease of carbonyl functionality coupled with an increase in hydroxyl groups.
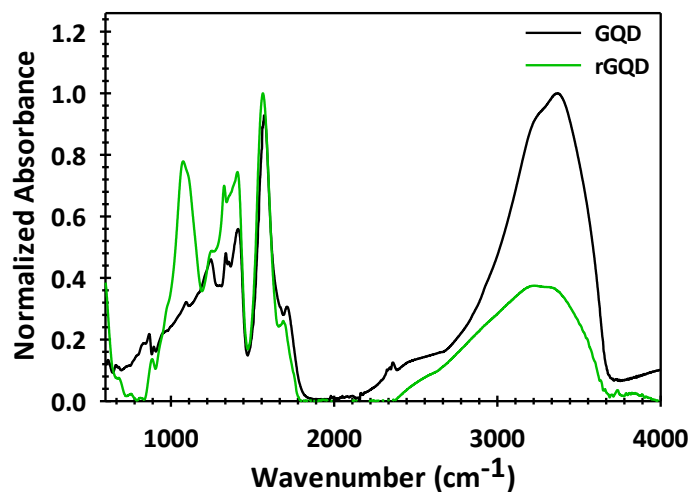
Figure 5.11: rGQD FT-IR Spectra. It can be seen that chemical reduction converts carbonyl groups (1750 cm^{-1}) to hydroxyl groups (1100 cm^{-1}, broadening of 3300-3400 cm^{-1}).
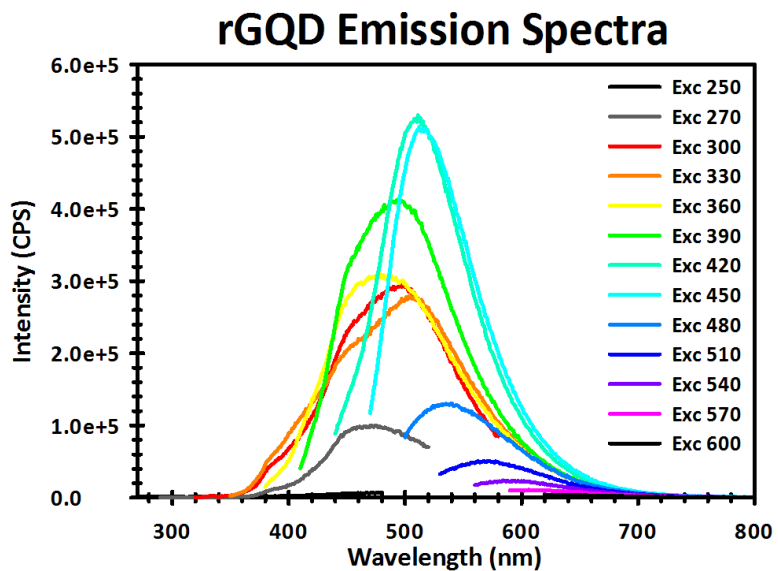
Figure 5.12: rGQD Emission Spectra. Compared to unmodified GQD, emission is shifted toward higher energy (lower wavelength) by the removal of carbonyl groups; reducing the π-conjugation of the quantum dot.
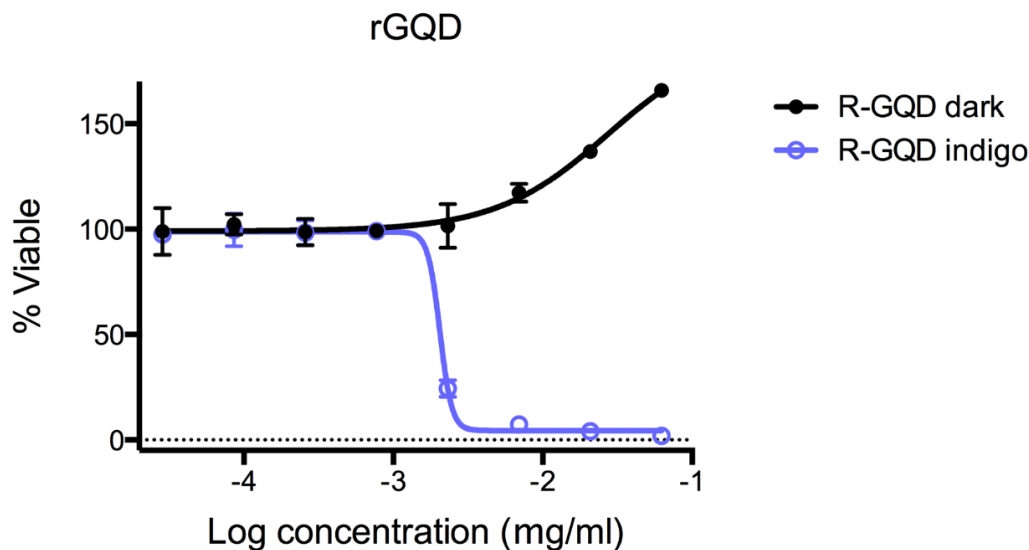
rGQD

Figure 5.13: rGQD cell viability results in the dark (black line) and with exposure to light (blue line). Compared to both unmodified and nitrogen-doped GQD, photo-induced cytotoxicity can only occur with higher concentrations.

CND grouped
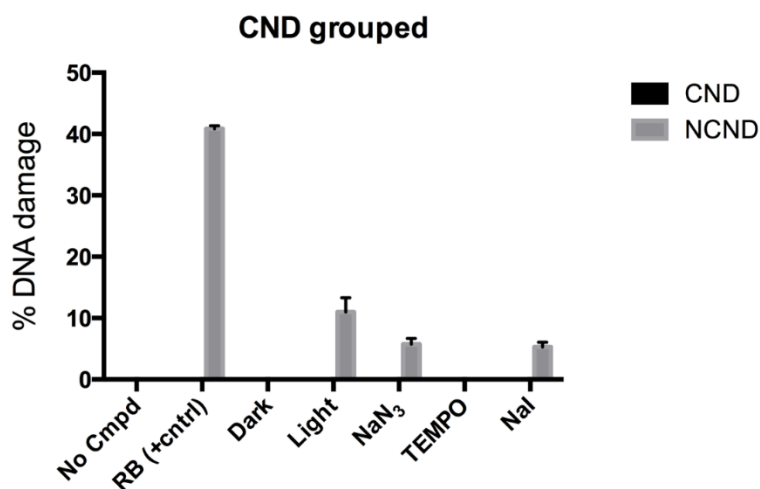
Figure 5.14: CND and NCND results from DNA damage experiment. As seen in cell viability experiments, unmodified CND show no appreciable photodynamic therapy effects. NCND on the other hand primarily act as PDT agents through radical compounds. When treated with sodium azide (NaN_3), TEMPO, or sodium iodide (NaI), the photodynamic performance is quenched by suppressing singlet oxygen, superoxide and hydroxyl radicals, respectively. Note: RB (+cntrl) refers to a control solution of 100 μM Rose Bengal which demonstrated roughly 40% DNA damage.

GQD grouped
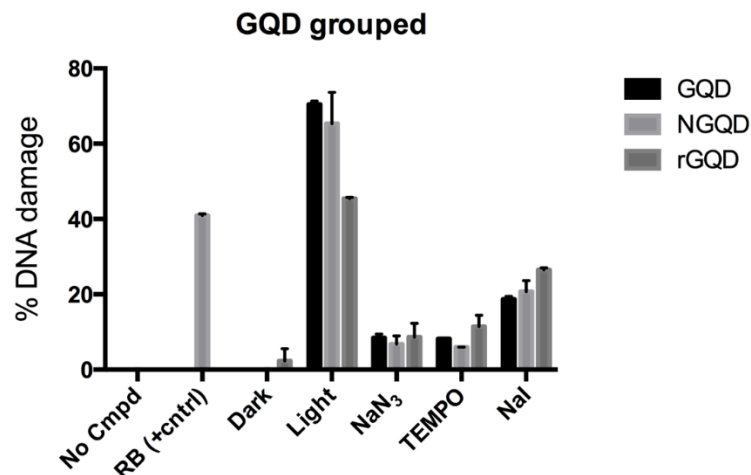
Figure 5.15: GQD, NGQD, and rGQD results from DNA damage experiment. As before, unmodified GQD exhibits the greatest photo-induced damage to the sample plasmid through a cocktail of singlet oxygen and radicalized species. Nitrogen-doping or chemical reduction suppress the PDT activity. Interestingly, rGQD experiences less singlet oxygen production and instead utilizes radical species (i.e. superoxide and hydroxyl radicals) as the dominant mechanism of photo-induced cytotoxicity. Note: RB (+cntrl) refers to a control solution of 100 µM Rose Bengal which demonstrated roughly 40% DNA damage.
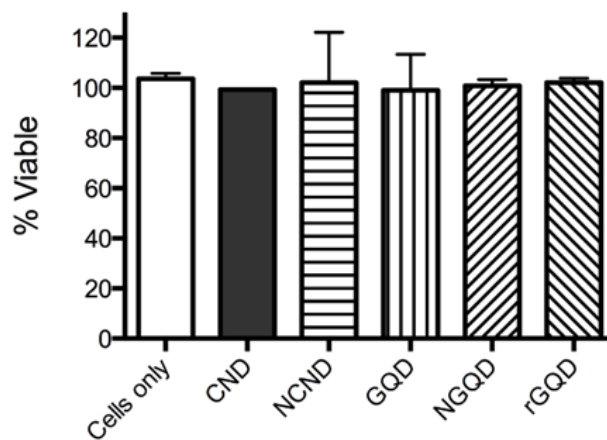
Figure 5.16: Cytotoxicity does not occur with CQD samples covalently mounted onto PDMS substrates. Results show that there is no significant amount of cell death by a contact-kill mechanism.

Lane #	Compound	% DNA Damaged
1	Ladder	–
2	No cmpd	0
3	100μM RB	40.518
4	GQD dark	0
5	GQD light	69.768
6	GQD NaN₃	7.722
7	GQD TEMPO	8.093
8	GQD NaI	18.223
9	NGQD dark	0
10	NGQD light	59.426
11	NGQD NaN₃	5.226
12	NGQD TEMPO	5.921
13	NGQD NaI	22.786
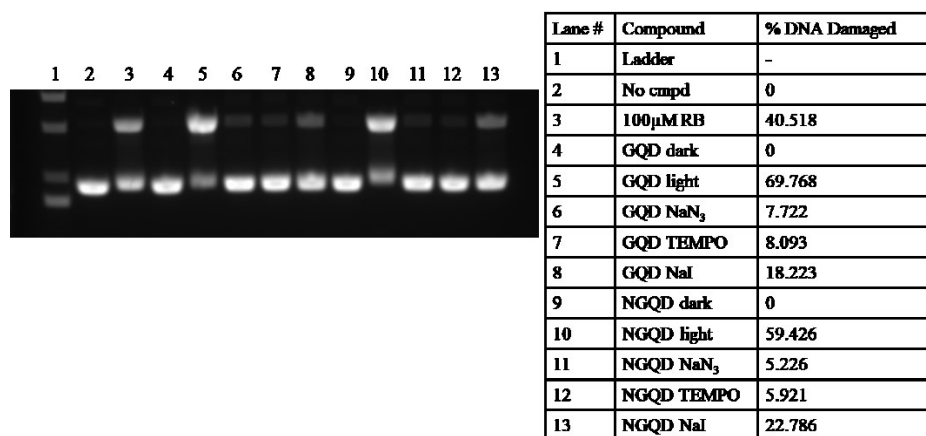
Figure 5.17: Photograph and quantitative results of DNA Damage with GQDs and NGQDs. NaN$_3$ was used as a $^1O_2$ quencher, TEMPO as a radical ROS quencher and NaI as a selective hydroxyl radical quencher.

Table 5.1: Quantitative results of sp^2 carbon, sp^3 carbon, and related functional groups determined by the deconvolution of XPS C1s Spectra.

	sp^2 Carbon (%)	sp^3 Carbon (%)	C-O (%)	C-N (%)	C=N (%)	C=O (%)	CO$_2$H (%)
GQD	56.51	12.56	6.92	---	---	14.14	9.87
NGQD	50.00	15.54	9.10	7.55	10.12	3.61	2.37
rGQD	34.47	33.27	14.36	---	---	8.95	8.94
CND	54.18	21.38	10.64	---	---	11.02	2.77
NCND	58.47	10.42	7.96	3.70	3.29	2.79	3.06

Table 5.2: Photoluminescence quantum yields of CQD samples measured with an integrating sphere.

	PLQY (%)
GQD	0.48 ± 0.067
NGQD	10.07 ± 0.109
rGQD	3.89 ± 0.084
CND	3.03 ± 0.041
NCND	11.12 ± 0.135

Table 5.3: Comparison of photodynamic index values of CQD samples and commercially available PDT drugs. Photodynamic index is defined as the dark cytotoxicity EC_{50} divided by the light cytotoxicity EC_{50}.[40]

	Dark Cytotoxicity EC_{50} (mg mL^{-1})	Light Cytotoxicity EC_{50} (mg mL^{-1})	Photodynamic Index
GQD	> 0.5	0.00069	724
NGQD	> 0.5	0.00098	510
rGQD	> 0.5	0.0025	200
CND	0.067	0.106	0.6
NCND	0.057	0.0016	36
ALA[40]	0.039	0.0021	19
Foscan®[41]	0.0020	0.00039	5

5.5   Chapter 5 References

1. Josefsen, L. B.; Boyle, R. W., Photodynamic Therapy and the Development of Metal-Based Photosensitisers. *Metal-Based Drugs* **2008,** *2008*, 276109.

2. Ericson, M. B.; Wennberg, A.-M.; Larkö, O., Review of photodynamic therapy in actinic keratosis and basal cell carcinoma. *Therapeutics and Clinical Risk Management* **2008,** *4*, 1-9.

3. Barun, V. V.; Ivanov, A. P.; Volotovskaya, A. V.; Ulashchik, V. S., Absorption spectra and light penetration depth of normal and pathologically altered human skin. *Journal of Applied Spectroscopy* **2007,** *74*, 430-439.

4. Wilson, B. C.; Jacques, S. L., Optical reflectance and transmittance of tissues: principles and applications. *IEEE Journal of Quantum Electronics* **1990,** *26*, 2186-2199.

5. Wang, Y.; Herron, N., Nanometer-sized semiconductor clusters: materials synthesis, quantum size effects, and photophysical properties. *Journal of Physical Chemistry* **1991,** *95*, 525-532.

6. Zhang, F.; Liu, F.; Wang, C.; Xin, X.; Liu, J.; Guo, S.; Zhang, J., Effect of Lateral Size of Graphene Quantum Dots on Their Properties and Application. *ACS Applied Material Interfaces* **2016,** *8*, 2104-2110.

7. Akizuki, N.; Aota, S.; Mouri, S.; Matsuda, K.; Miyauchi, Y., Efficient near-infrared up-conversion photoluminescence in carbon nanotubes. *Nature Communcations* **2015,** *6*, 8920.

8. Wick, P.; Manser, P.; Limbach, L. K.; Dettlaff-Weglikowska, U.; Krumeich, F.; Roth, S.; Stark, W. J.; Bruinink, A., The degree and kind of agglomeration affect carbon nanotube cytotoxicity. *Toxicology Letters* **2007,** *168*, 121-131.

9. Kang, S.; Herzberg, M.; Rodrigues, D. F.; Elimelech, M., Antibacterial Effects of Carbon Nanotubes: Size Does Matter! *Langmuir* **2008,** *24*, 6409-6413.

10. Sayes, C. M.; Liang, F.; Hudson, J. L.; Mendez, J.; Guo, W.; Beach, J. M.; Moore, V. C.; Doyle, C. D.; West, J. L.; Billups, W. E.; Ausman, K. D.; Colvin, V. L., Functionalization density dependence of single-walled carbon nanotubes cytotoxicity in vitro. *Toxicology Letters* **2006,** *161*, 135-142.

11. Bottini, M.; Bruckner, S.; Nika, K.; Bottini, N.; Bellucci, S.; Magrini, A.; Bergamaschi, A.; Mustelin, T., Multi-walled carbon nanotubes induce T lymphocyte apoptosis. *Toxicology Letters* **2006,** *160*, 121-126.

12. Dumortier, H.; Lacotte, S.; Pastorin, G.; Marega, R.; Wu, W.; Bonifazi, D.; Briand, J.-P.; Prato, M.; Muller, S.; Bianco, A., Functionalized Carbon Nanotubes Are Non-Cytotoxic and Preserve the Functionality of Primary Immune Cells. *Nano Letters* **2006,** *6*, 1522-1528.

13. Zhou, F.; Wu, S.; Yuan, Y.; Chen, W. R.; Xing, D., Mitochondria-Targeting Photoacoustic Therapy Using Single-Walled Carbon Nanotubes. *Small* **2012,** *8*, 1543-1550.

14. Simon-Deckers, A.; Gouget, B.; Mayne-L'Hermite, M.; Herlin-Boime, N.; Reynaud, C.; Carrière, M., In vitro investigation of oxide nanoparticle and carbon nanotube toxicity and intracellular accumulation in A549 human pneumocytes. *Toxicology* **2008,** *253*, 137-146.

15. Yudasaka, M.; Yomogida, Y.; Zhang, M.; Tanaka, T.; Nakahara, M.; Kobayashi, N.; Okamatsu-Ogura, Y.; Machida, K.; Ishihara, K.; Saeki, K.; Kataura, H., Near-Infrared Photoluminescent Carbon Nanotubes for Imaging of Brown Fat. *Scientific Reports* **2017,** *7*, 44760.

16. Huang, P.; Lin, J.; Wang, X.; Wang, Z.; Zhang, C.; He, M.; Wang, K.; Chen, F.; Li, Z.; Shen, G.; Cui, D.; Chen, X., Light-Triggered Theranostics Based on Photosensitizer-Conjugated Carbon Dots for Simultaneous Enhanced-Fluorescence Imaging and Photodynamic Therapy. *Advanced Materials* **2012,** *24*, 5104-5110.

17. Hola, K.; Zhang, Y.; Wang, Y.; Giannelis, E. P.; Zboril, R.; Rogach, A. L., Carbon dots-Emerging light emitters for bioimaging, cancer therapy and optoelectronics. *Nano Today* **2014,** *9*, 590-603.

18. Choi, Y.; Kim, S.; Choi, M. H.; Ryoo, S. R.; Park, J.; Min, D. H.; Kim, B. S., Highly Biocompatible Carbon Nanodots for Simultaneous Bioimaging and Targeted Photodynamic Therapy In Vitro and In Vivo. *Advanced Functional Materials* **2014,** *24*, 5781-5789.

19. Ge, J.; Lan, M.; Zhou, B.; Liu, W.; Guo, L.; Wang, H.; Jia, Q.; Niu, G.; Huang, X.; Zhou, H.; Meng, X.; Wang, P.; Lee, C. S.; Zhang, W.; Han, X., A graphene quantum dot photodynamic therapy agent with high singlet oxygen generation. *Nature Communication* **2014,** *5*, 4596.

20. Tetsuka, H.; Asahi, R.; Nagoya, A.; Okamoto, K.; Tajima, I.; Ohta, R.; Okamoto, A., Optically Tunable Amino-Functionalized Graphene Quantum Dots. *Advanced Materials* **2012,** *24*, 5333-5338.

21. Li, T. F.; Li, Y. W.; Xiao, L.; Yu, H. T.; Fan, L. Z., Electrochemical Preparation of Color-Tunable Fluorescent Carbon Quantum Dots. *Acta Chimica Sinica (Engl. Ed.)* **2014,** *72*, 227-232.

22. Chen, M. Y.; Wang, W. Z.; Wu, X. P., One-pot green synthesis of water-soluble carbon nanodots with multicolor photoluminescence from polyethylene glycol. *Journal of Materials Chemistry B* **2014,** *2*, 3937-3945.

23. Sarswat, P. K.; Free, M. L., Light emitting diodes based on carbon dots derived from food, beverage, and combustion wastes. *Physical Chemistry Chemical Physics* **2015,** *17*, 27642-27652.

24. Wang, L.; Li, B.; Xu, F.; Shi, X.; Feng, D.; Wei, D.; Li, Y.; Feng, Y.; Wang, Y.; Jia, D.; Zhou, Y., High-yield synthesis of strong photoluminescent N-doped carbon nanodots derived from hydrosoluble chitosan for mercury ion sensing via smartphone APP. *Biosensors and Bioelectronics* **2016,** *79*, 1-8.

25. Dong, Y.; Wang, R.; Li, H.; Shao, J.; Chi, Y.; Lin, X.; Chen, G., Polyamine-functionalized carbon quantum dots for chemical sensing. *Carbon* **2012,** *50*, 2810-2815.

26. Diac, A.; Focsan, M.; Socaci, C.; Gabudean, A. M.; Farcau, C.; Maniu, D.; Vasile, E.; Terec, A.; Veca, L. M.; Astilean, S., Covalent conjugation of carbon dots with Rhodamine B and assessment of their photophysical properties. *RSC Advances* **2015,** *5*, 77662-77669.

27. Zhu, S.; Zhang, J.; Tang, S.; Qiao, C.; Wang, L.; Wang, H.; Liu, X.; Li, B.; Li, Y.; Yu, W.; Wang, X.; Sun, H.; Yang, B., Surface Chemistry Routes to Modulate the Photoluminescence of Graphene Quantum Dots: From Fluorescence Mechanism to Up-Conversion Bioimaging Applications. *Advanced Functional Materials* **2012,** *22*, 4732-4740.

28. Fan, Z. T.; Li, S. H.; Yuan, F. L.; Fan, L. Z., Fluorescent graphene quantum dots for biosensing and bioimaging. *RSC Advances* **2015,** *5*, 19773-19789.

29. Zhao, A. D.; Chen, Z. W.; Zhao, C. Q.; Gao, N.; Ren, J. S.; Qu, X. G., Recent advances in bioapplications of C-dots. *Carbon* **2015,** *85*, 309-327.

30. Dong, Y.; Shao, J.; Chen, C.; Li, H.; Wang, R.; Chi, Y.; Lin, X.; Chen, G., Blue luminescent graphene quantum dots and graphene oxide prepared by tuning the carbonization degree of citric acid. *Carbon* **2012,** *50*, 4738-4743.

31. Zhai, X.; Zhang, P.; Liu, C.; Bai, T.; Li, W.; Dai, L.; Liu, W., Highly luminescent carbon nanodots by microwave-assisted pyrolysis. *Chemical Communication* **2012,** *48*, 7955-7957.

32. Peng, J.; Gao, W.; Gupta, B. K.; Liu, Z.; Romero-Aburto, R.; Ge, L.; Song, L.; Alemany, L. B.; Zhan, X.; Gao, G.; Vithayathil, S. A.; Kaipparettu, B. A.; Marti, A. A.; Hayashi, T.; Zhu, J.-J.; Ajayan, P. M., Graphene Quantum Dots Derived from Carbon Fibers. *Nano Letters* **2012,** *12*, 844-849.

33. Hu, C.; Yu, C.; Li, M. Y.; Wang, X. N.; Yang, J. Y.; Zhao, Z. B.; Eychmuller, A.; Sun, Y. P.; Qiu, J. S., Chemically Tailoring Coal to Fluorescent Carbon Dots with Tuned Size and Their Capacity for Cu(II) Detection. *Small* **2014,** *10*, 4926-4933.

34. Sun, H.; Gao, N.; Dong, K.; Ren, J.; Qu, X., Graphene Quantum Dots-Band-Aids Used for Wound Disinfection. *ACS Nano* **2014,** *8*, 6202-6210.

35. Ristic, B. Z.; Milenkovic, M. M.; Dakic, I. R.; Todorovic-Markovic, B. M.; Milosavljevic, M. S.; Budimir, M. D.; Paunovic, V. G.; Dramicanin, M. D.; Markovic, Z. M.; Trajkovic, V. S., Photodynamic antibacterial effect of graphene quantum dots. *Biomaterials* **2014,** *35*, 4428-4435.

36. Fowley, C.; Nomikou, N.; McHale, A. P.; McCaughan, B.; Callan, J. F., Extending the tissue penetration capability of conventional photosensitisers: a carbon quantum dot-protoporphyrin IX conjugate for use in two-photon excited photodynamic therapy. *Chemical Communication* **2013,** *49*, 8934-8936.

37. Mueller, M. L.; Yan, X.; McGuire, J. A.; Li, L.-s., Triplet States and Electronic Relaxation in Photoexcited Graphene Quantum Dots. *Nano Letters* **2010,** *10*, 2679-2682.

38. Kumawat, M. K.; Thakur, M.; Gurung, R. B.; Srivastava, R., Graphene Quantum Dots from Mangifera indica: Application in Near-Infrared Bioimaging and Intracellular Nanothermometry. *ACS Sustainable Chemical Engineering* **2017,** *5*, 1382-1391.

39. Fan, T. J.; Zeng, W. J.; Tang, W.; Yuan, C. Q.; Tong, S. Z.; Cai, K. Y.; Liu, Y. D.; Huang, W.; Min, Y.; Epstein, A. J., Controllable size-selective method to prepare graphene quantum dots from graphene oxide. *Nanoscale Research Letters* **2015,** *10*, 1-8.

40. Howerton, B. S.; Heidary, D. K.; Glazer, E. C., Strained Ruthenium Complexes Are Potent Light-Activated Anticancer Agents. *Journal of the American Chemical Society* **2012,** *134*, 8324-8327.

41. Dong, Y.; Chen, C.; Zheng, X.; Gao, L.; Cui, Z.; Yang, H.; Guo, C.; Chi, Y.; Li, C. M., One-step and high yield simultaneous preparation of single- and multi-layer graphene quantum dots from CX-72 carbon black. *Journal of Materials Chemistry* **2012,** *22*, 8764-8766.

42. Shinde, D. B.; Pillai, V. K., Electrochemical Preparation of Luminescent Graphene Quantum Dots from Multiwalled Carbon Nanotubes. *Chemistry –A European Journal* **2012,** *18*, 12522-12528.

43. Tan, X.; Li, Y.; Li, X.; Zhou, S.; Fan, L.; Yang, S., Electrochemical synthesis of small-sized red fluorescent graphene quantum dots as a bioimaging platform. *Chemical Communications* **2015,** *51*, 2544-2546.

44. Zhang, Y. L.; Wang, L.; Zhang, H. C.; Liu, Y.; Wang, H. Y.; Kang, Z. H.; Lee, S. T., Graphitic carbon quantum dots as a fluorescent sensing platform for highly efficient detection of Fe3+ ions. *RSC Advances* **2013,** *3*, 3733-3738.

45. Xu, M. H.; Xu, S. S.; Yang, Z.; Shu, M. J.; He, G. L.; Huang, D.; Zhang, L. L.; Li, L.; Cui, D. X.; Zhang, Y. F., Hydrophilic and blue fluorescent N-doped carbon dots from tartaric acid and various alkylol amines under microwave irradiation. *Nanoscale* **2015,** *7*, 15915-15923.

46. Huang, H.; Li, C. G.; Zhu, S. J.; Wang, H. L.; Chen, C. L.; Wang, Z. R.; Bai, T. Y.; Shi, Z.; Feng, S. H., Histidine-Derived Nontoxic Nitrogen-Doped Carbon Dots for Sensing and Bioinnaging Applications. *Langmuir* **2014,** *30*, 13542-13548.

47. Du, F. Y.; Li, J. A.; Hua, Y.; Zhang, M. M.; Zhou, Z.; Yuan, J.; Wang, J.; Peng, W. X.; Zhang, L.; Xia, S.; Wang, D. Q.; Yang, S. M.; Xu, W. R.; Gong, A. H.; Shao, Q. X., Multicolor Nitrogen-Doped Carbon Dots for Live Cell Imaging. *Journal of Biomedical Nanotechnology.* **2015,** *11*, 780-788.

48. Ding, H.; Xiong, H. M., Exploring the blue luminescence origin of nitrogen-doped carbon dots by controlling the water amount in synthesis. *RSC Advances* **2015,** *5*, 66528-66533.

49. Wang, L.; Zhu, S. J.; Wang, H. Y.; Wang, Y. F.; Hao, Y. W.; Zhang, J. H.; Chen, Q. D.; Zhang, Y. L.; Han, W.; Yang, B.; Sun, H. B., Unraveling Bright Molecule-Like State and Dark Intrinsic State in Green-Fluorescence Graphene Quantum Dots via Ultrafast Spectroscopy. *Advanced Optical Materials* **2013,** *1*, 264-271.

50. Luo, P. H.; Qiu, Y.; Guan, X. F.; Jiang, L. Q., Regulation of photoluminescence properties of graphene quantum dots via hydrothermal treatment. *Physical Chemistry Chemical Physics* **2014,** *16*, 19011-19016.

51. Feng, Y.; Zhao, J.; Yan, X.; Tang, F.; Xue, Q., Enhancement in the fluorescence of graphene quantum dots by hydrazine hydrate reduction. *Carbon* **2014,** *66*, 334-339.

52. Zhu, S.; Shao, J.; Song, Y.; Zhao, X.; Du, J.; Wang, L.; Wang, H.; Zhang, K.; Zhang, J.; Yang, B., Investigating the surface state of graphene quantum dots. *Nanoscale* **2015,** *7*, 7927-7933.

53. Dai, Y.; Long, H.; Wang, X.; Wang, Y.; Gu, Q.; Jiang, W.; Wang, Y.; Li, C.; Zeng, T. H.; Sun, Y.; Zeng, J., Doping: Versatile Graphene Quantum Dots with Tunable Nitrogen Doping (Part. Part. Syst. Charact. 5/2014). *Particle & Particle Systems Characterization* **2014,** *31*, 509-509.

54. Li, Y.; Zhao, Y.; Cheng, H.; Hu, Y.; Shi, G.; Dai, L.; Qu, L., Nitrogen-Doped Graphene Quantum Dots with Oxygen-Rich Functional Groups. *Journal of the American Chemical Society* **2012,** *134*, 15-18.

Chapter 6: Conclusions and Future Directions

6.1   Synopsis

This chapter serves as the foundation for future work that has not yet been performed. The first section of this chapter will address questions related to scarcely studied topics in CQD research. It is intended to serve as an inspiration for future students to critically think upon the challenges of this research such that better CQDs can be tailor-made for optoelectronic, catalytic and biomedical applications. Secondly, as there are many new reports in CQD research being published, the most recent trends and ideologies will be addressed. Unfortunately, there are many reports that aim only to make CQD out of some material without much thought to its future purpose nor the advantage of using one method or reagent to another. This author wishes that the results and their implications within this dissertation can assist future students in order to produce high quality work in this exciting field. Finally, the last section of this chapter will propose the use of CQD as opioid and nicotine cessation agents. After explaining the need for these kinds of agents, a brief explanation of the relevant biochemical mechanisms will provide hypotheses in which CQDs can be engineered toward this goal.

6.2   Conclusions and Discussion

The work presented in Chapters 2 through 5 provides new information on the often overlooked structure-function relationship. Chapter 2 demonstrates the structural differences in CQDs synthesized by top-down and bottom-up approaches. Though having similar structural motifs such as a fused aromatic ring region with some amount of edge-terminating functional groups; it was found through a series of rigorous characterization methods that bottom-up and top-down produced CQDs carry very different functional group distributions as well as sp^2:sp^3-carbon ratios.

Chapter 3 highlights the use of a hydrothermal reactor to control over heteroatom dopants by varying oven temperature. It was hypothesized and shown that there would be a temperature limit at which hydrothermal treatment would negatively impact N-doping efficiency. To that end, it was determined that temperatures above 150 °C would

cause hydrothermal cutting effects and ultimately cleave edge-terminating functional groups such as amines and amides from the GQD. It was found that various nitrogen-related functional groups (pyridinic, pyrrolic, and graphitic N) can be formed by the reaction between existing GQD defects and nitrogen precursors.

Chapter 4 investigated CNDs further by analyzing the effect of pyrolysis time on the chemical structure as well as optical and catalytic properties. The processes of H_2O and CO_2 elimination as well as C-C condensation are not new, but disordered systems like carbon quantum dots are worth investigating just how these processes influence chemical structure and thus, function over time. It was found that as time progresses during pyrolysis, the CND actually evolves into a more GQD-like structure. As first observed by Dong *et al.*[1], there is a point in which the GQD-like structure grows into a graphene oxide-like structure. Therefore, the bottom-up synthesis is found to be useful at shorter periods of time to finely tune the inherent fluorescence and post-synthesis modifications such as hydrothermal treatment or EDC/NHS coupling to an amine-containing compound. Longer periods of pyrolysis time prevent heteroatom doping due to the removal of defects and collapse of a three-dimensional sp^3-carbon passivation layer into a planar sp^2-carbon nanographene sheet. It was found that this change brought very serious changes to the catalytic activity toward the oxygen reduction reaction. This result provided an insight into all-carbon catalyst engineering in that heteroatom dopants must be able to easily insert themselves into the carbon backbone of CQDs. This allows for the development of catalysts that contain a high density of active sites per CQD. Compared to other popular nanomaterials that have heteroatom dopants introduced (such as CNTs, GO, etc.) the uptake of heteroatoms would be kinetically and thermodynamically more favorable in bottom-up synthesized CQDs.

Chapter 5 sought to use the structure-function relationship of both unmodified CNDs and GQDs as well as modified CNDs and GQDs for the purposes of anti-cancer photodynamic therapy. Interestingly, unmodified GQDs performed the best of all samples with unmodified CNDs performing the worst. Adding nitrogen heteroatoms or chemically reducing GQDs suppressed the amount of singlet oxygen produced and enhanced the production of species like hydroxyl and superoxide radicals. To our

surprise, nitrogenation of CNDs switched on the photodynamic effect, producing an even mixture of singlet oxygen and radical species as seen from the DNA damage experiments.

6.2.1 Heteroatom Doping Effects

In carbon quantum dot research, one of the most promising ways to improve performance (i.e.: optical, catalytic) is through heteroatom doping. Adding in a more-electron rich heteroatom than carbon such as nitrogen produced the results as seen in previous chapters such as shifting the photoluminescence toward each end of the visible spectrum or tuning the inherent brightness of the nanoparticles. In this regard, it would be insightful to explore atomic doping percentages of greater than 10 %. As before, the addition of a high percentage of graphitic and pyrrolic N dopants would greatly enhance the low PLQY of GQDs. Post-synthetic modification would allow for fine-tuning the spectral position while retaining the inherent brightness of the CQD.

A recent report states that incorporating multiple heteroatom dopants – boron, nitrogen and sulfur in this case – all improve the quantum yield of CQDs.[2] This report is intriguing as it states that any elements either with less electrons (boron) or more electrons (nitrogen, sulfur) improve photoluminescent quantum yield uniformly. As dopants influence changes in the dipole moment, absorption is increased which leads to enhanced PLQY. Much research into heteroatom doping has concluded that, like nitrogen, specific chemical states influence optical properties differently. For example, the removal of oxygen heteroatoms increases the photoluminescence and shifts emission toward the blue.[3] Thus, the addition of sulfur atoms, which have the same valence electrons as oxygen, have produced similar results including a red-shifting of emission compared to undoped quantum dots.[4] Boron is an interesting case as it is the only heteroatom in this report that is electron-deficient compared to carbon. Other studies have reported boron-doping of various carbon-based nanomaterials with opposing photoluminescence changes.[5-7] These optical differences may originate from differing chemical states though none of the authors of these works mention a correlation between these two ideas. As shown in Chapter 3, hydrothermal treatment can be utilized to give extensive control over doping quantities as well as functional

group distribution. Combining a parameterized HT treatment (e.g.: temperature- or time-dependence) with varying concentrations of heteroatom precursor (i.e.: boric acid, sulfate, etc.) would allow for a critical analysis of the role of boron not unlike chapter 3. The results gained from these experiments would greatly enhance current knowledge of tuning the carbon quantum dot fluorescence and properties as researchers could utilize a wider range of dopants.

6.2.2 Isolation of Functional Groups

In order to further elucidate the structure-property relationship including heteroatom dopants, the need arises to isolate the distribution of functional groups into one specific functional group. For example, could an N-doped CQD be made with only amines, pyridines, pyrrolic, or quaternary amines? Unfortunately, kinetic and thermodynamic barriers during synthesis prevent carbon quantum dots from only containing one functional group. This notion is the greatest challenge in CQD research with equally great promise upon completion. By synthesizing CQDs with only one functional group, experimentalists could compare their data with theoretical work. Fundamental understanding of the electronic interaction between heteroatoms and carbon could give rise to carbon-based nanomaterials whose properties are as monodisperse as inorganic quantum dots. Additionally, this knowledge could unlock the potential to produce tailor-made quantum dots for specific applications. Until then, chemists and material scientists must rely on theoretical studies to understand how singly disperse functional groups affect optoelectronic and catalytic performance.

As a proposed work, it would be useful for computational chemists to model a hydrothermal reactor system and fundamentally understand the mechanism behind nitrogen doping. From the results of Chapter 3, it can be simply stated that a kinetic model of doping occurs below treatment temperatures of 150 °C and that the majority of functional groups exist as amines and pyridines. Above 150 °C, it becomes thermodynamically favorable for dopants to penetrate the sp^2-nanodomain to form graphitic N. In the absence of literature on this exact topic, the common question can be drawn from our previous results: what is happening in the hydrothermal reactor at each of these temperatures? First, an assumption must be made that amine substitution

is a kinetically favorable process since carboxyl and hydroxyl functional groups are present at the edge of CQDs. This is coupled with the fact that from aqueous ammonia, three events must occur, the two bonds that break (N-H and C-O), and the newly formed C-N bond. Secondly, it can be hypothesized that oxygen defects such as the aromatic furan and the non-aromatic pyran – both of which would look like ethers in a CQD - are respectively converted into pyrrole and pyridine. Additionally, pyrroles and pyridines could be formed from the ring closure of a free amine as it is converted from a primary amine to a secondary amine. This kind of process would require a high amount of energy and would be classified as a thermodynamically driven process. In support of this idea, furans have been reacted with gaseous ammonia (at 400 °C) over an alumina bed to form pyrroles.[8] Instead of a substitution, this reaction proceeds by ring opening then the step-wise addition of ammonia and simultaneous ring closure and conversion to a secondary amine. Since then, this reaction has been developed to lower the energy needed to drive the reaction to completion by using the furan as an intermediate which may suggest a simple nitrogen substitution is possible under the right conditions.[9] In Figure 6.1, graphitic N is hypothesized to form under a completely thermodynamic process and can only form if there is a defect including one heteroatom (oxygen, in this case) and neighboring sp^2 or sp^3 carbon atoms.
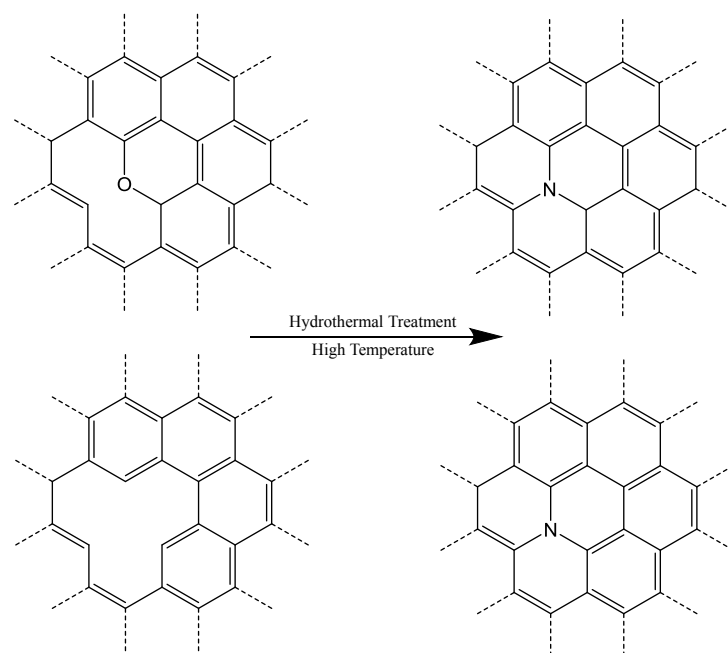
Figure 6.1: Possibilities in which nitrogen can be inserted into the sp^2 matrix of a CQD. Without an existing defect, the energy required to replace a carbon in the matrix with nitrogen would likely harm another part of the CQD.

There has been some computational work on the optoelectronic relationship of nitrogen-doped GQD. Recently, Margraf *et al*. reports calculated band gap differences between undoped carbon quantum dots and up to 5 atom % N in the form of amines and cyano groups.[10] It is further discussed that the addition of nitrogen only modifies the band gap slightly, stating little significance to the dopant effect. Referring back to our work with N-doped GQDs, this theoretical work agrees with our NGQDs that primarily consist of amine functionalities. However, the red-shifting nature from our work is greatly enhanced compared to Margraf's report. This is likely due to the sheer number of functional groups added to each NGQD. As stated in previous chapters, theoretical simulations show that increasing the density of amine functional groups progressively red-shits the emission further.[11] Interestingly, there are few papers that concern calculating optoelectronic properties of carbon quantum dots. Most theoretical studies on NCQDs aim to isolate a specific N-containing functional group for the ORR or CO_2 reduction (CRR) pathways. Saidi *et al*. found that pyridinic and graphitic N are ideal for electrocatalyzing the ORR reaction, however with large overpotentials.[12] Unique to this study, the pyridinic and graphitic N sites catalyse ORR separately in

dissociative and associative pathways, respectively. Generally, dissociative pathways split oxygen molecules into atoms once reaching the N active site. Associative pathways, on the other hand, carry out the reduction on the whole oxygen molecule where bound O_2 is reduced to bound OOH.

Zou *et al*. reports a detailed analysis on the N active sites in N-doped CQDs.[13] This work focuses specifically on the use of pyridinic N as the active site in a multi-step process to convert CO_2 to CH_4. This multi-step reaction is shown below in Figure 6.2. Briefly, this process starts with the binding of CO_2 to the pyridinic N, proton addition to one of the carbon dioxide oxygen atoms to form bound formate, electrochemical removal of –OH to form bound CO, two proton additions to the carbon attached to the pyridinic N and one to the remaining carbonyl oxygen. Then, another electrochemical removal of hydroxide to form bound CH_2 radical, hydration with water to form a bound primary alcohol and the addition of another proton to the bound carbon, one last removal of hydroxide to form CH_3 radical, and the addition of one last proton to form the volatile CH_4 molecule which is easily removed from solution. According to this report, a similar, more energetically favorable pathway occurs for much larger negative potentials.
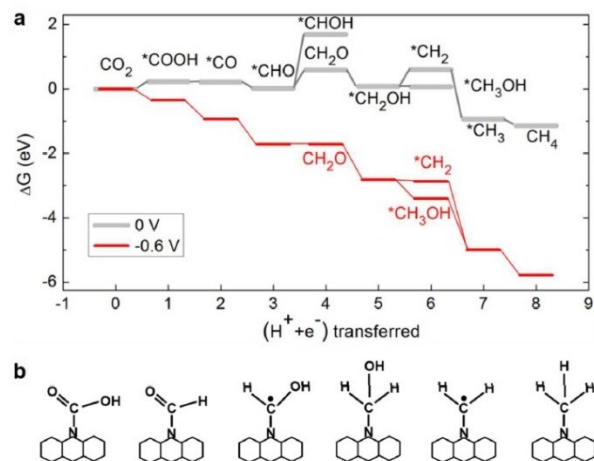
Figure 3. (a) Energy pathways for electrochemical reduction of CO_2 to CH_3OH and CH_4 at 0 V (black) and -0.6 V (red). (b) Schematic for selected intermediate states, including *COOH, *CHO, *CHOH, *CH_2OH, *CH_2, and *CH_3 adsorbed on NGQDs.

Figure 6.2: Reprinted with permission from Ref. 13. Copyright 2017 American Chemical Society.

It is hypothesized that synthesizing singly disperse functional groups within CQDs can be accomplished; however, low yields and difficult purification steps are likely to occur. Unsurprisingly, controlling the distribution of oxygen-containing functional groups has proven difficult with conventional methods such as chemical oxidation and reduction for fear of completely destroying the CQD. For external modification techniques, it may be more effective to use a top-down synthesized GQD to limit further condensation reactions that bottom-up synthesis would undergo. A GQD with carboxylic and carbonyl groups could be reduced down to only hydroxyl groups with $LiAlH_4$ - an extremely potent and dangerous reducing agent. Fortunately, $LiAlH_4$ does not reduce any aromatic or aliphatic C-C bonds so the risk of fragmenting the CQD is low with this process. Using this reagent could be effective if coupled with a GQD that has been mildly reduced with $NaBH_4$ to enhance solubility in non-aqueous media. As such, a glove box would be required for the synthesis as $LiAlH_4$ reacts violently with water (atmospheric moisture is a problem) and the pure material itself is pyrophoric. With all of the oxygen-containing functional groups converted to alcohols, a low temperature hydrothermal treatment with dilute aqueous ammonia would be performed to produce an amine-only CQD. From here, a reaction with methyl iodide would change

the primary amines (R-NH$_2$) into the tertiary dimethyl amines (R-N(CH$_3$)$_2$) which make all nitrogen quaternary. A synthetic scheme for modifying GQDs in these ways is shown in Figure 6.3. Pyridinic- and pyrrolic-only CQDs could be made using a bottom-up approach from the compounds 5-hydroxy-pyridine-2-carboxylic acid methyl ester, 6-hydroxymethyl-pyridine-2-carboxylic acid and 5-formyl-1H-pyrrole-2-carboxylic acid shown below in Figure 6.4. Employing higher temperatures and longer pyrolysis time compared to citric acid, N-doped CQDs with only pyridinic or pyrrolic functional groups can be made. It is important that the bottom-up approach be used for pyridinic and pyrrolic N compared to the top-down approach for avoiding the broad distribution of N chemical states.
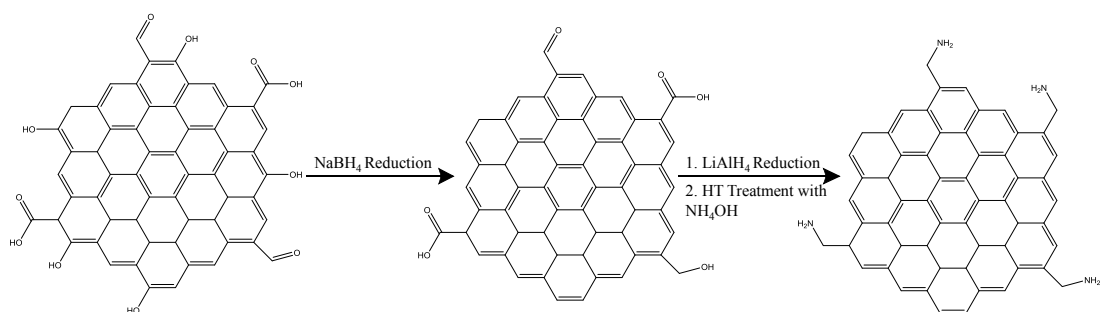
Figure 6.3: Potential synthetic route to amine-only graphene quantum dots. An ice bath and a glove box should be used to control the NaBH$_4$ and LiAlH$_4$ reductions, respectively. Low-temperature hydrothermal treatment with aqueous ammonia can be used to convert hydroxyl moieties to primary amines. Quaternary nitrogen functionalities could be made from further methylation of the amines.

5-hydroxy-pyridine-2-carboxylic acid methyl ester

6-hydroxymethyl-pyridine-2-carboxylic acid

5-formyl-1H-pyrrole-2-carboxylic acid
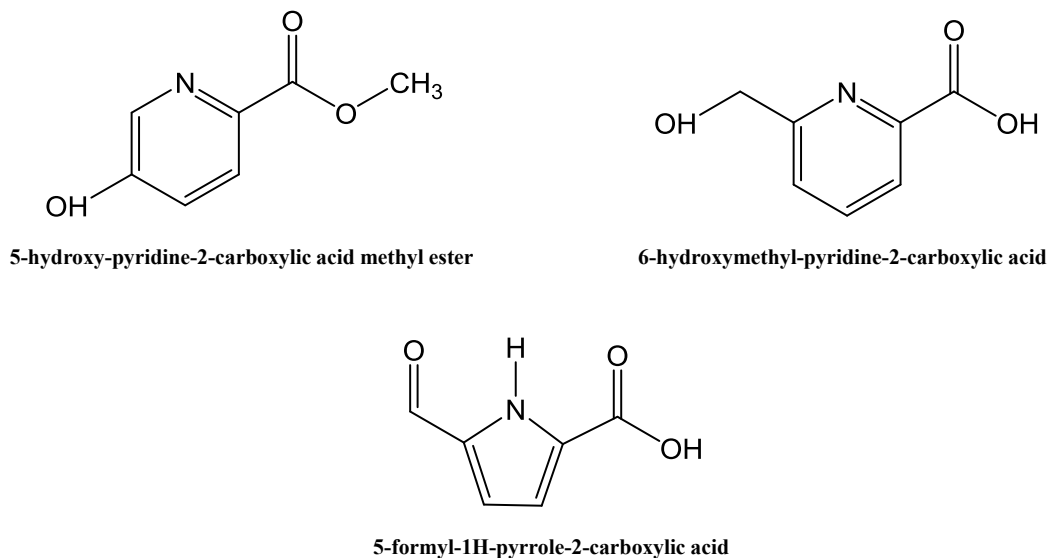
Figure 6.4: Possible compounds that could produce pyridine- or pyrrole-only carbon nanodots. The dehydration and condensation reactions aid in forming the carbon backbone of the CND while the very stable nitrogen-containing heterocycles remain intact during pyrolysis.

6.3   Carbon Quantum Dots as Opioid and Nicotine Cessation Agents

Carbon quantum dots have seen many uses in biomedical research as bioimaging, photodynamic anti-cancer and naturally anti-viral agents. This section proposes two new uses of CQDs as nicotine and opioid cessation agents by utilizing the similar chemical makeup of N-doped CQDs as a competitive mimic to nicotine and other opioids. Both of these drugs are highly addictive and are inevitably harmful to the body – potentially causing death from a variety of causes. Nicotine (3-[(2S)-1-methyl-2-pyrrolidinyl]-pyridine) is a readily available substance from tobacco leaves (up to 3 wt% in dry tobacco). When nicotine is taken up into the body and transported through the bloodstream, it ultimately reaches the brain. The high binding affinity of nicotine toward acetylcholine receptors (AChR) causes a chain reaction of signals that invoke feelings of stress reduction, pleasure, and enhanced mental focus. From here, two factors that contribute to the overarching behaviors associated with addiction are tolerance and dependence.

Tolerance is the need to uptake more of a substance to achieve the same effects. Mechanistically, this is done by a number of factors. AChRs typically bind to acetylcholine, an important chemical that transmits and modulates signals in the

brain.[14] Conversely, this neurochemical is regularly broken down by the enzyme acetylcholinesterase (AChE). Thus, neurochemical balance is achieved through synaptic activation by AChR coupled with synaptic termination by AChE. The combination of the high local concentration of acetylcholine (about 1 mM), the short pulse of receptor activation (a couple of ms) and fast degradation of acetylcholne by AChE prevent desensitization of the receptor. However nicotine is not enzymatically removed AChE like acetylcholine and is present at concentrations of less than 0.1 μM. Both of these factors favor receptor desensitization which requires even higher concentrations to achieve the initial desired effect.

Drug dependence occurs when uptake of a substance is required to avoid withdrawal symptoms.[15] In nicotine, this is done by the increased release of dopamine upon uptake. Dopamine is the neurotransmitter responsible for much of the action in the brain's reward and pleasure centers. Increased amounts of dopamine released upon uptake of a substance leads to a learned behavior associated with that uptake. In other words, the brain perceives the uptake of nicotine as a reward even though the act of smoking tobacco is harmful itself. If nicotine is not regularly delivered to the brain, neurological withdrawal symptoms from the lack of dopamine can start such as depressed mood, fatigue, irritability, and a lack of focus. With increased nicotinic abstinence, the onset of somatic withdrawal symptoms appear due to the body's need for rewarding stimuli.

Addiction is the mind's response to the body's biochemical changes made while under the effects of substance tolerance and dependence. Unsurprisingly, the mind and body are intimately connected and often, one influences the other. In other words, addiction is the behavior in which a user seeks a substance despite potential consequences. This is due to the need to reduce or eliminate withdrawal symptoms from the dependence as well as the high amount needed for a chronic user to overcome their tolerance. In the United States, nearly $300 billion dollars were spent on smoking-related illness which includes nearly half of that in direct medical care.[16] Additionally, nearly 480,000 people die from smoking-related illness a year and have life expectancies ten years less than those who don't smoke. However, if smokers quit

smoking before age 40, their chances of dying from a smoking-related illness decreases by roughly 90%. There are many available methods for nicotine cessation. Most of these include prescription or over-the-counter patches or gum but these are simply nicotine replacement agents that aid the user in titrating down off of the addiction instead of suffering withdrawal symptoms. Some non-nicotine cessation agents have been developed, notably bupropion and varenicline tartrate which are both shown below.

Opioid addiction could be another application for CQD use in the biomedical industry. Like nicotine, opioids (i.e.: heroin, morphine, fentanyl, prescription opioids) activate the same pleasure and reward centers of the brain.[17-19] One key difference between nicotine and opioids is the degree of legality each is allowed as well as the setting in which each is used. Where nicotine is grown through tobacco in farms and sold as cigarette and cigar products, opioids are highly illegal substances as in heroin or used in the medical industry as pain relievers such as fentanyl, morphine and other prescription-strength painkillers. Interestingly, the production of prescription opioids which include hydrocodone, methadone, and oxycodone have skyrocketed since the turn of the century. These opioids, originally for the purpose of relieving chronic pain, have created an epidemic of opioid abuse. As patients heal from their injuries, their need for medication is reduced. However, extended doses of these medications cause both tolerance and dependence in a similar mechanism to nicotine. The opioid receptors in the brain are, as before, repeatedly activated and desensitized which require higher or more frequent uptake to produce the pleasurable feelings (e.g. increased dopamine release) associated with the drug. With this information in mind, the so-called "opioid epidemic" has emerged from the combination of the elevated sale and use of heroin, the addition of fentanyl (a highly potent synthetic opioid) into heroin, and the rush of former prescription opioid users engaging in drug-seeking behavior. Presently, nearly half of all opioid-related overdoses stem from prescription opioids and nearly a quarter of all prescription opioid users struggle with addiction. Current opioid cessation agents include methadone, buprenorphine, and naloxone. Methadone and buprenorphine are useful in titration therapies designed to wean addicts off of opioids over a period of time. Naloxone and naltrexone are overdose-prevention agents that bind to free opioids

stronger than the opioid receptors, essentially returning potentially deadly concentrations to normally tolerated levels.

Nitrogen-doped carbon quantum dots could be a useful compound to combat the problems associated with nicotine and opioid addiction as shown in Figure 6.5. As an inexpensive high yield nanomaterial with a rich diversity of nitrogenous functional groups, a single N-doped CQD could act as a similar target for many of the AChR and opioid receptors. This would allow patients to receive treatment for a variety of substances while maintaining low costs and high accessibility. Additionally, dark cytotoxicity results from our photodynamic anti-cancer studies suggest that only high concentrations (mg/mL) induce negative effects. Shown below is a comparison of the chemical structure of an N-doped CQD to nicotine and other opioids. The secondary amines and aromatic nitrogen heterocycles present in these drugs act as targets that for AChR and mu opioid receptors which provide the brain with the rewarding release of dopamine without the need to intake and with easier to manage withdrawal symptoms after medication has been stopped. It is hypothesized that the nitrogen-containing functional groups (amines, pyridines, pyrroles and quaternary nitrogen) of CQDs can be engineered to act as a competitive agent with nicotine and opioids in smoking cessation. The mechanism of this inhibition (e.g.: competitive, non-competitive, etc.) could be studied by varying the amount of a specific functional group. Further work in this regard can be expanded toward other biological targets by exploiting the three greatest advantages to CQD: inexpensive, facile synthesis; a robust scaffold that can stand up to a variety of post-synthetic modifications, and easily tunable chemical functionalization.

This thesis has provided deeper understanding toward the newest class of carbon nanomaterials, carbon quantum dots, by critically analyzing and correlating the chemical structure and the resulting observed functions in optical, catalytic, and biological studies. Future work on heteroatom doping CQD has been discussed in several facets from changing the heteroatom dopant to narrowing the distribution of functional groups to developing new and exciting ways to use carbon nanomaterials. From here, CQD could be used in a variety of biological targets with the right

combination of chemical design and synthetic work. By taking great care of controlling the chemical structure, future generations of researchers can begin to develop tailor-made carbon quantum dots to replace current materials in optoelectronics, electro- and photo-catalysis, and biomedical applications. It is my hope that this work is continued and that deeper understanding can be reached such that CQD can be utilized as an easily accessible and effective material in many applications.
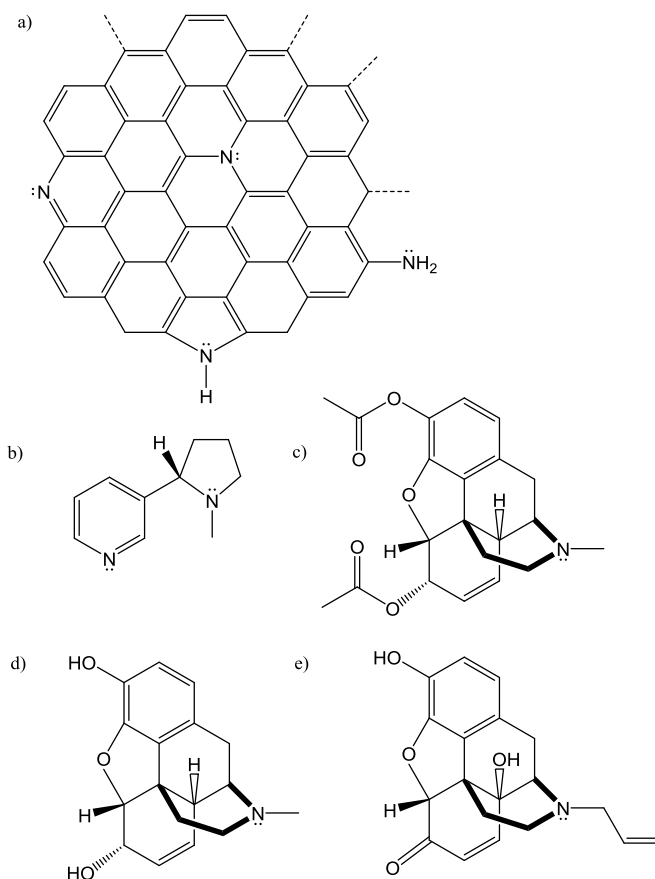
Figure 6.5: Comparison of an a) N-doped CQD to b) nicotine, c) heroin d) morphine, and e) naloxone. Each of these structures contain graphitic N; making NCQD an ideal macromolecule for nicotine and opioid cessation agents.

6.4   Chapter 6 References

1.   Dong, Y.; Shao, J.; Chen, C.; Li, H.; Wang, R.; Chi, Y.; Lin, X.; Chen, G., Blue luminescent graphene quantum dots and graphene oxide prepared by tuning the carbonization degree of citric acid. *Carbon* **2012,** *50* (12), 4738-4743.

2.   Das, R. K.; Mohapatra, S., Highly luminescent, heteroatom-doped carbon quantum dots for ultrasensitive sensing of glucosamine and targeted imaging of liver cancer cells. *Journal of Materials Chemistry B* **2017,** *5* (11), 2190-2197.

3.   Luo, P. H.; Qiu, Y.; Guan, X. F.; Jiang, L. Q., Regulation of photoluminescence properties of graphene quantum dots via hydrothermal treatment. *Physical Chemistry Chemical Physics* **2014,** *16* (35), 19011-19016.

4.   Bian, S.; Shen, C.; Hua, H.; Zhou, L.; Zhu, H.; Xi, F.; Liu, J.; Dong, X., One-pot synthesis of sulfur-doped graphene quantum dots as a novel fluorescent probe for highly selective and sensitive detection of lead(ii). *RSC Advances* **2016,** *6* (74), 69977-69983.

5.   Shan, X.; Chai, L.; Ma, J.; Qian, Z.; Chen, J.; Feng, H., B-doped carbon quantum dots as a sensitive fluorescence probe for hydrogen peroxide and glucose detection. *Analyst* **2014,** *139* (10), 2322-2325.

6.   Noor Ul, A.; Eriksson, O. M.; Schmidt, S.; Asghar, M.; Lin, P.-C.; Holtz, O. P.; Syväjärvi, M.; Yazdi, R. G., Tuning the Emission Energy of Chemically Doped Graphene Quantum Dots. *Nanomaterials* **2016,** *6* (11).

7.   Dey, S.; Govindaraj, A.; Biswas, K.; Rao, C. N. R., Luminescence properties of boron and nitrogen doped graphene quantum dots prepared from arc-discharge-generated doped graphene samples. *Chemical Physics Letters* **2014,** *595*, 203-208.

8.   Elming, N.; Clauson-Kaas, N., The preparation of pyrroles from furans. *Acta Chem. Scand* **1952,** *6*, 867-874.

9.   Amarnath, V.; Amarnath, K., Intermediates in the Paal-Knorr Synthesis of Furans. *The Journal of Organic Chemistry* **1995,** *60* (2), 301-307.

10. Margraf, J. T.; Strauss, V.; Guldi, D. M.; Clark, T., The Electronic Structure of Amorphous Carbon Nanodots. *Journal of Physical Chemistry B* **2015,** *119* (24), 7258-7265.

11. Jin, S. H.; Kim, D. H.; Jun, G. H.; Hong, S. H.; Jeon, S., Tuning the Photoluminescence of Graphene Quantum Dots through the Charge Transfer Effect of Functional Groups. *ACS Nano* **2013,** *7* (2), 1239-1245.

12. Saidi, W. A., Oxygen Reduction Electrocatalysis Using N-Doped Graphene Quantum-Dots. *The Journal of Physical Chemistry Letters* **2013,** *4* (23), 4160-4165.

13. Zou, X.; Liu, M.; Wu, J.; Ajayan, P. M.; Li, J.; Liu, B.; Yakobson, B. I., How Nitrogen-Doped Graphene Quantum Dots Catalyze Electroreduction of CO2 to Hydrocarbons and Oxygenates. *ACS Catalysis* **2017**, 6245-6250.

14. Benowitz, N. L., Pharmacology of Nicotine: Addiction, Smoking-Induced Disease, and Therapeutics. *Annual review of pharmacology and toxicology* **2009,** *49*, 57-71.

15. Ortells, M. O.; Barrantes, G. E., Tobacco addiction: A biochemical model of nicotine dependence. *Medical Hypotheses 74* (5), 884-894.

16. Xu, X.; Bishop, E. E.; Kennedy, S. M.; Simpson, S. A.; Pechacek, T. F., Annual Healthcare Spending Attributable to Cigarette Smoking. *American Journal of Preventive Medicine 48* (3), 326-333.

17. Benyhe, S.; Zádor, F.; Ötvös, F., Biochemistry of opioid (morphine) receptors: binding, structure and molecular modelling. *Acta Biol. Szeged.* **2015,** *59* (Suppl. 1), 17-37.

18. Kosten, T. R.; George, T. P., The neurobiology of opioid dependence: implications for treatment. *Science & Practice Perspectives* **2002,** *1* (1), 13.

19. Al-Hasani, R.; Bruchas, M. R., Molecular mechanisms of opioid receptor-dependent signaling and behavior. *Anesthesiology: The Journal of the American Society of Anesthesiologists* **2011,** *115* (6), 1363-1381.

BIBLIOGRAPHY

1. A. V. Naumkin, A. K.-V., S. W. Gaarenstroom, C. J. Powell NIST XPS Standard Reference Database. Version 4.1.

2. Administration, U. S. E. I., ELECTRIC POWER MONTHLY: with data for January 2016. Energy, U. S. D. o., Ed. 2016.

3. Akizuki, N.; Aota, S.; Mouri, S.; Matsuda, K.; Miyauchi, Y., Efficient near-infrared up-conversion photoluminescence in carbon nanotubes. *Nature Communications* **2015,** *6*, 8920.

4. Algarra, M.; Campos, B. B.; Radotic, K.; Mutavdzic, D.; Bandosz, T.; Jimenez-Jimenez, J.; Rodriguez-Castellon, E.; da Silva, J., Luminescent carbon nanoparticles: effects of chemical functionalization, and evaluation of Ag+ sensing properties. *Journal of Materials Chemistry A* **2014,** *2* (22), 8342-8351.

5. Al-Hasani, R.; Bruchas, M. R., Molecular mechanisms of opioid receptor-dependent signaling and behavior. *Anesthesiology: The Journal of the American Society of Anesthesiologists* **2011,** *115* (6), 1363-1381.

6. Al-Rasbi, N. K.; Sabatini, C.; Barigelletti, F.; Ward, M. D., Red-shifted luminescence from naphthalene-containing ligands due to [small pi]-stacking in self-assembled coordination cages. *Dalton Transactions* **2006,** (40), 4769-4772.

7. Alves, L. A.; de Castro, A. H.; de Mendonça, F. G.; de Mesquita, J. P., Characterization of acid functional groups of carbon dots by nonlinear regression data fitting of potentiometric titration curves. *Applied Surface Science* **2016,** *370*, 486-495.

8. Amarnath, V.; Amarnath, K., Intermediates in the Paal-Knorr Synthesis of Furans. *The Journal of Organic Chemistry* **1995,** *60* (2), 301-307.

9. Aoshima, H.; Kokubo, K. E. N.; Shirakawa, S.; Ito, M.; Yamana, S.; Oshima, T., Antimicrobial Activity of Fullerenes and Their Hydroxylated Derivatives. *Biocontrol Science* **2009,** *14* (2), 69-72.

10. Aparna, M.; Pankaj, K.; Kamalasanan, M. N.; Subhas, C., White organic LEDs and their recent advancements. *Semiconductor Science and Technology* **2006,** *21* (7), R35.

11. Aqel, A.; El-Nour, K. M. M. A.; Ammar, R. A. A.; Al-Warthan, A., Carbon nanotubes, science and technology part (I) structure, synthesis and characterisation. *Arabian Journal of Chemistry* **2012,** *5* (1), 1-23.

12. Arash, B.; Park, H. S.; Rabczuk, T., Mechanical properties of carbon nanotube reinforced polymer nanocomposites: A coarse-grained model. *Composites Part B: Engineering* **2015,** *80*, 92-100.

13. Arora, N. D.; Hauser, J. R.; Roulston, D. J., Electron and hole mobilities in silicon as a function of concentration and temperature. *IEEE Transactions on Electron Devices* **1982,** *29* (2), 292-295.

14. Asada, R.; Liao, F.; Saitoh, Y.; Miwa, N., Photodynamic anti-cancer effects of fullerene [C60]–PEG complex on fibrosarcomas preferentially over normal fibroblasts in terms of fullerene uptake and cytotoxicity. *Molecular and Cellular Biochemistry* **2014,** *390* (1), 175-184.

15. Barbose, G., J. Miller, B. Sigrin, E. Reiter, K. Cory, J. McLaren, J. Seel, A. Mills, N. Darghouth, and A. Satchwell. , On the Path to SunShot: Utility Regulatory and Business Model Reforms for Addressing the Financial Impacts of Distributed Solar on Utilities. Laboratory, N. R. E., Ed. Golden, CO, 2016.

16. Bartelmess, J.; Giordani, S., Carbon nano-onions (multi-layer fullerenes): chemistry and applications. *Beilstein Journal of Nanotechnology* **2014,** *5*, 1980-1998.

17. Barun, V. V.; Ivanov, A. P.; Volotovskaya, A. V.; Ulashchik, V. S., Absorption spectra and light penetration depth of normal and pathologically altered human skin. *Journal of Applied Spectroscopy* **2007,** *74* (3), 430-439.

18. Benowitz, N. L., Pharmacology of Nicotine: Addiction, Smoking-Induced Disease, and Therapeutics. *Annual review of pharmacology and toxicology* **2009,** *49*, 57-71.

19. Benyhe, S.; Zádor, F.; Ötvös, F., Biochemistry of opioid (morphine) receptors: binding, structure and molecular modelling. *Acta Biol. Szeged.* **2015,** *59* (Suppl. 1), 17-37.

20. Bhunia, S. K.; Saha, A.; Maity, A. R.; Ray, S. C.; Jana, N. R., Carbon Nanoparticle-based Fluorescent Bioimaging Probes. *Scientific Reports* **2013,** *3*.

21. Bian, S.; Shen, C.; Hua, H.; Zhou, L.; Zhu, H.; Xi, F.; Liu, J.; Dong, X., One-pot synthesis of sulfur-doped graphene quantum dots as a novel fluorescent probe for highly selective and sensitive detection of lead(ii). *RSC Advances* **2016,** *6* (74), 69977-69983.

22. Bolotin, K. I.; Sikes, K. J.; Jiang, Z.; Klima, M.; Fudenberg, G.; Hone, J.; Kim, P.; Stormer, H. L., Ultrahigh electron mobility in suspended graphene. *Solid State Communications* **2008,** *146* (9), 351-355.

23. Bottini, M.; Balasubramanian, C.; Dawson, M. I.; Bergamaschi, A.; Bellucci, S.; Mustelin, T., Isolation and Characterization of Fluorescent Nanoparticles from Pristine and Oxidized Electric Arc-Produced Single-Walled Carbon Nanotubes. *The Journal of Physical Chemistry B* **2006,** *110* (2), 831-836.

24. Bottini, M.; Bruckner, S.; Nika, K.; Bottini, N.; Bellucci, S.; Magrini, A.; Bergamaschi, A.; Mustelin, T., Multi-walled carbon nanotubes induce T lymphocyte apoptosis. *Toxicology Letters* **2006,** *160* (2), 121-126.

25. Bourlinos, A. B.; Stassinopoulos, A.; Anglos, D.; Zboril, R.; Karakassides, M.; Giannelis, E. P., Surface functionalized carbogenic quantum dots. *Small* **2008,** *4* (4), 455-458.

26. Brodie, B. C., Sur le poids atomique du graphite. *Ann. Chim. Phys* **1860,** *59* (466), e472.

27. Cady-Pereira, K. E.; Payne, V. H.; Neu, J. L.; Bowman, K. W.; Miyazaki, K.; Marais, E. A.; Kulawik, S.; Tzompa-Sosa, Z. A.; Hegarty, J. D., Seasonal and Spatial Changes in Trace Gases over Megacities from AURA TES Observations. *Atmos. Chem. Phys. Discuss.* **2017,** *2017*, 1-31.

28. Center, E. T. LED Lights - How It Works - History. http://www.edisontechcenter.org/LED.html (accessed July 5, 2017).

29. Chandra, S.; Pathan, S. H.; Mitra, S.; Modha, B. H.; Goswami, A.; Pramanik, P., Tuning of photoluminescence on different surface functionalized carbon quantum dots. *RSC Advances* **2012,** *2* (9), 3602-3606.

30. Chen, J.; Yao, B.; Li, C.; Shi, G., An improved Hummers method for eco-friendly synthesis of graphene oxide. *Carbon* **2013,** *64*, 225-229.

31. Chen, M. Y.; Wang, W. Z.; Wu, X. P., One-pot green synthesis of water-soluble carbon nanodots with multicolor photoluminescence from polyethylene glycol. *Journal of Materials Chemistry B* **2014,** *2* (25), 3937-3945.

32. Chen, T.; Baoqing, Z.; Liu, J. L.; Dong, J. H.; Liu, X. Q.; Wu, Z.; Yang, X. Z.; Li, Z. M., High throughput exfoliation of graphene oxide from expanded graphite with assistance of strong oxidant in modified Hummers method. *Journal of Physics: Conference Series* **2009,** *188* (1), 012051.

33. Chen, X. X.; Jin, Q. Q.; Wu, L. Z.; Tung, C. H.; Tang, X. J., Synthesis and Unique Photoluminescence Properties of Nitrogen-Rich Quantum Dots and Their Applications. *Angewandte Chemie-International Edition* **2014,** *53* (46), 12542-12547.

34. Chen, Y.; Mastalerz, M.; Schimmelmann, A., Characterization of chemical functional groups in macerals across different coal ranks via micro-FTIR spectroscopy. *International Journal of Coal Geology* **2012,** *104*, 22-33.

35. Chen, Z.; Wang, X. C.; Li, H.; Li, C.; Lu, Q. H.; Yang, G.; Long, J. G.; Meng, L. J., Controllable and mass fabrication of highly luminescent N-doped carbon dots for bioimaging applications. *RSC Advances* **2015,** *5* (29), 22343-22349.

36. Cheong, W. F.; Prahl, S. A.; Welch, A. J., A review of the optical properties of biological tissues. *IEEE Journal of Quantum Electronics* **1990,** *26* (12), 2166-2185.

37. Choi, Y.; Kim, S.; Choi, M. H.; Ryoo, S. R.; Park, J.; Min, D. H.; Kim, B. S., Highly Biocompatible Carbon Nanodots for Simultaneous Bioimaging and Targeted Photodynamic Therapy In Vitro and In Vivo. *Advanced Functional Materials* **2014,** *24* (37), 5781-5789.

38. Choi, Y. C.; Bae, D. J.; Lee, Y. H.; Lee, B. S.; Han, I. T.; Choi, W. B.; Lee, N. S.; Kim, J. M., Low temperature synthesis of carbon nanotubes by microwave plasma-enhanced chemical vapor deposition. *Synthetic Metals* **2000,** *108* (2), 159-163.

39. Chung, C.; Kim, Y.-K.; Shin, D.; Ryoo, S.-R.; Hong, B. H.; Min, D.-H., Biomedical Applications of Graphene and Graphene Oxide. *Accounts of Chemical Research* **2013,** *46* (10), 2211-2224.

40. Chung, D., K. Horowitz, and P. Kurup., On the Path to SunShot: Emerging Opportunities and Challenges in U.S. Solar Manufacturing. Laboratory, N. R. E., Ed. Golden, CO, 2016.

41. Colomban, P., The Use of Metal Nanoparticles to Produce Yellow, Red and Iridescent Colour, from Bronze Age to Present Times in Lustre Pottery and Glass: Solid State Chemistry, Spectroscopy and Nanostructure. *Journal of Nano Research* **2009,** *8*, 109-132.

42. Colombeau, L.; Acherar, S.; Baros, F.; Arnoux, P.; Gazzali, A. M.; Zaghdoudi, K.; Toussaint, M.; Vanderesse, R.; Frochot, C., Inorganic Nanoparticles for Photodynamic Therapy. In *Light-Responsive Nanostructured Systems for Applications in Nanomedicine*, Sortino, S., Ed. Springer International Publishing: Cham, 2016; pp 113-134.

43. Coropceanu, V.; Cornil, J.; da Silva Filho, D. A.; Olivier, Y.; Silbey, R.; Brédas, J.-L., Charge Transport in Organic Semiconductors. *Chemical Reviews* **2007,** *107* (4), 926-952.

44. Dai, Y.; Long, H.; Wang, X.; Wang, Y.; Gu, Q.; Jiang, W.; Wang, Y.; Li, C.; Zeng, T. H.; Sun, Y.; Zeng, J., Doping: Versatile Graphene Quantum Dots with Tunable Nitrogen Doping (Part. Part. Syst. Charact. 5/2014). *Particle & Particle Systems Characterization* **2014,** *31* (5), 509-509.

45. Das, R.; Ali, M. E.; Hamid, S. B. A.; Ramakrishna, S.; Chowdhury, Z. Z., Carbon nanotube membranes for water purification: A bright future in water desalination. *Desalination* **2014,** *336*, 97-109.

46. Das, R. K.; Mohapatra, S., Highly luminescent, heteroatom-doped carbon quantum dots for ultrasensitive sensing of glucosamine and targeted imaging of liver cancer cells. *Journal of Materials Chemistry B* **2017,** *5* (11), 2190-2197.

47. Deng, L.; Wang, X. L.; Kuang, Y.; Wang, C.; Luo, L.; Wang, F.; Sun, X. M., Development of hydrophilicity gradient ultracentrifugation method for photoluminescence investigation of separated non-sedimental carbon dots. *Nano Research* **2015,** *8* (9), 2810-2821.

48. Denholm, P., K. Clark, and M. O'Connell, On the Path to SunShot: Emerging Issues and Challenges in Integrating High Levels of Solar into the Electrical Generation and Transmission System. Laboratory., N. R. E., Ed. Golden, CO, 2016.

49. Dey, S.; Govindaraj, A.; Biswas, K.; Rao, C. N. R., Luminescence properties of boron and nitrogen doped graphene quantum dots prepared from arc-discharge-generated doped graphene samples. *Chemical Physics Letters* **2014,** *595*, 203-208.

50. Diac, A.; Focsan, M.; Socaci, C.; Gabudean, A. M.; Farcau, C.; Maniu, D.; Vasile, E.; Terec, A.; Veca, L. M.; Astilean, S., Covalent conjugation of carbon dots with Rhodamine B and assessment of their photophysical properties. *RSC Advances* **2015,** *5* (95), 77662-77669.

51. Ding, H.; Xiong, H. M., Exploring the blue luminescence origin of nitrogen-doped carbon dots by controlling the water amount in synthesis. *RSC Advances* **2015,** *5* (82), 66528-66533.

52. Do, S.; Kwon, W.; Rhee, S.-W., Soft-template synthesis of nitrogen-doped carbon nanodots: tunable visible-light photoluminescence and phosphor-based light-emitting diodes. *Journal of Materials Chemistry C* **2014,** *2* (21), 4221-4226.

53. Dong, Y.; Chen, C.; Zheng, X.; Gao, L.; Cui, Z.; Yang, H.; Guo, C.; Chi, Y.; Li, C. M., One-step and high yield simultaneous preparation of single- and multi-layer graphene quantum dots from CX-72 carbon black. *Journal of Materials Chemistry* **2012,** *22* (18), 8764-8766.

54. Dong, Y.; Shao, J.; Chen, C.; Li, H.; Wang, R.; Chi, Y.; Lin, X.; Chen, G., Blue luminescent graphene quantum dots and graphene oxide prepared by tuning the carbonization degree of citric acid. *Carbon* **2012,** *50* (12), 4738-4743.

55. Dong, Y.; Wang, R.; Li, H.; Shao, J.; Chi, Y.; Lin, X.; Chen, G., Polyamine-functionalized carbon quantum dots for chemical sensing. *Carbon* **2012,** *50* (8), 2810-2815.

56. Dreyer, D. R.; Park, S.; Bielawski, C. W.; Ruoff, R. S., The chemistry of graphene oxide. *Chemical Society Reviews* **2010,** *39* (1), 228-240.

57. Du, F. Y.; Li, J. A.; Hua, Y.; Zhang, M. M.; Zhou, Z.; Yuan, J.; Wang, J.; Peng, W. X.; Zhang, L.; Xia, S.; Wang, D. Q.; Yang, S. M.; Xu, W. R.; Gong, A. H.; Shao, Q. X., Multicolor Nitrogen-Doped Carbon Dots for Live Cell Imaging. *Journal of Biomedical Nanotechnology* **2015,** *11* (5), 780-788.

58. Dumortier, H.; Lacotte, S.; Pastorin, G.; Marega, R.; Wu, W.; Bonifazi, D.; Briand, J.-P.; Prato, M.; Muller, S.; Bianco, A., Functionalized Carbon Nanotubes Are Non-Cytotoxic and Preserve the Functionality of Primary Immune Cells. *Nano Letters* **2006,** *6* (7), 1522-1528.

59. Eatemadi, A.; Daraee, H.; Karimkhanloo, H.; Kouhi, M.; Zarghami, N.; Akbarzadeh, A.; Abasi, M.; Hanifehpour, Y.; Joo, S. W., Carbon nanotubes: properties, synthesis, purification, and medical applications. *Nanoscale Research Letters* **2014,** *9* (1), 393.

60. Ebenhoch, B.; Thomson, S. A. J.; Genevičius, K.; Juška, G.; Samuel, I. D. W., Charge carrier mobility of the organic photovoltaic materials PTB7 and PC71BM and its influence on device performance. *Organic Electronics* **2015,** *22*, 62-68.

61. Elming, N.; Clauson-Kaas, N., The preparation of pyrroles from furans. *Acta Chem. Scand* **1952,** *6*, 867-874.

62. Energy), D. U. S. D. o., SunShot Vision Study. Energy), D. U. S. D. o., Ed. Washington, DC, 2012.

63. Ericson, M. B.; Wennberg, A.-M.; Larkö, O., Review of photodynamic therapy in actinic keratosis and basal cell carcinoma. *Therapeutics and Clinical Risk Management* **2008,** *4* (1), 1-9.

64. Essner, J. B.; Laber, C. H.; Ravula, S.; Polo-Parada, L.; Baker, G. A., Pee-dots: biocompatible fluorescent carbon dots derived from the upcycling of urine. *Green Chemistry* **2016,** *18* (1), 243-250.

65. Fan, T. J.; Zeng, W. J.; Tang, W.; Yuan, C. Q.; Tong, S. Z.; Cai, K. Y.; Liu, Y. D.; Huang, W.; Min, Y.; Epstein, A. J., Controllable size-selective method to prepare graphene quantum dots from graphene oxide. *Nanoscale Research Letters* **2015,** *10*, 1-8.

66. Fan, Z.; Sun, K.; Wang, J., Perovskites for photovoltaics: a combined review of organic-inorganic halide perovskites and ferroelectric oxide perovskites. *Journal of Materials Chemistry A* **2015,** *3* (37), 18809-18828.

67. Fan, Z. T.; Li, S. H.; Yuan, F. L.; Fan, L. Z., Fluorescent graphene quantum dots for biosensing and bioimaging. *RSC Advances* **2015,** *5* (25), 19773-19789.

68. Feldman, D., and M. Bolinger, On the Path to SunShot: Emerging Opportunities and Challenges in Financing Solar. Laboratory, N. R. E., Ed. Golden, CO, 2016.

69. Feng, Y.; Zhao, J.; Yan, X.; Tang, F.; Xue, Q., Enhancement in the fluorescence of graphene quantum dots by hydrazine hydrate reduction. *Carbon* **2014,** *66*, 334-339.

70. Fowley, C.; Nomikou, N.; McHale, A. P.; McCaughan, B.; Callan, J. F., Extending the tissue penetration capability of conventional photosensitisers: a carbon quantum dot-protoporphyrin IX conjugate for use in two-photon excited photodynamic therapy. *Chemical Communications* **2013,** *49* (79), 8934-8936.

71. Fu, M.; Ehrat, F.; Wang, Y.; Milowska, K. Z.; Reckmeier, C.; Rogach, A. L.; Stolarczyk, J. K.; Urban, A. S.; Feldmann, J., Carbon Dots: A Unique Fluorescent Cocktail of Polycyclic Aromatic Hydrocarbons. *Nano Letters* **2015,** *15* (9), 6030-6035.

72. Funke, A.; Ziegler, F., Hydrothermal carbonization of biomass: A summary and discussion of chemical mechanisms for process engineering. *Biofuels Bioproducts & Biorefining-Biofpr* **2010,** *4* (2), 160-177.

73. Gaddam, R. R.; Vasudevan, D.; Narayan, R.; Raju, K., Controllable synthesis of biosourced blue-green fluorescent carbon dots from camphor for the detection of heavy metal ions in water. *RSC Advances* **2014,** *4* (100), 57137-57143.

74. Gao, X.; Jang, J.; Nagase, S., Hydrazine and Thermal Reduction of Graphene Oxide: Reaction Mechanisms, Product Structures, and Reaction Design. *The Journal of Physical Chemistry C* **2010,** *114* (2), 832-842.

75. Ge, J.; Jia, Q.; Liu, W.; Lan, M.; Zhou, B.; Guo, L.; Zhou, H.; Zhang, H.; Wang, Y.; Gu, Y.; Meng, X.; Wang, P., Carbon Dots with Intrinsic Theranostic Properties for Bioimaging, Red-Light-Triggered Photodynamic/Photothermal Simultaneous Therapy In Vitro and In Vivo. *Advanced Healthcare Materials* **2016,** *5* (6), 665-675.

76. Ge, J.; Lan, M.; Zhou, B.; Liu, W.; Guo, L.; Wang, H.; Jia, Q.; Niu, G.; Huang, X.; Zhou, H.; Meng, X.; Wang, P.; Lee, C.-S.; Zhang, W.; Han, X., A graphene quantum dot photodynamic therapy agent with high singlet oxygen generation. *Nature Communications* **2014,** *5*, 4596.

77. Ge, J.; Li, Y.; Zhang, B. P.; Ma, N.; Wang, J.; Pu, C.; Xiang, Y. C., Electrochemical tuning of optical properties of graphitic quantum dots. *Journal of Luminescence* **2015,** *166*, 322-327.

78. Geim, A. K.; Novoselov, K. S., The rise of graphene. *Nature Materials* **2007,** *6* (3), 183-191.

79. Ghosh Chaudhuri, R.; Paria, S., Core/Shell Nanoparticles: Classes, Properties, Synthesis Mechanisms, Characterization, and Applications. *Chemical Reviews* **2012,** *112* (4), 2373-2433.

80. Gong, K.; Du, F.; Xia, Z.; Durstock, M.; Dai, L., Nitrogen-Doped Carbon Nanotube Arrays with High Electrocatalytic Activity for Oxygen Reduction. *Science* **2009,** *323* (5915), 760.

81. Gong, X.; Lu, W.; Paau, M. C.; Hu, Q.; Wu, X.; Shuang, S.; Dong, C.; Choi, M. M. F., Facile synthesis of nitrogen-doped carbon dots for Fe3+ sensing and cellular imaging. *Analytica Chimica Acta* **2015,** *861*, 74-84.

82. Haddon, R. C.; Brus, L. E.; Raghavachari, K., Electronic structure and bonding in icosahedral C60. *Chemical Physics Letters* **1986,** *125* (5), 459-464.

83. Hall, A. H.; Rumack, B. H., Clinical toxicology of cyanide. *Annals of emergency medicine* **1986,** *15* (9), 1067-1074.

84. Han, X. G.; Zhong, S. H.; Pan, W.; Shen, W. Z., A simple strategy for synthesizing highly luminescent carbon nanodots and application as effective down-shifting layers. *Nanotechnology* **2015,** *26* (6).

85. Hata, M.; Chomanee, J.; Thongyen, T.; Bao, L.; Tekasakul, S.; Tekasakul, P.; Otani, Y.; Furuuchi, M., Characteristics of nanoparticles emitted from burning of biomass fuels. *Journal of Environmental Sciences* **2014,** *26* (9), 1913-1920.

86. Hill, G. B.; Lyon, L. B., A NEW CHEMICAL STRUCTURE FOR COAL. *Industrial & Engineering Chemistry* **1962,** *54* (6), 36-41.

87. Hofmann, S.; Csányi, G.; Ferrari, A. C.; Payne, M. C.; Robertson, J., Surface Diffusion: The Low Activation Energy Path for Nanotube Growth. *Physical Review Letters* **2005,** *95* (3), 036101.

88. Hola, K.; Zhang, Y.; Wang, Y.; Giannelis, E. P.; Zboril, R.; Rogach, A. L., Carbon dots-Emerging light emitters for bioimaging, cancer therapy and optoelectronics. *Nano Today* **2014,** *9* (5), 590-603.

89. Hövel, H.; Bödecker, M.; Grimm, B.; Rettig, C., Growth mechanisms of carbon nanotubes using controlled production in ultrahigh vacuum. *Journal of Applied Physics* **2002,** *92* (2), 771-777.

90. Howerton, B. S.; Heidary, D. K.; Glazer, E. C., Strained Ruthenium Complexes Are Potent Light-Activated Anticancer Agents. *Journal of the American Chemical Society* **2012,** *134* (20), 8324-8327.

91. Hu, C.; Yu, C.; Li, M.; Wang, X.; Dong, Q.; Wang, G.; Qiu, J., Nitrogen-doped carbon dots decorated on graphene: a novel all-carbon hybrid electrocatalyst for enhanced oxygen reduction reaction. *Chemical Communications* **2015,** *51* (16), 3419-3422.

92. Hu, C.; Yu, C.; Li, M. Y.; Wang, X. N.; Yang, J. Y.; Zhao, Z. B.; Eychmuller, A.; Sun, Y. P.; Qiu, J. S., Chemically Tailoring Coal to Fluorescent Carbon Dots with Tuned Size and Their Capacity for Cu(II) Detection. *Small* **2014,** *10* (23), 4926-4933.

93. Hu, X.; An, X.; Li, L., Easy synthesis of highly fluorescent carbon dots from albumin and their photoluminescent mechanism and biological imaging applications. *Materials Science & Engineering C-Materials for Biological Applications* **2016,** *58*, 730-736.

94. Hu, X.; Cheng, L.; Wang, N.; Sun, L.; Wang, W.; Liu, W., Surface passivated carbon nanodots prepared by microwave assisted pyrolysis: effect of carboxyl group in precursors on fluorescence properties. *Rsc Advances* **2014,** *4* (36), 18818-18826.

95. Hu, Y. P.; Yang, J.; Tian, J. W.; Jia, L.; Yu, J. S., Green and size-controllable synthesis of photoluminescent carbon nanoparticles from waste plastic bags. *RSC Advances* **2014,** *4* (88), 47169-47176.

96. Hu, Y. P.; Yang, J.; Tian, J. W.; Yu, J. S., How do nitrogen-doped carbon dots generate from molecular precursors? An investigation of the formation mechanism and a solution-based large-scale synthesis. *Journal of Materials Chemistry B* **2015,** *3* (27), 5608-5614.

97. Huang, H.; Li, C. G.; Zhu, S. J.; Wang, H. L.; Chen, C. L.; Wang, Z. R.; Bai, T. Y.; Shi, Z.; Feng, S. H., Histidine-Derived Nontoxic Nitrogen-Doped Carbon Dots for Sensing and Bioinnaging Applications. *Langmuir* **2014,** *30* (45), 13542-13548.

98. Huang, H.; Liao, L.; Xu, X.; Zou, M.; Liu, F.; Li, N., The electron-transfer based interaction between transition metal ions and photoluminescent graphene quantum dots (GQDs): A platform for metal ion sensing. *Talanta* **2013,** *117*, 152-157.

99. Huang, J.; Deming, C. P.; Song, Y.; Kang, X.; Zhou, Z.-Y.; Chen, S., Chemical analysis of surface oxygenated moieties of fluorescent carbon nanoparticles. *Nanoscale* **2012,** *4* (3), 1010-1015.

100. Huang, P.; Lin, J.; Wang, X.; Wang, Z.; Zhang, C.; He, M.; Wang, K.; Chen, F.; Li, Z.; Shen, G.; Cui, D.; Chen, X., Light-Triggered Theranostics Based on Photosensitizer-Conjugated Carbon Dots for Simultaneous Enhanced-Fluorescence Imaging and Photodynamic Therapy. *Advanced Materials* **2012,** *24* (37), 5104-5110.

101. Hummers Jr, W. S.; Offeman, R. E., Preparation of graphitic oxide. *Journal of the American Chemical Society* **1958,** *80* (6), 1339-1339.

102. Iijima, S., Helical microtubules of graphitic carbon. *Nature* **1991,** *354* (6348), 56-58.

103. Islam, A.; Rabbani, M.; Bappy, M. H.; Miah, M. A. R.; Sakib, N. In *A review on fabrication process of organic light emitting diodes*, 2013 International Conference on Informatics, Electronics and Vision (ICIEV), 17-18 May 2013; 2013; pp 1-5.

104. Jawhari, T.; Roid, A.; Casado, J., Raman spectroscopic characterization of some commercially available carbon black materials. *Carbon* **1995,** *33* (11), 1561-1565.

105. Ji, S.-R.; Liu, C.; Zhang, B.; Yang, F.; Xu, J.; Long, J.; Jin, C.; Fu, D.-l.; Ni, Q.-X.; Yu, X.-J., Carbon nanotubes in cancer diagnosis and therapy. *Biochimica et Biophysica Acta (BBA) - Reviews on Cancer* **2010,** *1806* (1), 29-35.

106. Jia, X.; Li, J.; Wang, E., One-pot green synthesis of optically pH-sensitive carbon dots with upconversion luminescence. *Nanoscale* **2012,** *4* (18), 5572-5575.

107. Jiang, Z.; Nolan, A.; Walton, J. G. A.; Lilienkampf, A.; Zhang, R.; Bradley, M., Photoluminescent Carbon Dots from 1,4-Addition Polymers. *Chemistry-a European Journal* **2014,** *20* (35), 10926-10931.

108. Jin, S. H.; Kim, D. H.; Jun, G. H.; Hong, S. H.; Jeon, S., Tuning the Photoluminescence of Graphene Quantum Dots through the Charge Transfer Effect of Functional Groups. *ACS Nano* **2013,** *7* (2), 1239-1245.

109. Josefsen, L. B.; Boyle, R. W., Photodynamic Therapy and the Development of Metal-Based Photosensitisers. *Metal-Based Drugs* **2008,** *2008*, 276109.

110. Journet, C.; Maser, W. K.; Bernier, P.; Loiseau, A.; de la Chapelle, M. L.; Lefrant, S.; Deniard, P.; Lee, R.; Fischer, J. E., Large-scale production of single-walled carbon nanotubes by the electric-arc technique. *Nature* **1997,** *388* (6644), 756-758.

111. Ju, J.; Chen, W., Synthesis of highly fluorescent nitrogen-doped graphene quantum dots for sensitive, label-free detection of Fe (III) in aqueous media. *Biosensors & Bioelectronics* **2014,** *58*, 219-225.

112. Jung, K. H.; Boo, J.-H.; Hong, B., Synthesis of carbon nanotubes grown by hot filament plasma-enhanced chemical vapor deposition method. *Diamond and Related Materials* **2004,** *13* (2), 299-304.

113. Kang, S.; Herzberg, M.; Rodrigues, D. F.; Elimelech, M., Antibacterial Effects of Carbon Nanotubes: Size Does Matter! *Langmuir* **2008,** *24* (13), 6409-6413.

114. Khodashenas, B.; Ghorbani, H. R., Synthesis of silver nanoparticles with different shapes. *Arabian Journal of Chemistry* **2015**.

115. Kim, H.; Kwon, W.; Choi, M.; Rhee, S. W.; Yong, K., Photoelectrochemical Hydrogen Generation Using C-dot/ZnO Hierarchical Nanostructure as an Efficient Photoanode. *Journal of the Electrochemical Society* **2015,** *162* (6), H366-H370.

116. Kim, H.; Namgung, R.; Singha, K.; Oh, I.-K.; Kim, W. J., Graphene Oxide–Polyethylenimine Nanoconstruct as a Gene Delivery Vector and Bioimaging Tool. *Bioconjugate Chemistry* **2011,** *22* (12), 2558-2567.

117. Kim, T. H.; Ho, H. W.; Brown, C. L.; Cresswell, S. L.; Li, Q., Amine-rich carbon nanodots as a fluorescence probe for methamphetamine precursors. *Analytical Methods* **2015,** *7* (16), 6869-6876.

118. Kirner, S.; Sekita, M.; Guldi, D. M., 25th Anniversary Article: 25 Years of Fullerene Research in Electron Transfer Chemistry. *Advanced Materials* **2014,** *26* (10), 1482-1493.

119. Kolasinski, K. W., Catalytic growth of nanowires: Vapor–liquid–solid, vapor–solid–solid, solution–liquid–solid and solid–liquid–solid growth. *Current Opinion in Solid State and Materials Science* **2006,** *10* (3), 182-191.

120. Konkena, B.; Vasudevan, S., Understanding Aqueous Dispersibility of Graphene Oxide and Reduced Graphene Oxide through pKa Measurements. *The Journal of Physical Chemistry Letters* **2012,** *3* (7), 867-872.

121. Koole, R.; Groeneveld, E.; Vanmaekelbergh, D.; Meijerink, A.; de Mello Donegá, C., Size Effects on Semiconductor Nanoparticles. In *Nanoparticles: Workhorses of Nanoscience,* de Mello Donegá, C., Ed. Springer Berlin Heidelberg: Berlin, Heidelberg, 2014; pp 13-51.

122. Kosten, T. R.; George, T. P., The neurobiology of opioid dependence: implications for treatment. *Science & Practice Perspectives* **2002,** *1* (1), 13.

123. Kroto, H. W.; Allaf, A. W.; Balm, S. P., C60 - BUCKMINSTERFULLERENE. *Chemical Reviews* **1991,** *91* (6), 1213-1235.

124. Kumawat, M. K.; Thakur, M.; Gurung, R. B.; Srivastava, R., Graphene Quantum Dots from Mangifera indica: Application in Near-Infrared Bioimaging and Intracellular Nanothermometry. *ACS Sustainable Chemistry & Engineering* **2017,** *5* (2), 1382-1391.

125. Kundu, A.; Nandi, S.; Das, P.; Nandi, A. K., Facile and green approach to prepare fluorescent carbon dots: Emergent nanomaterial for cell imaging and detection of vitamin B2. *Journal of Colloid and Interface Science* **2016,** *468*, 276-83.

126. Lee, B.; Baek, Y.; Lee, M.; Jeong, D. H.; Lee, H. H.; Yoon, J.; Kim, Y. H., A carbon nanotube wall membrane for water treatment. *Nature Communications* **2015,** *6*, 7109.

127. Lei, Z.; Xu, S.; Wan, J.; Wu, P., Facile synthesis of N-rich carbon quantum dots by spontaneous polymerization and incision of solvents as efficient bioimaging probes and advanced electrocatalysts for oxygen reduction reaction. *Nanoscale* **2016,** *8* (4), 2219-2226.

128. Li, D.; Muller, M. B.; Gilje, S.; Kaner, R. B.; Wallace, G. G., Processable aqueous dispersions of graphene nanosheets. *Nature Nanotechnology* **2008,** *3* (2), 101-105.

129. Li, F.; Tian, F.; Liu, C.; Wang, Z.; Du, Z.; Li, R.; Zhang, L., One-step synthesis of nanohybrid carbon dots and TiO2composites with enhanced ultraviolet light active photocatalysis. *RSC Advances* **2015,** *5* (11), 8389-8396.

130. Li, L. L.; Wu, G. H.; Yang, G. H.; Peng, J.; Zhao, J. W.; Zhu, J. J., Focusing on luminescent graphene quantum dots: current status and future perspectives. *Nanoscale* **2013,** *5* (10), 4015-4039.

131. Li, Q.; Yan, H.; Zhang, J.; Liu, Z., Effect of hydrocarbons precursors on the formation of carbon nanotubes in chemical vapor deposition. *Carbon* **2004,** *42* (4), 829-835.

132. Li, Q.; Zhang, S.; Dai, L.; Li, L.-s., Nitrogen-Doped Colloidal Graphene Quantum Dots and Their Size-Dependent Electrocatalytic Activity for the Oxygen Reduction Reaction. *Journal of the American Chemical Society* **2012,** *134* (46), 18932-18935.

133. Li, T. F.; Li, Y. W.; Xiao, L.; Yu, H. T.; Fan, L. Z., Electrochemical Preparation of Color-Tunable Fluorescent Carbon Quantum Dots. *Acta Chimica Sinica* **2014,** *72* (2), 227-232.

134. Li, Y.; Hu, Y.; Zhao, Y.; Shi, G.; Deng, L.; Hou, Y.; Qu, L., An Electrochemical Avenue to Green-Luminescent Graphene Quantum Dots as Potential Electron-Acceptors for Photovoltaics. *Advanced Materials* **2011,** *23* (6), 776-780.

135. Li, Y.; Shu, H.; Niu, X.; Wang, J., Electronic and Optical Properties of Edge-Functionalized Graphene Quantum Dots and the Underlying Mechanism. *The Journal of Physical Chemistry C* **2015,** *119* (44), 24950-24957.

136. Li, Y.; Zhao, Y.; Cheng, H.; Hu, Y.; Shi, G.; Dai, L.; Qu, L., Nitrogen-Doped Graphene Quantum Dots with Oxygen-Rich Functional Groups. *Journal of the American Chemical Society* **2012,** *134* (1), 15-18.

137. Li, Z.; Yu, H.; Bian, T.; Zhao, Y.; Zhou, C.; Shang, L.; Liu, Y.; Wu, L.-Z.; Tung, C.-H.; Zhang, T., Highly luminescent nitrogen-doped carbon quantum dots as effective fluorescent probes for mercuric and iodide ions. *Journal of Materials Chemistry C* **2015,** *3* (9), 1922-1928.

138. Liu, J.; Erogbogbo, F.; Yong, K.-T.; Ye, L.; Liu, J.; Hu, R.; Chen, H.; Hu, Y.; Yang, Y.; Yang, J.; Roy, I.; Karker, N. A.; Swihart, M. T.; Prasad, P. N., Assessing Clinical Prospects of Silicon Quantum Dots: Studies in Mice and Monkeys. *ACS Nano* **2013,** *7* (8), 7303-7310.

139. Liu, J.; Tu, G.; Zhou, Q.; Cheng, Y.; Geng, Y.; Wang, L.; Ma, D.; Jing, X.; Wang, F., Highly efficient green light emitting polyfluorene incorporated with 4-diphenylamino-1,8-naphthalimide as green dopant. *Journal of Materials Chemistry* **2006,** *16* (15), 1431-1438.

140. Liu, L.; Li, Y.; Zhan, L.; Liu, Y.; Huang, C., One-step synthesis of fluorescent hydroxyls-coated carbon dots with hydrothermal reaction and its application to optical sensing of metal ions. *Science China Chemistry* **2011,** *54* (8), 1342.

141. Liu, M. Y.; Zhang, X. Q.; Yang, B.; Li, Z.; Deng, F. J.; Yang, Y.; Zhang, X. Y.; Wei, Y., Fluorescent nanoparticles from starch: Facile preparation, tunable luminescence and bioimaging. *Carbohydrate Polymers* **2015,** *121*, 49-55.

142. Liu, R.-M.; Ting, J.-M., Growth of carbon nanotubes using microwave plasma-enhanced chemical vapor deposition process. *Materials Chemistry and Physics* **2003,** *82* (3), 571-574.

143. Liu, S. Y.; Zhao, N.; Cheng, Z.; Liu, H. G., Amino-functionalized green fluorescent carbon dots as surface energy transfer biosensors for hyaluronidase. *Nanoscale* **2015,** *7* (15), 6836-6842.

144. Liu, Y.; Liao, M.; He, X. L.; Liu, X.; Kou, X. M.; Xiao, D., One-step Synthesis of Highly Luminescent Nitrogen-doped Carbon Dots for Selective and Sensitive Detection of Mercury(II) Ions and Cellular Imaging. *Analytical Sciences* **2015,** *31* (10), 971-977.

145. Liu, Y.; Lin, M.; Zhao, Y., Intersystem Crossing Rates of Isolated Fullerenes: Theoretical Calculations. *The Journal of Physical Chemistry A* **2017,** *121* (5), 1145-1152.

146. Lopez, T. D. F.; Gonzalez, A. F.; Diaz-Garcia, M. E.; Badia-Laino, R., Highly efficient Forster resonance energy transfer between carbon nanoparticles and europium-tetracycline complex. *Carbon* **2015,** *94*, 142-151.

147. Lu, W. J.; Gong, X. J.; Yang, Z. H.; Zhang, Y. X.; Hu, Q.; Shuang, S. M.; Dong, C.; Choi, M. M. F., High-quality water-soluble luminescent carbon dots for multicolor patterning, sensors, and bioimaging. *RSC Advances* **2015,** *5* (22), 16972-16979.

148. Luo, P. H.; Qiu, Y.; Guan, X. F.; Jiang, L. Q., Regulation of photoluminescence properties of graphene quantum dots via hydrothermal treatment. *Physical Chemistry Chemical Physics* **2014,** *16* (35), 19011-19016.

149. Ma, Z.; Ming, H.; Huang, H.; Liu, Y.; Kang, Z., One-step ultrasonic synthesis of fluorescent N-doped carbon dots from glucose and their visible-light sensitive photocatalytic ability. *New Journal of Chemistry* **2012,** *36* (4), 861-864.

150. Margraf, J. T.; Strauss, V.; Guldi, D. M.; Clark, T., The Electronic Structure of Amorphous Carbon Nanodots. *Journal of Physical Chemistry B* **2015,** *119* (24), 7258-7265.

151. Markovic, Z. M.; Ristic, B. Z.; Arsikin, K. M.; Klisic, D. G.; Harhaji-Trajkovic, L. M.; Todorovic-Markovic, B. M.; Kepic, D. P.; Kravic-Stevovic, T. K.; Jovanovic, S. P.; Milenkovic, M. M.; Milivojevic, D. D.; Bumbasirevic, V. Z.; Dramicanin, M. D.; Trajkovic, V. S., Graphene quantum dots as autophagy-inducing photodynamic agents. *Biomaterials* **2012,** *33* (29), 7084-7092.

152. Martindale, B. C. M.; Hutton, G. A. M.; Caputo, C. A.; Reisner, E., Solar Hydrogen Production Using Carbon Quantum Dots and a Molecular Nickel Catalyst. *Journal of the American Chemical Society* **2015,** *137* (18), 6018-6025.

153. Martins, N. C. T.; Ângelo, J.; Girão, A. V.; Trindade, T.; Andrade, L.; Mendes, A., N-doped carbon quantum dots/TiO2 composite with improved photocatalytic activity. *Applied Catalysis B: Environmental* **2016,** *193*, 67-74.

154. Maruyama, J.; Okamura, J.; Miyazaki, K.; Uchimoto, Y.; Abe, I., Hemoglobin Pyropolymer Used as a Precursor of a Noble-Metal-Free Fuel Cell Cathode Catalyst. *The Journal of Physical Chemistry C* **2008,** *112* (7), 2784-2790.

155. Mehos, M., C. Turchi, J. Jorgensen, P. Denholm, C. Ho, and K. Armijo, On the Path to SunShot: Advancing Concentrating Solar Power Technology, Performance, and Dispatchability. Laboratory, N. R. E., Ed. Golden, CO, 2016.

156. Mei, Q.; Zhang, K.; Guan, G.; Liu, B.; Wang, S.; Zhang, Z., Highly efficient photoluminescent graphene oxide with tunable surface properties. *Chemical Communications* **2010,** *46* (39), 7319-7321.

157. Miles, R. W.; Zoppi, G.; Forbes, I., Inorganic photovoltaic cells. *Materials Today* **2007,** *10* (11), 20-27.

158. Necas, D.; Klapetek, P., Gwyddion: an open-source software for SPM data analysis. *Central European Journal of Physics* **2012,** *10* (1), 181-188.

159. Nessim, G. D., Properties, synthesis, and growth mechanisms of carbon nanotubes with special focus on thermal chemical vapor deposition. *Nanoscale* **2010,** *2* (8), 1306-1323.

160. Neyerlin, K. C.; Gu, W.; Jorne, J.; Gasteiger, H. A., Study of the Exchange Current Density for the Hydrogen Oxidation and Evolution Reactions. *Journal of The Electrochemical Society* **2007,** *154* (7), B631-B635.

161. Niu, W. J.; Li, Y.; Zhu, R. H.; Shan, D.; Fan, Y. R.; Zhang, X. J., Ethylenediamine-assisted hydrothermal synthesis of nitrogen-doped carbon quantum dots as fluorescent probes for sensitive biosensing and bioimaging. *Sensors and Actuators B-Chemical* **2015,** *218*, 229-236.

162. Noor Ul, A.; Eriksson, O. M.; Schmidt, S.; Asghar, M.; Lin, P.-C.; Holtz, O. P.; Syväjärvi, M.; Yazdi, R. G., Tuning the Emission Energy of Chemically Doped Graphene Quantum Dots. *Nanomaterials* **2016,** *6* (11).

163. Ortells, M. O.; Barrantes, G. E., Tobacco addiction: A biochemical model of nicotine dependence. *Medical Hypotheses 74* (5), 884-894.

164. Palmintier, B., R. Broderick, B. Mather, M. Coddington, K. Baker, F. Ding, M. Reno, M. Lave, and A. Bharatkumar, On the Path to SunShot: Emerging Issues and Challenges in Integrating Solar with the Distribution System. Laboratory, N. R. E., Ed. 2016.

165. Pan, D. Y.; Zhang, J. C.; Li, Z.; Wu, M. H., Hydrothermal Route for Cutting Graphene Sheets into Blue-Luminescent Graphene Quantum Dots. *Advanced Materials* **2010,** *22* (6), 734-738.

166. Paulo, S.; Palomares, E.; Martinez-Ferrero, E., Graphene and Carbon Quantum Dot-Based Materials in Photovoltaic Devices: From Synthesis to Applications. *Nanomaterials* **2016,** *6* (9).

167. Peng, J.; Gao, W.; Gupta, B. K.; Liu, Z.; Romero-Aburto, R.; Ge, L.; Song, L.; Alemany, L. B.; Zhan, X.; Gao, G.; Vithayathil, S. A.; Kaipparettu, B. A.; Marti, A. A.; Hayashi, T.; Zhu, J.-J.; Ajayan, P. M., Graphene Quantum Dots Derived from Carbon Fibers. *Nano Letters* **2012,** *12* (2), 844-849.

168. Puretzky, A. A.; Geohegan, D. B.; Jesse, S.; Ivanov, I. N.; Eres, G., In situ measurements and modeling of carbon nanotube array growth kinetics during chemical vapor deposition. *Applied Physics A* **2005,** *81* (2), 223-240.

169. Qian, Z.; Ma, J.; Shan, X.; Feng, H.; Shao, L.; Chen, J., Highly Luminescent N-Doped Carbon Quantum Dots as an Effective Multifunctional Fluorescence Sensing Platform. *Chemistry-a European Journal* **2014,** *20* (11), 2983-2983.

170. Qu, D.; Zheng, M.; Zhang, L.; Zhao, H.; Xie, Z.; Jing, X.; Haddad, R. E.; Fan, H.; Sun, Z., Formation mechanism and optimization of highly luminescent N-doped graphene quantum dots. *Scientific Reports* **2014,** *4*, 5294.

171. Rao, C. N. R.; Voggu, R.; Govindaraj, A., Selective generation of single-walled carbon nanotubes with metallic, semiconducting and other unique electronic properties. *Nanoscale* **2009,** *1* (1), 96-105.

172. Reibold, M.; Paufler, P.; Levin, A. A.; Kochmann, W.; Patzke, N.; Meyer, D. C., Materials: Carbon nanotubes in an ancient Damascus sabre. *Nature* **2006,** *444* (7117), 286-286.

173. Reiss, P.; Protiere, M.; Li, L., Core/Shell Semiconductor Nanocrystals. *Small* **2009,** *5* (2), 154-168.

174. Rietmeijer, F. J. M.; Mackinnon, I. D. R., Poorly graphitized carbon as a new cosmothermometer for primitive extraterrestrial materials. *Nature* **1985,** *315* (6022), 733-736.

175. Ristic, B. Z.; Milenkovic, M. M.; Dakic, I. R.; Todorovic-Markovic, B. M.; Milosavljevic, M. S.; Budimir, M. D.; Paunovic, V. G.; Dramicanin, M. D.; Markovic, Z. M.; Trajkovic, V. S., Photodynamic antibacterial effect of graphene quantum dots. *Biomaterials* **2014,** *35* (15), 4428-4435.

176. Roduner, E., Size matters: why nanomaterials are different. *Chemical Society Reviews* **2006,** *35* (7), 583-592.

177. S. Isaacs, N.; van Eldik, R., A mechanistic study of the reduction of quinones by ascorbic acid. *Journal of the Chemical Society, Perkin Transactions 2* **1997,** (8), 1465-1468.

178. Saidi, W. A., Oxygen Reduction Electrocatalysis Using N-Doped Graphene Quantum-Dots. *The Journal of Physical Chemistry Letters* **2013,** *4* (23), 4160-4165.

179. Salar Bagherpour, D. H. E.-D. S. E., Fibre Reinforced Polyester Composites. *InTech* **2012**.

180. Samia, A. C. S.; Chen, X.; Burda, C., Semiconductor Quantum Dots for Photodynamic Therapy. *Journal of the American Chemical Society* **2003,** *125* (51), 15736-15737.

181. Sarkar, S.; Das, K.; Ghosh, M.; Das, P. K., Amino acid functionalized blue and phosphorous-doped green fluorescent carbon dots as bioimaging probe. *RSC Advances* **2015,** *5* (81), 65913-65921.

182. Sarswat, P. K.; Free, M. L., Light emitting diodes based on carbon dots derived from food, beverage, and combustion wastes. *Physical Chemistry Chemical Physics* **2015,** *17* (41), 27642-27652.

183. Sayes, C. M.; Liang, F.; Hudson, J. L.; Mendez, J.; Guo, W.; Beach, J. M.; Moore, V. C.; Doyle, C. D.; West, J. L.; Billups, W. E.; Ausman, K. D.; Colvin, V. L., Functionalization density dependence of single-walled carbon nanotubes cytotoxicity in vitro. *Toxicology Letters* **2006,** *161* (2), 135-142.

184. Schaeffer, W. D.; Smith, W. R., Effect of Heat Treatment on Reinforcing Properties of Carbon Black. *Industrial & Engineering Chemistry* **1955,** *47* (6), 1286-1290.

185. Scherf, U.; List, E. J. W., Semiconducting Polyfluorenes—Towards Reliable Structure–Property Relationships. *Advanced Materials* **2002,** *14* (7), 477-487.

186. Schwager, I.; Yen, T. F., Determination of nitrogen and oxygen functional groups in coal-derived asphaltenes. *Analytical Chemistry* **1979,** *51* (4), 569-571.

187. Scott, C. D.; Arepalli, S.; Nikolaev, P.; Smalley, R. E., Growth mechanisms for single-wall carbon nanotubes in a laser-ablation process. *Applied Physics A* **2001,** *72* (5), 573-580.

188. Shan, X.; Chai, L.; Ma, J.; Qian, Z.; Chen, J.; Feng, H., B-doped carbon quantum dots as a sensitive fluorescence probe for hydrogen peroxide and glucose detection. *Analyst* **2014,** *139* (10), 2322-2325.

189. Sharma, P. P.; Wu, J.; Yadav, R. M.; Liu, M.; Wright, C. J.; Tiwary, C. S.; Yakobson, B. I.; Lou, J.; Ajayan, P. M.; Zhou, X.-D., Nitrogen-Doped Carbon Nanotube Arrays for High-Efficiency Electrochemical Reduction of CO2: On the Understanding of Defects, Defect Density, and Selectivity. *Angewandte Chemie International Edition* **2015,** *54* (46), 13701-13705.

190. Shen, J.; Li, Y.; Su, Y.; Zhu, Y.; Jiang, H.; Yang, X.; Li, C., Photoluminescent carbon-nitrogen quantum dots as efficient electrocatalysts for oxygen reduction. *Nanoscale* **2015,** *7* (5), 2003-2008.

191. Shi, W. J.; Fan, H.; Ai, S. Y.; Zhu, L. S., Preparation of fluorescent graphene quantum dots from humic acid for bioimaging application. *New Journal of Chemistry* **2015,** *39* (9), 7054-7059.

192. Shi, Z.; Lian, Y.; Liao, F. H.; Zhou, X.; Gu, Z.; Zhang, Y.; Iijima, S.; Li, H.; Yue, K. T.; Zhang, S.-L., Large scale synthesis of single-wall carbon nanotubes by arc-discharge method. *Journal of Physics and Chemistry of Solids* **2000,** *61* (7), 1031-1036.

193. Shinde, D. B.; Pillai, V. K., Electrochemical Preparation of Luminescent Graphene Quantum Dots from Multiwalled Carbon Nanotubes. *Chemistry-a European Journal* **2012,** *18* (39), 12522-12528.

194. Shinozaki, K.; Zack, J. W.; Richards, R. M.; Pivovar, B. S.; Kocha, S. S., Oxygen Reduction Reaction Measurements on Platinum Electrocatalysts Utilizing Rotating Disk Electrode Technique: I. Impact of Impurities, Measurement Protocols and Applied Corrections. *Journal of the Electrochemical Society* **2015,** *162* (10), F1144-F1158.

195. Shui, J.; Chen, C.; Grabstanowicz, L.; Zhao, D.; Liu, D.-J., Highly efficient nonprecious metal catalyst prepared with metal–organic framework in a continuous carbon nanofibrous network. *Proceedings of the National Academy of Sciences* **2015,** *112* (34), 10629-10634.

196. Simon-Deckers, A.; Gouget, B.; Mayne-L'Hermite, M.; Herlin-Boime, N.; Reynaud, C.; Carrière, M., In vitro investigation of oxide nanoparticle and carbon nanotube toxicity and intracellular accumulation in A549 human pneumocytes. *Toxicology* **2008,** *253* (1), 137-146.

197. Singh, H.; Khurana, H.; Singh, H.; Singh, M., Photodynamic therapy: Truly a marriage between a drug and a light. *Muller Journal of Medical Sciences and Research* **2014,** *5* (1), 48-55.

198. Sk, M. A.; Ananthanarayanan, A.; Huang, L.; Lim, K. H.; Chen, P., Revealing the tunable photoluminescence properties of graphene quantum dots. *Journal of Materials Chemistry C* **2014,** *2* (34), 6954-6960.

199. Song, C.; Zhang, J., Electrocatalytic Oxygen Reduction Reaction. In *PEM Fuel Cell Electrocatalysts and Catalyst Layers: Fundamentals and Applications*, Zhang, J., Ed. Springer London: London, 2008; pp 89-134.

200. Song, Y. B.; Zhu, S. J.; Yang, B., Bioimaging based on fluorescent carbon dots. *RSC Advances* **2014,** *4* (52), 27184-27200.

201. Song, Y. B.; Zhu, S. J.; Zhang, S. T.; Fu, Y.; Wang, L.; Zhao, X. H.; Yang, B., Investigation from chemical structure to photoluminescent mechanism: a type of carbon dots from the pyrolysis of citric acid and an amine. *Journal of Materials Chemistry C* **2015,** *3* (23), 5976-5984.

202. Spano, F. C.; Silva, C., H-and J-aggregate behavior in polymeric semiconductors. *Annual review of physical chemistry* **2014,** *65*, 477-500.

203. Stankovich, S.; Dikin, D. A.; Piner, R. D.; Kohlhaas, K. A.; Kleinhammes, A.; Jia, Y.; Wu, Y.; Nguyen, S. T.; Ruoff, R. S., Synthesis of graphene-based nanosheets via chemical reduction of exfoliated graphite oxide. *Carbon* **2007,** *45* (7), 1558-1565.

204. Staudenmaier, L., Verfahren zur darstellung der graphitsäure. *European Journal of Inorganic Chemistry* **1898,** *31* (2), 1481-1487.

205. Strauss, V.; Margraf, J. T.; Dolle, C.; Butz, B.; Nacken, T. J.; Walter, J.; Bauer, W.; Peukert, W.; Spiecker, E.; Clark, T.; Guldi, D. M., Carbon Nanodots: Toward a Comprehensive Understanding of Their Photoluminescence. *Journal of the American Chemical Society* **2014,** *136* (49), 17308-17316.

206. Sun, H.; Gao, N.; Dong, K.; Ren, J.; Qu, X., Graphene Quantum Dots-Band-Aids Used for Wound Disinfection. *Acs Nano* **2014,** *8* (6), 6202-6210.

207. Sun, H.; Gao, N.; Wu, L.; Ren, J.; Wei, W.; Qu, X., Highly Photoluminescent Amino-Functionalized Graphene Quantum Dots Used for Sensing Copper Ions. *Chemistry-a European Journal* **2013,** *19* (40), 13362-13368.

208. Sun, J.; Yang, S.; Wang, Z.; Shen, H.; Xu, T.; Sun, L.; Li, H.; Chen, W.; Jiang, X.; Ding, G.; Kang, Z.; Xie, X.; Jiang, M., Ultra-High Quantum Yield of Graphene Quantum Dots: Aromatic-Nitrogen Doping and Photoluminescence Mechanism. *Particle & Particle Systems Characterization* **2015,** *32* (4), 434-440.

209. Sun, Y.; Wang, S.; Li, C.; Luo, P.; Tao, L.; Wei, Y.; Shi, G., Large scale preparation of graphene quantum dots from graphite with tunable fluorescence properties. *Physical Chemistry Chemical Physics* **2013,** *15* (24), 9907-9913.

210. Sun, Y. X.; He, Z. W.; Sun, X. B.; Zhao, Z. D., Synthesis of Water-soluble Fluorescent Carbon Dots from a One-step Hydrothermal Method with Potato. In *Eighth China National Conference on Functional Materials and Applications*, Zhao, G. M.; Chen, L.; Tang, Y.; Long, B.; Nie, Z.; He, L.; Chen, H., Eds. 2014; Vol. 873, pp 770-776.

211. Tan, X.; Li, Y.; Li, X.; Zhou, S.; Fan, L.; Yang, S., Electrochemical synthesis of small-sized red fluorescent graphene quantum dots as a bioimaging platform. *Chemical Communications* **2015,** *51* (13), 2544-2546.

212. Tang, L.; Ji, R.; Li, X.; Teng, K. S.; Lau, S. P., Energy-level structure of nitrogen-doped graphene quantum dots. *Journal of Materials Chemistry C* **2013,** *1* (32), 4908-4915.

213. Tao, H.; Yang, K.; Ma, Z.; Wan, J.; Zhang, Y.; Kang, Z.; Liu, Z., In Vivo NIR Fluorescence Imaging, Biodistribution, and Toxicology of Photoluminescent Carbon Dots Produced from Carbon Nanotubes and Graphite. *Small* **2012,** *8* (2), 281-290.

214. Tetsuka, H.; Asahi, R.; Nagoya, A.; Okamoto, K.; Tajima, I.; Ohta, R.; Okamoto, A., Optically Tunable Amino-Functionalized Graphene Quantum Dots. *Advanced Materials* **2012,** *24* (39), 5333-5338.

215. Toh, S. Y.; Loh, K. S.; Kamarudin, S. K.; Daud, W. R. W., Graphene production via electrochemical reduction of graphene oxide: Synthesis and characterisation. *Chemical Engineering Journal* **2014,** *251*, 422-434.

216. Tuci, G.; Zafferoni, C.; Rossin, A.; Luconi, L.; Milella, A.; Ceppatelli, M.; Innocenti, M.; Liu, Y.; Pham-Huu, C.; Giambastiani, G., Chemical functionalization of N-doped carbon nanotubes: a powerful approach to cast light on the electrochemical role of specific N-functionalities in the oxygen reduction reaction. *Catalysis Science & Technology* **2016,** *6* (16), 6226-6236.

217. Uchida, H.; Curtis, C. J.; Kamat, P. V.; Jones, K. M.; Nozik, A. J., Optical properties of gallium arsenide nanocrystals. *The Journal of Physical Chemistry* **1992,** *96* (3), 1156-1160.

218. Ugarte, D., Curling and closure of graphitic networks under electron-beam irradiation. *Nature* **1992,** *359* (6397), 707-709.

219. Velasco-Santos, C.; Martı; x; nez-Hernández, A. L.; Consultchi, A.; Rodrı; x; guez, R.; Castaño, V. M., Naturally produced carbon nanotubes. *Chemical Physics Letters* **2003,** *373* (3), 272-276.

220. von Schneidemesser, E.; Monks, P. S.; Allan, J. D.; Bruhwiler, L.; Forster, P.; Fowler, D.; Lauer, A.; Morgan, W. T.; Paasonen, P.; Righi, M.; Sindelarova, K.; Sutton, M. A., Chemistry and the Linkages between Air Quality and Climate Change. *Chemical Reviews* **2015,** *115* (10), 3856-3897.

221. Wang, H.; Sun, P.; Cong, S.; Wu, J.; Gao, L.; Wang, Y.; Dai, X.; Yi, Q.; Zou, G., Nitrogen-Doped Carbon Dots for "green" Quantum Dot Solar Cells. *Nanoscale Research Letters* **2016,** *11* (1), 27.

222. Wang, J.; Sahu, S.; Sonkar, S. K.; Tackett Ii, K. N.; Sun, K. W.; Liu, Y.; Maimaiti, H.; Anilkumar, P.; Sun, Y.-P., Versatility with carbon dots - from overcooked BBQ to brightly fluorescent agents and photocatalysts. *RSC Advances* **2013,** *3* (36), 15604-15607.

223. Wang, K.; Zhang, X. Y.; Zhang, X. Q.; Yang, B.; Li, Z.; Zhang, Q. S.; Huang, Z. F.; Wei, Y., Fluorescent Glycopolymer Nanoparticles Based on Aggregation-Induced Emission Dyes: Preparation and Bioimaging Applications. *Macromolecular Chemistry and Physics* **2015,** *216* (6), 678-684.

224. Wang, L.; Li, B.; Xu, F.; Shi, X.; Feng, D.; Wei, D.; Li, Y.; Feng, Y.; Wang, Y.; Jia, D.; Zhou, Y., High-yield synthesis of strong photoluminescent N-doped carbon nanodots derived from hydrosoluble chitosan for mercury ion sensing via smartphone APP. *Biosenors and Bioelectronics* **2016,** *79*, 1-8.

225. Wang, L.; Zhu, S. J.; Wang, H. Y.; Qu, S. N.; Zhang, Y. L.; Zhang, J. H.; Chen, Q. D.; Xu, H. L.; Han, W.; Yang, B.; Sun, H. B., Common Origin of Green Luminescence in Carbon Nanodots and Graphene Quantum Dots. *ACS Nano* **2014,** *8* (3), 2541-2547.

226. Wang, L.; Zhu, S. J.; Wang, H. Y.; Wang, Y. F.; Hao, Y. W.; Zhang, J. H.; Chen, Q. D.; Zhang, Y. L.; Han, W.; Yang, B.; Sun, H. B., Unraveling Bright Molecule-Like State and Dark Intrinsic State in Green-Fluorescence Graphene Quantum Dots via Ultrafast Spectroscopy. *Advanced Optical Materials* **2013,** *1* (3), 264-271.

227. Wang, S.; Yu, D.; Dai, L., Polyelectrolyte Functionalized Carbon Nanotubes as Efficient Metal-free Electrocatalysts for Oxygen Reduction. *Journal of the American Chemical Society* **2011,** *133* (14), 5182-5185.

228. Wang, W.; Lu, Y.-C.; Huang, H.; Wang, A.-J.; Chen, J.-R.; Feng, J.-J., Facile synthesis of N, S-codoped fluorescent carbon nanodots for fluorescent resonance energy transfer recognition of methotrexate with high sensitivity and selectivity. *Biosensors & Bioelectronics* **2015,** *64*, 517-522.

229. Wang, Y.; Herron, N., Nanometer-sized semiconductor clusters: materials synthesis, quantum size effects, and photophysical properties. *The Journal of Physical Chemistry* **1991,** *95* (2), 525-532.

230. Wang, Y.; Li, Z.; Wang, J.; Li, J.; Lin, Y., Graphene and graphene oxide: biofunctionalization and applications in biotechnology. *Trends in Biotechnology* **2011,** *29* (5), 205-212.

231. Wen, X. M.; Yu, P.; Toh, Y. R.; Ma, X. Q.; Tang, J., On the upconversion fluorescence in carbon nanodots and graphene quantum dots. *Chemical Communications* **2014,** *50* (36), 4703-4706.

232. Wick, P.; Manser, P.; Limbach, L. K.; Dettlaff-Weglikowska, U.; Krumeich, F.; Roth, S.; Stark, W. J.; Bruinink, A., The degree and kind of agglomeration affect carbon nanotube cytotoxicity. *Toxicology Letters* **2007,** *168* (2), 121-131.

233. Wilson, B. C.; Jacques, S. L., Optical reflectance and transmittance of tissues: principles and applications. *IEEE Journal of Quantum Electronics* **1990,** *26* (12), 2186-2199.

234. Wilson, M. A.; Tran, N. H.; Milev, A. S.; Kannangara, G. S. K.; Volk, H.; Lu, G. Q. M., Nanomaterials in soils. *Geoderma* **2008,** *146* (1), 291-302.

235. Wiser, R., T. Mai, D. Millstein, J. Macknick, A. Carpenter, S. Cohen, W. Cole, B. Frew, and G. A. Heath, On the Path to SunShot: The Environmental and Public Health Benefits of Achieving High Penetrations of Solar Energy in the United States. Laboratory, N. R. E., Ed. Golden, CO, 2016.

236. Woodhouse, M., R. Jones-Albertus, D. Feldman, R. Fu, K. Horowitz, D. Chung, D. Jordan, and S. Kurtz, On the Path to SunShot: The Role of Advancements in Solar Photovoltaic Efficiency, Reliability, and Costs. Laboratory, N. R. E., Ed. 2016.

237. Wu, C.; Wang, C.; Han, T.; Zhou, X.; Guo, S.; Zhang, J., Insight into the Cellular Internalization and Cytotoxicity of Graphene Quantum Dots. *Advanced Healthcare Materials* **2013,** *2* (12), 1613-1619.

238. Xu, J.; Sahu, S.; Cao, L.; Bunker, C. E.; Peng, G.; Liu, Y.; Fernando, K. A. S.; Wang, P.; Guliants, E. A.; Meziani, M. J.; Qian, H.; Sun, Y.-P., Efficient Fluorescence Quenching in Carbon Dots by Surface-Doped Metals - Disruption of Excited State Redox Processes and Mechanistic Implications. *Langmuir* **2012,** *28* (46), 16141-16147.

239. Xu, M. H.; Xu, S. S.; Yang, Z.; Shu, M. J.; He, G. L.; Huang, D.; Zhang, L. L.; Li, L.; Cui, D. X.; Zhang, Y. F., Hydrophilic and blue fluorescent N-doped carbon dots from tartaric acid and various alkylol amines under microwave irradiation. *Nanoscale* **2015,** *7* (38), 15915-15923.

240. Xu, Q.; Zhao, J.; Liu, Y.; Pu, P.; Wang, X.; Chen, Y.; Gao, C.; Chen, J.; Zhou, H., Enhancing the luminescence of carbon dots by doping nitrogen element and its application in the detection of Fe(III). *Journal of Materials Science* **2015,** *50* (6), 2571-2576.

241. Xu, X.; Bishop, E. E.; Kennedy, S. M.; Simpson, S. A.; Pechacek, T. F., Annual Healthcare Spending Attributable to Cigarette Smoking. *American Journal of Preventive Medicine 48* (3), 326-333.

242. Xu, X.; Ray, R.; Gu, Y.; Ploehn, H. J.; Gearheart, L.; Raker, K.; Scrivens, W. A., Electrophoretic Analysis and Purification of Fluorescent Single-Walled Carbon Nanotube Fragments. *Journal of the American Chemical Society* **2004,** *126* (40), 12736-12737.

243. Yang, Z.; Xu, M.; Liu, Y.; He, F.; Gao, F.; Su, Y.; Wei, H.; Zhang, Y., Nitrogen-doped, carbon-rich, highly photoluminescent carbon dots from ammonium citrate. *Nanoscale* **2014,** *6* (3), 1890-1895.

244. Yang, Z.-C.; Wang, M.; Yong, A. M.; Wong, S. Y.; Zhang, X.-H.; Tan, H.; Chang, A. Y.; Li, X.; Wang, J., Intrinsically fluorescent carbon dots with tunable emission derived from hydrothermal treatment of glucose in the presence of monopotassium phosphate. *Chemical Communications* **2011,** *47* (42), 11615-11617.

245. Yoo, E.; Kim, J.; Hosono, E.; Zhou, H.-s.; Kudo, T.; Honma, I., Large Reversible Li Storage of Graphene Nanosheet Families for Use in Rechargeable Lithium Ion Batteries. *Nano Letters* **2008,** *8* (8), 2277-2282.

246. Yu, H.; Zhao, Y.; Zhou, C.; Shang, L.; Peng, Y.; Cao, Y.; Wu, L.-Z.; Tung, C.-H.; Zhang, T., Carbon quantum dots/TiO2 composites for efficient photocatalytic hydrogen evolution. *Journal of Materials Chemistry A* **2014,** *2* (10), 3344-3351.

247. Yu, J.; Zheng, Y.; Huang, J., Towards High Performance Organic Photovoltaic Cells: A Review of Recent Development in Organic Photovoltaics. *Polymers* **2014,** *6* (9).

248. Yudasaka, M.; Yomogida, Y.; Zhang, M.; Tanaka, T.; Nakahara, M.; Kobayashi, N.; Okamatsu-Ogura, Y.; Machida, K.; Ishihara, K.; Saeki, K.; Kataura, H., Near-Infrared Photoluminescent Carbon Nanotubes for Imaging of Brown Fat. *Scientific Reports* **2017,** *7*, 44760.

249. Zeng, D.; Cheng, J.; Ren, S.; Sun, J.; Zhong, H.; Xu, E.; Du, J.; Fang, Q., A new sensor for copper(II) ion based on carboxyl acid groups substituted polyfluoreneethynylene. *Reactive and Functional Polymers* **2008,** *68* (12), 1715-1721.

250. Zhai, X.; Zhang, P.; Liu, C.; Bai, T.; Li, W.; Dai, L.; Liu, W., Highly luminescent carbon nanodots by microwave-assisted pyrolysis. *Chemical Communications* **2012,** *48* (64), 7955-7957.

251. Zhai, Y.; Zhu, Z.; Zhu, C.; Ren, J.; Wang, E.; Dong, S., Multifunctional water-soluble luminescent carbon dots for imaging and Hg2+ sensing. *Journal of Materials Chemistry B* **2014,** *2* (40), 6995-6999.

252. Zhang, F.; Liu, F.; Wang, C.; Xin, X.; Liu, J.; Guo, S.; Zhang, J., Effect of Lateral Size of Graphene Quantum Dots on Their Properties and Application. *ACS Applied Materials & Interfaces* **2016,** *8* (3), 2104-2110.

253. Zhang, R.; Chen, W., Nitrogen-doped carbon quantum dots: Facile synthesis and application as a "turn-off" fluorescent probe for detection of Hg^{2+} ions. *Biosensors & Bioelectronics* **2014,** *55*, 83-90.

254. Zhang, R.; Liu, Y. B.; Sun, S. Q., Preparation of highly luminescent and biocompatible carbon dots using a new extraction method. *Journal of Nanoparticle Research* **2013,** *15* (10).

255. Zhang, R.; Liu, Y. B.; Yu, L. B.; Li, Z.; Sun, S. Q., Preparation of high-quality biocompatible carbon dots by extraction, with new thoughts on the luminescence mechanisms. *Nanotechnology* **2013,** *24* (22).

256. Zhang, W.; Yu, S. F.; Fei, L.; Jin, L.; Pan, S.; Lin, P., Large-area color controllable remote carbon white-light light-emitting diodes. *Carbon* **2015,** *85*, 344-350.

257. Zhang, W. F.; Jin, L. M.; Yu, S. F.; Zhu, H.; Pan, S. S.; Zhao, Y. H.; Yang, H. Y., Wide-bandwidth lasing from C-dot/epoxy nanocomposite Fabry-Perot cavities with ultralow threshold. *Journal of Materials Chemistry C* **2014,** *2* (8), 1525-1531.

258. Zhang, X.; Zhang, Y.; Wang, Y.; Kalytchuk, S.; Kershaw, S. V.; Wang, Y.; Wang, P.; Zhang, T.; Zhao, Y.; Zhang, H.; Cui, T.; Wang, Y.; Zhao, J.; Yu, W. W.; Rogach, A. L., Color-Switchable Electroluminescence of Carbon Dot Light-Emitting Diodes. *ACS Nano* **2013,** *7* (12), 11234-11241.

259. Zhang, Y.; Gu, H.; Iijima, S., Single-wall carbon nanotubes synthesized by laser ablation in a nitrogen atmosphere. *Applied Physics Letters* **1998,** *73* (26), 3827-3829.

260. Zhang, Y.; He, J. H., Facile synthesis of S, N co-doped carbon dots and investigation of their photoluminescence properties. *Physical Chemistry Chemical Physics* **2015,** *17* (31), 20154-20159.

261. Zhang, Y. L.; Wang, L.; Zhang, H. C.; Liu, Y.; Wang, H. Y.; Kang, Z. H.; Lee, S. T., Graphitic carbon quantum dots as a fluorescent sensing platform for highly efficient detection of Fe^{3+} ions. *RSC Advances* **2013,** *3* (11), 3733-3738.

262. Zhang, Z.; Zheng, T.; Li, X.; Xu, J.; Zeng, H., Progress of Carbon Quantum Dots in Photocatalysis Applications. *Particle & Particle Systems Characterization* **2016,** *33* (8), 457-472.

263. Zhao, A. D.; Chen, Z. W.; Zhao, C. Q.; Gao, N.; Ren, J. S.; Qu, X. G., Recent advances in bioapplications of C-dots. *Carbon* **2015,** *85*, 309-327.

264. Zhao, L. X.; Di, F.; Wang, D. B.; Guo, L. H.; Yang, Y.; Wan, B.; Zhang, H., Chemiluminescence of carbon dots under strong alkaline solutions: a novel insight into carbon dot optical properties. *Nanoscale* **2013,** *5* (7), 2655-2658.

265. Zheng, B. Z.; Liu, T.; Paau, M. C.; Wang, M. N.; Liu, Y.; Liu, L.; Wu, C. F.; Du, J.; Xiao, D.; Choi, M. M. F., One pot selective synthesis of water and organic soluble carbon dots with green fluorescence emission. *Rsc Advances* **2015,** *5* (15), 11667-11675.

266. Zheng, M.; Liu, S.; Li, J.; Xie, Z.; Qu, D.; Miao, X.; Jing, X.; Sun, Z.; Fan, H., Preparation of highly luminescent and color tunable carbon nanodots under visible light excitation for in vitro and in vivo bio-imaging. *Journal of Materials Research* **2015,** *30* (22), 3386-3393.

267. Zheng, Y.; Zhu, P., Carbon nano-onions: large-scale preparation, functionalization and their application as anode material for rechargeable lithium ion batteries. *RSC Advances* **2016,** *6* (95), 92285-92298.

268. Zhou, F.; Wu, S.; Yuan, Y.; Chen, W. R.; Xing, D., Mitochondria-Targeting Photoacoustic Therapy Using Single-Walled Carbon Nanotubes. *Small* **2012,** *8* (10), 1543-1550.

269. Zhu, S.; Meng, Q.; Wang, L.; Zhang, J.; Song, Y.; Jin, H.; Zhang, K.; Sun, H.; Wang, H.; Yang, B., Highly Photoluminescent Carbon Dots for Multicolor Patterning, Sensors, and Bioimaging. *Angewandte Chemie-International Edition* **2013,** *52* (14), 3953-3957.

270. Zhu, S.; Shao, J.; Song, Y.; Zhao, X.; Du, J.; Wang, L.; Wang, H.; Zhang, K.; Zhang, J.; Yang, B., Investigating the surface state of graphene quantum dots. *Nanoscale* **2015,** *7* (17), 7927-7933.

271. Zhu, S.; Zhang, J.; Qiao, C.; Tang, S.; Li, Y.; Yuan, W.; Li, B.; Tian, L.; Liu, F.; Hu, R.; Gao, H.; Wei, H.; Zhang, H.; Sun, H.; Yang, B., Strongly green-photoluminescent graphene quantum dots for bioimaging applications. *Chemical Communications* **2011,** *47* (24), 6858-6860.

272. Zhu, S.; Zhang, J.; Tang, S.; Qiao, C.; Wang, L.; Wang, H.; Liu, X.; Li, B.; Li, Y.; Yu, W.; Wang, X.; Sun, H.; Yang, B., Surface Chemistry Routes to Modulate the Photoluminescence of Graphene Quantum Dots: From Fluorescence Mechanism to Up-Conversion Bioimaging Applications. *Advanced Functional Materials* **2012,** *22* (22), 4732-4740.

273. Zhu, S. J.; Shao, J. R.; Song, Y. B.; Zhao, X. H.; Du, J. L.; Wang, L.; Wang, H. Y.; Zhang, K.; Zhang, J. H.; Yang, B., Investigating the surface state of graphene quantum dots. *Nanoscale* **2015,** *7* (17), 7927-7933.

274. Zhu, S. J.; Song, Y. B.; Zhao, X. H.; Shao, J. R.; Zhang, J. H.; Yang, B., The photoluminescence mechanism in carbon dots (graphene quantum dots, carbon nanodots, and polymer dots): current state and future perspective. *Nano Research* **2015,** *8* (2), 355-381.

275. Zhu, S. J.; Zhang, J. H.; Liu, X.; Li, B.; Wang, X. F.; Tang, S. J.; Meng, Q. N.; Li, Y. F.; Shi, C.; Hu, R.; Yang, B., Graphene quantum dots with controllable surface oxidation, tunable fluorescence and up-conversion emission. *RSC Advances* **2012,** *2* (7), 2717-2720.

276. Zhu, S. J.; Zhang, J. H.; Song, Y. B.; Zhang, G. Y.; Zhang, H.; Yang, B., Fluorescent Nanocomposite Based on PVA Polymer Dots. *Acta Chimica Sinica* **2012,** *70* (22), 2311-2315.

277. Zhu, S. J.; Zhang, J. H.; Tang, S. J.; Qiao, C. Y.; Wang, L.; Wang, H. Y.; Liu, X.; Li, B.; Li, Y. F.; Yu, W. L.; Wang, X. F.; Sun, H. C.; Yang, B., Surface Chemistry Routes to Modulate the Photoluminescence of Graphene Quantum Dots: From Fluorescence Mechanism to Up-Conversion Bioimaging Applications. *Advanced Functional Materials* **2012,** *22* (22), 4732-4740.

278. Zhu, S. J.; Zhou, N.; Hao, Z. Y.; Maharjan, S.; Zhao, X. H.; Song, Y. B.; Sun, B.; Zhang, K.; Zhang, J. H.; Sun, H. C.; Lu, L. J.; Yang, B., Photoluminescent graphene quantum dots for in vitro and in vivo bioimaging using long wavelength emission. *RSC Advances* **2015,** *5* (49), 39399-39403.

279. Zhu, Y.; Murali, S.; Cai, W.; Li, X.; Suk, J. W.; Potts, J. R.; Ruoff, R. S., Graphene and Graphene Oxide: Synthesis, Properties, and Applications. *Advanced Materials* **2010,** *22* (35), 3906-3924.

280. Zou, X.; Liu, M.; Wu, J.; Ajayan, P. M.; Li, J.; Liu, B.; Yakobson, B. I., How Nitrogen-Doped Graphene Quantum Dots Catalyze Electroreduction of CO2 to Hydrocarbons and Oxygenates. *ACS Catalysis* **2017**, 6245-6250.

281. Zrazhevskiy, P.; Sena, M.; Gao, X., Designing multifunctional quantum dots for bioimaging, detection, and drug delivery. *Chemical Society Reviews* **2010,** *39* (11), 4326-4354.

282. Züttel, A.; Remhof, A.; Borgschulte, A.; Friedrichs, O., Hydrogen: the future energy carrier. *Philosophical Transactions of the Royal Society A: Mathematical, Physical and Engineering Sciences* **2010,** *368* (1923), 3329.

VITA

Timothy Pillar-Little was born in Acworth, Georgia which is 20 miles northeast of Atlanta. After finishing high school in 2007, he started attending Southern Polytechnic State University in Marietta, Georgia. Between 2007 and 2011, he studied chemistry and was awarded a Bachelor's of Science in Chemistry in December 2011. In his time at the University of Kentucky starting in August 2012, he has been presented awards and fellowships that include an Outstanding General Chemistry Teaching Award, the H.H. Griffiths Outstanding General Chemistry Teaching Award, and two Max Steckler Fellowship Awards. His professional publications during this time are listed below:

Pillar-Little, T.J.; Kim, D.Y. Differentiating the impact of nitrogen chemical states on optical properties of nitrogen-doped graphene quantum dots. RSC Adv., 2017, 7, 48263.

Pillar-Little, T.J.; Kim, D.Y. Investigation of localized nitrogen addition and photoluminescent properties in carbon nanodots. 2017. Submitted.

Pillar-Little, T.J.; Kim, D.Y. Structure-Function Comparison of Bottom-Up and Top-Down Approaches to Carbon Quantum Dot Synthesis. 2017. In preparation.

Pillar-Little, T.J.; Wanninayake, N.; Nease, L.; Glazer, E.; Heidary, D.; Kim, D.Y. Carbon Quantum Dots Exhibit Strong Type I and Type II Photodynamic Anti-Cancer Effects. 2017. Submitted.